Mechanistic Investigation of Polyhydroxybutyrate (PHB) Synthases and Elucidation of PHB Biosynthesis and Degradation Process in *Wautersia eutropha* H16

By

Jiamin Tian

B.A. *1997 Chemistry, University of Virginia*

Submitted to the Department of Chemistry in Partial Fulfillment of the Requirements for the Degree of

Doctor of Philosophy in Biochemistry

at the

MASSACHUSETTS INSTITUTE OF TECHNOLOGY

February 2005

Signature of Author: _____

Department of Chemistry
14 December 2004

Certified by: _____

Professor JoAnne Stubbe
Novartis Professor of Chemistry and Professor of Biology

Accepted by: _____

Professor Robert W. Field
Haslam and Dewey Professor of Chemistry
Chairman, Department Committee on Graduate Studies

This doctoral thesis has been examined by a Committee of the Department of Chemistry and Biology as follows.

Professor Catherine L. Drennan
Green Career Development Assistant Professor of Chemistry
Chairperson

Professor JoAnne Stubbe
Novartis Professor of Chemistry and Professor of Biology
Thesis Supervisor

Professor Anthony J. Sinskey
Professor of Microbiology

To my dearest mom, dad, and Jimmy

ACKNOWLEDGEMENTS

I would like to thank my parents for everything. Their unconditional love and support have and will always be a constant source of strength for me. I am grateful for all that they endured to give me a future. They are my inspiration for science and for life. Science can be at times all consuming. When I least expected it, Jimmy came into my life. He brought me warmth, joy, and comfort when I needed it the most. I will always cherish his kindness, patience, and most of all his love. For the rest of our lives, I will always love him and be there for him just as he has been there for me.

I am extremely grateful to my advisor, Prof. Stubbe. Beyond shaping my approach to science, she has had a profound impact on me as a person. She inspired me to pursue everything in life with dedication, passion, and tenacity. I have learned so much from her, and sometimes, just by simply watching her. I am grateful for all she has done for me. I thank her for guidance, and know that I am very fortunate and honored to have JoAnne as my advisor.

I am also fortunate to have Prof. Sinskey, one of the founding fathers of the PHB field, as my second advisor. Throughout my graduate career, he has given me advice, support, and motivation. It has been a pleasure to have subgroup with Tony and his PHB group. I would also like to thank Prof. Drennan, my thesis chair, for her advice, attentiveness, and support over the years.

Whenever I needed a helping hand, Dr. Jennie Ge was there. I am so lucky to have her as a dear friend. I will always cherish those memories with her in and outside the lab, and our late night restaurant runs. I was also lucky to have overlapped with Dr. Greg York on the PHB project in my first two years. I thank him for his patience, mentorship, and friendship. I would like to thank Dr. Ute Müh for her work on the Class III synthase and saturated trimer. I wish I had an opportunity to overlap with her. I thank Dr. Jimmy Jia for his work on characterizing the numerous synthase mutants, and Joe Kappock for generating the threading model of the Class III synthase. I would like to thank Dr. Wei Yuan for synthesizing the substrates or substrate analogues and leaving behind detailed procedures for their synthesis. All of their studies laid down the foundation to my thesis project.

I would like to thank Nicki Watson for training and helping me on TEM. She has been incredibly patient and generous, giving me support whenever 'disasters' strike. I thank Dr. Peter Mouton for his consultation on stereology and providing us with the probes. I also thank my dad who helped me tremendously in understanding the principles of unbiased stereology so that it could be applied to our system. I also would like to thank Jimmy and Jialin for helping me out on the stereology counting.

I especially would like to thank the entire Stubbe Lab, present and past members. I am thankful for all the help you have given me. I wish the best of luck to all of you. Last but not least, thanks to little Zymie who has brought me much joy.

Mechanistic Investigation of Polyhydroxybutyrate (PHB) Synthases and Elucidation of PHB Biosynthesis and Degradation Processes in *Wautersia eutropha* H16

By

Jiamin Tian

Submitted to the Department of Chemistry on 14 December 2004, in partial fulfillment of the requirements for the Degree of Doctor of Philosophy

ABSTRACT

Polyhydroxyalkanoate (PHA) synthase from various bacterial organisms is able to catalyze the polymerization of (*R*)-hydroxyalkanoate-CoAs into high molecular weight PHAs under nutrient-limited conditions in the presence of a carbon source. PHA synthases are representative of enzymes involved in polymerizations in which a soluble substrate is transformed into an insoluble inclusion during the polymerization process. The initiation, elongation, and termination phases of this non-template driven polymerization process are not well understood. This thesis is focused on the initiation and the elongation phases leading to granule formation. For the first time, we have observed intermediate species in the *in vitro* reaction containing a mutant Class III synthase, D302A-PhaCPhaE$_{Av}$, with its natural substrate (*R*)-3-hydroxybutyryl-CoA (HB-CoA). Analysis of reaction products by SDS-PAGE gel, Westerns with PHA and PhaCPhaE$_{Av}$ antibodies, and autoradiography showed different migratory properties of the mutant synthase after its reaction with substrate at various substrate to enzyme ratios (S/E). These results indicate that PhaC$_{Av}$ has been modified with hydroxybutyrate oligomers ((HB)$_n$). The site of labeling was established to be C149, by trypsin digestion of the (HB)$_n$ modified synthase (n=3~10 at S/E = 5), reverse-phase HPLC separation of peptides, and mass spectrometry analysis. Similar intermediates have also been detected with the wild-type (wt) PhaCPhaE$_{Av}$, and shown to be chemically competent. Thus, the mechanism of initiation of this synthase is through self-priming. Kinetic analysis of the reaction of HB-CoA with the wt synthase at S/E ratios of 70,000 was mechanistically informative. The Western blots using antibodies to PhaCPhaE$_{Av}$ revealed the disappearance of PhaC$_{Av}$ (migrating as a 40 KDa protein) at early time points and the reappearance of PhaC$_{Av}$ as the molecular weight of the polymer approached ~ 1 MDa. The results suggest that an inherent property of the synthase is chain termination and perhaps re-priming and re-initiation. The requirement of synthase to re-initiate *in vivo* has also been demonstrated by measuring the amount of PHB produced and the amount of synthase present inside the cell under defined growth conditions. Together, the *in vitro and in vivo* results strongly suggest that the synthase plays an important role in polymer chain termination, most likely through polymer chain transfer onto a second nucleophile that is solvent accessible. The chain can then be removed through hydrolysis, thus allowing the synthase to reinitiate new polymer synthesis.

We also report the kinetic studies of PHB granule initiation and growth in *W. eutropha* H16 studied with transmission electron microscopy (TEM). Analysis of the TEM images by the

method of unbiased stereology provided the estimated parameters of cell volume and granule surface area per cell as a function of time. Assuming the proteins identified to be involved in PHB homeostasis are globular and are granule bound, the values of cell and granule dimensions allowed the calculation of granule surface area coverage by these proteins, whose amounts in the cell at each time point were quantitated by Western analysis. The phasin protein (PhaP) was shown to cover up to 30% of the cell surface, while the others were less than 1%. Thus, additional compounds, such as lipids, are required to cover the remainder of the surface of granules. The TEM images at the early stages of PHB granule formation under nitrogen-limited conditions revealed dark-stained features near the center of the cells adjacent to the growing granules. These observations have led to a new model for granule formation involving some type of scaffolding. Information learned from the *in vitro* and *in vivo* studies presented in this thesis should help us in unraveling the mechanism of PHB synthases, and that of the granule formation and degradation processes.

Thesis Advisor: Professor JoAnne Stubbe
Title: Novartis Professor of Chemistry and Professor of Biology

Table of Contents

Acknowledgments 4

Abstract 5

Table of Contents 7

List of Schemes, Tables, and Figures 16

List of Abbreviations 24

Chapter 1 Polyhydroxyalkanoate (PHA) Homeostasis 26

1.1 Homopolymerization Reactions 27

1.2 Players in the PHA Biosynthetic Pathway 28

1.3 PHA Synthases 30

1.3.1 A structural model based on α/β hydrolase superfamily 31

1.3.2 Proposed mechanism for PHB formation 32

1.3.3 Properties of the Class I synthase 33

1.3.4 Insight into the initiation process of the Class I synthase using synthetic primers 36

1.3.5 Properties of the Class III synthase 40

1.3.6 Insight into the initiation and elongation process of the Class IIII synthase using synthetic primers 41

1.3.7 Mutagenesis studies used to probe residues involved in catalysis 42

1.3.8 Models for the conversion of primed synthase to granules 45

1.4 Other Players in PHB Homeostasis 48

1.4.1 The role of PhaP and PhaR in the elongation process in Wautersia eutropha 48

1.4.2 The role of the depolymerases 51

1.5 Summary and Overview 53

1.6 References 54

1.7 Tables and Figures 67

Chapter 2 Detection of Intermediates from the Polymerization Reaction Catalyzed by a D302A Mutant of Class III Polyhydroxyalkanoate (PHA) Synthase **84**

2.1 Abstract 85

2.2 Introduction 86

2.3 Materials and Methods 89

2.3.1 Materials 89

2.3.2 Over-expression and purification of D302A-PhaCPhaE$_{Av}$ 89

2.3.3 Incubation of D302A-PhaCPhaE$_{Av}$ with [^{14}C]-HB-CoA 90

2.3.4 Analysis of reaction products by SDS-PAGE: Coomassie staining and autoradiography 90

2.3.5 Extraction of radioactivity from SDS-PAGE gel 90

2.3.6 Kinetics of D302A-PhaCPhaE$_{Av}$ modification monitored by SDS-PAGE gel, Western blotting, and autoradiography 91

2.3.7 Stability of the covalently bound HB-oligomers/D302A-PhaCPhaE$_{Av}$ complex using dialysis 91

2.3.8 Isolation by HPLC of peptides from D302A-PhaCPhaE$_{Av}$ labeled with [^{14}C]-HB-oligomers 92

2.3.9 Analysis of peptides by Mass Spectrometry 93

2.3.10 Transmission electron microscopy (TEM) 93

2.4 Results 94

2.4.1 Evidence for covalent labeling of PhaC$_{Av}$ by [^{14}C]-HB-CoA 94

2.4.2 Kinetics of D302A-synthase monitored by Western blotting and autoradiography 96

2.4.3 Stability of (HB)$_n$-PhaC$_{Av}$ 97

2.4.4 Isolation of HB$_n$-bound PhaC$_{Av}$ peptide(s) 98

2.4.5 Characterization and identification of the radiolabeled peptide(s) 99

2.4.6 TEM of W. eutropha with its Class I synthase gene replaced with D302A-PhaCPhaE$_{Av}$ 101

2.5 Discussion 101

2.6 Acknowledgement 104

2.7 Reference 105

2.8 Tables and Figures 110

Chapter 3 Class III Polyhydroxyalkanoate Synthase: Involvement in Chain Termination and Re-initiation **121**

3.1 Abstract 122

3.2 Introduction 123

3.3 Materials and Methods 126

3.3.1 Materials 126

3.3.2 Purification of recombinant PHA synthases 127

3.3.3 Incubation of wt PhaCPhaE$_{Av}$, C149A-PhaCPhaE$_{Av}$, or PhaC$_{We}$ with (R)-HB-CoA or [^{14}C]-HB-CoA 127

3.3.4 Analysis of reaction products by SDS-PAGE: Coomassie staining, autoradiography, and Western blotting 127

3.3.5 Isolation of HPLC of peptides from wt PhaCPhaEAv incubated with 1 equivalent of [^{14}C]-HB-CoA followed by digestion with trypsin 128

3.4 Results 128

3.4.1 Evidence for covalent labeling of wt PhaCPhaE$_{Av}$ by [^{14}C]-HB-CoA 128

3.4.2 Chemical competence of species I 130

3.4.3 Time-dependence phenomenon 131

3.4.4 Removal of CoA can stop the time-dependence phenomenon 132

3.4.5 D302A-PhaCPhaE$_{Av}$ also prevents the time-dependence phenomenon 132

3.4.6 Chasing of radiolabeled species I with cold HB-CoA: species I is chemically competent 133

3.4.7 Reactivity of species I, II and III 134

3.4.8 Kinetics of the polymerization reaction catalyzed by wt PhaCPhaE$_{Av}$ monitored by anti-PhaCPhaE$_{Av}$ Western blot 136

3.4.9 Labeling of recombinant Class I synthase $PhaC_{We}$ 137
3.5 Discussion 138
3.6 Acknowledgement 145
3.7 Reference 145
3.8 Schemes and Figures 149

Chapter 4 Mechanistic Investigation of the Class I Synthase 161
4.1 Abstract 162
4.2 Introduction 163
4.3 Materials and Methods 165
4.3.1 Materials 165
4.3.2 Over-expression and purification of $(His)_6$-tagged W. eutropha synthase 165
4.3.3 Over-expression and purification of non-$(His)_6$-tagged W. eutropha synthase 166
4.3.4 Enzyme assay 167
4.3.5 Isolation of aggregate, dimer, and monomer fractions of the synthase 167
4.3.6 Kinetic studies of dimer-monomer interconversion at 0°C 168
4.3.7 Kinetic studies of dimer-monomer interconversion at 22°C 168
4.3.8 Growth of W. eutropha gene replacement strains 169
4.3.9 PHB quantitation 170
4.3.10 Purification of $(His)_6$-PhaC from its native host W. eutropha ($PhaC_{We\_N}$) using Ni-NTA column 170
4.3.11 *Purification of $(His)_6$-PhaC from W. eutropha using methyl-HIC column* 170
4.4 Results 171
4.4.1 Purification and characterization of recombinant W. eutropha PHB synthase with and without $(His)_6$ 171
4.4.2 Effect of fructose 172

4.4.3 Determination of K_D for D↔M and k_d for dissociation of dimer (D) to monomer (M) 173
4.4.4 Isolation and specific activity of synthase dimer and monomer 175
4.4.5 Growth of W. eutropha under different conditions and quantitation of their PHB content 178
4.4.6 Isolation of $(His)_6$-$PhaC_{We}$ from W. eutropha using Ni-NTA column 177
4.4.7 Isolation of $(His)_6$-$PhaC_{We}$ from W. eutropha using methyl-HIC column 177
4.5 Discussion 178
4.6 Reference 181
4.7 Figures 184

Chapter 5 Kinetic Studies of Polyhydroxybutyrate Granule Formation in *Wautersia eutropha* H16 by Transmission Electron Microscopy 196

5.1 Abstract 197
5.2 Introduction 198
5.3 Materials and Methods 200
5.3.1 Cultivation conditions 200
5.3.2 TEM reagents 201
5.3.3 Fixation 201
5.3.4 Dehydration 202
5.3.5 Embedding 203
5.3.6 Sectioning and scoping 203
5.3.7 TEM image data analysis: calculation of the average cell volume at 5 h of wt strain grown in PHB_P 203
5.3.8 Calculation of the area of cell profiles on 2-D images using unbiased stereology at given times 204
5.3.9 Calculation of the average volume of cells at each time point 205

using A_{CP} of the corresponding sample and V_{Csh}

5.3.10 Calculation of the total surface area of granules per cell (S_G) using unbiased stereology 207

5.3.11 Measurement of the size distribution of cell and granule profiles on 2-D images 208

5.4 Results 208

5.4.1 Transition of cells from nutrient-rich medium (TSB) to PHB_P 208

5.4.2 Kinetics of wt W. eutropha H16: unusual features accommodating small granules at early time points 209

5.4.3 Changes of the cell volume during PHB production and utilization 211

5.4.4 *Changes of the surface area of granules in wt W. eutropha H16 during PHB_P* 215

5.5 Discussion 217

5.6 Acknowledgements 219

5.7 Reference 220

5.8 Tables and Figures 225

Chapter 6 Analysis of Polyhydroxybutyrate Biosynthesis and Degradation in *Wautersia eutropha* H16 by Quantitative Westerns and Transmission Electron Microscopy **237**

6.1 Abstract 238

6.2 Introduction 239

6.3 Materials and Methods 241

6.3.1 Cultivation conditions 241

6.3.2 Cell counting 241

6.3.3 Preparation of cell samples cultivated in TSB medium for Western analysis 242

6.3.4 Solubilizing proteins from PHB granules generated under TSB growth conditions by SDS or using an extracellular PHB depolymerase 243

6.3.5 Extraction of PHB and M_W determination 244

6.3.6 Transmission electron microscopy 244

6.3.7 TEM data analysis 245

6.3.8 Determination of the average number of granules per cell at 4 and 24 h in TSB medium using stereology 245

6.4 Results 247

6.4.1 Choice of TSB medium to study granule formation 247

6.4.2 Determination of the average number of granules per cell at 4 and 24 h in TSB medium 248

6.4.3 Quantitative Western analysis 249

6.4.4 Analysis of proteins in wt W. eutropha H16 250

6.4.5 Relationship between PhaP and PHB 251

6.4.6 Time course of $PhaC_{We}$ 251

6.4.7 In vivo concentrations and molecules per cell of $PhaC_{We}$ and PhaP at 4 and 24 h in TSB medium 252

6.4.8 Protein coverage of granule surface area per cell at 4 and 24 h in TSB medium 253

6.4.9 Protein coverage of granule surface area per cell at 24 h in PHB_P 254

6.4.10 M_W of PHB at 4 h in TSB medium and 24 h in PHB_P allows determination of the $PhaC_{We}$/PHB and PhaP/PHB ratios: Evidence for re-initiation of PHB biosynthesis in vivo 257

6.4.11 Localization of granules observed in ΔphaR W. eutropha H16 strain 258

6.5 Discussion 259

6.6 Acknowledgement 263

6.7 Reference 264

6.8 Tables and Figures 268

Chapter 7 Additional Observations and Proposal for Future Experiments **280**

7.1 Introduction 281

7.2 Oligomeric state of the Class III Synthase 282

7.2.1 Introduction 282

7.2.2 Materials and methods 283

7.2.3 Results and discussion 285

7.3 The Role of $PhaE_{Av}$ 287

7.3.1 Introduction 287

7.3.2 Materials and methods 288

7.3.3 Results and discussion 289

7.4 Preliminary Studies of Mutant S90A Class III Synthase 290

7.4.1 Introduction 290

7.4.2 Materials and methods 290

7.4.3 Results and discussion 291

7.5 Probing the Function(s) of Other Conserved Amino Acid Residues of Class III Synthase by SDS-PAGE Gel and Autoradiography 295

7.6 Further Investigation of Class I Synthase 295

7.6.1 Introduction 295

7.6.2 Materials and methods 296

7.6.3 Results and discussion 297

7.7 Characterization of intracellular depolymerase deletion strains *in vivo* 299

7.7.1 Introduction 299

7.7.2 Materials and methods 300

7.7.3 Results and discussion 301

7.8 Studies of Dark-Stained Structures 302

7.9 Preliminary TEM Studies of Deletion Strains of *W. eutropha* 305

7.9.1 Introduction 305

7.9.2 ΔphaC W. eutropha H16 strain 306

7.9.3 ΔphaR W. eutrophaH16 strain 308

7.9.4 ΔphaP W. eutropha H16 strains 310

7.9.5 *$\Delta phaZ1_a$, $\Delta phaZ1_b$, $\Delta phaZ1_c$, and $\Delta phaZ1_{abc}$ W. eutropha H16 strains* 311

7.10 Cryoelectron Microscopy 312

7.11 Reference 317

7.12 Tables and Figures 323

List of Tables, Schemes, and Figures

Chapter 1

Table 1.1	List of the conserved amino acid residues in Class I, II, and III synthases.	67
Table 1.2	Specific activity *in vitro* and amounts of PHB *in vivo* of the synthase mutants.	68
Figure 1.1	PHAs generated by PHA synthases in bacteria.	69
Figure 1.2	Operon organization of the *W. eutropha* Class I and *A. vinosum* Class III PHA synthases, and the biosynthetic pathway for PHB production from acetyl-CoA.	70
Figure 1.3	TEM images of PHB granules accumulated in wt, Δ*phaP*, and PhaP over-expressing *W. eutropha* strains under nutrient-limited conditions.	71
Figure 1.4	Proteins required for PHA homeostasis and a cartoon of the proposed granule structure.	72
Figure 1.5	Interaction of a lipase with the surface of a TAG micelle, and Proposed mechanism of hydrolysis of a fatty acid from a TAG within the micelle by interfacial catalysis.	73
Figure 1.6	Cyclization catalyzed by the thioesterase domain of the surfactin synthase.	74
Figure 1.7	Current working models for PHB initiation and granule formation. The active site in this mechanism is formed at the interface of two monomers. Each cysteine is involved in covalent catalysis. Alternatively, X could be a thiol from a phosphopantetheine.	75
Figure 1.8	Current working models for PHB initiation and granule formation. In this mechanism, the active site contains a single cysteine and the polymerization involves covalent and non-covalent catalysis.	76
Figure 1.9	Hydroxybutyrate-CoA analogues used as putative primers of the polymerization process or chain terminators.	77
Figure 1.10	Threading model of *A. vinosum* synthase based on the crystallographic structure of *Pseudomonas* lipases showing conserved amino acids.	78

Figure 1.11	Proposed mechanism of hydrolysis of sT by the conserved D302 of the Class III synthase from *A. vinosum*.	79
Figure 1.12	Granule formation through micelle formation from hydroxybutyrate $(HB)_n$ chains covalently attached to PhaC.	80
Figure 1.13	Granule formation through budding from the inner leaflet of the plasma membrane.	81
Figure 1.14	TEM images revealing the kinetics of PHB granule formation and degradation in nutrient-rich, PHB production, and PHB utilization media.	82
Figure 1.15	Regulation of PhaP expression by PhaR. PhaR is a proposed repressor. De-repression requires active PhaC.	83

Chapter 2

Table 2.1	Radioactivity extracted from SDS-PAGE gel containing polymerization reactions catalyzed by D302A-PhaCPhaE$_{Av}$ with [^{14}C]-HB-CoA at indicated S/E ratios.	110
Table 2.2	N-terminal sequence of peptides purified from fractions indicated in Figure 2.4A (F5-F8).	111
Table 2.3	MALDI-TOF and ESI spectrum analysis: assignment of the peaks of interest.	112
Figure 2.1	SDS-PAGE gel (10%) monitoring the end products of the polymerization catalyzed by D302A-PhaCPhaE$_{Av}$ at various S/E ratios.	113
Figure 2.2	Kinetics of the polymerization reaction catalyzed by D302A-PhaCPhaE$_{Av}$ using [^{14}C]-HB-CoA at S/E of 100 monitored by Western blotting with Abs to PhaCPhaE$_{Av}$ and by autoradiography.	114
Figure 2.3	HPLC profile of peptides monitored at A_{214nm} resulting from trypsin digestion of D302A-PhaCPhaE$_{Av}$ produced by incubation of [^{14}C]-HB-CoA at a S/E ratio of 5.	115
Figure 2.4	Expanded elution profile of the HB-modified-peptides monitored at A_{214nm} and A_{280nm}.	116
Figure 2.5	MALDI-TOF Mass spectrum in the reflection mode of F7.	117

Figure 2.6	Candidate for the 50-mer and 52-mer peptide of PhaC proposed to be associated with HB oligomers.	118
Figure 2.7	ESI Mass spectra of F5.	119
Figure 2.8	TEM images of wt *W. eutropha* and *W. eutropha* with its synthase gene replaced with D302A-PhaCPhaE$_{Av}$.	120

Chapter 3

Scheme 3.1	Hydrolysis of covalently attached HB oligomer by D302 of PhaC$_{Av}$ at low S/E ratios.	149
Scheme 3.2	Regeneration of HB-CoA through transesterification by the synthase at low S/E ratios.	150
Scheme 3.3	A nucleophile of the synthase is proposed to catalyze the polymer chain transfer, resulting in primed synthase.	151
Figure 3.1	10% SDS-PAGE gel containing wt PhaCPhaE$_{Av}$ with [^{14}C]-HB-CoA at various S/E ratios analyzed by phosphorimaging.	152
Figure 3.2	Coomassie-stained SDS-PAGE gel shows disappearance of PhaC$_{Av}$ as the S/E ratio increases.	153
Figure 3.3	Western blot using PHB Abs showing the time-dependence associated with species I.	154
Figure 3.4	Time-dependence phenomenon observed with wt PhaCPhaE$_{Av}$ and [^{14}C]-HB-CoA.	155
Figure 3.5	Autoradiography demonstrating the elimination of the time-dependence phenomenon by removal of CoA or use of D302A-PhaCPhaE$_{Av}$.	156
Figure 3.6	Chasing radiolabeled species with cold HB-CoA	157
Figure 3.7	Autoradiography revealing the reactivity of species I, II, III, and IV.	158
Figure 3.8	Kinetics of wt PhaCPhaE$_{Av}$ monitored by Western blot using Abs to PhaCPhaE$_{Av}$ and by the release of CoA using DTNB.	159

Figure 3.9 Autoradiography of products from reactions containing recombinant $PhaC_{We}$ and [^{14}C]-HB-CoA at various S/E ratios. 160

Chapter 4

Figure 4.1 SDS-PAGE gel examining the over-expression and purification of recombinant $(His)_6$-$PhaC_{We}$. 184

Figure 4.2 Time course of CoA release from HB-CoA catalyzed by protein aggregate and synthase dimer + monomer. 185

Figure 4.3 Bio-Silect SEC250 size-exclusion chromatography analysis of recombinant synthase and fractions collected. 186

Figure 4.4 SEC chromatographs showing protein aggregate of recombinant $PhaC_{We}$, once separated from the synthase dimer and monomer, does not reform dimer or monomer. 187

Figure 4.5 Time course of CoA release from HB-CoA catalyzed by protein aggregate, synthase dimer, and synthase monomer. 188

Figure 4.6 Effect of fructose on the lag phase examined by the synthase assay 189

Figure 4.7 SEC chromatographs of two independent experiments demonstrating the reproducibility of the methods used: HPLC and manual collection of the dimer fraction 190

Figure 4.8 SEC chromatographs showing dimer↔monomer interconvation at 0°C. 191

Figure 4.9 SEC chromatographs showing dimer↔monomer interconvation at 22°C. The integrity of the synthase was also examined by SDS-PAGE gel. 192

Figure 4.10 Dissociation of synthase dimer to monomer at 22°C. 193

Figure 4.11 Purification of $(His)_6$-$PhaC_{We}$ from *W. eutropha* whose synthase gene was replaced with $(His)_6$-synthase. 194

Figure 4.12 Activity assay measuring the rate of CoA release by $PhaC_{We\_N}$. No lag-phase was observed. 195

Chapter 5

Table 5.1	Estimated average cell volume (V_C) and total surface area of granules per *W. eutropha* H16 cell (S_G) by the method of stereology are reported as a function of time and cultivation condition.	225
Table 5.2	Estimated average cell volume calculated using the average length of longest cell profiles (~ 4% of the total cell profiles measured, see histograms of Figure 5.4) at each time point.	226
Figure 5.1	Multipurpose testing system used for stereology analysis.	227
Figure 5.2	Derivation of the S_V equation.	228
Figure 5.3	TEM images of wt *W. eutropha* H16 grown in TSB medium for 24 h and in PHB_P for 2.5 h after 24 h in TSB medium.	229
Figure 5.4	TEM images of wt *W. eutropha* H16 during its growth in PHB_P and PHB_U.	230
Figure 5.5	TEM images of wt *W. eutropha* H16 at 2.5 h in PHB_P.	231
Figure 5.6	TEM images of wt *W. eutropha* H16 at 2.5, 5, 9, and 24 h in PHB_P.	232
Figure 5.7	TEM image of *W. eutropha* H16 with its synthase gene replaced with D302A-PhaCPhaE$_{Av}$ from *Allochromatium vinosum*, grown for 24 h in PHB_P.	233
Figure 5.8	TEM image of *W. eutropha* H16 at 73 h in PHB_P.	234
Figure 5.9	TEM image of *W. eutropha* H16 at 48 h in PHB_U.	235
Figure 5.10	TEM images of consecutive serial sections (**A→B→C**) of the sample at 5 h in PHB_P.	236

Chapter 6

Table 6.1	*In vivo* concentration of PhaC$_{We}$, PhaP, PhaR, and PhaZ1$_a$ in wt *W. eutropha* H16 at 4 and 24 h in TSB medium, assuming that all proteins were soluble. Number of molecules of each protein is also reported.	268

Table 6.2	Protein coverage of the granule surface at 4 h and 24 h time points in TSB medium.	269
Table 6.3	Protein coverage of granule surface area per cell at 24 h in PHB_P using S_G (Method 1)	270
Table 6.4	Protein coverage of granule surface area per mL of cell culture at 24 h in PHB_P using density of amorphous PHB (Method 2).	271
Figure 6.1	Disector probes used to quantitate the number of granules per cell using images of consecutive serial sections.	272
Figure 6.2	Profile of PHB accumulation by wt *W. eutropha* H16 in TSB medium, expression of PhaC and PhaP in wt *W. eutropha* in TSB medium, and Western blots of PhaC and PhaP in crude extract of wt *W. eutropha*.	273
Figure 6.3	TEM images of wt *W. eutropha* H16 grown in TSB medium for 4 h and 24 h.	274
Figure 6.4	TEM images of consecutive serial sections of wt *W. eutropha* H16 grown in TSB medium for 4 h.	275
Figure 6.5	Control experiment for Western analyses.	276
Figure 6.6	Expression of $PhaC_{We}$ and PhaP in wt *W. eutropha* H16 in PHB_P and PHB_U.	277
Figure 6.7	TEM images of wt *W. eutropha* H16 cells at 4 h and 24 h showing dark-stained structures.	278
Figure 6.8	TEM image of Δ*phaR W. eutropha* H16 grown in TSB medium for 4 h showing localization of small granules.	279

Chapter 7

Table 7.1	Summary of Light Scattering Data Analyzed by ASTRA Software.	323
Table 7.2	Outer and inner oligonucleotides used in the construction of truncated versions of $PhaE_{Av}$ gene.	324
Table 7.3	Summary of ESI-MS data of recombinant $(His)_6$-$PhaC_{We}$ and $PhaC_{We}$.	325

Figure 7.1	Analysis of wt PhaCPhaE$_{Av}$ by SEC coupled to multiangle light scattering instrument (MALS) and a refractive index detector (RI).	326
Figure 7.2	Analysis of W248A-PhaCPhaE$_{Av}$ by SEC coupled to MALS and RI.	327
Figure 7.3	Coomassie-stained gel showing purified two truncated versions of PhaCPhaE$_{Av}$.	328
Figure 7.4	Size-exclusion chromatography analysis of PhaCPhaE-A and PhaCPhaE-B.	329
Figure 7.5	Phosphorimage of reaction products from reactions containing S90A-PhaCPhaE$_{Av}$ and [^{14}C]-HB-CoA.	330
Figure 7.6	TEM of *W. eutropha* H16 with its synthase gene replaced with S90A-PhaCPhaE$_{Av}$.	331
Figure 7.7	ESI mass spectra of recombinant (His)$_6$-PhaC$_{We}$ and PhaC$_{We}$.	332
Figure 7.8	Western blot using PhaC$_{We}$ Abs detected two bands near the MW of PhaC$_{We}$ in crude extract of *W. eutropha*.	333
Figure 7.9	PHB production and utilization in TSB medium by intracellular depolymerase deletion strains.	334
Figure 7.10	PHB production in PHB$_P$ and PHB utilization in PHB$_U$ by intracellular depolymerase deletion strains.	335
Figure 7.11	TEM photograph of wt and Δ*phaC W. eutropha* H16 in TSB medium at 4 h.	336
Figure 7.12	TEM images of Δ*phaC W. eutropha* H16 strain grown in PHB$_P$ for 72 h and PHB$_U$ for 48 h.	337
Figure 7.13	TEM images of Δ*phaC W. eutropha* H16 strain grown in PHB$_P$ for 72 h (a blow up).	338
Figure 7.14	TEM image of Δ*phaR W. eutropha* H16 at 72 h in PHB$_P$.	339
Figure 7.15	TEM image of Δ*phaR W. eutropha* H16 strain at 72 h in PHB$_P$, in comparison to wt *W. eutropha* H16 at the same time point.	340
Figure 7.16	TEM image of Δ*phaR W. eutropha* H16 strain at 48 h in PHB$_U$, in comparison to wt *W. eutropha* H16 at the same time point.	341

Figure 7.17 TEM image of Δ*phaP W. eutropha* H16 strain grown in PHB_P for 72 h. 342

Figure 7.18 TEM images of Δ*phaZ1*$_a$, Δ*phaZ1*$_b$, and Δ*phaZ1*$_c$ *W. eutropha* H16 strains at 72 h in PHB_U. 343

Figure 7.19 TEM images of Δ*phaZ1*$_a$, Δ*phaZ1*$_b$, and Δ*phaZ1*$_c$ *W. eutropha* H16 strains at 48 h in PHB_U. 344

Figure 7.20 TEM images of Δ*phaZ1*$_{abc}$ *W. eutropha* H16 strain at 72 h in PHB_P and 48 h in PHB_U. 345

List of Abbreviations

Abs	antibodies
CoA	coenzyme A
D	protein fraction containing mostly dimeric synthase
dn/dc	change of refractive index/change of concentration
DTNB	5,5′-dithiobis-(2-nitrobenzoic acid)
ESI-MS	electrospray ionization mass spectrometry
HB	hydroxybutyrate
HB-CoA	(*R*)-3-hydroxybutyryl-CoA
HIC	hydrophobic interaction column
HV	hydroxyvalerate
Imid	imidazole
M	protein fraction containing mostly monomeric synthase
MALDI-TOF	matrix assisted laser desorption/ionization, time-of-flight mass spectrometry
NMR	nuclear magnetic resonance
IPTG	isopropyl-β-D-thiogalactopyranoside
k_d	rate constant for dissociation of D to M
K_D	equilibrium constant for D↔M
KPi	potassium phosphate
MALS	multiangle light scattering instrument
M_W	weight-average molar mass
PHA	polyhydroxyalkanoate
$PhaC_{We}$	Class I synthase from *Wautersia eutropha*
$PhaC_{We\_N}$	native Class I synthase purified from *Wautersia eutropha*
$PhaCPhaE_{Av}$	Class III synthase from *Allochromatium vinosum*; PhaC and PhaE coexpressed and copurified
PHB	polyhydroxybutyrate
PHB_P	PHB production medium
PHB_U	PHB utilization medium
RI	refractive index
SA	specific activity
SDS-PAGE	sodium dodecyl sulfate-polyacrylamide gel electrophoresis
S/E	substrate to enzyme ratio
SEC	size-exclusion chromatography
sT	a trimer of 3-hydroxybutyrate in which the terminal hydroxyl is replaced with a hydrogen
sT-CoA	saturated trimer-CoA
TAG	triacylglycerol
TEM	Transmission Electron Microscopy
TSB	tryptic soy broth-dextrose free, nutrient-rich medium
wt	wild-type

Stereology terms

a(p)	area per point
A_A	area fraction (ratio of area of cell profiles to area of reference space)
A_{CP}	area of cell profiles
A_{ref}	area of reference space that contains A_{CP}
CP	cell profiles, refer to the cross-sections of cells resulting from a cut
CE	coefficient of error or sampling error
I	number of granule surface – test-line intersections
N_{CP}	number of cell profiles in the reference space
P	number of points intersecting cell profiles
S_G	total surface area of granules in one cell
S_V	average volume of a cell
V_{CP}	volume of cell profiles
V_{ref}	volume of reference space
V_V	volume fraction (ratio of volume of cell profiles to volume of reference space)

CHAPTER 1

Polyhydroxyalkanoate (PHA) Homeostasis

Polyhydroxyalkanoates (PHAs) are biodegradable polymers synthesized by the PHA synthase(s) inside various microorganisms when they encounter nutrient-limited conditions. PHAs have properties of plastics ranging from brittle to pliable to elastic. Production of these polymers in an economically competitive fashion via bioengineering requires an understanding of the biosynthetic pathway and its regulation. This chapter provides the background information on the Class I and III PHA synthases and briefly summarizes the major conclusions presented in Chapter 2, 3 and 4 that have contributed to our current understanding of the mechanism of the synthase in initiation, elongation, and termination of the polymerization process. This chapter also provides an overview of the phase transition process in which soluble substrates (coenzyme A esters of β-hydroxyalkanoates) are polymerized into insoluble polymers and players other than the synthase that are involved in this process. Results presented in Chapter 5 and 6 that have contributed to our current understanding of the PHA biosynthesis and degradation in *Wautersia eutropha* are also briefly described.

1 .1 HOMO-POLYMERIZATION REACTIONS

Template based polymerization reactions involving amino acid and nucleotide building blocks to generate polypeptides and nucleic acids respectively have been studied in detail. Their mechanisms of initiation, elongation, termination, and regulation of polymer formation are moderately well understood. In contrast to these complex processes, the mechanisms of the simpler homo-polymerization reactions such as formation of glycogen or starch from UDP-glucose and ADP-glucose respectively (*1, 2*), poly-γ-glutamate formation from glutamate (*3*), rubber from isopentenyl pyrophosphate (*4, 5*), or polyoxoesters from 3-hydroxyalkanoate thioesters (*6-8*) have received less attention. These homo-polymerization reactions as with

template based polymerization reactions, utilize soluble substrates. However, during the polymerization process, the polymers generated undergo a phase transition to produce insoluble inclusions or granules. Their mechanisms of initiation, elongation, termination, and regulation of the phase transitions remain largely unexplored. Over the past 15 years, our lab has been focusing on one homo-polymerization process: the conversion of β-hydroxyalkanoate thioesters to polyoxoesters or polyhydroxyalkanoates (PHAs), more specifically the coenzyme A (CoA) ester of β-hydroxybutyrate (HB-CoA) to polyhydroxybutyrate (PHB) (Figure 1.1).

PHAs have been on the radar screens of those interested in biomaterials for over a decade as they have properties that range from thermoplastics (R = H, CH_3, C_2H_5) to elastomers (R = C_3H_7 – $C_{13}H_{27}$) (Figure 1.1) and they are biodegradable (*8*). The amount of plastic waste produced from oil based feed stocks, the desire to become independent of oil based products, and the environmental problems associated with biodegradation of these materials has fueled efforts to make more environmental friendly plastics in an economically competitive fashion (*9-13*). We are still a long way from these goals.

1.2 PLAYERS IN THE PHA BIOSYNTHETIC PATHWAY

Most of the genes involved in PHA biosynthesis reside within an operon, which includes a thiolase (*phaA*), a reductase (*phaB*), and the synthase (or polymerase, *phaC*) (Figure 1.2) (*14-18*). The thiolase and reductase generate the starting material HB-CoA and the synthase is thought to catalyze all the steps in the polymerization process. Thus far, no protein involved in initiation or priming of polymer formation has been identified. In addition, genes for an intracellular depolymerase(s) (*phaZ*) (*19*), a phasin protein (*phaP*) (*20*) and a regulatory protein (*phaR*) (*21-24*) are also often found adjacent to the biosynthetic genes and are involved in

controlling polymer homeostasis. Many excellent reviews have been published on the genetic organization of the genes involved in PHA biosynthesis (*6-8, 25*) and biotechnological advances to generate these materials in a useful and cost effective fashion (*9, 12, 26-28*). These reviews should be referred to for detailed information on these topics.

Our lab focuses specifically on the role of the synthase in the production of short chain PHAs (R = H, CH_3, and C_2H_5, Figure 1.1). PHBs are generated by many species of bacteria when they find themselves in a nutrient-limited environment and they have a readily available carbon source (a sugar or a fatty acid) that can be fashioned into HB-CoA (*28, 29*). This polymer is an excellent way to store energy and precursors to essential building blocks in times of nutrient limitation. Under these growth conditions, as revealed in Figure 1.3A, the entire inside to the bacterium fills with PHB polymer in its insoluble granule form. The sizes of the granules typically range from 0.2 to 0.5 microns (*6*). The granules from *Bacillus megaterium* are reported to contain PHB (97.7%), phospholipid (0.46%), and protein (0.47%) (*30*). The composition of granules from other sources has not yet been reported (*31*). When the bacteria find themselves in more growth accommodating environments, they sense the environmental change and use their intracellular PHA depolymerases to degrade these polymers to generate energy and 3-hydroxybutyrate (HB) (*25, 32*). Generation of these water insoluble granules so that they can be reused in an expeditious fashion plays an important role in the organism's survival. The proteins required for PHB production and re-utilization identified thus far and their putative functions are shown in Figure 1.4. The biochemistry and biology of each of these proteins with the focus on the synthase and the regulation of PHB production and utilization will be discussed.

1.3 PHA SYNTHASES

Two synthases have been purified to homogeneity and studied in some mechanistic detail: the Class I synthase from *Wautersia eutropha* (formerly known as *Ralstonia eutropha*) (*33-35*) and the Class III synthase from *Allochromatium vinosum* (*18, 36, 37*). Both of these proteins use HB-CoA as a substrate. A third PHA synthase that uses medium chain 3-hydroxyalkanoates as substrates (Class II synthase, R = $C_3H_7 - C_{14}H_{29}$, Figure 1.1) has also recently been purified (*38-40*). Its turnover number, however, is very low in comparison with the Class I and III synthases. Finally two recent reports of synthases from *B. megaterium* and *Bacillus sp.* INT005 suggest that a fourth class of synthase has been identified (*41, 42*). Mechanistic studies on the Class II synthase and this new class of proteins are still in a preliminary state and hence will not be discussed further.

Both the Class I and III synthases catalyze the same chemical transformation (Figure 1.2B), but as outlined subsequently have distinct protein structures and exhibit distinct kinetics *in vitro*. The working model for polyoxoester formation was originally based on our understanding of the fatty acid synthase, the observation that HB-CoA was the substrate, and that a cysteine of the synthase was required for activity (*30, 33, 43-46*). However, our recent studies have shown this model to be incorrect and that a mechanism similar to that reported for lipases provides a hypothesis more consistent with the present experimental data (*18, 28, 37*). Lipases use interfacial and covalent catalysis to hydrolyze a fatty acid from a triacylglycerol (TAG) by binding to the surface of a micelle made from the TAGs (Figure 1.5A). TAGs in plants are stored as granules covered by proteins called oleosins in a fashion similar to PHBs (*47*). Thus the use of a structurally homologous enzyme for PHB synthesis (see below) is intriguing. Hydrolysis with lipases requires a serine, histidine and possibly an aspartic acid (Figure 1.5B) for

catalysis (*48-50*). The role of the aspartate is open to debate based on mutagenesis experiments (*50-52*). All lipase catalyzed reactions involve a covalent acyl enzyme intermediate.

1.3.1 A structural model based on the α/β hydrolase superfamily

Sequence alignments of the synthases reveal that they are homologous to lipases (40 KDa monomers) and are members of the α/β hydrolase superfamily of proteins (*37*). All enzymes in this superfamily possess an active site nucleophile (cysteine, serine, or aspartate) that resides in a sharp elbow between a strand and a helix of the α/β structure (*53*). Recently, a structure of one of these superfamily members, the thioesterase (TE) domain of surfactin synthase, was reported (*54*). This protein possesses the catalytic apparatus required to form an acyl enzyme intermediate from an acyl-carrier protein (ACP)-linked peptide (Figure 1.6). Surfactin, a lactone, is generated from this acylated enzyme by cyclization with the hydroxyl group of a 3-*R*-hydroxyalkanoate (C13 to C15 fatty acid). This ester bond formation is remarkably similar to the reaction catalyzed by the PHB synthases (compare Figure 1.2B and 1.6). The TE domain of surfactin synthase possesses a long tunnel into its active site that allows delivery of a peptide attached as a thioester to the phosphopantetheine of ACP to the active site serine. The protein also possesses a tunnel for binding of the long chain fatty acid that may be analogous to the binding site for the extended chain of the polyoxoester generated by the PHB synthase. Most of the α/β hydrolase superfamily proteins are monomeric. Those that are dimeric possess independent active sites. At present, there is no superfamily member that possesses a single active site formed at the interface of the two monomers. Any mechanistic hypothesis for the PHB polymerization process must take these observations into account when using lipase as a model system.

1.3.2 Proposed mechanisms for PHB formation

Our original model for PHB formation was that the active site of the PHB synthase was formed at the interface of the two monomers with one cysteine from each monomer involved in covalent catalysis (Figure 1.7) (*33, 34, 36, 37, 55*). While many aspects of this model are still appealing, the structural constraints of positioning one cysteine from each monomer adjacent to each other and biochemical studies presented in Chapter 2, 3 and 4 have suggested that alternative models such as that shown in Figure 1.8 must also be considered. Both proposed mechanisms involve covalent catalysis by a cysteine/histidine pair and the general base catalysis of an aspartate to activate the 3-hydroxyl of a second HB-CoA for ester bond formation. The model in Figure 1.7 involves covalent catalysis with the second HB-CoA, while the model in Figure 1.8 involves non-covalent catalysis with the second HB-CoA. Precedent for each mechanism exists in the literature. The mechanism in Figure 1.7 requires two different covalent intermediates. Fatty acid synthases or more recently polyketide synthases use a cysteine and a phosphopantetheine thiol in covalent catalysis and serve as the paradigm (*43, 56, 57*). For precedence of the mechanism in Figure 1.8, chalcone synthase uses three malonyl-CoAs to form chalcone via a combination of non-covalent and covalent intermediates (*58*). In both mechanisms, the cysteine is activated for nucleophilic attack by a histidine in the active site. The hydroxyl group of the second HB-CoA, covalently or non-covalently bound, is then activated for nucleophilic attack to form a dimeric oxoester that is covalently or non-covalently bound to the synthase. In the latter case, this intermediate then becomes covalently attached to the cysteine in the active site, the CoA is removed and the process repeats itself. The growing chain of the polymer exits through a tunnel accommodating an oligomeric HB. The proposal in Figure 1.8

predicts that one would have covalently bound and non-covalently bound polymers of HB that could potentially be identified by rapid chemical quench experiments.

1.3.3 Properties of the Class I synthase

The Class I synthase from *W. eutropha* ($PhaC_{We}$, a paradigm for the Class I enzymes) has a subunit molecular weight of 64 KDa and can be over-expressed and isolated from a recombinant source with a specific activity (SA) of 40 U/mg ((*33, 59*), and Chapter 4). The protein under physiological conditions as isolated from recombinant sources is largely monomeric and can be induced to dimerize as described subsequently.

Several assays have been developed to examine the kinetic mechanism of the synthase reaction. The most reliable assay monitors the release of CoA (*36, 60*). However, CoA release can result from hydrolysis as well as ester bond formation and thus this assay can be problematic when examining substrate analogs with low activities. PHB production can also be monitored using [3-^{3}H]-HB-CoA by stopping the reaction and extracting the polymer into chloroform (*6, 33*). However, the ease of extraction of the polymer changes with its chain length and hence this is not an ideal assay either. The Class I synthase from *W. eutropha* exhibits unusual kinetics: a lag phase precedes a linear phase for CoA release (*33*). The basis(es) of this lag phase is not yet understood. Models involving rate determining priming or synthase dimerization have been considered as mechanistic options (*33, 34, 61*). Studies presented in Chapter 4, however, indicate otherwise. When protein fractions containing mostly monomeric or dimeric form of the synthase were assayed, their length of the lag phase was similar.

The inability to interpret kinetic results of $PhaC_{We}$ has required the use of additional methods to examine the initiation and elongation steps of the polymerization process (*33*). Early sucrose density centrifugation experiments examining product formation from reaction mixtures in which

the substrate (HB-CoA) to enzyme ratios (S/E) were varied from 1:1 to 10^3:1 suggested that the elongation rate for polymer formation of this recombinant synthase is much greater than the initiation rate. In the sucrose gradient, most of the protein remained unmodified with substrate at the top of the gradient and a small amount of the protein migrated with the PHB polymer as a large molecular weight aggregate (unpublished). Recent experiments (described in Chapter 3) in which products were generated under similar S/E ratios and examined by polyacrylamide gel electrophoresis support this model. Most of the protein migrated as monomer in the gel, whereas a small amount of protein complexed with all the PHB failed to enter the gel (Chapter 3). These studies revealed that at ratios of S/E of 10^3:1 or less, a very small amount of the protein contains a large molecule of polymer attached, while most of the protein has remained untouched by HB-CoA. This situation is unlikely to occur *in vivo* as it would be very difficult to control granule formation for polymer reuse. It would also be difficult to prevent aggregation of hydrophobic patches of proteins inside the cell with the hydrophobic polymer. The kinetics of this synthase has therefore limited our ability to study the mechanism of this enzyme due to the heterogeneity of the enzyme population. This heterogeneity has been under appreciated by those studying the Class I synthase (*61, 62*). The kinetics suggest that a component of the polymerase system is still missing.

To date, no polymerase has been purified from the host organism. Many early attempts to isolate the *W. eutropha* synthase resulted in low recoveries of inhomogeneous protein with low specific activity (*63*). Efforts to purify the recombinant *W. eutropha* synthase were also unsuccessful until it was discovered that the non-ionic detergent, hecameg, at a concentration well below its critical micelle concentration, prevented non-specific surface binding of the synthase to "everything" (*33*). The inability to purify the synthase from the host bacterium

suggests that it may be bound to some cellular constituent which has altered its solubility properties. The chameleon behavior of the synthase is not surprising as it spends most of its time bound to granules.

We have recently engineered *W. eutropha* to contain a gene for N-terminal $(His)_6$-tagged synthase in place of the wild-type (wt) synthase gene in an effort to isolate the protein from the host organism (G. York, unpublished). As noted above, the same $(His)_6$-tagged construct has been successfully used to isolate the synthase over-expressed in *Escherichia coli* (Chapter 4, (*59*)). Efforts to purify this tagged protein from *W. eutropha* under conditions in which PHB production was minimized have had limited success. The protein "sticks" to many resins used in chromatographic separations in a non-specific fashion in the presence or absence of hecameg. These results are reminiscent of our efforts to purify the recombinant protein from *E. coli* in the absence of hecameg. In contrast to the protein expressed in *E. coli*, the $(His)_6$-tagged synthase expressed in *W. eutropha* does not appear to have its tail accessible for binding to the Ni affinity column to facilitate purification. The $(His)_6$-tagged protein from *W. eutropha* has been purified to approximately 20-30% homogeneity in 1.4 % overall yield. Antibodies to the synthase and Western blots were used to determine the protein concentration that allowed determination of a SA of 180 U/mg. Recall that the SA of the recombinant protein is 40 U/mg. The kinetics of the release of CoA with this protein is also distinct from the same protein isolated from *E. coli*. There is no longer a lag phase, although the kinetics are still multi-phasic. These results support our proposal that the constitutively expressed protein is covalently modified in *W. eutropha*, perhaps residing in the host organism in the primed form. Alternatively the inhomogeneous purified protein could contain the missing factor(s) that facilitates the polymerization reaction. The details of this work have been presented in Chapter 4. The studies on the synthase isolated

from *W. eutropha* and *E. coli* clearly identify differences that need to be resolved. In addition, studies described subsequently on substrate specificity further suggest differences between the *in vitro* recombinant synthase and the polymer composition generated in the host organism *in vivo*. Taken together, it is clear that a basic piece to the puzzle is missing with the *W. eutropha* synthase.

1.3.4 Insight into the initiation process of the Class I synthase using synthetic primers

Lessons from enzymes catalyzing other homo-polymerization reactions (e.g., glycogen/glycogenin) suggest that a protein could potentially serve as a primer of the polymerization process (*64*). In the case of the *W. eutropha* synthase isolated from *E. coli*, the observed kinetic lag phase could be associated with the absence of the priming apparatus. Thus an effort was made to identify a priming protein using crude extracts from Δ*pha*C *W. eutropha* or *W. eutropha* containing an inactive PhaC (active site cysteine was changed to an alanine). These strains were grown under conditions known to produce PHB. The crude extracts from these growth conditions were then added into an assay mixture in an effort to eliminate the kinetic lag phase. The lag phase however, was unaffected (Tian, unpublished results).

The lack of success in identifying a protein primer caused us to focus on small molecule primers also observed to successfully prime a number of homo-polymerization processes (*65-67*). The mechanism of initiation has therefore been investigated using a series of oligomers of HB-CoA as potential primers (Figure 1.9). The results from experiments using these analogs have been mechanistically informative regardless of their relevance to the priming process *in vivo*. To study "priming", the Class I synthase was incubated with a large excess of dimer (**1**), trimer (**2**), tetramer (**3**) or saturated trimer (sT) (**4**) of HB-CoA (Figure 1.9). The synthase was then isolated by size exclusion chromatography and further incubated with HB-CoA.

Monitoring this reaction revealed a decrease in the lag phase for CoA release, an increase in the rate of CoA release relative to the synthase that had not been pre-incubated with a primer, and an increase in the dimeric form of the synthase (*55*). Studies further revealed that these oligomeric HB analogs covalently labeled the single conserved cysteine within the synthase and that the label was chemically stable. The stability of **4** attached to the synthase allowed isolation of a peptide containing the labeled primer and demonstrated it to be attached to C319 (Table 1.1). Size exclusion chromatography of synthase incubated with [^{3}H]-sT-CoA (**4**, Figure 1.9) showed that only the dimeric form of the synthase was labeled. Quantitation of the label covalently bound indicated a single chain of **4** per dimer of synthase (*34*). The chemical competence of this species was established as the label from **4** attached to the enzyme could be chased into PHB polymer upon addition of HB-CoA. These experiments established that C319 is involved in covalent catalysis. These studies were the basis for the hypothesis that the active form of the synthase is a dimer, and that the active site is at the interface of the two monomers (Figure 1.7).

Recent papers of Zhang *et al* have also suggested, based on studies with the natural substrate HB-CoA, that the active form of the *W. eutropha* synthase is the dimer and that this dimer supports a single PHB chain (*61, 68*). Two types of experiments were carried out that led them to this model. In one set of experiments, the synthase was placed into solutions of 70% fructose to foster dimeric synthase formation through macromolecular crowding. In our hands, assays in the presence of fructose give drastically reduced rates of polymer formation relative to assays in its absence (unpublished results described in Chapter 4), in contrast with their reported activities. The combination of their use of a poor assay, monitoring loss of the thioester of HB-CoA at 236 nm, and the slow rates, led them to the incorrect conclusion that the lag phase in the kinetic assay

had been removed and that the lag phase is associated with slow synthase dimerization to generate the active dimeric form of the enzyme.

In a second set of experiments, Zhang *et al* generated putative heterodimers of the synthase with one wt-monomer and one C319A monomer(*61*). The model in Figure 1.7 would predict this form of the synthase should be inactive. Furthermore, the model predicts that incubation of equal amounts of wt-homodimer and C319A-homodimer would result in 50% the activity of the wt-homodimer. However their failure to take into account the equilibration between the heterodimeric and homodimeric forms of the synthase, their inability to prime synthase in a homogeneous fashion, and their use of high concentrations of fructose to facilitate dimer formation, suggest that the conclusions from these studies used to support a single active site within dimer, need to be re-examined. The kinetic complexity associated with the *W. eutropha* enzyme needs to be resolved before an informative experiment can be executed.

We have sought unsuccessfully to obtain support for Figure 1.7 by attempting to trap the second covalent intermediate using potential chain terminators: 3-methoxy (**5**) and 3-fluoro (**6**) butyryl-CoA (Figure 1.9). Generation of $PhaC_{We}$ with one equivalent of [^{3}H]-sT-CoA (**4**) bound per dimer of the synthase followed by its incubation with either **5** or **6** failed to reveal any CoA release. Thus, these experiments failed to provide support for a second covalent intermediate (Y. Jia and W. Yuan, unpublished results).

A modified version of the mechanism in Figure 1.7, not requiring a single active site per dimer, but still involving two covalent intermediates has also been considered. This model is based on fatty acid synthase and more recently polyketide synthase mechanisms (*43, 57*). In this modified version of Figure 1.7, the second thiol involved in covalent catalysis is generated by post-translational modification of the synthase by CoA and a phosphopantetheinyl transferase

(*33, 69*). In an effort to detect this modification, an *E. coli* strain lacking the gene (*panD*) for making β-alanine, an essential precursor to CoA, was used. Δ*panD E. coli* is auxotrophic for β-alanine. Using this strain transformed with plasmids containing *phaC* from either the Class I or III synthase and grown on radiolabeled β-alanine, we observed radiolabel in both the Class I and III synthases (*33*). These results suggested that the synthases were post-translationally modified. In these early experiments, however, the extent of label incorporation was not quantified (*33*). Our more recent studies have shown that the level of incorporation was very low (at most 1% of the protein) suggesting this modification is not catalytically important (*59*). Genetic studies in *W. eutropha*, in which the gene that makes β-alanine was knocked out with a Tn5 insertion, also suggest that post-translational modification is not involved in creation of a second thiol that could be used by PHB synthase (*70*). Thus at present, there is no evidence for any mechanism involving two covalent thiol intermediates.

At this stage, the model of the active site at the interface of two monomers seems unlikely given the large amount of structural data now available on the α/β hydrolase superfamily and the biochemical experiments conducted to date. Thus an explanation for a single PHB chain per dimeric form of the synthase remains elusive. However, in the light of our recent *in vitro* (presented in Chapter 3) and *in vivo* (presented in Chapter 6) results demonstrating the need for the synthase to re-initiate during PHB granule synthesis, a new explanation proposed in Chapter 3 needs to be considered. Although the dimeric form of the synthase was found to be associated with a single PHB chain, one monomer could be responsible for polymer synthesis while the other carries out the steps necessary for the synthase to re-initiate.

1.3.5 Properties of the Class III synthase

The Class III synthase from *A. vinosum* (PhaCPhaE$_{Av}$, a paradigm for the Class III enzymes) is distinct from the Class I enzymes as it is composed of two subunits, PhaC and PhaE. This synthase does not require a non-ionic detergent such as hecameg for protein solubilization, and is chromatographically well behaved (*71*). Based on sequence homology, PhaC is the synthase. PhaE has no sequence homology to any known protein in the protein data base. The Class III synthase has only been isolated from a recombinant source as well. From *E. coli*, the protein is isolated as a 1:1 complex of PhaC$_{Av}$ and PhaE$_{Av}$. Each protein is approximately 40 KDa and the native form of the protein appears to be a tetramer (~ 320,000 Da, unpublished results described in Chapter 7). The genes for both PhaC and PhaE were constructed with a N-terminal $(His)_6$-tag which allowed each protein to be expressed and isolated in the absence of the second protein (*36*). Only PhaC$_{Av}$ was able to catalyze the release of CoA from HB-CoA and it did so at a rate of $1/10^3$ that of the wt-PhaCPhaE$_{Av}$. The PhaE protein had no detectable activity. Titration of the tagged-PhaC$_{Av}$ with tagged PhaE$_{Av}$ resulted in recovery of activity similar to that observed with a 1:1 complex of co-expressed PhaCPhaE$_{Av}$. The ratio of PhaE$_{Av}$ added to PhaC$_{Av}$ to achieve this activity, however, was 10:1. The tagged-PhaC$_{Av}$ was very unstable and prone to aggregation and precipitation, reminiscent of the behavior of the Class I synthase. The kinetics of the Class III synthase are distinct from the recombinant Class I synthase and in fact are similar to the native Class I enzyme isolated from *W. eutropha*. In this system, as outlined subsequently, the initiation rate appears to be greater than or comparable with the elongation rate and thus this synthase has been much more amenable to examination of its mechanism of polymerization (*36*).

1.3.6 Insight into the initiation and elongation process of the Class III synthase using synthetic primers

Similar studies with the small molecule primers (Figure 1.9) were also carried out with the Class III enzyme. The results were mechanistically more informative than those obtained from studies with the Class I enzyme. The results suggested that the enzyme was caught in the act of elongation through a covalent intermediate (*36*). The Class III enzyme was incubated with the [^{3}H]-sT-CoA (**4**). In contrast with the results from the Class I enzyme, however, the label covalently attached to the synthase was chemically labile, thus complicating analysis. In a serendipitous finding, the [^{3}H]-sT-CoA that was incubated with the enzyme contained a small amount of HB-CoA due to hydrolysis of **4** on storage. Because of the chemical lability of labeled synthase, the stoichiometry of labeling of the enzyme was monitored as CoA release. Approximately one equivalent of CoA per dimer of PhaCPhaE$_{Av}$, similar to the results with the Class I enzyme, was observed, despite the differences in the protein's quaternary structures. The synthase was covalently labeled in a ratio of ~0.2:1 (**4**:E(dimer)), instead of the 1:1 (**4**:E) observed with the Class I enzyme. The labeled protein was digested with trypsin and the peptides were separated by HPLC. Three [^{3}H]-sT labeled peptides in a ratio of 1:1:1 were identified and sequencing revealed that all three peptides were identical. MS/MS sequencing of each peptide revealed that one peptide contained the sT, the second contained a HB unit in addition to the sT, and the third contained two HBs attached to the sT. In all three cases, the conserved C149 of PhaC$_{Av}$ was the only residue in the peptide labeled. The enzyme had thus been caught in the act of elongation due to the fortuitous presence of small amounts of HB-CoA in **4**. More importantly, the results support a model of "uniform" loading of this Class III synthase with closely matched initiation and elongation rates (*36*). These studies have laid a

foundation to the studies presented in Chapter 2 and 3, in which the initiation and elongation steps of the PHB polymerization process catalyzed by PhaCPhaE$_{Av}$ were examined in more detail using a mutant (D302A) and wt-PhaCPhaE$_{Av}$ with their natural substrate HB-CoA. Intermediate species, that is PhaC$_{Av}$ with short HB oligomer bound, have been isolated and characterized. Their presence suggests that PhaCPhaE$_{Av}$ initiates polymerization through self-priming. Further investigation of these intermediate species provided evidence for additional roles of the synthase: the ability to control the polymer chain size by termination and the ability to re-initiate. The stoichiometry of sT to PhaCPhaE$_{Av}$ reveals that there is also one polymer chain per dimer of synthase in this system (*36*). While a structure of a synthase is required to resolve this conundrum, a possible role of the second synthase in chain termination as mentioned above should be considered.

1.3.7 Mutagenesis studies to probe residues involved in catalysis

A threading model for the Class III synthase and more recently the Class I synthase have been generated using structures of bacterial lipases (*37, 72*). Identification of 13 conserved amino acids by sequence alignment (Table 1.1) and mapping these residues onto the models have provided guidance for mutagenesis studies (Figure 1.10). A variety of these mutants in *W. eutropha* and *A. vinosum* synthases have been examined *in vitro* and *in vivo*. The *in vivo* experiments were possible as the wt gene for the synthase in *W. eutropha* has been replaced using homologous recombination methods by the mutant genes from *W. eutropha* (Table 1.2) and the wt and mutant synthase genes from *A. vinosum* (*73*). The ability of the wt and mutant synthases to make PHB in these engineered organisms has been examined. The results from the studies *in vivo* can be compared, with caution, to the turnover numbers for polymer formation of the mutant enzymes *in vitro*. Several mutants have thus far been mechanistically informative.

Their phenotypes are similar *in vitro* and *in vivo*. The data suggest that as with the lipases and the proposed mechanisms (Figure 1.7 and 1.8), a histidine (508 and 331 in the Class I and III synthases, respectively) is the general base catalyst that activates the active site cysteine to a thiolate to facilitate the formation of the acylated enzyme. We have not yet studied the aspartate corresponding to the one in the catalytic triad of the α/β hydrolases. Aspartate 350 in *W. eutropha* and 177 in *A. vinosum* would be the best candidates, based on the threading model. Aspartate 480 and 302 from the Class I and III enzymes, respectively, are proposed to be the general base catalyst that activate the 3'-OH for nucleophilic attack on the acylated enzyme (*34, 37*). The location of this residue in the threading model suggests that a conformational change would be required to function in this capacity. The proposed function for this residue in both Class I and III synthases is based on the observed interaction of sT-CoA (**4**) with the D to N mutant relative to the wt-enzyme. Both wt and mutant synthases are readily acylated by **4**, suggesting that this residue is not part of a catalytic triad proposed to be important in acylation of bacterial lipases. Subsequent to acylation with **4**, however, the thiol ester linkage of the mutant is much more stable than that of the corresponding wt-synthase. These results suggested that the D in the wt-enzyme activates water in the absence of HB-CoA and facilitates deacylation of the acylated enzyme (Figure 1.11). The asparagine mutant can no longer activate water and the acylated enzyme is more stable (*37*). This hypothesis has been confirmed by the studies presented in Chapter 2. We now understand much more about the role of the D302 residue in the Class III PhaCPhaE$_{Av}$ synthase.

The differences in the properties of the synthase isolated from host cells vs. a heterologous expression system suggested that it was important to compare the behavior of each mutant observed *in vitro* to its ability to make PHB *in vivo*. As expected, the C319A (C149A) and

H508A (H331A) mutants of the Class I and III synthases are unable to produce PHB *in vivo* in *W. eutropha* (Table 1.2). The phenotypes of several other conserved residues that have been examined thus far, however, are not as mechanistically transparent (Table 1.2). For example, the S260A (S90A) and W425F (W248F) mutants have low specific activity *in vitro* (Table 2). These mutants, however, make amounts of PHB *in vivo* comparable to those observed with the wt-synthase. Once the appropriate set of assays are established, a comparison of polymer made by the mutant proteins *in vitro* and in different engineered organisms should be mechanistically informative.

Differences in polymer production by mutant synthases *in vitro* vs. *in vivo* are also mirrored by differences in the results from substrate specificity studies *in vitro* and *in vivo*. *In vivo*, over 100 different monomers can be incorporated into polymers under different growth conditions (*29*). *In vitro* studies, on the other hand, suggest the proteins have much more stringent substrate specificity (*59, 68*). One example will be presented as a case in point. CoA release from 3-hydroxyhexanoyl-CoA *in vitro* occurs at 1/500 the rate of 3-HB-CoA in *W. eutropha* and 1/100 the rate in *A. vinosum*. *In vivo* however, in a Δ*phaA W. eutropha* strain, PHB containing 7% 3-hydroxyhexanoate has been reported (*74*). (Note: HB-CoA can still be generated by a second thiolase encoded by the *bktB* gene (*75*).) Under the growth conditions producing this polymer, however, only 2% of the dry cell weight was polymer and its molecular weight was 10^5 Da. In wt *W. eutropha,* 85% of the dry cell weight can be polymer with PHB molecular weights ranging from 1 to 5 x 10^6 Da. The mutant synthase studies and the substrate specificity studies thus suggest that the environment in which the polymer is generated *in vivo* is significantly different from the biochemical studies *in vitro*. Identifying the basis of the kinetic differences between synthase expressed in *W. eutropha* or *A. vinosum* and *E. coli* is important. Furthermore, how

other proteins involved in PHB homeostasis effect specificity and polymer molecular weight also requires additional analysis.

1.3.8 Models for the conversion of primed synthases to granules

Polymer formation from the primed synthase is complex as the homo-polymerization reaction starts with soluble substrate monomers and progresses to generate insoluble inclusions. The mechanism of the biogenesis, the structures of these inclusion bodies, and the mechanism by which they can be reused rapidly under defined conditions remains to be unraveled (*31*). Perhaps the best studied model systems for granule formation involve storage of energy as triacylglycerols or esterified sterols in lipid bodies (*76*). In plants, as much as 50% of the dry cell weight of seeds can be lipid bodies. Breakdown of the lipids by lipases provides the energy required for seed germination and post-germinative growth of the seedings. There are some striking parallels between these systems and PHB storage and re-utilization. The lipid bodies are composed largely of TAGs and the organelle is thought to be surrounded by one mono-layer of membrane (*47*). Structural proteins called oleosins are embedded in this monolayer. The biogenesis of the plant oil bodies is not understood in detail. However, one working model is that plant oil bodies bud off of the endoplasmic reticulum (ER) with one lipid leaflet and oleosins on the exterior bringing with it the TAGs which accumulate between the lipid leaflets of the ER (similar to that shown Figure 1.13). This model is similar to ones proposed for formation of very low density lipoproteins (VLDL) in liver (*76*) or lipid particles observed in yeast (*77*). The timing of oleosin production relative to TAG production and its role in orchestration of 'lipid body' formation is at present unresolved. The proposed function of the oleosins which have a central hydrophobic structure that interacts with the lipid oil bodies is to: (1) stabilize the TAG during seed desiccation and quiescence; (2) prevent fusion with adjacent oil bodies; and (3) act

as receptors for lipase binding to activate storage oil mobilization. Phasin proteins (PhaP) that are known to play an important role in PHB homeostasis have been proposed to be similar to the oleosins (Figure 1.4, Figure 1.12, Figure 1.13) (*20*). The role of PhaP will be discussed subsequently.

In the case of PHBs, several models for elongation need to be considered in the conversion of a soluble form of the primed synthase to the insoluble granule state. Each will be discussed in turn. A number of experimental observations must be accommodated within any model. Electron microscopy (EM) studies using antibodies to the synthase and phasin and uranyl-acetate staining suggest that both proteins are located only on the granule surface (*24, 71, 78*). This location has important mechanistic implications. One model for granule formation involves the aggregation of PHB-linked synthases to generate micelle like structures (Figure 1.12) (*33*). The distribution of sizes of the oligomeric HBs required to effect these structures has not been described. In this model, the synthases reside on the surface of the micelle structure, obtain the soluble substrate HB-CoA from the cytosol and contain the growing insoluble PHB chains within the micelle. No specific location of this synthesis is required. The phasin proteins, with their carefully regulated rate of production might serve, as with the oleosins, to prevent fusion of granules. Solid-state NMR methods have suggested that PHB within the granules is maintained in an amorphous state (*79, 80*). The phasins, therefore, might also prevent small molecules from nucleating crystallization of the PHB polymer within the growing granules. Crystallization might dramatically reduce the rate at which PHB can be utilized by the intracellular depolymerases. PhaP could also protect the cell from the hydrophobic surface of the growing PHB polymer that could lead to aggregation of cellular proteins and their unfolding.

A second model for granule formation, proposed by our lab, would be analogous to that proposed for lipid body biogenesis. In this model, the synthases would be peripheral membrane bound proteins, adhering to the inner face of the plasma membrane. Their association with the membrane could be facilitated by a primer molecule (a long chain fatty acid or oligomers of HB) covalently attached to the active site cysteine of the synthase (Figure 1.13). As the PHB chains extend and the PhaP phasin is produced, budding of a vesicle with a monolayer or partial monolayer of lipid could ensue, leading to granule formation (Figure 1.13). Again, PhaC and PhaP are expected to be on the exterior of the granule which is consistent with experimental results. Additional evidence supporting this model is the atypical membrane layer (3 – 20 nm in thickness) surrounding the granules often observed in several bacteria systems by EM (*81-83*). The amount of phospholipid associated with each granule, whether the granule is composed of a monolayer as shown in Figure 1.13 or more likely a combination of phospholipid and protein, still requires careful quantitation of the granule constituents. Calculation of the surface area of granules relative to the size of the bacteria suggests that a model with a lipid monolayer would require extensive phopholipid biosynthesis during granule formation (*31*). Thus, the PHB budding model predicts that granule biogenesis would occur close to the inner cell membrane of bacteria.

Recent kinetic transmission electron microscopy (TEM) studies described in Chapter 5 and 6 have suggested that a third model of granule formation should be considered. As revealed in Figure 1.14C, at early times when *W. eutropha* cells are placed in PHB production medium, very small, discrete granules appear to be localized to a dark-stained feature located in the center of the bacterium. With time, the granules increase in size and remain localized to the same features (Figure 1.14D, 1.14E). By 24 h (Figure 1.14F) the dark-stained feature, proposed to be a

putative scaffold for PHB nucleation, is no longer observed. The granule localization and putative scaffold is also apparent under other growth conditions and in other gene replacement strains of *W. eutropha*. The basis for this localization is presently unknown, but appears to be central to understanding granule formation. This information must be considered for any granule biogenesis model.

1.4 OTHER PLAYERS IN PHB HOMEOSTASIS

1.4.1 The role of PhaP and PhaR in the elongation process in Wautersia eutropha

PhaP, a 'phasin', was discovered by the Steinbuchel lab and proposed to play a role in PHB homeostasis (*20*). Phasin proteins are a component of the operon for PHB production of most PHB producing bacteria (Figure 1.2). The phasins are unusual in that in contrast to all the other proteins involved in PHB homeostasis, they are not conserved between organisms and come in many different sizes and sequences. No structures of phasin proteins have yet been reported. PhaP from *W. eutropha* is the best studied phasin. Studies with *W. eutropha* indicate that when mature granules are generated, the phasin PhaP can account for 3 to 5% of the total protein in the organism (*31*). While the function of this protein still remains unknown, a number of hypotheses for its function have been suggested as noted above. Further insight into PhaP's role(s) has been provided by genetic studies (*20, 31*). Steinbuchel's lab used Tn5 insertion mutagenesis to demonstrate that *W. eutropha* cells that express lower than normal amounts of PhaP can produce PHB, but that the PHB is present in one single large granule in the cell (Figure 1.3B). Over-expression of PhaP, on the other hand, results in formation of many small granules within the cell (Figure 1.3C). Thus PhaP, as noted above, prevents granule fusion. Gene deletion experiments of PhaP demonstrated that the amount of PHB under a defined set of growth

conditions was reduced 25-50% with respect to wt *W. eutropha* (*73*). Thus PhaP also affects the amount of PHB that the cell makes.

Further insight into the role of PhaP was provided by the discovery of a transcription factor PhaR in *Paracoccus denitrificans* that regulates production of PhaP (Figure 1.4) (*22*). PhaR in this organism interacts with up-stream regulatory sequences of both *phaP* and *phaR*. Using the *P. denitrificans* PhaR sequence and the BLAST algorithm, proteins homologous to PhaR were identified in *W. eutropha, A. vinosum*, and a number of additional PHB producing organisms. A common regulatory mechanism for PHB production thus appears to be operative. A number of *W. eutropha* deletion strains were constructed to examine the role of PhaR in PHB production (*23*). The model resulting from these studies and the studies of Maehara is shown in Figure 1.15. PhaR is proposed to be a repressor protein that binds to the upstream region of *phaP* in *W. eutropha*. Efforts to find consensus sequences for PhaR binding in the upstream regions of other *pha* genes within the PHB operon in *W. eutropha* have thus far not been successful. In the presence of PhaR, the production of PhaP is repressed. De-repression of PhaR requires the synthesis of PHB. In the Δ*phaR* strain, PhaP is constitutively expressed at high levels. If *phaC* is deleted, then no PhaP is produced; PhaR is proposed to remain bound to the DNA. Importantly, deletion of both *phaR* and *phaC* results in high levels of PhaP expression, even though the cells cannot produce PHB (*23*). Thus the presence of some product produced by the synthase has been suggested to function either directly or indirectly in the de-repression process through PhaR (Figure 1.15). Several groups have suggested that PHB granules or oligomers are responsible for the de-repression of PhaR and that PhaR subsequent to its dissociation from the DNA binds to the granule surface (*22-24*). The evidence that PhaR binds to the PHB granules is based on Western blots, using antibodies to PhaR and proteins that co-purify with the granules.

In vitro studies also revealed that *P. denitrificans* PhaR was able to cause a gel shift of a sequence of DNA to which it is proposed to bind and that this gel shift was reversed in the presence of PHB (*84*).

Genetic studies also demonstrated in *W. eutropha* that deletion of both *phaP* and *phaR* resulted in an even greater reduction in PHB production than deletion of either of the genes alone (*23*). These studies suggested that PhaR has a role or roles in addition to regulation of PhaP. *E. coli* strains have been engineered to contain *phaA*, *phaB*, *phaC* in the absence of *phaP* and/or *phaR*. Studies with these strains revealed that PhaR can regulate PhaP production in *E. coli* and that the uncontrolled production of PhaP extensively inhibited PHB production in the early stages of its biosynthesis.

Recently, detailed analyses of the concentration of proteins at various stages of PHB biosynthesis and degradation in *W. eutropha* have been carried out using quantitative Westerns (Chapter 6, (*85, 86*)). In addition, as described in Chapter 5 and 6, TEM images of *W. eutropha* cells at these stages were used to estimate the cell and granule dimensions by the method of unbiased stereology. Dynamic light scattering was also used to determine the molecular weight of a PHB polymer chain (*85*). Information from all these studies have allowed us for the first time to determined the relationship between the size of the granules, the molecular weight of the polymers within the granules, the number of synthases, the number of polymer chains per synthase, the number of phasin proteins covering the surface of granules, and the approximate *in vivo* concentration of all proteins involved in PHB biosynthesis and degradation. Chapter 6 presents these results in details. All of this information and how these numbers change as a function of time during granule assembly are essential for obtaining a realistic model for formation of inclusions.

1.4.2 The role of the depolymerases

To understand PHB homeostasis, one also needs to understand the mechanism of mobilization of the HB unit under appropriate metabolic conditions. Many investigators have studied the extracellular depolymerases, proteins that degrade PHB found in the environment released from dead bacteria (*87*). PHBs in this form serve as a source of nutrients. Several excellent reviews have recently summarized our knowledge of the depolymerases (*88, 89*). These extracellular depolymerases are of interest as they are the enzymes responsible for the biodegradability of the polymer and hence the development of the polymer as a biodegradable counterpart to polyethylenes and polypropylenes. These enzymes in general work on crystalline PHB and not on the amorphous PHB found in the granules *in vivo*.

The first intracellular depolymerase to be characterized genetically and *in vitro* is $PhaZ1_a$ (*19, 90*), formerly known as PhaZ1. The sequence of this protein showed no similarity to the sequence of the extracellular PHB depolymerases. Studies in wt and $\Delta phaZ1_a$ *W. eutropha* monitoring the rate of PHB utilization under different growth conditions, suggested that additional intracellular depolymerases are required to mobilize the PHB (*19, 91*). Recently, the availability of the complete genome of *Wautersia metallidurans* CH34 and the $phaZ1_a$ sequence from *W. eutropha* H16 allowed the design of degenerate primers that led to the identification of two additional putative intracellular depolymerase genes, $phaZ1_b$ and $phaZ1_c$ (formerly known as *phaZ2* and *phaZ3*), in *W. eutropha* H16 (*92*). Generation of a variety of *W. eutropha* deletion strains of these putative depolymerases ($\Delta phaZ1_{abc}$, $\Delta phaZ1_{ab}$, $\Delta phaZ1_{ac}$, $\Delta phaZ1_{bc}$, and each single deletion strain) and examination of their ability to use PHB under defined growth conditions suggested that $PhaZ1_b$ is also an intracellular depolymerase. No phenotype for $PhaZ1_c$, although it is 45% sequence homologous with $PhaZ1_a$ and 42%% sequence homologous

with PhaZ1$_b$, has yet been identified. Very recently, an intracellular oligomer hydrolase (designated as PhaZ2) has also been identified (*93*). In addition to degrading trimers of HB, this protein has also been shown to degrade amorphous PHB *in vitro* and *in vivo* under a defined set of growth conditions. The size of this oligomer hydrolase (78 KDa) and its sequence are completely different from PhaZ1$_a$, PhaZ1$_b$, and PhaZ1$_c$. Recently, our lab has also undertaken time-resolved mRNA profiling and Western analysis of these putative depolymerases (*85, 86, 94*). These results revealed that the expression pattern of these proteins varies from each other. While PhaZ1$_a$ is constitutively present under both nutrient-rich and limited conditions, PhaZ1$_b$ has only been detected upon exhaustion of nitrogen. PhaZ1$_c$ has not been observed under any growth conditions studied thus far, although its expression could have been missed if it is transient. The oligomer hydrolase, on the other hand, was found be to be expressed at a higher level during the PHB degradation phase. These results suggest that each of these putative depolymerases, with the exception of PhaZ1$_c$, has a specific function. Unfortunately, nothing is known about the regulation of expression of these depolymerases or their actual substrates. Thus far, no detailed mechanistic studies on the intracellular depolymerases have been reported. Understanding the function and regulation of these proteins is essential for understanding PHB homeostasis.

1.5 SUMMARY AND OVERVIEW

Homo-polymerization reactions are common in biology. Glucose can be converted to starch or cellulose in plants or glycogen in bacteria and humans. More complex polysaccharides such as heparin, keratin, chondroitin are generated from several sugar building blocks and are subsequently decorated (*95, 96*). These polymers can function as scaffolds playing important structural roles or as storage bins for energy. The genes have been identified and cloned for many of these proteins through sequencing projects. Expression efforts have revealed, however, that many of these proteins are membrane associated at some phase in their lifetime, making studies on polymer formation and utilization challenging (*95*). The mechanism(s) by which these polymers undergo phase transitions or can be rapidly mobilized from insoluble inclusions remain a mystery. PHB generation is one of the simpler polymerization processes. PHB formation and utilization thus may serve as a paradigm for understanding the mechanism of a controlled phase transition of a soluble substrate to an insoluble biopolymer of defined structure.

In general, mechanisms of initiation, elongation, and chain termination in most systems are not well understood. The function of the proteins involved in polymer homeostasis and how they modulate the phase transition and the flux of the monomeric building block away from central metabolism under different metabolic states are all problems that remain to be answered.

Understanding PHB homeostasis is essential for effective metabolic engineering. The regulation may have to be recapitulated in the heterologous expression systems to prevent toxicity to the host system in which the genes are being expressed (*26, 97*). Generation of new materials requires an understanding of specificity *in vivo* and the role of lipid and membranes. The control of the initiation and elongation rates and the control of concentrations of required substrates at various phases in the growth of the organism are essential to understand. Much has

been learned about the machinery required to make PHAs since the discovery of the polymerases in the late 1980s. The studies presented in the subsequent chapters have shed new light on the makings of PHB. The PHB synthase story reinforces the importance of the marriage between biochemistry and biology. The next decade will reveal new secrets about the complex biology that in turn may lead to new materials that can be generated in an economically competitive fashion.

1.6 REFERENCES

1. Smith, A.M. (2001) The biosynthesis of starch granules, *Biomacromolecules 2*, 335-341.
2. Shearer, J. and Graham, T.E. (2002) New perspectives on the storage and organization of muscle glycogen, *Can J Appl Physiol 27*, 179-203.
3. Ashiuchi, M. and Misono, H. (2002) Biochemistry and molecular genetics of poly-gamma-glutamate synthesis, *Appl Microbiol Biotechnol 59*, 9-14.
4. Archer, B.L. and Audley, B.G. (1967) Biosynthesis of rubber, *Adv Enzymol Relat Areas Mol Biol 29*, 221-257.
5. Cornish, K. (2001) Biochemistry of natural rubber, a vital raw material, emphasizing biosynthetic rate, molecular weight and compartmentalization, in evolutionarily divergent plant species, *Nat Prod Rep 18*, 182-189.
6. Anderson, A.J. and Dawes, E.A. (1990) Occurrence, Metabolism, Metabolic Role, and Industrial Uses of Bacterial Polyhydroxyalkanoates, *Microbiol. Rev. 54*, 450-472.
7. Lee, S.Y. (1996) Bacterial Polyhydroxyalkanoates, *Biotechnol. Bioeng. 49*, 1-14.

8. Steinbuchel, A. and Hein, S. (2001) Biochemical and molecular basis of microbial synthesis of polyhydroxyalkanoates in microorganisms, *Adv Biochem Eng Biotechnol 71*, 81-123.

9. Gerngross, T.U. (1999) Can biotechnology move us toward a sustainable society?, *Nat. Biotechnol. 17*, 541-544.

10. Page, W.J. (1995) Bacterial Polyhydroxyalkanoates, Natural Biodegradable Plastics with a Great Future, *Can. J. Microbiol. 41 (suppl. 1)*, 1-3.

11. Gross, R.A. and Kalra, B. (2002) Biodegradable polymers for the environment, *Science 297*, 803-807.

12. Snell, K.D. and Peoples, O.P. (2002) Polyhydroxyalkanoate polymers and their production in transgenic plants, *Metab Eng 4*, 29-40.

13. Slater, S., Mitsky, T.A., Houmiel, K.L., Hao, M., Reiser, S.E., Taylor, N.B., Tran, M., Valentin, H.E., Rodriguez, D.J., Stone, D.A., Padgette, S.R., Kishore, G., and Gruys, K.J. (1999) Metabolic engineering of *Arabidopsis* and *Brassica* for poly(3- hydroxybutyrate-co-3-hydroxyvalerate) copolymer production, *Nat. Biotechnol. 17*, 1011-1016.

14. Schubert, P., Steinbüchel, A., and Schlegel, H.G. (1988) Cloning of the *Alcaligenes eutrophus* genes for synthesis of poly-β-hydroxybutyric acid (PHB) and synthesis of PHB in *Escherichia coli*, *J. Bacteriol. 170*, 5837-5847.

15. Peoples, O.P. and Sinskey, A.J. (1989) Poly-β-hydroxybutyrate (PHB) biosynthesis in *Alcaligenes eutrophus* H16: Identification and characterization of the PHB polymerase gene (phbC), *J. Biol. Chem. 264*, 15298-15303.

16. Peoples, O.P. and Sinskey, A.J. (1989) Poly-β-hydroxybutyrate biosynthesis in *Alcaligenes eutrophus* H16: Characterization of the genes encoding β-ketothiolase and acetoacetyl-CoA reductase, *J. Biol. Chem. 264*, 15293-15297.

17. Slater, S.C., Voige, W.H., and Dennis, D.E. (1988) Cloning and Expression in *Escherichia coli* of the *Alcaligenes eutrophus* H16 Poly-β-Hydroxybutyrate Biosynthetic Pathway, *J. Bacteriol. 170*, 4431-4436.

18. Liebergesell, M. and Steinbüchel, A. (1992) Cloning and nucleotide sequences of genes relevant for biosynthesis of poly(3-hydroxybutyric acid) in *Chromatium vinosum* strain D, *Eur. J. Biochem. 209*, 135-150.

19. Saegusa, H., Shiraki, M., Kanai, C., and Saito, T. (2001) Cloning of an intracellular Poly[D(-)-3-Hydroxybutyrate] depolymerase gene from *Ralstonia eutropha* H16 and characterization of the gene product, *J Bacteriol 183*, 94-100.

20. Wieczorek, R., Pries, A., Steinbüchel, A., and Mayer, F. (1995) Analysis of a 24-kilodalton protein associated with the polyhydroxyalkanoic acid granules in *Alcaligenes eutrophus*, *J. Bacteriol. 177*, 2425-2435.

21. Maehara, A., Ueda, S., Nakano, H., and Yamane, T. (1999) Analyses of a polyhydroxyalkanoic acid granule-associated 16-kilodalton protein and its putative regulator in the *pha* locus *Paracoccus denitrificans*, *J. Bacteriol. 181*, 2914-2921.

22. Maehara, A., Doi, Y., Nishiyama, T., Takagi, Y., Ueda, S., Nakano, H., and Yamane, T. (2001) PhaR, a protein of unknown function conserved among short-chain-length polyhydroxyalkanoic acids producing bacteria, is a DNA-binding protein and represses *Paracoccus denitrificans* phaP expression in vitro, *FEMS Microbiol Lett 200*, 9-15.

23. York, G.M., Stubbe, J., and Sinskey, A.J. (2002) The *Ralstonia eutropha* PhaR protein couples synthesis of the PhaP phasin to the presence of polyhydroxybutyrate in cells and promotes polyhydroxybutyrate production, *J Bacteriol 184*, 59-66.

24. Potter, M., Madkour, M.H., Mayer, F., and Steinbuchel, A. (2002) Regulation of phasin expression and polyhydroxyalkanoate (PHA) granule formation in *Ralstonia eutropha* H16, *Microbiology 148*, 2413-2426.

25. Doi, Y., *Microbial Polyesters*. (1990) VCH Publishers, Inc., Weinheim.

26. Poirier, Y., Dennis, D.E., Klomparens, K., and Somerville, C. (1992) Polyhydroxybutyrate, a biodegradable thermoplastic produced in transgenic plants, *Science 256*, 520-522.

27. Marchessault, R.H. (1996) Tender Morsels for Bacteria: Recent Developments in Microbial Polyesters, *Trends Polym. Sci. 4*, 163-168.

28. Madison, L.L. and Huisman, G.W. (1999) Metabolic engineering of poly(3-hydroxyalkanoates): From DNA to plastic, *Microbiol. Mol. Biol. Rev. 63*, 21-53.

29. Rehm, B.H. and Steinbüchel, A. (1999) Biochemical and genetic analysis of PHA synthases and other proteins required for PHA synthesis, *Int. J. Biol. Macromol. 25*, 3-19.

30. Griebel, R., Smith, Z., and Merrick, J.M. (1968) Metabolism of poly-β-hydroxybutyrate. I. Purification, composition, and properties of native poly-β-hydroxybutyrate granules from *Bacillus megaterium*, *Biochemistry 7*, 3676-3681.

31. Steinbüchel, A., Aerts, K., Babel, W., Föllner, C., Liebergesell, M., Madkour, M.H., Mayer, F., Pieper-Fürst, U., Pries, A., Valentin, H., and Wieczorek, R. (1995) Considerations on the structure and biochemistry of bacterial polyhydroxyalkanoic acid inclusions, *Can. J. Microbiol. 41 (suppl. 1)*, 94-105.

32. Steinbüchel, A. (1991) *Polyhydroxyalkanoic Acids*, in *Biomaterials. Novel Materials and Biological Sources.* Macmillan Publishers Ltd., Basingstoke, U. K. p. 123-213.

33. Gerngross, T.U., Snell, K.D., Peoples, O.P., Sinskey, A.J., Cushai, E., Masamune, S., and Stubbe, J. (1994) Overexpression and purification of the soluble polyhydroxyalkanoate synthase from *Alcaligenes eutrophus*: Evidence for a required posttranslational modification for catalytic activity, *Biochemistry 33*, 9311-9320.

34. Jia, Y., Yuan, W., Wodzinska, J., Park, C., Sinskey, A.J., and Stubbe, J. (2001) Mechanistic studies of Class I polyhydroxybutyrate (PHB) synthase from *Ralstonia eutropha*: Class I and III synthases share a similar catalytic mechanism, *Biochemistry 40*, 1011-1019.

35. Song, J.J., Zhang, S., Lenz, R.W., and Goodwin, S. (2000) *In vitro* polymerization and copolymerization of 3-hydroxypropionyl-CoA with the PHB synthase from *Ralstonia eutropha*, *Biomacromolecules 1*, 433-439.

36. Müh, U., Sinskey, A.J., Kirby, D.P., Lane, W.S., and Stubbe, J. (1999) PHA synthase from *Chromatium vinosum*: Cysteine 149 is involved in covalent catalysis, *Biochemistry 38*, 826-837.

37. Jia, Y., Kappock, T.J., Frick, T., Sinskey, A.J., and Stubbe, J. (2000) Lipases provide a new mechanistic model for polyhydroxybutyrate (PHB) synthases: Characterization of the functional residues in *Chromatium vinosum* PHB synthase, *Biochemistry 39*, 3927-3936.

38. Qi, Q., Steinbüchel, A., and Rehm, B.H. (2000) *In vitro* synthesis of poly(3-hydroxydecanoate): purification and enzymatic characterization of type II

polyhydroxyalkanoate synthases PhaC1 and PhaC2 from *Pseudomonas aeruginosa*, *Appl. Microbiol. Biotechnol. 54*, 37-43.

39. Ren, Q., De Roo, G., Kessler, B., and Witholt, B. (2000) Recovery of active medium-chain-length-poly-3-hydroxyalkanoate polymerase from inactive inclusion bodies using ion-exchange resin, *Biochem J 349*, 599-604.

40. Rehm, B.H., Qi, Q., Beermann, B.B., Hinz, H.J., and Steinbuchel, A. (2001) Matrix-assisted in vitro refolding of *Pseudomonas aeruginosa* class II polyhydroxyalkanoate synthase from inclusion bodies produced in recombinant *Escherichia coli*, *Biochem J 358*, 263-268.

41. McCool, G.J. and Cannon, M.C. (2001) PhaC and PhaR are required for polyhydroxyalkanoic acid synthase activity in *Bacillus megaterium*, *J Bacteriol 183*, 4235-4243.

42. Satoh, Y., Minamoto, N., Tajima, K., and Munekata, M. (2002) Polyhydroxyalkanoate Synthase from *Bacillus* sp. INT005 Is Composed of PhaC and PhaR, *Journal of B ioscience and Bioengineering 94*, 343-350.

43. Smith, S. (1994) The animal fatty acid synthase: One gene, one polypeptide, seven enzymes, *FASEB J. 8*, 1248-1259.

44. Griebel, R.J. and Merrick, J.M. (1971) Metabolism of poly-b-hydroxybutyrate: Effect of mild alkaline extraction on native poly-b-hydroxybutyrate granules, *J. Bacteriol. 108*, 782-789.

45. Ballard, D.G., Holmes, P.A., and Senior, P.J. (1987) *Formation of polymers of β-hydroxybutyric acid in bacteria cells and a comparison of the morphology of growth with the formation of polyethylene in the solid state*, in *Recent Advances in Mechanistic and*

Synthetic Aspects of Polymerization. D. Reidel Publishing Company, Lancaster, U.K. p. 293-314.

46. Kawaguchi, Y. and Doi, Y. (1992) Kinetics and Mechanism of Synthesis and Degradation of Poly(3-Hydroxybutyrate) in *Alcaligenes eutrophus*, *Macromolecules 25*, 2324-2329.

47. Huang, A.H. (1996) Oleosins and oil bodies in seeds and other organs, *Plant Physiol 110*, 1055-1061.

48. Karlsson, M., Contreras, J.A., Hellman, U., Tornqvist, H., and Holm, C. (1997) cDNA cloning, tissue distribution, and identification of the catalytic triad of monoglyceride lipase. Evolutionary relationship to esterases, lysophospholipases, and haloperoxidases, *J. Biol. Chem. 272*, 27218-27223.

49. Brumlik, M.J. and Buckley, J.T. (1996) Identification of the catalytic triad of the lipase/acyltransferase from *Aeromonas hydrophila*, *J. Bacteriol. 178*, 2060-2064.

50. Frenken, L.G., Egmond, M.R., Batenburg, A.M., Bos, J.W., Visser, C., and Verrips, C.T. (1992) Cloning of the *Pseudomonas glumae* lipase gene and determination of the active site residues, *Appl. Environ. Microbiol. 58*, 3787-3791.

51. Kingma, R.L., Fragiathaki, M., Snijder, H.J., Dijkstra, B.W., Verheij, H.M., Dekker, N., and Egmond, M.R. (2000) Unusual Catalytic Triad of *Escherichia coli* Outer Membrane Phospholipase A, *Biochemistry 39*, 10017-10022.

52. Lang, D., Hofmann, B., Haalck, L., Hecht, H.J., Spener, F., Schmid, R.D., and Schomburg, D. (1996) Crystal structure of a bacterial lipase from *Chromobacterium viscosum* ATCC 6918 refined at 1.6 angstroms resolution, *J. Mol. Biol. 259*, 704-717.

53. Ollis, D.L., Cheah, E., Cygler, M., Dijkstra, B., Frolow, F., Franken, S.M., Harel, M., Remington, S.J., Silman, I., Schrag, J., Sussman, J.L., Verschueren, K.H.G., and Goldman, A. (1992) The alpha/beta hydrolase fold, *Protein Eng. 5*, 197-211.

54. Bruner, S.D., Weber, T., Kohli, R.M., Schwarzer, D., Marahiel, M.A., Walsh, C.T., and Stubbs, M.T. (2002) Structural basis for the cyclization of the lipopeptide antibiotic surfactin by the thioesterase domain SrfTE, *Structure (Camb) 10*, 301-310.

55. Wodzinska, J., Snell, K.D., Rhomberg, A., Sinskey, A.J., Biemann, K., and Stubbe, J. (1996) Polyhydroxybutyrate synthase: Evidence for covalent catalysis, *J. Am. Chem. Soc. 118*, 6319-6320.

56. Wakil, S.J. (1989) Fatty acid synthase, a proficient multifunctional enzyme, *Biochemistry 28*, 4523-4530.

57. Staunton, J. and Weissman, K.J. (2001) Polyketide biosynthesis: a millennium review, *Nat Prod Rep 18*, 380-416.

58. Austin, M.B. and Noel, J.P. (2003) The chalcone synthase superfamily of type III polyketide synthases, *Nat Prod Rep 20*, 79-110.

59. Yuan, W., Jia, Y., Tian, J., Snell, K.D., Muh, U., Sinskey, A.J., Lambalot, R.H., Walsh, C.T., and Stubbe, J. (2001) Class I and III polyhydroxyalkanoate synthases from *Ralstonia eutropha* and *Allochromatium vinosum*: characterization and substrate specificity studies, *Arch Biochem Biophys 394*, 87-98.

60. Valentin, E.H. and Steinbüchel, A. (1994) Application of enzymatically synthesized short-chain-length hydroxy fatty acid coenzyme A thioester for assay of polyhydroxyalkanoic acid synthases, *Appl. Microbiol. Biotechnol. 40*, 699-709.

61. Zhang, S., Kolvek, S., Lenz, R.W., and Goodwin, S. (2003) Mechanism of the polymerization reaction initiated and catalyzed by the polyhydroxybutyrate synthase of *Ralstonia eutropha*, *Biomacromolecules 4*, 504-509.

62. Nobes, G.A.R., Jurasek, L., Marchessault, R.H., Martin, D.P., Putaux, J.L., and Chanzy, H. (2000) Growth and kinetics of *in vitro* poly([*R*]-3-hydroxybutyrate) granules interpreted as particulate polymerization with coalescence, *Macromol. Rapid Commun. 21*, 77-84.

63. Haywood, G.W., Anderson, A.J., and Dawes, E.A. (1989) The Importance of PHB-Synthase Substrate Specificity in Polyhydroxyalkanoate Synthesis by *Alcaligenes eutrophus*, *FEMS Microbiol. Letts. 57*, 1-6.

64. Smythe, C. and Cohen, P. (1991) The discovery of glycogenen and the priming mechanism for glycogen biogenesis, *Eur. J. Biochem. 200*, 625-631.

65. Kornberg, A., Rao, N.N., and Ault-Riche, D. (1999) Inorganic polyphosphate: A molecule of many functions, *Annu. Rev. Biochem. 68*, 89-125.

66. Fritz, T.A., Gabb, M.M., Wei, G., and Esko, J.D. (1994) Two N-acetylglucosaminyl transferases catalyze the biosynthesis of heparan sulfate, *J. Biol. Chem. 269*, 28809-28814.

67. Mooibroek, H. and Cornish, K. (2000) Alternative sources of natural rubber, *Appl. Microbiol. Biotechnol. 53*, 355-365.

68. Zhang, S., Yasuo, T., Lenz, R.W., and Goodwin, S. (2000) Kinetic and mechanistic characterization of the polyhydroxybutyrate synthase from *Ralstonia eutropha*, *Biomacromolecules 1*, 244-251.

69. Walsh, C.T., Gehring, A.M., Weinreb, P.H., Quadri, L.E., and Flugel, R.S. (1997) Post-translational modification of polyketide and nonribosomal peptide synthases, *Curr. Opin. Chem. Biol. 1*, 309-315.

70. Hoppensack, A., Rehm, B.H., and Steinbüchel, A. (1999) Analysis of 4-phosphopantetheinylation of polyhydroxybutyrate synthase from *Ralstonia eutropha*: generation of beta-alanine auxotrophic Tn5 mutants and cloning of the *pan*D gene region, *J. Bacteriol. 181*, 1429-1435.

71. Liebergesell, M., Sonomoto, K., Madkour, M., Mayer, F., and Steinbuchel, A. (1994) Purification and characterization of the poly(hydroxyalkanoic acid) synthase from *Chromatium vinosum* and localization of the enzyme at the surface of poly(hydroxyalkanoic acid) granules, *Eur J Biochem 226*, 71-80.

72. Rehm, B.H., Antonio, R.V., Spiekermann, P., Amara, A.A., and Steinbuchel, A. (2002) Molecular characterization of the poly(3-hydroxybutyrate) (PHB) synthase from *Ralstonia eutropha*: in vitro evolution, site-specific mutagenesis and development of a PHB synthase protein model, *Biochim Biophys Acta 1594*, 178-190.

73. York, G.M., Junker, B.H., Stubbe, J.A., and Sinskey, A.J. (2001) Accumulation of the PhaP phasin of *Ralstonia eutropha* is dependent on production of polyhydroxybutyrate in cells, *J Bacteriol 183*, 4217-4226.

74. Dennis, D., McCoy, M., Stangl, A., Valentin, H.E., and Wu, Z. (1998) Formation of poly(3-hydroxybutyrate-co-3-hydroxyhexanoate) by PHA synthase from *Ralstonia eutropha*, *J. Biotechnol. 64*, 177-186.

75. Slater, S., Houmiel, K.L., Tran, M., Mitsky, T.A., Taylor, N.B., Padgette, S.R., and Gruys, K.J. (1998) Multiple beta-ketothiolases mediate poly(beta-hydroxyalkanoate) copolymer synthesis in *Ralstonia eutropha*, *J. Bacteriol. 180*, 1979-1987.

76. Murphy, D.J. and Vance, J. (1999) Mechanisms of lipid-body formation, *Trends Biochem Sci 24*, 109-115.

77. Sorger, D. and Daum, G. (2003) Triacylglycerol biosynthesis in yeast, *Appl Microbiol Biotechnol 61*, 289-99.

78. Gerngross, T.U., Reilly, P., Stubbe, J., Sinskey, A.J., and Peoples, O.P. (1993) Immunocytochemical analysis of poly-β-hydroxybutyrate (PHB) synthase in *Alcaligenes eutrophus* H16: Localization of the synthase enzyme at the surface of PHB granules, *J. Bacteriol. 175*, 5289-5293.

79. Barnard, G.N. and Sanders, J.K.M. (1989) The poly-β-hydroxybutyrate granule *in vivo*, *J. Biol. Chem. 264*, 3286-3291.

80. Horowitz, D.M. and Sanders, J.K.M. (1994) Amorphous, biomimetic granules of polyhydroxybutyrate: Preparation, characterization, and biological implications, *J. Am. Chem. Soc. 116*, 2695-2702.

81. Boatman, E.S. (1964) Observations on the Fine Structure of Spheroplasts of *Rhodospirillum Rubrum*, *J Cell Biol 20*, 297-311.

82. Lundgren, D.G., Alper, R., Schnaitman, C., and Marchessault, R.H. (1965) Characterization of Poly-Beta-Hydroxybutyrate Extracted from Different Bacteria, *J Bacteriol 89*, 245-251.

83. Jensen, T.E. and Sicko, L.M. (1971) Fine structure of poly-beta-hydroxybutyric acid granules in a blue-green alga, *Chlorogloea fritschii*, *J Bacteriol 106*, 683-686.

84. Maehara, A., Taguchi, S., Nishiyama, T., Yamane, T., and Doi, Y. (2002) A repressor protein, PhaR, regulates polyhydroxyalkanoate (PHA) synthesis via its direct interaction with PHA, *J Bacteriol 184*, 3992-4002.

85. Tian, J., He, A., Lawrence, A., Liu, P., Watson, N., Sinskey, A.J., and Stubbe, J. (2004) Analysis of Transient Polyhydroxybutyrate Production in *Wautersia eutropha* H16 by Quantitative Westerns and Transmission Electron Microscopy, *manuscript submitted for publication.*

86. He, A., Tian, J., Lawrence, A., Liu, P., Sinskey, A.J., and Stubbe, J. (2004) Expression Analysis of Proteins Involved in Polyhydroxybutyrate Homeostasis in *Wautersia eutropha* H16, *submitted for publication.*

87. Jendrossek, D. (1998) Microbial degradation of polyesters: a review on extracellular poly(hydroxyalkanoic acid) depolymerases, *Polym. Degrad. Stab. 59*, 317-325.

88. Jendrossek, D. (2001) Microbial degradation of polyesters, *Adv Biochem Eng Biotechnol 71*, 293-325.

89. Jendrossek, D. and Handrick, R. (2002) Microbial degradation of polyhydroxyalkanoates, *Annu Rev Microbiol 56*, 403-432.

90. Saito, T., Takizawa, K., and Saegusa, H. (1995) Intracellular poly(3-hydroxybutyrate) depolymerase in *Alcaligenes eutrophus*, *Can. J. Microbiol. 41 (suppl. 1)*, 187-191.

91. Handrick, R., Reinhardt, S., and Jendrossek, D. (2000) Mobilization of poly(3-hydroxybutyrate) in *Ralstonia eutropha*, *J Bacteriol 182*, 5916-5918.

92. York, G.M., Lupberger, J., Tian, J., Lawrence, A.G., Stubbe, J., and Sinskey, A.J. (2003) *Ralstonia eutropha* H16 Encodes Two and Possibly Three Intracellular Poly[D-(-)-3-Hydroxybutyrate] Depolymerase Genes, *J Bacteriol 185*, 3788-3794.

93. Kobayashi, T., Shiraki, M., Abe, T., Sugiyama, A., and Saito, T. (2003) Purification and Properties of an Intracellular 3-Hydroxybutyrate-Oligomer Hydrolase (PhaZ2) in *Ralstonia eutropha* H16 and Its Identification as a Novel Intracellular Poly(3-Hydroxybutyrate) Depolymerase, *J Bacteriol 185*, 3485-3490.

94. Lawrence, A.G., Schoenheit, J., He, A., Tian, J., Liu, P., Stubbe, J., and Sinskey, A.J. (2004) Time-resolved expression profiling of *Wautersia eutropha* genes related to poly-(*R*)-hydroxybutyrate homeostasis during bach fermentation, *manuscript submitted for publication.*

95. Sugahara, K. and Kitagawa, H. (2002) Heparin and heparan sulfate biosynthesis, *IUBMB Life 54*, 163-175.

96. Silbert, J.E. and Sugumaran, G. (2002) Biosynthesis of chondroitin/dermatan sulfate, *IUBMB Life 54*, 177-186.

97. Bohmert, K., Balbo, I., Steinbuchel, A., Tischendorf, G., and Willmitzer, L. (2002) Constitutive expression of the beta-ketothiolase gene in transgenic plants. A major obstacle for obtaining polyhydroxybutyrate-producing plants, *Plant Physiol 128*, 1282-1290.

1.7 TABLES AND FIGURES

Table 1.1 List of the conserved amino acid residues in Class I, II, and III synthases.

Class I (*W. eutropha*)	Class III (*A. vinosum*)
P239	P69
Y251	Y81
D254	D84
S260	S90
C319	C149
G322	G152
D350	D177
W425	W248
D428	D251
D480	D302
H481	H303
G507	G330
H508	H331

Table 1.2 Specific activity *in vitro* and amounts of PHB *in vivo* of the synthase mutants.

Class I (*W . eutropha*)	Specific Activity % of wt (*in vitro*)	Amounts of PHB % of wt (*in vivo*)	Class III (*A. vinosum*)	Specific Activity % of wt (*in vitro*)	Amounts of PHB % of wt (*in vivo*)
wild-type	100	100	wild-type	100	100
C319A	0	0	C149A	0	0
C319C	0	0	C149S	0.1	0.09
H508Q	0	0	H331Q	0.01	0.11
D480N	0.004	0.03	D302N	0.25	0.38
W425A	0.003	19	W248A	0.29	2
W425F	2	80	W248F	5	94
D254N	58	39	D84N	3	92
S260A	5	90	S90A	0.75	81

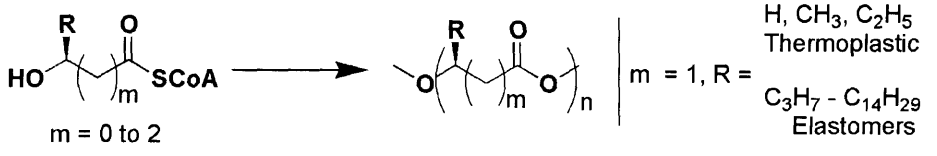

Figure 1.1 PHAs generated by PHA synthases in bacteria.

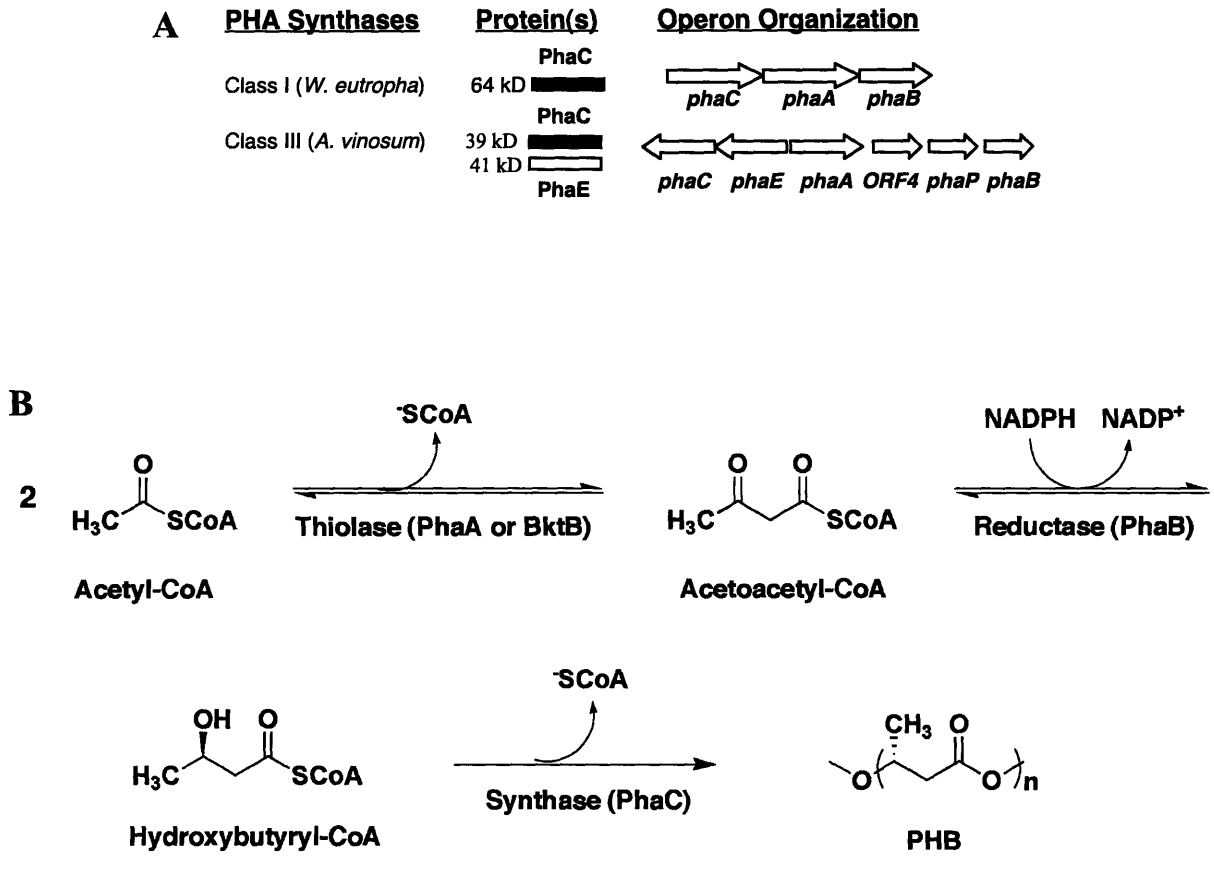

Figure 1.2 Operon organization of the *W. eutropha* Class I and *A. vinosum* Class III PHA synthases (**A**), and the biosynthetic pathway for PHB production from acetyl-CoA (**B**).

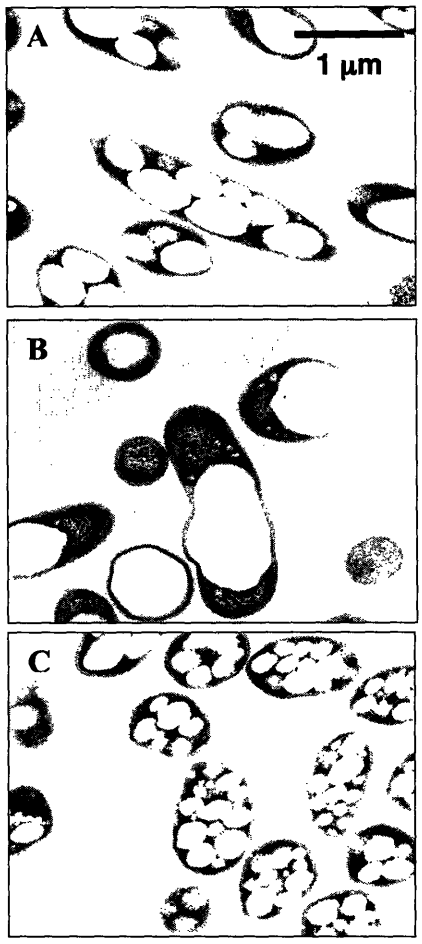

Figure 1.3 TEM images (by G. York) of PHB granules accumulated in *W. eutropha* strains under nutrient-limited conditions. (**A**) wild-type (**B**) Δ*phaP* and (**C**) PhaP over-expressed.

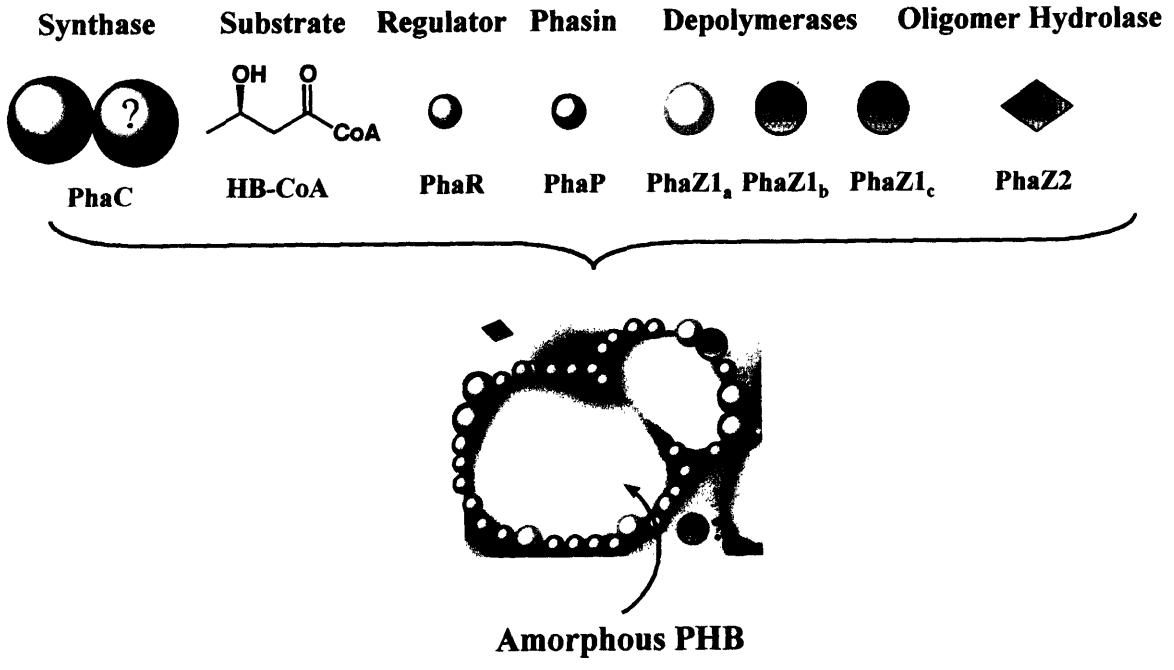

Figure 1.4 Proteins required for PHA homeostasis and a cartoon of the proposed granule structure.

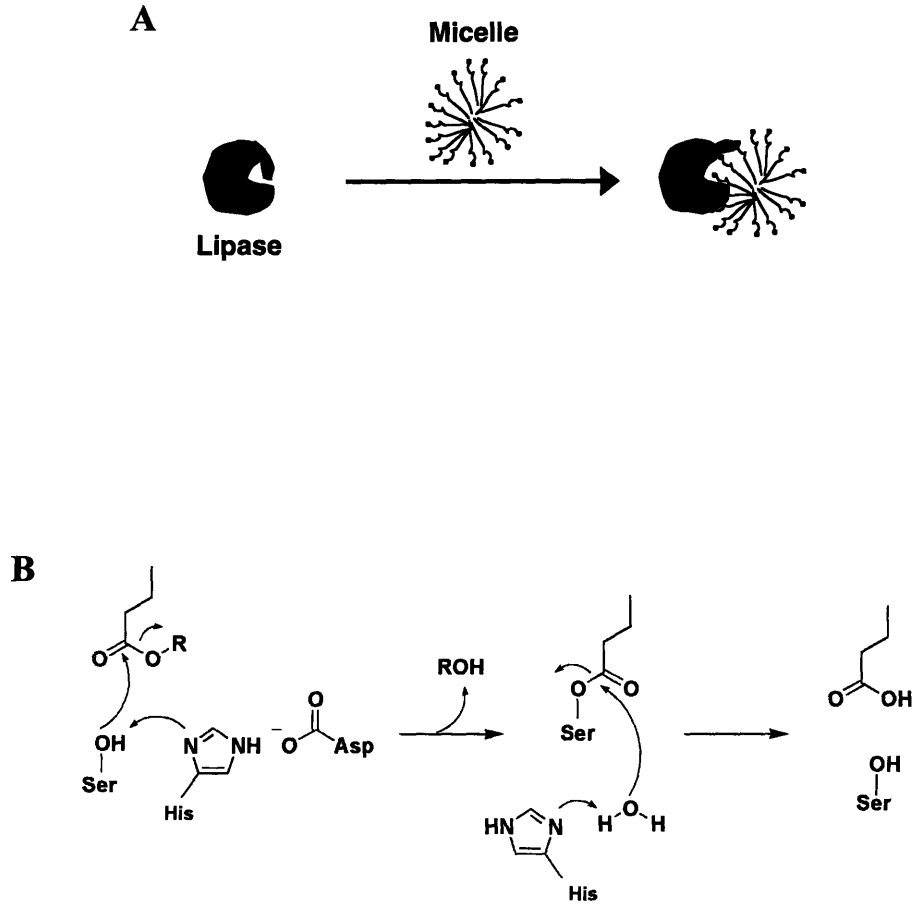

Figure 1.5 (**A**) Interaction of a lipase with the surface of a TAG micelle. (**B**) Proposed mechanism of hydrolysis of a fatty acid from a TAG within the micelle by interfacial catalysis.

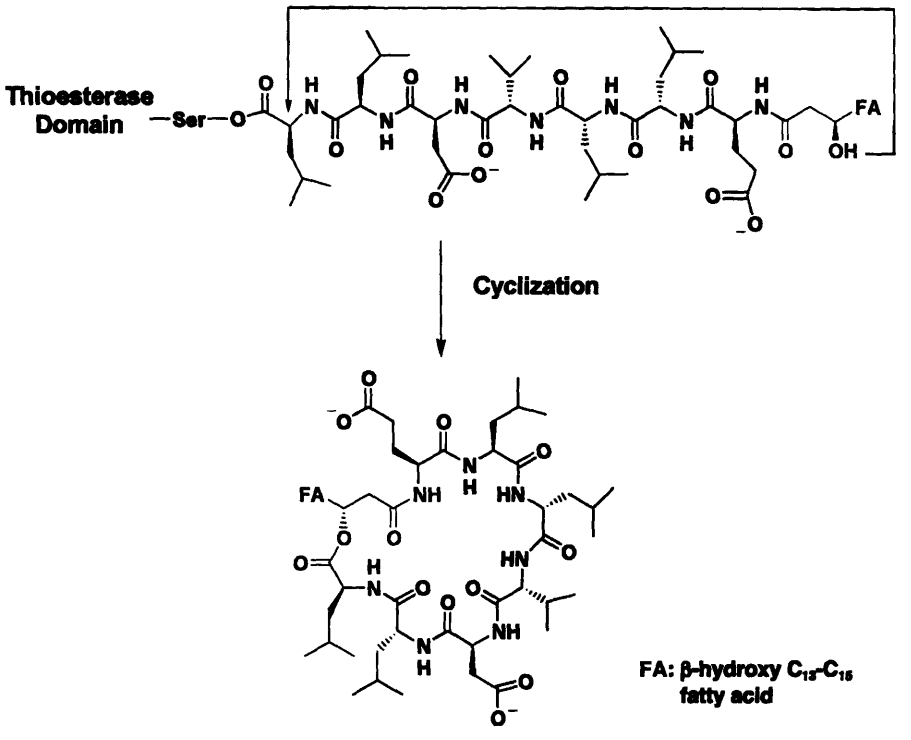

Figure 1.6 Cyclization catalyzed by the thioesterase domain of the surfactin synthase.

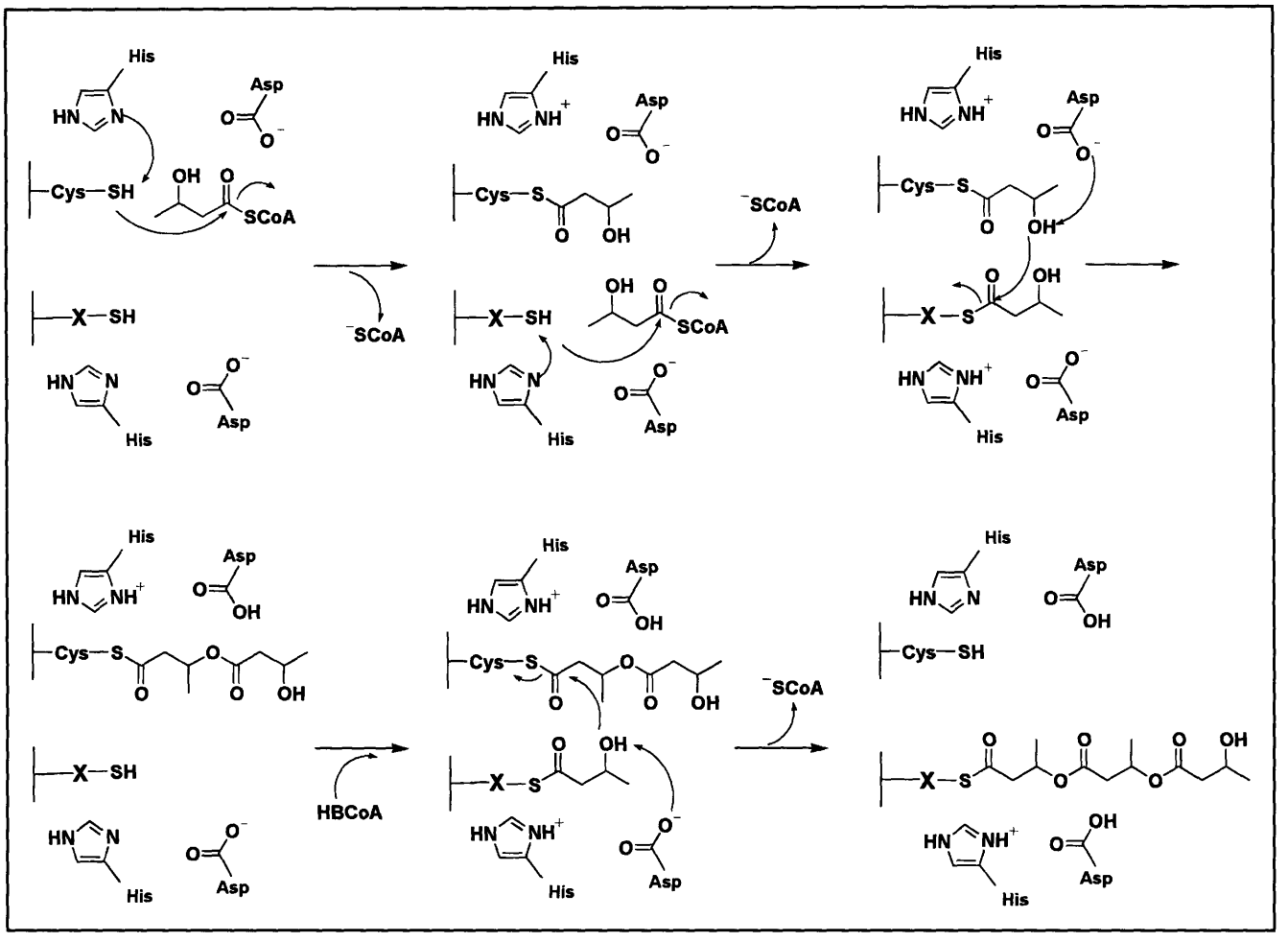

Figure 1.7 Current working models for PHB initiation and granule formation. The active site in this mechanism is formed at the interface of two monomers. Each cysteine is involved in covalent catalysis. Alternatively, X could be a thiol from a phosphopantetheine.

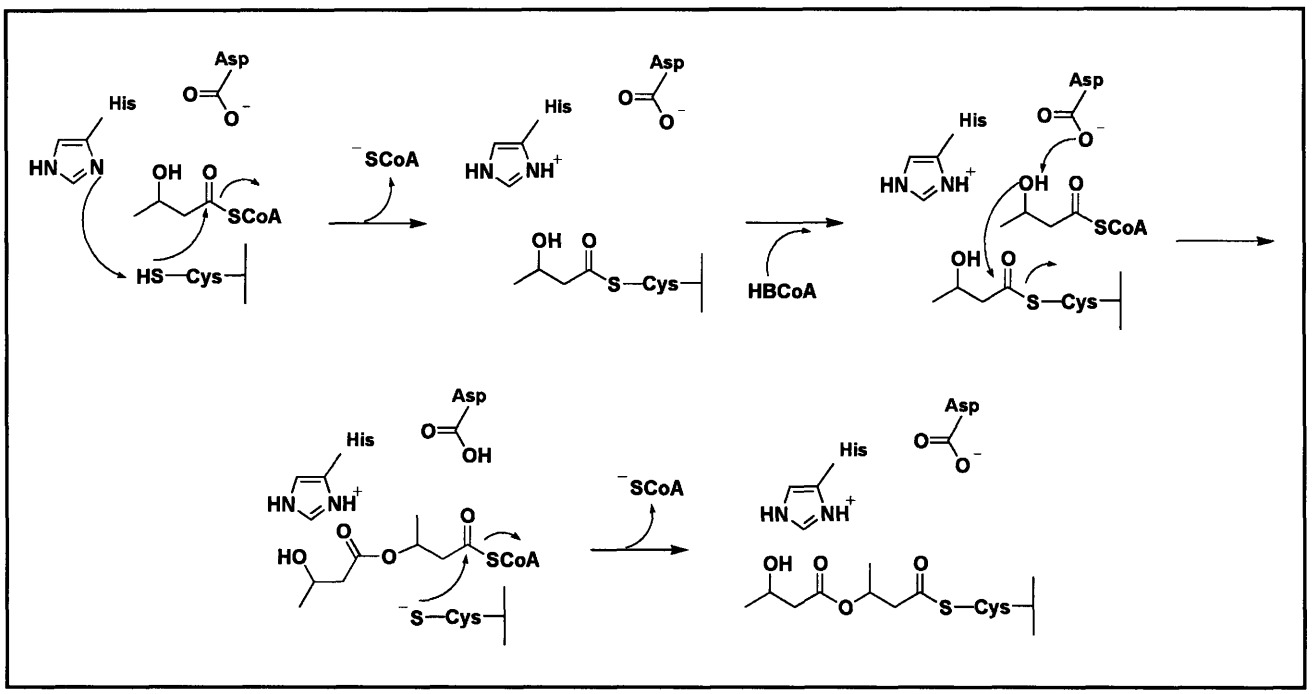

Figure 1.8 Current working models for PHB initiation and granule formation. In this mechanism, the active site contains a single cysteine and the polymerization involves covalent and non-covalent catalysis.

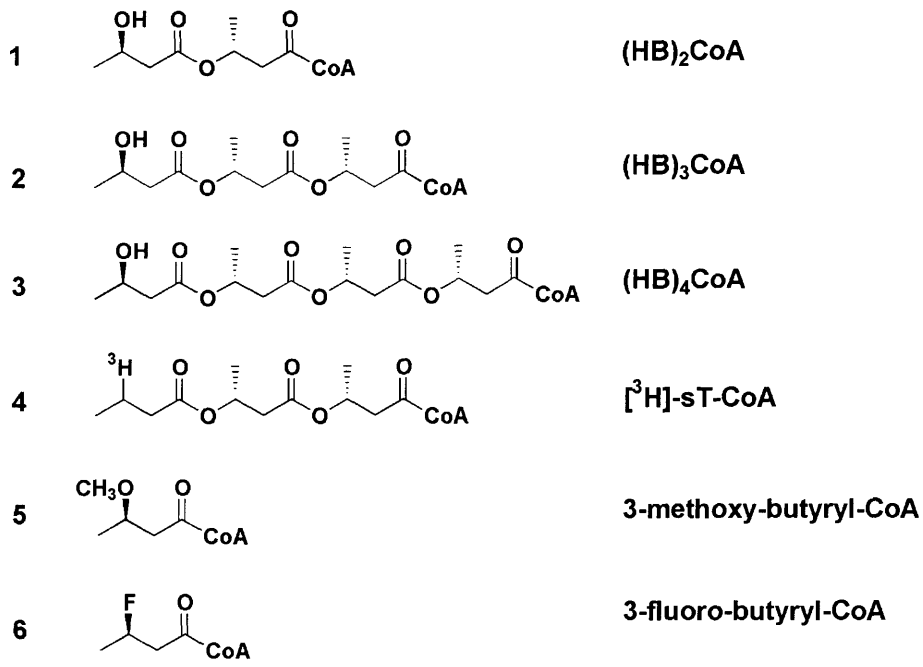

Figure 1.9 Hydroxybutyrate-CoA analogues used as putative primers of the polymerization process (**1-4**) or chain terminators (**5**, **6**).

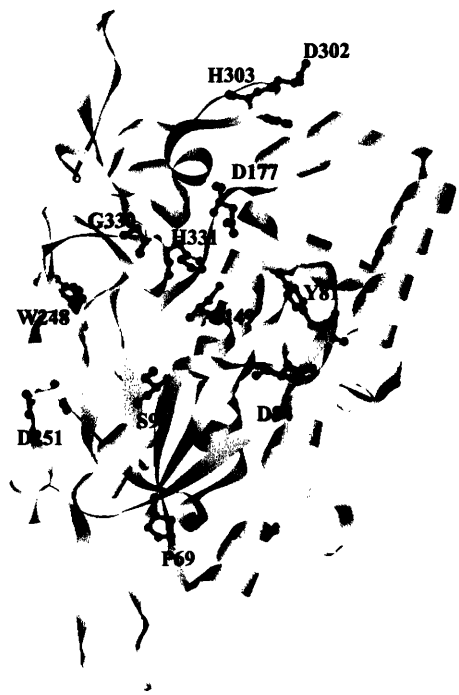

Figure 1.10 Threading model of *A. vinosum* synthase based on the crystallographic structure of *Pseudomonas* lipases showing conserved amino acids (Table 1.1). (Note: G152 is not shown.)

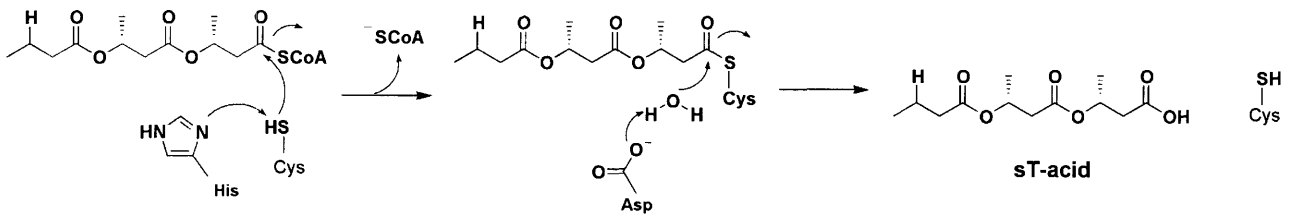

Figure 1.11 Proposed mechanism of hydrolysis of sT, **4** (Figure 1.9), by the conserved D302 of the Class III synthase from *A. vinosum*.

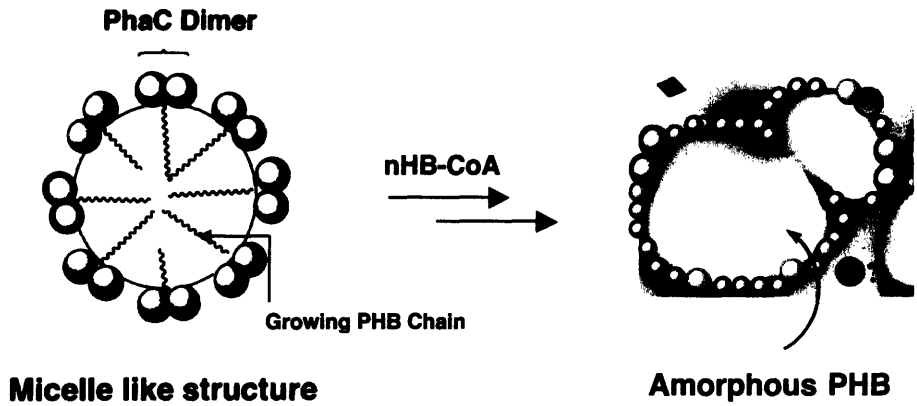

Figure 1.12 Granule formation through micelle formation from hydroxybutyrate $(HB)_n$ chains covalently attached to PhaC. Colored spheres shown on amorphous PHB represent proteins that have been shown to or are proposed to associate with the granule surface. Gray, PhaC; blue, PhaP; red, PhaR; green, $PhaZ1_a$; purple, $PhaZ1_b$; orange, $PhaZ1_c$; brown diamond, oligomer hydrolase.

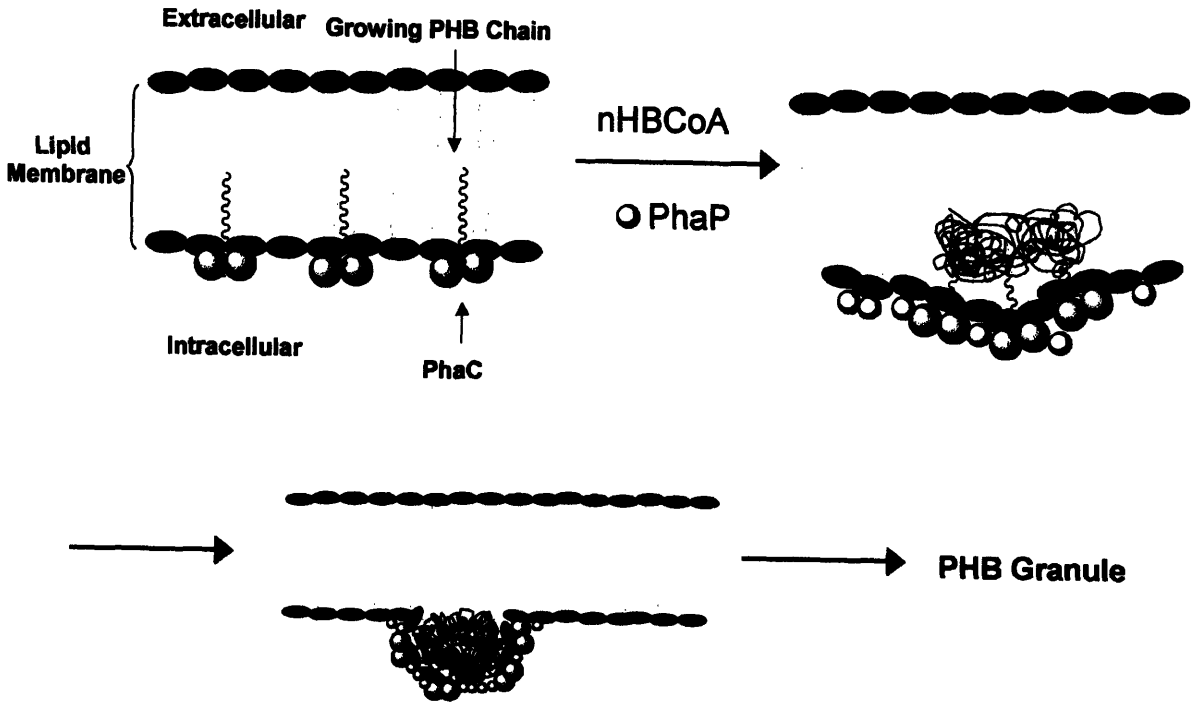

Figure 1.13 Granule formation through budding from the inner leaflet of the plasma membrane.

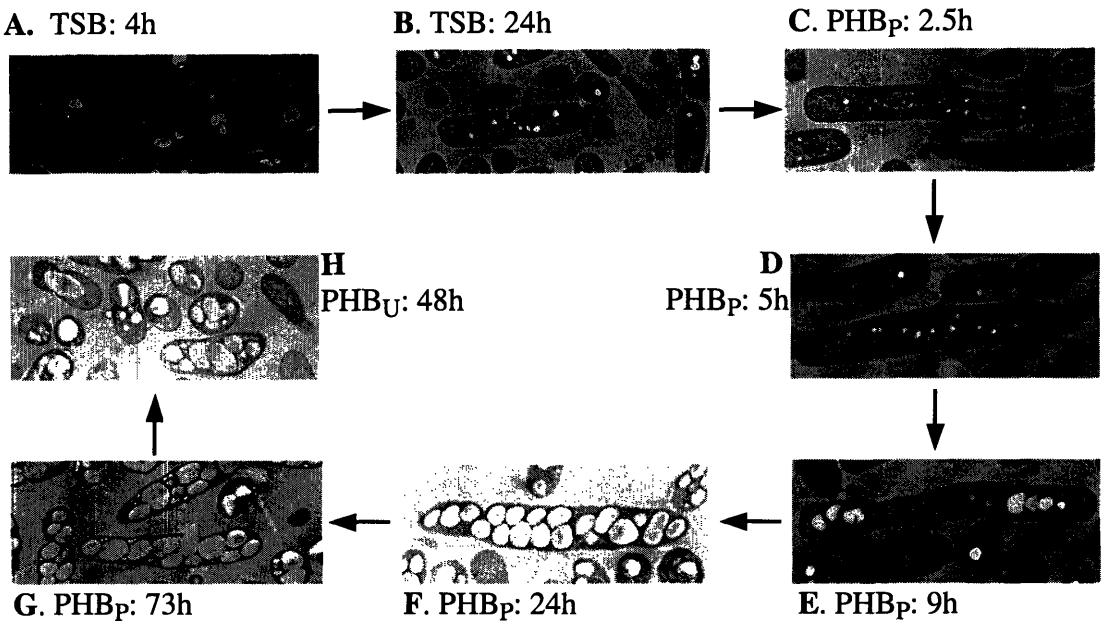

Figure 1.14 TEM images revealing the kinetics of PHB granule formation and degradation in nutrient-rich medium at 4 h (**A**) and 24 (**B**), in PHB production medium at 2.5 h (**C**), 5 h (**D**), 9 h (**E**), 24 h (**F**), and 73 h (**G**), and in PHB utilization medium at 48 h (**H**). All images are at the same magnification.

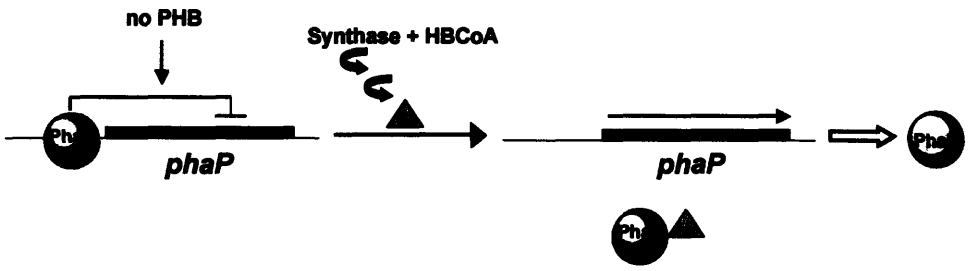

Figure 1.15 Regulation of PhaP expression by PhaR. PhaR is a proposed repressor. De-repression requires active PhaC.

CHAPTER 2

Detection of Intermediates from the Polymerization Reaction Catalyzed by a D302A Mutant of Class III Polyhydroxyalkanoate (PHA) Synthase

2.1 ABSTRACT

Polyhydroxybutyrate (PHB) synthases catalyze the polymerization of (*R*)-3-hydroxybutyryl-CoA (HB-CoA) into high molecular weight PHB, biodegradable polymers. The Class III PHB synthase from *Allochromatium vinosum* is composed of a 1:1 mixture of two ~40 KDa proteins: $PhaC_{Av}$ and $PhaE_{Av}$. Previous studies using site-directed mutagenesis and a saturated trimer of hydroxybutyryl-CoA have suggested the importance of C149 (in covalent catalysis), H331 (in activation of C149), and D302 (in hydroxyl group activation for ester bond formation) in the polymerization process. All three residues are located on $PhaC_{Av}$. We now report that incubation of D302A-PhaCPhaE with [^{14}C]-HB-CoA results in detection, for the first time, of oligomeric HBs covalently bound to $PhaC_{Av}$. The reaction products have been analyzed by SDS-PAGE, Westerns with $PhaCPhaE_{Av}$ antibodies, and autoradiography. Different migratory properties of D302A-$PhaC_{Av}$ on SDS-PAGE have been observed at [^{14}C]-HB-CoA to enzyme (S/E) ratios between 5 and 100. Trypsin digestion and HPLC analysis of the D302A-$PhaCPhaE_{Av}$ (from a reaction with S/E of 5) allowed isolation of multiple radiolabeled peptides. N-terminal sequencing, MALDI-TOF, and ESI mass spectrometric analysis of these peptides revealed that all the peptides were identical, but were modified by $(HB)_n$ ranging in size from n = 3 to 10. The *in vitro* results support the role of D302 in elongation rather then in activating the active site cysteine for acylation. This proposal has been further supported by our *in vivo* studies on a *Wautersia eutropha* strain in which the Class I synthase gene has been replaced with the D302A-$PhaCPhaE_{Av}$ gene and the organism examined under PHB production conditions by transmission electron microscopy. Very small granules (< 0.05 microns) were observed in contrast to the 0.2 to 0.5 micron granules observed with the wt-strain. Use of the D302A-

synthase has allowed successful interrogation of the initiation and elongation steps catalyzed by the Class III synthase.

2.2 INTRODUCTION

Polyhydroxyalkanoate (PHA) synthases from various bacteria are able to catalyze the polymerization of coenzyme A (CoA) esters of (*R*)-hydroxyalkanoates into high molecular weight PHAs under nutrient-limited conditions in the presence of a carbon source (*1-4*). Many different PHAs are generated by bacteria (Figure 1.1). The biodegradability and the thermoplastic or elastomeric properties of PHAs have provided the impetus for many research groups to study the mechanism of polymerization, the regulation of the polymerization process, and the substrate specificity of the synthases (*5-7*). The long-range goal is to produce PHAs in a bio-renewable source, in a fashion that is economically competitive with the oil-based polymers.

There are now four classes of PHA synthases. The classification is based on their substrate specificities and subunit composition (*4*). The Class I synthases (designated as PhaC) use short-chain CoA esters of 3-hydroxyalkanoates (C_3 to C_5) as substrates and are composed of one subunit of molecular weight 64 KDa (*8*). *Wautersia eutropha,* formerly known as *Ralstonia eutropha*, contains the best characterized Class I synthase and this organism has also been the system of choice for genetic analyses to understand PHA homeostasis. The Class II synthases, which use CoA esters of 3-hydroxyalkanoate (C_6 to C_{17}) as substrates, are also composed of one type of subunit of molecular weight between 61 to 73 KDa; *Pseudomonas* synthases are representatives of this class (*9*). The Class III synthases have substrate specificity similar to the Class I synthases. However these proteins, typified by the extensively characterized *Allochromatium vinosum* enzyme, consist of a 1:1 mixture of two different types of subunits:

$PhaE_{Av}$ (~40 KDa) and $PhaC_{Av}$ (~39 KDa) (*10, 11*). The native protein is thought to be a tetramer (Tian, unpublished data described in Chapter 7). $PhaC_{Av}$ is sequence homologous to the Class I synthase and is the site of polymerization. $PhaE_{Av}$ potentiates the polymerization process by a mechanism that is not understood. Recently, a fourth class of synthase has been identified in *Bacillus megaterium* and *Bacillus sp. INT005*, but remains to be characterized in detail (*12, 13*).

PHA synthases are representative of enzymes involved in polymerization processes in which a soluble substrate is transformed into insoluble inclusions during the polymerization process. This process requires careful orchestration of a number of proteins such that the polymer can be degraded and the monomeric units and energy generated can be reused in times of need. PHA granule formation and PHA homeostasis requires the synthase, several intracellular depolymerases, an oligomer hydrolase, phasin(s), transcription factor(s), and most likely additional factors that have not yet been identified (*14-21*). Recombinant PHA synthases from *W. eutropha* (*8, 22, 23*) and *A. vinosum* (*10, 11, 24*) have been expressed in *Escherichia coli* and purified to homogeneity. Both synthases incorporate HB-CoA into long chains of PHB *in vitro* in the absence of any other proteins. The granules formed *in vitro* are different from those observed *in vivo* (*25*). These proteins *in vitro* can thus serve only as a paradigm for studying the initiation and the early steps of elongation of the non-template driven polymerization processes. Understanding these processes may provide a basis for understanding other non-template dependent polymerization processes such as those catalyzed by glycogen synthase, starch synthases, and rubber synthase, among others (*26-28*).

Our thinking about the mechanism of $PhaCPhaE_{Av}$ was influenced by a 45 amino acid stretch of PhaC, which shares 42% sequence identity with several bacterial lipases (*24*). Clustal W

alignments of $PhaC_{Av}$ from the Class III synthases with these lipases and their available structures allowed generation of a threading model of the synthase. This model suggested that C149, H331, and D302 might be similar to the catalytic triad involved in lipase catalysis (*Pseudomonas cepacia, Pseudomonas sp. KWI-56,* and *Pseudomonas luteola*). Our initial studies focused on use of site-directed mutagenesis and use of a primer, a saturated trimer of HB-CoA in which the terminal hydroxyl has been replaced with a tritium ([^{3}H]-sT-CoA, **4** in Figure 1.9)(*11*) to investigate the initiation process. The studies with the [^{3}H]-sT-CoA and a C149A mutant provided the first direct evidence for the importance of C149 of the Class III synthase in covalent catalysis and the importance of H331 in the activation of this cysteine. The studies further suggested that D302 was not part of a catalytic triad, but functions as a general base catalyst in the activation of the 3-HO of HB-CoA for nucleophilic attack to generate the oxygen ester linkage, thus playing a role in elongation rather then loading of the substrate onto C149. Our mechanistic model for PHB synthases is at present based on the results from studies with this artificial primer (sT-CoA), and it is important to establish that a similar set of reactions occurs with the natural substrate, HB-CoA.

Taking advantage of the hypothesis developed from our studies with the sT-CoA, we reasoned that mutation of D302 to an A would slow down the rate of elongation, potentially allowing us to examine the priming process and the early stages in the elongation with HB-CoA. Results of studies are now presented in which the [^{14}C]-HB-CoA/PhaCPhaE$_{Av}$ ratio (S/E) was varied from 5 to 300 and the resulting products analyzed by SDS-PAGE, Western blots with antibodies (Abs) to PhaCPhaE$_{Av}$, and autoradiography. The intermediates formed at the priming stage have been isolated covalently bound to $PhaC_{Av}$. Their identity and the site of attachment has been established by trypsin digestion of the protein followed by HPLC separation of the

resulting peptides, identification of those peptides with radiolabeled $(HB)_n$ attached, followed by mass spectrometric analysis to determine the sizes of the $(HB)_n$. Furthermore, transmission electron microscopy (TEM) has been used to study a *W. eutropha* strain with its Class I synthase replaced by D302A-PhaCPhaE$_{Av}$. Instead of being able to accumulate large granules (0.2 - 0.5 μm in diameter (*2*)) under PHB production conditions similar to the wild-type (wt) strain, this gene-replacement strain is only able to generate granules <0.05 μm in diameter. The results with D302A-PhaCPhaE$_{Av}$ support a model in which C149 is involved in covalent catalysis and D302 is involved with self-priming and elongation.

2.3 MATERIALS AND METHODS

2.3.1 Materials. Racemic [1-^{14}C]-HB-CoA was obtained from the American Radiolabeled Chemicals, Inc. The racemic [1-^{14}C]-HB-CoA was diluted with (*R*)-HB-CoA synthesized by the method of Wei *et al* (*29*). *S*-[1-^{14}C]- HB-CoA has previously been shown not to be a substrate for the synthase (*29*). Edman sequencing of peptides was carried out by the MIT Biopolymers Laboratory. HPLC was performed with a Waters 510 HPLC system equipped with a Waters Automated Gradient Controller and a Waters Tunable Absorbance Detector, or a Rainin Dynamax model SD-200 HPLC system equipped with a Dynamax Diode Array Detector (model PDA-1).

2.3.2 Over-expression and purification of D302A-PhaCPhaE$_{Av}$. The synthase was over-expressed and purified to homogeneity by the procedure of Müh *et al* (*11*). Its specific activity was measured to be 0.13 U/mg.

2.3.3 Incubation of D302A-PhaCPhaE$_{Av}$ with [^{14}C]-HB-CoA. In a final volume of 21 µL, 10 µM of D302A-PhaCPhaE$_{Av}$ was incubated with 150 µM to 3 mM [^{14}C]-HB-CoA (specific activity ranging from 2.5 x 10^6 cpm/µmol to 3.3 x 10^7 cpm/µmol) in 20 mM Tris-HCl, pH 7.5, 50 mM NaCl (assay buffer) for 20 min at 30°C. Experiments with S/E ratios of 5, 60, 100 and 300 were carried out.

2.3.4 Analysis of reaction products by SDS-PAGE: Coomassie staining and autoradiography. The reaction was stopped by addition of an equal volume of Laemmli buffer (*30*) with no reducing reagent. Furthermore, the sample was not boiled. From each quenched reaction mixture, 10 µL was loaded onto a 10% SDS-PAGE gel of 0.7 mm thickness. Duplicates of reactions were resolved on the same gel, which was then cut in half. One half was stained with Coomassie for 10 min, destained in fast destain solution for 30 min, transferred to slow destain solution for 15 min, rinsed in dH_2O for less then 10 sec and dried immediately. The other half was not stained and was dried directly after being soaked in dH_2O for less then 10 sec. The purpose of the latter was to determine whether the Coomassie staining/destaining process resulted in loss of label or quenching of radioactivity. The dried gels were exposed to the Low-energy Screen (Molecular Dynamics) for ~15 h, and then scanned using the Storm Imaging System and analyzed using ImageQuant™ TL software (Amersham Biosciences).

2.3.5 Extraction of radioactivity from SDS-PAGE gel. Ten µL of each quenched reaction mixture described above was also resolved by SDS-PAGE. The gel was stained with Coomassie, destained as described above and quickly rinsed in water. Each gel was cut into columns which were then cut into ~1-3 mm slices. The resulting 17 acrylamide bands were each transferred to scintillation vials, to which 0.5 mL of dH_2O and 1 mL of SOLVABLE™ (PerkinElmer) was

added. The vials were incubated at 55°C for 36 h with shaking. Scintillation fluid Emulsifier-Safe™ (PerkinElmer), 9 mL, was then added and the samples analyzed by liquid scintillation counting. A control containing gel slices from a lane that contained the same amount of only PhaCPhaE was included for background correction. A second control contained a known amount of radioactivity and a non-radioactive gel slice to assess the extent of quenching.

2.3.6 Kinetics of D302A-PhaCPhaE$_{Av}$ modification monitored by SDS-PAGE gel, Western blotting and autoradiography. D302A-PhaCPhaE$_{Av}$, 10 μM, was incubated with 1 mM of [^{14}C]-HB-CoA (2.5 x 10^6 cpm/μmol) in assay buffer in a final volume of 100 μL at 30°C. At times from 0.5 to 20 min, 10 μL aliquots were removed from the reaction mixture and quenched with 10 μL of Laemmli buffer without reducing reagent. The samples, 17 μL each, were separated on a 10% SDS-PAGE gel that was then dried and exposed to the Low-energy Screen for 15 h.

For Western blotting, 8 ng of protein was loaded into each lane for SDS-PAGE analysis. Subsequent to electrophoresis, the proteins were electro-blotted onto a PVDF membrane (Millipore) using a Mini Trans-Blot Cell (Bio-Rad) at 100V for 1.5 h. The membrane was then treated with PhaCPhaE$_{Av}$ Ab (*11*) at a 1:1000 dilution for 1 h. After three washings with blocking buffer, the membrane was incubated with secondary Ab (goat anti-rabbit) at a 1:5000 dilution for 45 min. Blocking buffer and secondary Ab were obtained from the Western-Light Chemiluminescence Detection System (Tropix, Inc) which was used to detect the signals on the membrane. All reagents were used as described by the manufacturer.

2.3.7 Stability of the covalently bound HB-oligomers/D302A-PhaCPhaE$_{Av}$ complex using dialysis. D302A-PhaCPhaE$_{Av}$ (103 μM) was incubated with [^{14}C]-HB-CoA (514 μM) in assay

buffer for 5 min at 25°C. Concentrated guanidine HCl solution, 8M, was then added to the reaction mixture (final guanidine HCl concentration was 6M) for 10 min at room temperature. The protein/polymer complex was isolated by Sephadex G50 column chromatography (1 cm x 30 cm). The column was equilibrated and eluted with 2M urea, 0.1M KPi (pH 6) buffer. Thirty μL (30 μL) of the pooled fractions (~1.5 mL) containing protein was analyzed by liquid scintillation counting. The remainder of the material was then transferred to a slide-A-lyzer (Pierce, MWCO=10,000), and dialyzed against the elution buffer at 37°C. At times ranging from 15 to 360 min, aliquots were removed and 30 μL was analyzed by scintillation counting.

2.3.8 Isolation by HPLC of peptides from D302A-PhaCPhaE$_{Av}$ labeled with [^{14}C]-HB-oligomers. In a final volume of 60 μL, 103 μM of D302A-PhaCPhaE$_{Av}$ (500 μg), 514 μM of [^{14}C]-HB-CoA (5.7 x 10^6 cpm/μmol), and assay buffer were incubated at room temperature for 5 min. The reaction mixture was immediately loaded onto a Sephadex G-50 column (~22 mL, equilibrated in elution buffer) and eluted with the same buffer. Fractions that contained protein (based on a Bradford assay) were pooled and analyzed by scintillation counting. The combined mixture was then measured for A_{280nm} and digested with trypsin (TPCK-treated, Sigma) at a trypsin-to-synthase ratio of 1:4 for 30 min at 37°C. The reaction was stopped by making the sample 5% in acetonitrile and adjusting the pH to ~2 with trifluoroacetic acid (TFA). The entire mixture was injected onto a RP-C4 column (4.6 x 250 mm, Vydac) equilibrated in 5% acetonitrile and 0.08% TFA in water. The peptides were eluted using a linear gradient with 0.08% TFA in acetonitrile as follows: 5 – 30% in 0 – 50 min; 30 – 50% in 50 – 80 min; 50 – 95% in 80 – 160 min. The flow rate was 0.8 mL/min. Fractions were collected manually based on peak appearance, and were analyzed for radioactivity. A control experiment was carried out on D302A-PhaCPhaE$_{Av}$ alone and worked up under identical conditions.

2.3.9 Analysis of Peptides by Mass Spectrometry: MALDI-TOF MS. Fractions from HPLC containing peptides and radioactivity were concentrated to a small volume (10 – 30 μL) by Speedvac and submitted to the MIT Biopolymer Laboratory for MALDI spectrometry analysis. All samples were analyzed in both linear and reflection mode on Voyager-DE^{TM} STR (Applied Biosystems) using sinapinic acid as the matrix.

ESI-MS. Several fractions from the HPLC analysis were concentrated to near dryness by Speedvac and 50 μL of 50% acetonitrile/0.2% acetic acid was then added. The samples were submitted to the MIT Biopolymers Laboratory for ESI analysis by direct infusion on PE SCIEX API 365 (PerkinElmer).

2.3.10 Transmission Electron Microscopy. *W. eutropha* wt and the strain that contains the Class III D302A-PhaCPhaE$_{Av}$ (from *A. vinosum*) replacing the native Class I synthase were cultivated in PHB production medium following the procedure described in York *et al* (*16*). At 24 h, cell cultures were collected for EM analysis. Samples were first fixed with glutaraldehyde and paraformaldehyde, osmium tetraoxide, and uranyl acetate, then dehydrated through a series of increasing concentrations of ethanol. The samples were then embedded into 100% low viscosity embedding resin. All reagents were purchased from Electron Microscopy Sciences (Hatfield, PA). The detailed procedure for sample preparation is described in Chapter 5. The block containing the sample was sectioned at a thickness of ~70 nm using a Diatome diamond knife on a Reichert Ultracut E microtome. The sections were examined using a Philips EM410 electron microscope at 80 kV.

2.4 RESULTS

2.4.1 Evidence for covalent labeling of $PhaC_{Av}$ by [^{14}C]-HB-CoA. Our initial efforts to isolate covalently labeled wt-PhaCPhaE$_{Av}$ upon incubation with [^{14}C]-HB-CoA at low S/E ratios were deterred by the observation that reaction products appeared non-uniform when analyzed by SDS-PAGE gel and autoradiography. A small amount of protein contained highly polymerized HB units, while much of the protein contained shorter oligomers of HB that varied in length significantly. Our previous studies suggested a solution to this problem. As outlined in the introduction, studies with sT-CoA (**4**, Figure 1.9) suggested that D302 plays a key role in the elongation process. Thus its mutation to an alanine might decrease the elongation rate, facilitating detection of early steps in the polymerization process with HB-CoA. Second, our studies with the sT-CoA also demonstrated that D302A slowed the hydrolysis of the covalently sT-labeled PhaC relative to wt PhaC, suggesting that D302 also activated water in the hydrolysis process (Figure 1.11). Thus to look for labeled PhaC$_{Av}$ using [^{14}C]-HB-CoA, we initially focused our efforts on the D302A-PhaCPhaE$_{Av}$. Incubations at S/E ratios from 5 to 300 were carried out and the products analyzed by SDS-PAGE followed by autoradiography. To minimize loss of label from protein, mercaptoethanol was omitted from the loading buffer and the samples were not boiled. The results of a typical experiment are shown in Figure 2.1A (Coomassie staining) and 2.1B (autoradiography). A control experiment in which PhaCPhaE$_{Av}$ was replaced with C149A-PhaCPhaE$_{Av}$ and was reacted with [^{14}C]-HB-CoA showed no radioactivity by autoradiography (data not shown). These results establish that the radiolabeled HB oligomeric products are attached covalently to the synthase, and are able to withstand SDS-PAGE methods of analysis and most likely are attached to C149, at least initially.

Several observations made from the results presented in Figure 2.1A and B are interesting. First as the S/E ratio increases, the migratory properties of $PhaC_{Av}$ decrease (compare lower band in lane 2 with the slowest moving band in lane 5, Figure 2.1A). Autoradiography of the same gel reveals that only $PhaC_{Av}$ appears to be labeled (compare lanes 2 and 4, Figure 2.1B) and that as the S/E ratio increases, the intensity of the band associated with the slow migrating PhaC increases. By a ratio of S/E of 300, aggregates of HB oligomers are likely formed that dramatically alter the migratory properties of PhaC (Figure 2.1B, lane 5). Control experiments revealed that Coomassie staining and destaining does not alter the extent of labeling. The gels also show that the migration of $PhaE_{Av}$ does not appear to be changed with differing S/E ratios. This phenomenon is observed much more clearly when the wt-PhaCPhaE$_{Av}$ reacts with [^{14}C]-HB-CoA at high S/E ratios, such as 300, 1000, and higher; while 'unmodified' $PhaC_{Av}$ completely disappears, migration and intensity of the $PhaE_{Av}$ band remains unchanged (unpublished).

A second observation is that when the S/E ratio is greater than 5:1, the amount of 'unmodified' $PhaC_{Av}$ (Figure 2.1A, the fastest migrating protein in lanes 3, 4, and 5) does not appear to change. Coomassie staining suggests that it represents 20 to 30% of the starting $PhaC_{Av}$. No radioactivity appears to be associated with this 'unmodified' $PhaC_{Av}$ (Figure 2.1B, lane 3, 4, and 5) at least under the 15 h exposure to the intensifying screen. There are at least three possible interpretations of this observation. One is that 20 to 30% of $PhaC_{Av}$ over-expressed via recombinant methods is inactive. A second is that a very short $(HB)_n$ oligomer is actually attached to this protein, but it is not detectable due to the specific activity of [^{14}C]-HB-CoA used in the experiment. A third, and the most likely, is that a very short HB oligomer attached to PhaC has been removed by hydrolysis or aminolysis. In fact, it is surprising that we

have been able to observe radioactivity attached to protein given that the gels are run in Tris buffer. One might have expected the amine to react with the putative thiol ester intermediate. It is possible that the hydrophobic HB-oligomers are able to protect the active site from aminolysis or hydrolysis. It is also possible that the HB-oligomers are attached to a site other than C149 (*31, 32*). Recent SDS-PAGE analyses of a number of proteins, for example those involved in polyketide biosynthetic pathways, that use covalent catalysis by cysteines also retain their thiol esters during electrophoresis (*33, 34*).

An alternative method of gel analysis, cutting the columns of the acrylamide gels into 17 slices followed by extraction and scintillation counting, gave results very similar to those observed by autoradiography (Table 2.1). With S/E of 5 and 60, it was impossible to determine whether $PhaC_{Av}$, $PhaE_{Av}$ or both proteins were labeled as their migratory properties on the gels overlapped. However, at S/E ratios of 100 and 300, all of the radioactivity migrated more slowly than PhaE, whose appearance by Coomassie staining was identical to the no substrate controls. Thus, this data also supports the conclusion that only $PhaC_{Av}$ is labeled. The recovery of the expected radioactivity was ~ 60% for the S/E ratio of 5, ~30% for the S/E ratio of 60 and 100, and ~19% for the S/E ratio of 300.

2.4.2 Kinetics of D302A-synthase monitored by Western Blotting and autoradiography. The rate of polymer formation with D302A-$PhaCPhaE_{Av}$ is approximately 1/1000 of the rate of the wt synthase (*24*). Using a S/E ratio of 100 and a high protein concentration (10 μM), we monitored the kinetics of HB oligomers covalently attached to $PhaC_{Av}$ by SDS-PAGE with either Western blotting and $PhaCPhaE_{Av}$ Abs or directly by autoradiography of the dried gel. Western analysis was chosen over Coomassie staining since it is much more sensitive and would allow us to observe the minute change in the migratory properties of $PhaC_{Av}$ as a function of

reaction time. However, this method requires blotting and the ability to electroblot $PhaC_{Av}$ with HB oligomers attached could be different from 'unmodified' $PhaC_{Av}$. In addition, our previous studies established that under conditions in which $PhaC_{Av}$ is completely transferred to the PVDF membranes, the transfer of $PhaE_{Av}$ is limited and variable (data not shown). These transfer problems thus complicate quantitative analysis. Despite these problems, the Western blot (Figure 2.2A) revealed that 'unmodified' $PhaC_{Av}$ decreased in intensity throughout the reaction. As the reaction approached completion, $PhaC_{Av}$ migrated more slowly than $PhaE_{Av}$. At each time point, $PhaC_{Av}$ did not shift as a single band, but rather as a smear, consistent with it being modified by HB oligomers differing slightly in their length. The smearing observed near the $PhaE_{Av}$ band is also believed to be due to $PhaC_{Av}$ with longer oligomer attached. The presence of these HB oligomer(s) on $PhaC_{Av}$ was confirmed by autoradiography (Figure 2.2B). The intensity of the radioactive band increased and its migration within the gel decreased as a function of time. The combination of these results establishes that the D302A-synthase can elongate the PHB polymer chain. Some 'unmodified' $PhaC_{Av}$ is again observed at 20 min. Thus for the first time, we have been able to visualize the formation of HB-oligomers attached to $PhaC_{Av}$ as a function of time. The ability to observe these discrete intermediates suggests that with the aspartate mutant, the rate of chain extension has reduced to such an extent that relatively uniform loading of $PhaCPhaE_{Av}$ with HB-CoA is observed.

2.4.3 Stability of $(HB)_n$-$PhaC_{Av}$. In order to identify the site or sites of labeling of $PhaC_{Av}$ observed in Figure 2.1 and 2.2, it must be established that the label is stable under the conditions required to degrade the $PhaC_{Av}$ with trypsin and separate the resulting peptides by HPLC. We have previously established that the thioester linkage between $PhaC_{Av}$ and sT (**4**, Figure 1.9) was stable to acid, once the $PhaC_{Av}$ was denatured. Dialysis studies were thus carried out with [^{14}C]-

$(HB)_n$-$PhaC_{Av}$ in 2M urea, 0.1M KPi, pH 6 at 37°C. Under these conditions, the half-life of the label was 80 min. Trypsin digestion was thus carried out for only 30 min with a trypsin-to-substrate ratio of 1:4 to minimize label loss.

2.4.4 Isolation of HB_n-bound $PhaC_{Av}$ peptide(s). A S/E of 5 was chosen to isolate the $(HB)_n$ species formed during the initiation stage of the polymerization. The oligomers were expected to be short because of relatively uniform enzyme loading. The D302A-PhaCPhaE$_{Av}$ was reacted with the [^{14}C]-HB-CoA for 5 min and the reaction was stopped by directly loading the reaction mixture onto the Sephadex G-50 column equilibrated in 2M urea, 0.1M KPi (pH 6). We initially used guanidine HCl to stop the reaction prior to Sephadex chromatography. However, the recovery of radioactivity was poor, with only ~ 0.4 label per PhaCPhaE$_{Av}$ monomer. Direct loading of the reaction mixture onto the Sephadex column resulted ~1.7 labeled HB units per PhaCPhaE$_{Av}$ monomer. The labeled synthase was digested with trypsin and the peptides were resolved using a reverse-phase C4 column. A typical profile is shown in Figure 2.3 with the labeled peptides indicated. The expanded elution profile from 88-110 min is shown in Figure 2.4A as monitoring at A_{214} and A_{280} nm. The elution profile between 97 and 104 min (fractions F5 to F8, Figure 2.4A) is distinctly different from that of the control in which trypsin was used to digest D302A-PhaCPhaE$_{Av}$ alone (Figure 2.4B, monitoring A_{214nm}), and indicates that new species are generated in the presence of HB-CoA. Comparison of the elution profile monitored at A_{214nm} with that monitored at A_{280nm} (Figure 2.4A) is also very informative. The peptide peaks and their relative intensities are strikingly similar. These results strongly suggested that the same peptide modified by differing numbers of $(HB)_n$s, or an extended peptide with no additional aromatic amino acids modified by$(HB)_n$, is being observed.

Approximately 50% of the radioactivity loaded onto the Vydac column eluted in this region and rechromatography of several of the fractions from this region established that the radioactivity was associated with peptide (data not shown). The remaining radioactivity eluted from 62% to 72% acetonitrile and could be associated with hydrolyzed HB oligomers or with $(HB)_n$ oligomers attached to peptides in very low concentrations. The recovery of radioactivity from HPLC analysis after trypsin digestion was quantitative.

2.4.5 Characterization and identification of the radiolabeled peptide(s). Fractions 5, 6, 7, and 8 (Figure 2.4A) were collected and submitted for N-terminal sequencing. The results shown in Table 2.2 establish that all four fractions contained a peptide(s) with ALTLDD at its (their) N-terminus. These residues are identical to residues 116 to 121 of $PhaC_{Av}$. These results support our model that the same peptide decorated with different length of HB oligomers elute in this region of the chromatogram.

To obtain further insight about the size of the peptide(s) and the number of HB units attached, both MALDI-TOF and ESI mass spectrometric methods have been employed. Peptide(s), F1-F8 (Figure 2.4A) were analyzed by MALDI mass spectroscopy in both the linear and reflection mode. These two detection methods differ in that the linear mode provides higher sensitivity for larger molecules and the reflection mode provides higher resolution (*35*). The linear detector was used to measure the increasing number of HB units per peptide, and the reflection mode was used to determine the exact molecular weights of individual peptide-HB species. Typical results from the linear mode showed that the peptides in F5, F6, F7, and F8, each of which eluted with increased retention times at higher concentration of acetonitrile, exhibit increasing masses from F5 to F8 (data not shown). This is the expected result if the same

peptide has an increasing numbers of hydrophobic HB units attached. The observed broad peaks (data not shown) indicate that more then one species is present in each fraction.

In the reflection mode, the spectrum for F7 is shown in Figure 2.5. The dominant feature in F7 has a mass of 6215.67 Da. Our previous studies with sT-CoA (**4**, Figure 1.9) labeling of $PhaC_{Av}$, identified a 32mer peptide (shown in red, Figure 2.6) that contained the active site C149 (arrow). Our N-terminal sequence information from the present studies (Table 2.2), in conjunction with the previous peptide mapping studies, suggested that the peptide(s) labeled in these experiments would be a 50-mer or a 52-mer (Figure 2.6). Recall that our trypsin digestion conditions were designed to limit thioester cleavage and $(HB)_n$ loss, resulting in a number of trypsin sites that remained uncleaved.

Using the mass of the 50-mer peptide, addition of $(HB)_8$ minus water or $(HB)_{10}$ minus water gives the two observed masses in F7 (Table 2.3). The requirement for water loss to obtain the observed mass was unexpected. We postulate that it results from dehydration of the terminal 3-hydroxyl group to yield a crotonate analog. Experiments in the reflective mode on F6 and F8 were unsuccessful due to sensitivity problems.

Experiments in the reflective mode on F5 gave results very similar to those obtained by ESI MS (Figure 2.7, data from MALDI not shown). The mass of the dominant peak given by MALDI was 6041.491 Da, and that given by ESI MS was 6039.0 Da. The assignment of a structure to this mass is complicated by the fact that two species could have molecular weight within the error of the mass data by each method. Candidate 1 is the 50-mer peptide labeled with $(HB)_6$ minus water, giving a final mass of 6041.62 Da. Candidate 2 is the 52-mer peptide with $(HB)_3$ minus water giving a final mass of 6038.34 Da. The presence of the 52-mer peptide is supported by assignment of the 6210.0 Da feature (Figure 2.7) to the 52-mer peptide decorated

with $(HB)_5$ minus water (final mass 6210.64 Da) (Table 2.3). Since we know that more than one species is present in each of the fractions (F5 to F8 from the MALDI in the linear mode), the presence of all these species is feasible.

2.4.6 TEM of W. eutropha with its Class I synthase gene replaced with D302A-PhaCPhaE$_{Av}$.

This genetically engineered *W. eutropha H16* strain was cultivated in nitrogen-limited medium to promote PHB production. WT *W. eutropha* was also included in the study as a control. At 24 h of cultivation, cell samples were collected and fixed for TEM analysis. The wt strain generated normal size granules, ~0.4 μm in diameter which is within the reported range in literature (Figure 2.8A) (*2*). With the mutant strain, very small granules with diameter less than 0.05 μm were observed (Figure 2.8B). One interpretation of these observations is that the average length of the PHB polymer in the granule is substantially less than that observed in the wt strain. This interpretation is consistent with the postulated role for D302 in the polymerization process.

2.5 DISCUSSION

A number of labs have proposed that the PHB synthases *in vivo*, *in vitro* or both can generate block co-polymers of oxopolyesters (R = CH_3 and C_2H_5, Figure 1.1), a process that requires the initiation and elongation rates of the polymerization process are comparable (*3, 23, 36, 37*). Our *in vitro* studies on the Class I *W. eutropha* synthase showed this hypothesis not to be the case. In fact, our initial studies to investigate the wt Class III synthase by its incubation with 1 to 5 equivalents of HB-CoA also suggested that strict uniform loading was not occurring in this system either (described in Chapter 3). In the case of the Class I synthase, the rate of elongation relative to initiation was sufficiently rapid to preclude detection of any covalently labeled $(HB)_n$s. In the case of the Class III synthase, the initiation and elongation rates appear to be

more balanced, but are still complicated by the fact that a wide distribution of products are present. Our efforts thus focused on finding a Class III synthase mutant in which the initiation and elongation rates are more comparable. Our previous mutagenesis studies and studies with the sT-CoA (**4**, Figure 1.9) suggested that the conserved D302 is involved in elongation mechanism. Our results were consistent with its role as a general base catalyst involved in deprotonation of the 3'- hydroxyl group of the incoming HB-CoA, activating it for nucleophilic attack on the carbonyl of the previous HB unit covalently attached to the cysteine in the active site (Figure 1.8). D302 was proposed to play a key role in extending the polymer chain and hence its modification would interfere with polymer elongation (*24*). The D302A synthase, therefore, became the focus of our attention. Results from this study provide direct support for this model *in vitro* and *in vivo*.

The availability of [^{14}C]-HB-CoA facilitated the study of reaction products from the polymerization reaction catalyzed by D302A-PhaCPhaE$_{Av}$. It allowed the use of SDS-PAGE and autoradiography to probe the product size and its distribution as a function of time. The S/E ratio was increased from 5 to 300, which corresponds to an increase in polymer size from 430 to 25,800 Da expected for a uniform loading model. The migratory properties of PhaC$_{Av}$ in the gel are consistent with this proposal. The apparent size of PhaC$_{Av}$ increased (Figure 2.1) at increasing S/E ratios. At S/E ratios > 100, however, the complexes of proteins with PHB polymers migrated much more slowly than expected based on size and in fact some of the material did not enter the gel. These results mirror the low recoveries of radioactivity from the gels by the crush and soak method as the ratio of S/E increased (Table 2.1). Despite the complications at these high S/E ratios which may be associated with polymer aggregation, the mutant synthase, at lower ratios shows relatively uniform loading of HB units.

The ability of the $(HB)_n$ to remain covalently bound to PhaC during electrophoresis initially seemed surprising given that the running buffer contains Tris which could potentially aminate the thioester linkage to PhaC, releasing $(HB)_n$s. However, there are now many examples from the polyketide synthase literature using SDS-PAGE (with no reductants) that have successfully detected substrate bound to proteins via thioester linkages. As noted above, we have considered the possibility that the HB oligomers are attached to a site other than the C149 on PhaC during some stage in the polymerization process. The alternate site could be involved in HB-CoA loading or polymer termination. An alternative site is supported by the observation that the recovery of radioactivity associated with protein through any type of manipulation (Sephadex G50, C4-Reverse phase column, and SDS-PAGE) is always less than 50%. The precedent for additional sites of covalent attachment is excellent based on the extensive literature on fatty acid synthases and polyketide synthases (*31, 32*). The actual distribution of $(HB)_n$s would be mechanistically informative regarding the uniform loading model. However, this information has been inaccessible due to the challenges associated with the separation and detection methods. The methods of analysis together provide compelling evidence that the D302A-PhaCPhaE$_{Av}$ can self-prime and generate covalently attached $(HB)_n$ that can be chain extended.

The proposal for the role of D302 in the polymerization process *in vivo* is supported by examination using TEM of the *W. eutropha* strain containing D302A-PhaCPhaE$_{Av}$ in place of its native Class I synthase. WT *W. eutropha* H16 is able to accumulate up to 85% of its cell dry weight (cdw) as PHB under nitrogen-limited growth conditions. The literature suggests that each cell typically contains ~12 granules, averaging 0.2 - 0.5 μm in diameter (*2*). When the *W. eutropha* Class I synthase was replaced by wt Class III-PhaCPhaE from *A. vinosum*, the genetically engineered *W. eutropha* was also able to accumulate 91% of PHB/cdw in granule

form (*20*). A similar gene replacement strain with D302N-PhaCPhaE$_{Av}$ has also been generated. Extracts of whole cells under maximum PHB production conditions and analysis for PHB revealed less than 1.6% PHB observed with the wt-strain, consistent with the TEM and *in vitro* studies. The observation of very small granules in the *W. eutropha* strain containing D302A-PhaCPhaE$_{Av}$ supports the role of D302 in elongation.

The studies presented herein have offered a glimpse into the initiation process *in vivo*. The D302A mutant synthase will serve as a useful reagent in preparation of HB oligomers of defined length ($1 < \sim(HB)_n$) for use as PHB molecular weight standards. Isolating the granules from this mutant strain and determination of the molecular weight of the PHB could potentially allow us to examine the ends of the polymer by NMR spectroscopy and allow identification of the priming mechanism *in vivo*.

2.6 ACKNOWLEDGEMENT

I would like to thank Dr. Gregory York for the construction of *W. eutropha* gene replacement strain containing D302A-PhaCPhaE$_{Av}$.

2.7 REFERENCE

1. Byrom, D. (1987) Polymer Synthesis by Microorganisms: Technology and Economics, *Trends Biotechnol. 5*, 246-250.
2. Anderson, A.J. and Dawes, E.A. (1990) Occurrence, Metabolism, Metabolic Role, and Industrial Uses of Bacterial Polyhydroxyalkanoates, *Microbiol. Rev. 54*, 450-472.
3. Madison, L.L. and Huisman, G.W. (1999) Metabolic engineering of poly(3-hydroxyalkanoates): From DNA to plastic, *Microbiol. Mol. Biol. Rev. 63*, 21-53.
4. Rehm, B.H. and Steinbüchel, A. (1999) Biochemical and genetic analysis of PHA synthases and other proteins required for PHA synthesis, *Int. J. Biol. Macromol. 25*, 3-19.
5. Stubbe, J. and Tian, J. (2003) Polyhydroxyalkanoate (PHA) homeostasis: the role of PHA synthase, *Nat Prod Rep 20*, 445-457.
6. Rehm, B.H. (2003) Polyester synthases: natural catalysts for plastics, *Biochem J 376*, 15-33.
7. Kessler, B. and Witholt, B. (2001) Factors involved in the regulatory network of polyhydroxyalkanoate metabolism, *J Biotechnol 86*, 97-104.
8. Gerngross, T.U., Snell, K.D., Peoples, O.P., Sinskey, A.J., Cushai, E., Masamune, S., and Stubbe, J. (1994) Overexpression and purification of the soluble polyhydroxyalkanoate synthase from *Alcaligenes eutrophus*: Evidence for a required posttranslational modification for catalytic activity, *Biochemistry 33*, 9311-9320.
9. Qi, Q., Steinbüchel, A., and Rehm, B.H. (2000) *In vitro* synthesis of poly(3-hydroxydecanoate): purification and enzymatic characterization of type II polyhydroxyalkanoate synthases PhaC1 and PhaC2 from *Pseudomonas aeruginosa*, *Appl. Microbiol. Biotechnol. 54*, 37-43.

10. Liebergesell, M. and Steinbüchel, A. (1992) Cloning and nucleotide sequences of genes relevant for biosynthesis of poly(3-hydroxybutyric acid) in *Chromatium vinosum* strain D, *Eur. J. Biochem. 209*, 135-150.

11. Müh, U., Sinskey, A.J., Kirby, D.P., Lane, W.S., and Stubbe, J. (1999) PHA synthase from *Chromatium vinosum*: Cysteine 149 is involved in covalent catalysis, *Biochemistry 38*, 826-837.

12. McCool, G.J. and Cannon, M.C. (2001) PhaC and PhaR are required for polyhydroxyalkanoic acid synthase activity in *Bacillus megaterium*, *J Bacteriol 183*, 4235-4243.

13. Satoh, Y., Minamoto, N., Tajima, K., and Munekata, M. (2002) Polyhydroxyalkanoate Synthase from *Bacillus* sp. INT005 Is Composed of PhaC and PhaR, *Journal of Bioscience and Bioengineering 94*, 343-350.

14. Peoples, O.P. and Sinskey, A.J. (1989) Poly-β-hydroxybutyrate (PHB) biosynthesis in *Alcaligenes eutrophus* H16: Identification and characterization of the PHB polymerase gene (phbC), *J. Biol. Chem. 264*, 15298-15303.

15. Saegusa, H., Shiraki, M., Kanai, C., and Saito, T. (2001) Cloning of an intracellular Poly[D(-)-3-Hydroxybutyrate] depolymerase gene from *Ralstonia eutropha* H16 and characterization of the gene product, *J Bacteriol 183*, 94-100.

16. York, G.M., Lupberger, J., Tian, J., Lawrence, A.G., Stubbe, J., and Sinskey, A.J. (2003) *Ralstonia eutropha* H16 Encodes Two and Possibly Three Intracellular Poly[D-(-)-3-Hydroxybutyrate] Depolymerase Genes, *J Bacteriol 185*, 3788-3794.

17. Maehara, A., Doi, Y., Nishiyama, T., Takagi, Y., Ueda, S., Nakano, H., and Yamane, T. (2001) PhaR, a protein of unknown function conserved among short-chain-length

polyhydroxyalkanoic acids producing bacteria, is a DNA-binding protein and represses *Paracoccus denitrificans* phaP expression in vitro, *FEMS Microbiol Lett 200*, 9-15.

18. Wieczorek, R., Pries, A., Steinbüchel, A., and Mayer, F. (1995) Analysis of a 24-kilodalton protein associated with the polyhydroxyalkanoic acid granules in *Alcaligenes eutrophus*, *J. Bacteriol. 177*, 2425-2435.

19. Steinbüchel, A., Aerts, K., Babel, W., Föllner, C., Liebergesell, M., Madkour, M.H., Mayer, F., Pieper-Fürst, U., Pries, A., Valentin, H., and Wieczorek, R. (1995) Considerations on the structure and biochemistry of bacterial polyhydroxyalkanoic acid inclusions, *Can. J. Microbiol. 41 (suppl. 1)*, 94-105.

20. York, G.M., Junker, B.H., Stubbe, J.A., and Sinskey, A.J. (2001) Accumulation of the PhaP phasin of *Ralstonia eutropha* is dependent on production of polyhydroxybutyrate in cells, *J Bacteriol 183*, 4217-4226.

21. Potter, M., Muller, H., Reinecke, F., Wieczorek, R., Fricke, F., Bowien, B., Friedrich, B., and Steinbuchel, A. (2004) The complex structure of polyhydroxybutyrate (PHB) granules: four orthologous and paralogous phasins occur in *Ralstonia eutropha*, *Microbiology 150*, 2301-2311.

22. Jia, Y., Yuan, W., Wodzinska, J., Park, C., Sinskey, A.J., and Stubbe, J. (2001) Mechanistic studies of Class I polyhydroxybutyrate (PHB) synthase from *Ralstonia eutropha*: Class I and III synthases share a similar catalytic mechanism, *Biochemistry 40*, 1011-1019.

23. Song, J.J., Zhang, S., Lenz, R.W., and Goodwin, S. (2000) In vitro polymerization and copolymerization of 3-hydroxypropionyl-CoA with the PHB synthase from *Ralstonia eutropha*, *Biomacromolecules 1*, 433-439.

24. Jia, Y., Kappock, T.J., Frick, T., Sinskey, A.J., and Stubbe, J. (2000) Lipases provide a new mechanistic model for polyhydroxybutyrate (PHB) synthases: Characterization of the functional residues in *Chromatium vinosum* PHB synthase, *Biochemistry 39*, 3927-3936.

25. Gerngross, T.U. and Martin, D.P. (1995) Enzyme-catalyzed synthesis of poly[(R)-(-)-3-hydroxybutyrate]: Formation of macroscopic granules in vitro, *Proc. Natl. Acad. Sci. USA 92*, 6279-6283.

26. Ugalde, J.E., Parodi, A.J., and Ugalde, R.A. (2003) De novo synthesis of bacterial glycogen: *Agrobacterium tumefaciens* glycogen synthase is involved in glucan initiation and elongation, *Proc Natl Acad Sci U S A 100*, 10659-10663.

27. Smith, A.M. (2001) The biosynthesis of starch granules, *Biomacromolecules 2*, 335-341.

28. Cornish, K. (2001) Biochemistry of natural rubber, a vital raw material, emphasizing biosynthetic rate, molecular weight and compartmentalization, in evolutionarily divergent plant species, *Nat Prod Rep 18*, 182-189.

29. Yuan, W., Jia, Y., Tian, J., Snell, K.D., Muh, U., Sinskey, A.J., Lambalot, R.H., Walsh, C.T., and Stubbe, J. (2001) Class I and III polyhydroxyalkanoate synthases from *Ralstonia eutropha* and *Allochromatium vinosum*: characterization and substrate specificity studies, *Arch Biochem Biophys 394*, 87-98.

30. Laemmli, U.K. (1970) Cleavage of structural proteins during the assembly of the head of bacteriophage T4., *Nature 227*, 680-685.

31. Shen, B. (2003) Polyketide biosynthesis beyond the type I, II and III polyketide synthase paradigms, *Curr Opin Chem Biol 7*, 285-295.

32. Smith, S., Witkowski, A., and Joshi, A.K. (2003) Structural and functional organization of the animal fatty acid synthase, *Prog Lipid Res 42*, 289-317.

33. Dreier, J., Li, Q., and Khosla, C. (2001) Malonyl-CoA:ACP transacylase from *Streptomyces coelicolor* has two alternative catalytically active nucleophiles, *Biochemistry 40*, 12407-12411.

34. Tang, Y., Lee, T.S., Kobayashi, S., and Khosla, C. (2003) Ketosynthases in the initiation and elongation modules of aromatic polyketide synthases have orthogonal acyl carrier protein specificity, *Biochemistry 42*, 6588-6595.

35. Rader, H.J. and Schrepp, W. (1998) MALDI-TOF mass spectrometry in the analysis of synthetic polymers, *Acta Polymer 49*, 272-293.

36. Luzier, W.D. (1992) Materials derived from biomass/biodegradable materials, *Proc Natl Acad Sci U S A 89*, 839-842.

37. Kelley, A.S. and Srienc, F. (1999) Production of two phase polyhydroxyalkanoic acid granules in *Ralstonia eutropha*, *Int. J. Biol. Macromol. 25*, 61-67.

2.8 TABLES AND FIGURES

Table 2.1 Radioactivity extracted from SDS-PAGE gel containing polymerization reactions catalyzed by D302A-PhaCPhaE$_{Av}$ with [^{14}C]-HB-CoA at indicated S/E ratios. Each lane was sliced from top to bottom and the gel bands were numbered as shown.

Band No.	S/E= 5 (cpm)	S/E=60 (cpm)	S/E=100 (cpm)	S/E=300 (cpm)
1	**102**	14	26	8
2	**895**	27	33	8
3	**1129**	**443**	**310**	29
4	**69**	**2064**	**446**	**117**
5	31	**311**	**3996**	**932**
6	25	26	**288**	**108**
7	28	6	37	6
8	17	4	16	7
9	129	0	3	10
10	44	5	5	6
11	5	13	1	5
12	15	10	3	24
13	5	2	4	21
14	7	11	2	**99**
15	23	5	12	**194**
16	16	30	30	**946**
17	6	19	0	0
% CPM Recovery	**60**	**31**	**33**	**19**

Table 2.2 N-terminal sequence of peptides purified from fractions indicated in Figure 2.4A (F5-F8).

Fraction No.	N-terminus Sequence
F5	ALTLDD
F6	ALTLDD
F7	ALTLDD
F8	ALTLDD

Table 2.3 MALDI-TOF and ESI spectrum analysis: assignment of the peaks of interest. Note that the molecular weight (MW) of a single HB unit is 86.15 Da.

Fraction	Method	MW of Peak $[M+H]^+$ (Da)	MW of the Predicted Peptide $[M+H]^+$ (Da)	Length of HB Oligomer Proposed	Calculated MW of the Proposed Species (Da)
F5	ESI	6039.0	5797.8926 (52mer)	3 mer - H_2O	5797.8926 + 86.15 x 3 - 18 = 6038.34
		6210.0		5 mer - H_2O	5797.8926 + 86.15 x 5 - 18 = 6210.64
	MALDI	6041.5	5542.7231 (50mer)	6 mer - H_2O	5542.7231 + 86.15 x 6 - 18 = 6041.62
F7	MALDI	6215.7	5542.7231	8mer -H_2O	5542.7231 + 86.15 x 8 - 18 = 6213.92
		6386.1	5542.7231	10mer -H_2O	5542.7231 + 86.15 x 10 - 18 = 6386.22

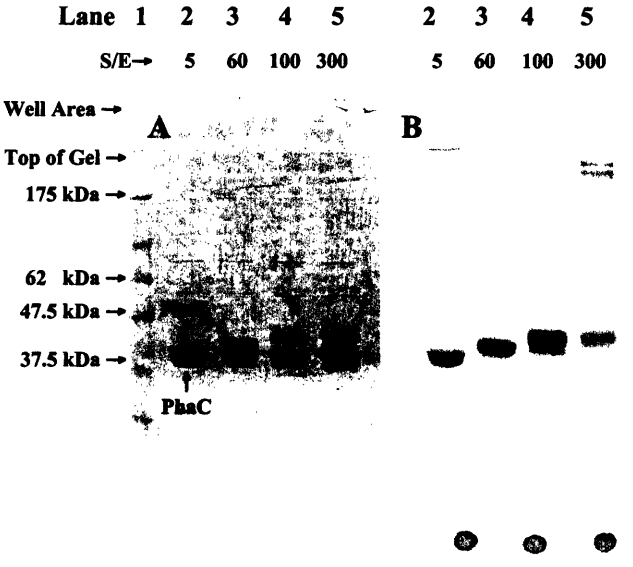

Figure 2.1 (**A**) SDS-PAGE gel (10%) monitoring the end products of the polymerization catalyzed by D302A-PhaCPhaE$_{Av}$ at various S/E ratios. The specific activity of [^{14}C]-HB-CoA used with S/E ratios of 5, 60, 100 and 300 was 3.3 x 10^7, 6.4 x 10^6, 6.4 x 10^6, and 2.5 x 10^6 cpm/μmol, respectively. (**A**) Coomassie staining of the gel; (**B**) Autoradiography of the gel.

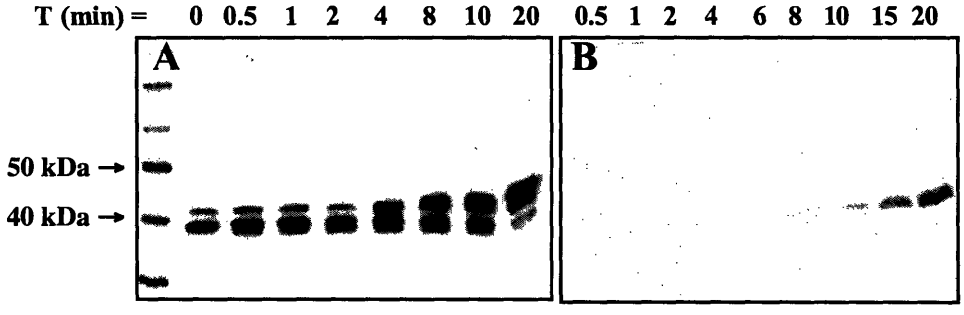

Figure 2.2 Kinetics of the polymerization reaction catalyzed by D302A-PhaCPhaE$_{Av}$ using [^{14}C]-HB-CoA at S/E of 100: (**A**) Monitoring the reaction by Western blotting with Abs to PhaCPhaE$_{Av}$; (**B**) By autoradiography.

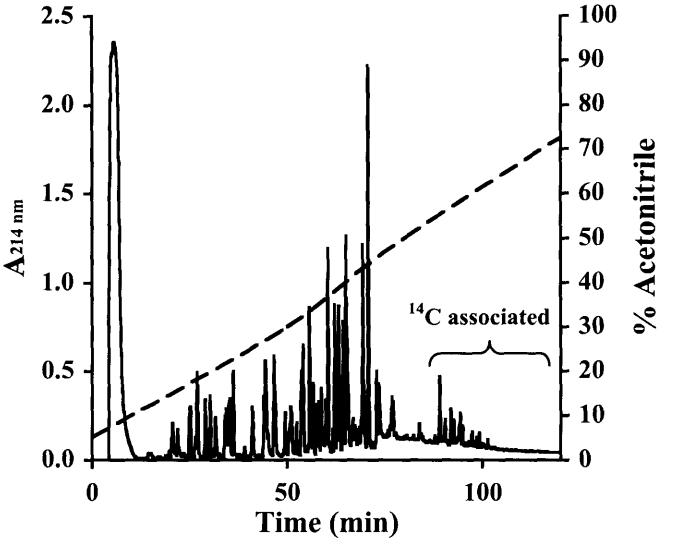

Figure 2.3 HPLC profile of peptides monitored at A_{214nm} resulting from trypsin digestion of D302A-PhaCPhaE$_{Av}$ produced by incubation of [^{14}C]-HB-CoA at a S/E ratio of 5. Acetonitrile gradient is shown as a dashed line. The flow rate was 0.8 mL/min. The region where radioactivity eluted is indicated.

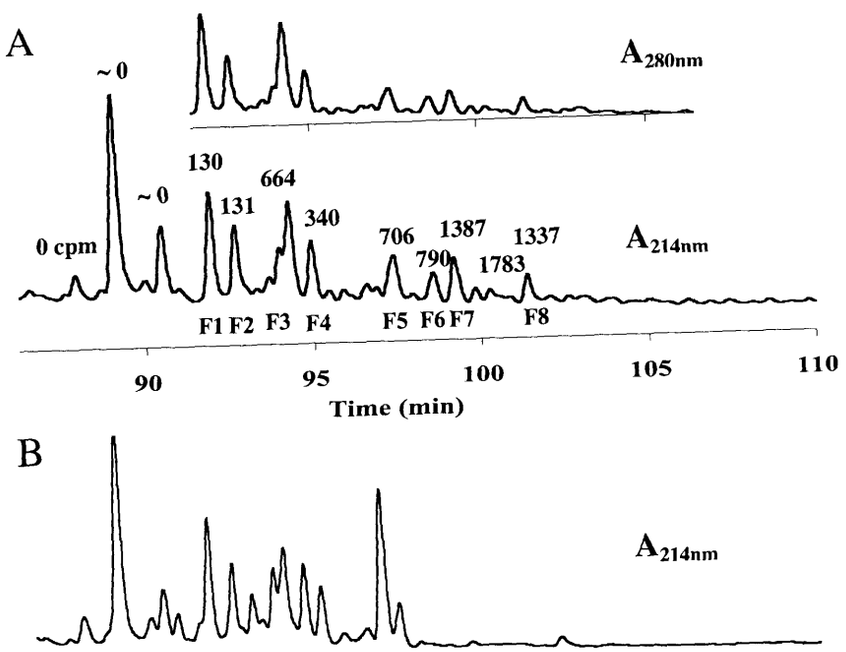

Figure 2.4 Expanded elution profile of the HB-modified-peptides (radioactivity associated) from Figure 2.3. (**A**) Expanded elution profile monitored at A_{214nm}, with elution profile monitored at A_{280nm} overlaid on top. (**B**) Expanded elution profile of the control trypsin digestion of D302A synthase monitored at A_{214nm}.

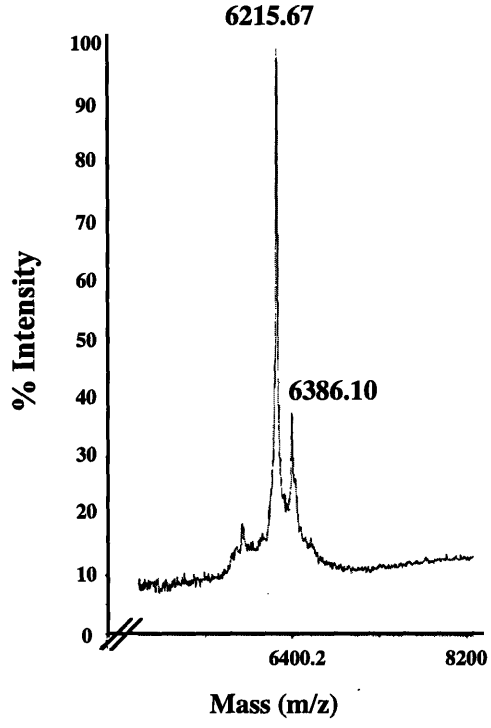

Figure 2.5 MALDI-TOF Mass spectrum in the reflection mode of F7 (from Figure 2.4A).

Figure 2.6 Candidate for the 50-mer and 52-mer peptide of PhaC proposed to be associated with HB oligomers. The 32-mer peptide identified previously is shown in red. The conserved cysteine (C149) proposed to be the site of covalent catalysis is pointed by an arrow. The sites where trypsin cleavage did not occur are indicated with a *.

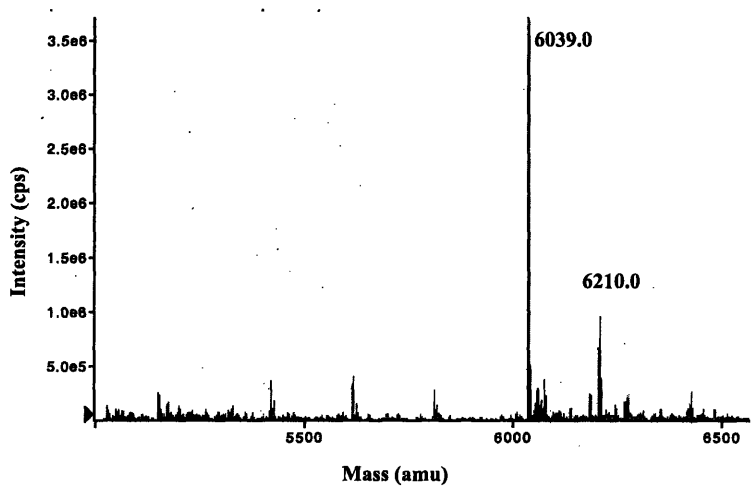

Figure 2.7 ESI Mass spectra of F5 (from Figure 2.4A).

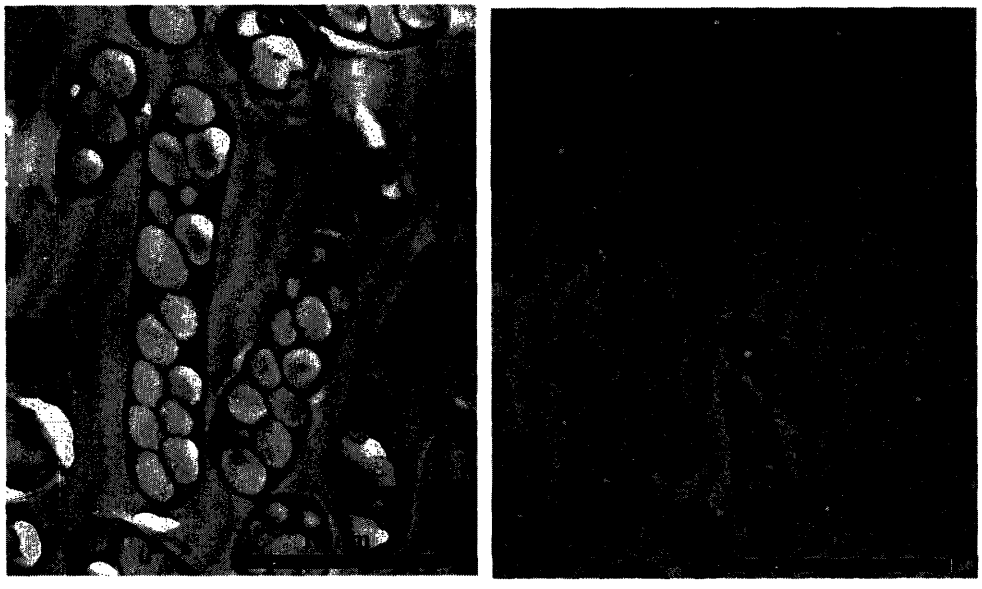

Figure 2.8 TEM images of (**A**) wt *W. eutropha* and (**B**) *W. eutropha* with its synthase gene replaced with D302A-PhaCPhaE$_{Av}$. Both strains were grown in PHB production medium for 24 h. Both photographs were taken at the same magnification and printed at a final magnification of 18933×. Bar size, 1.9 μm.

CHAPTER 3

Class III Polyhydroxyalkanoate Synthase: Involvement in Chain Termination and Re-Initiation

3.1 ABSTRACT

Polyhydroxybutyrate (PHB) synthase catalyzes the polymerization of (*R*)-3-hydroxybutyryl-CoA into high molecular weight polyhydroxybutyrate (PHB). Recombinant wt Class III synthase from *Allochromatium vinosum* (PhaCPhaE$_{Av}$), antibodies to this synthase and to PHB, and [^{14}C]-hydroxybutyryl-CoA (HB-CoA) have been used to detect oligomeric hydroxybutyrate (HB) units covalently bound to the synthase using SDS-PAGE analysis. Although a distribution of products is typically observed, short (HB)$_n$-bound synthases (designated species I) are most prevalent at low substrate to enzyme (S/E) ratios. Species I are similar to those (HB)$_n$-bound PhaC$_{Av}$ (n = 3 – 10) recently identified using D302A-PhaCPhaE$_{Av}$ (Tian, J., Sinskey, A.J., and Stubbe, J., *Biochemistry*, in press). Species I is shown to be an intermediate in the elongation process of PHB synthesis *in vitro*. The reaction catalyzed by the wt synthase *in vitro* was further studied under two sets of conditions: at low (< 200) and high (70,000) S/E ratios. Although these conditions may not be encountered under physiological conditions, results from these studies have been mechanistically informative. At low S/E ratios, species I was observed to increase with time subsequent to consumption of all of the HB-CoA. Kinetic analysis of the reaction of HB-CoA with the wt synthase at S/E ratios of 70,000 was equally intriguing. The Western blots using antibodies to PhaCPhaE$_{Av}$ revealed the disappearance of PhaC$_{Av}$ (migrating as a 40 KDa protein) at early time points and the reappearance of PhaC$_{Av}$ as the molecular weight of the polymer approached ~ 1 MDa. The results from studies under both sets of conditions suggest that an inherent property of the synthase is chain termination and re-initiation.

3.2 INTRODUCTION

Polyhydroxyalkanoate (PHA) synthases catalyze the polymerization of (*R*)-3-hydroxyalkanoate-CoA into high molecular weight polyoxoesters under nutrient-limited conditions in the presence of a carbon source (*1-4*). PHA synthases are representative of enzymes involved in polymerization processes in which a water-soluble substrate is transformed during the polymerization process into a water-insoluble granule or inclusion. The thermoplastic or elastomeric properties of PHAs (depending on R, Figure 1.1) have provided the impetus for many research groups to study the mechanism and the regulation of the polymerization process, as well as the substrate specificity of the synthase. The long-range goal is to make materials with novel properties in an economically competitive fashion with oil-based polymers.

The classification of PHA synthases, based on substrate specificity and subunit composition, has been described in detail in several reviews (*5, 6*). Our lab has focused on the Class I and Class III synthases that use (*R*)-3-hydroxybutyrate-CoA (HB-CoA) to form polyhydroxybutyrate (PHB). The Class I synthase from the prototypical *Wautersia eutropha* ($PhaC_{We}$) has a subunit molecular weight of 64 KDa (*7*). The Class III synthase from the prototypical *Allochromatium vinosum* is composed of two subunits, designated $PhaE_{Av}$ (~41 KDa) and $PhaC_{Av}$ (~39 KDa) (*8*). $PhaC_{Av}$ contains the site of catalysis, while the role of PhaE is unknown.

Different mechanisms of initiation are often observed in non-template driven polymerization systems. So far, examples of three models have been observed. The first involves priming by other protein(s) in addition to the synthase itself, exemplified by glycogenin in mammalian glycogen biosynthesis (*9*). The second involves oligomers of substrate unit, exemplified by malto-oligosaccharides (MOS, 2 to 7 residues) in starch biosynthesis (*10*). Finally, the polymerase can initiate through self-priming, a process exemplified by the bacterial glycogen

synthase from *Agrobacterium tumefaciens* (*11*). The mechanism of initiation by both the *W. eutropha* and *A. vinosum* synthases has been studied in some detail. These studies have resulted in the working model shown in Figure 1.7. In this early model, the active site is proposed to be at the interface of the two monomers; thus the dimeric synthase is thought to be the active form in elongation. Mutagenesis studies and studies with oligomeric HB-CoA analogs suggest that the single conserved cysteine is involved in covalent catalysis and that a conserved histidine activates this thiol for nucleophilic attack on HB-CoA (*12*). A conserved aspartate has been implicated in the activation of the hydroxyl of HB-CoA for nucleophilic attack and ester bond formation. In analogy with fatty acid synthases, a second covalent intermediate has been proposed to be involved in the catalysis. No evidence for this latter hypothesis is yet available and an alternative (Figure 1.8) involving a non-covalent mechanism is feasible (*6*). Sequence alignments of the Class III synthases revealed that they are structurally homologous to lipases and are members of the α/β hydrolase superfamily (*13*). So far, there are no examples of lipases having a single active site at a dimer interface. The threading models for Class I and III synthases, generated based on the structure of bacterial lipases, also predict that the active site is buried deep inside the monomer. Therefore, how two monomers of the synthase can come together to form the active site, as proposed in Figure 1.7, for initiation is still an enigma.

In our previous papers, we have demonstrated that the kinetics of the recombinant Class III synthase PhaCPhaE$_{Av}$ differ from that of the recombinant Class I synthase PhaC$_{We}$ (*7, 12*). The release of CoA from HB-CoA catalyzed by PhaCPhaE$_{Av}$ is multi-phasic with the initial phase being faster than the additional phase(s). With this enzyme, the initiation process is proposed to be faster than the elongation process. The evidence for this proposal is based on studies with a saturated trimer of HB-CoA in which the terminal hydroxyl has been replaced with a tritium (**4**

in Figure 1.9, [^{3}H]-sT-CoA). With this oligomer and low concentrations of HB-CoA, the enzyme was trapped in the process of elongation with a sT, sT+HB and a sT+$(HB)_2$ bound to the cysteine in the active site (*12*). Our initiation model is at present based on use of this artificial primer, **4** (Figure 1.9), and it is important to establish that a similar set of reactions occurs with the natural substrate HB-CoA.

Recently, we have for the first time observed intermediate species in the *in vitro* reaction containing a mutant Class III synthase, D302A-PhaCPhaE$_{Av}$, and its natural substrate HB-CoA (*14*). Analysis of reaction products by SDS-PAGE gel, Western, and autoradiography showed different migratory properties of the mutant synthase after its reaction with substrate at various substrate to enzyme (S/E) ratios. These results indicate that PhaC has been modified with hydroxybutyrate oligomers ($(HB)_n$). Substrate loading of the mutant synthase appeared to be uniform at S/E ratios lower than 100. Trypsin digestion of the $(HB)_n$ modified synthase at a S/E ratio of 5 followed by reverse-phase HPLC separation of peptides allowed the isolation of peptides modified with $(HB)_n$ (n = 3-10). N-terminal sequencing, MALDI-TOF, and ESI mass spectrometry of the peptides revealed that these intermediate species are attached to the active-site cysteine.

In this chapter, we describe our continuing effort in studying the initiation catalyzed by both Class I and III synthases. We report the first direct evidence of intermediate species(s) that are formed during the initiation stage of polymerization by the recombinant wild-type Class III synthase PhaCPhaE$_{Av}$ using its natural substrate, HB-CoA. Our results show that this Class III synthase initiates polymerization through self-priming. Uncovering its *in vitro* reactions via manipulation of the S/E ratios has give us new insight to the additional catalytic capabilities of this enzyme, despite the fact that some reaction conditions used may not be physiologically

relevant. Specifically, monitoring a PhaCPhaE$_{Av}$ reaction at a S/E ratio of 70,000 by Western blot using Abs to PhaCPhaE$_{Av}$ revealed the reappearance of polymer-free PhaC$_{Av}$ at the time when polymer of M_W 10^6 Da is formed. Thus, direct evidence for re-initiation of PhaCPhaE$_{Av}$ has been observed for the first time *in vitro*. It strongly suggests that additional chemical role for the synthase exists. The synthase most likely has the ability to sense polymer chain size and catalyzes the removal of the polymer chain from itself once the polymer reaches the desired molecular weight, thus allowing the synthesis of a new polymer chain.

Although intermediate species have also been observed in the recombinant Class I synthase, this synthase does not follow the same mechanism of initiation. Instead, large polymers or aggregates of polymers are formed by a small fraction of the enzyme immediately. The reason why recombinant Class I PhaC$_{We}$ does not load substrate uniformly could be that the protein is not appropriately modified or that a factor is missing when the enzyme is over-expressed in *Escherichia coli*.

3.3 MATERIALS AND METHODS

3.3.1 Materials. (*R, S*)-[1-^{14}C]-HB-CoA was obtained from American Radiolabeled Chemicals, Inc.. (*R,S*) -[1-^{14}C]-HB-CoA was diluted with (*R*)-HB-CoA synthesized by the method of Yuan *et al* (*15*). (*S*)-HB-CoA has previously been shown not to be a substrate for the synthase(*15*). Hecameg [6-*O*-(N-heptylcarbamoyl)methyl-α-D-glucopyranoside] was obtained from Vegatec, Villejuif, France. Wt PhaCPhaE$_{Av}$, C149A-PhaCPhaE$_{Av}$, and D302A-PhaCPhaE$_{Av}$ were over-expressed in plasmids pET-UM4, pET-UM21, and pET-YJ33, respectively, as previously described (*12, 13*). The expression of plasmid pKAS4 carrying *W. eutropha* PhaC$_{We}$ has also been reported (*7*). Preparation of antibodies (Abs) to PhaCPhaE$_{Av}$ has been described previously

(*12*). Abs to PHB were a kind gift from Metabolix, Cambridge, MA; the antigen was prepared by covalently attaching a synthetic PHB oligomer, $(HB)_8$, to keyhole limpet hemocyanin. Edman sequencing of peptides and ESI-MS analysis of the peptides were carried out by the MIT Biopolymer Laboratory. HPLC was performed with a Rainin Dynamax model SD-200 HPLC system equipped with a Dynamax Diode Array Detector (model PDA-1).

3.3.2 Purification of recombinant PHA synthases. Expression and purification of recombinant $PhaC_{We}$ was carried out following the procedure described previously (*15*). Recombinant wt and mutant Class III PHA synthases (C149A- and D302A-$PhaCPhaE_{Av}$) from *A. vinosum* were expressed and purified following the procedure described in Müh *et al* (*12*). All synthases were assayed by the discontinuous method using DTNB to monitor CoA release (*12*). $PhaC_{We}$ has activity of 40 U/mg, and $PhaCPhaE_{Av}$ has activity of 200 U/mg. D302A-$PhaCPhaE_{Av}$ has activity of 0.13 U/mg. C149A-$PhaCPhaE_{Av}$ has no detectable activity under our assay conditions.

3.3.3 Incubation of wt $PhaCPhaE_{Av}$, C149A-$PhaCPhaE_{Av}$, or $PhaC_{We}$ with (R)-HB-CoA or [^{14}C]-HB-CoA. All reactions containing Class III synthases are in 20 mM Tris/HCl, pH 7.8, 50 mM NaCl containing variable amounts of [^{14}C]-HB-CoA and are incubated at 30°C for 5 min, unless indicated otherwise. All reactions containing Class I synthase are in 150 mM KPi, pH 7.2, 0.2% glycerol with variable amounts of substrate and are incubated at 25°C for 1 h. The details of each specific experiment, such as concentration of the synthase and substrate, and the specific activity of the substrate are described in the figure legend.

3.3.4 Analysis of reaction products by SDS-PAGE: Coomassie staining, autoradiography, and Western blotting. All reactions were stopped by addition of an equal volume of Laemmli buffer

(*16*) with no reducing reagent. Furthermore, samples were not boiled (Note: boiling the samples at 95°C for 5 min does no effect the results as we have determined later). All samples were analyzed on 10% SDS-PAGE gels, followed by either Coomassie staining, autoradiography, Western blotting, or a combination of these methods, as specified in the figure legend. The details of these methods have been described in Chapter 2. Abs to PhaCPhaE$_{Av}$, and PHB were used at a 1:1000 dilution.

3.3.5 Isolation by HPLC of peptides from wt PhaCPhaE$_{Av}$ incubated with 1 equivalent of [^{14}C]-HB-CoA followed by digestion with trypsin. In a final volume of 112 μL, 56 μM of PhaCPhaE$_{Av}$ (500 μg) was reacted with [^{14}C]-HB-CoA (3.1 x 10^7 cpm/μmol) at a substrate/synthase (S/E) ratio of 1:1 in assay buffer for 5 min at room temperature. The reaction mixture was then processed following the procedure described in Chapter 2 and analyzed by N-terminal sequencing and ESI-MS. The recovery of radioactivity from the Sephadex G-50 column was 80%, which corresponds to 0.5 HB/PhaCPhaE$_{Av}$. The recovery of radioactivity from C4-Vydac column was 84%, indicating that some polymers failed to elute.

3.4 RESULTS

3.4.1 Evidence for covalent labeling of wt PhaCPhaE$_{Av}$ by [^{14}C]-HB-CoA. Chapter 2 reported that incubation of D302A-PhaCPhaE$_{Av}$ with [^{14}C]-HB-CoA resulted in detection, for the first time, of oligomeric (HB)$_n$ (n = 3-10) covalently bound to C149 in PhaC$_{Av}$ intermediate species. The (HB)$_n$-PhaC$_{Av}$ could be chased into longer HB oligomers. These species were thus proposed to play an important role in the polymerization process. To establish the relevance of the (HB)$_n$-PhaC$_{Av}$ in the polymerization reaction catalyzed by the wt synthase, we have therefore chosen to

study these species further using the wt PhaCPhaE$_{Av}$. Incubation of [^{14}C]-HB-CoA with PhaCPhaE$_{Av}$ at S/E ratio of 5:1, 15:1 and 45:1, and analysis by SDS-PAGE gel/autoradiography resulted in four distinct groups of products when analyzed by SDS-PAGE gels and autoradiography. These four species are numbered I through IV in Figure 3.1A; each species is composed of multiple products. No signals were detected on the phosphorimage when a similar experiment was carried out with C149A-PhaCPhaE$_{Av}$ and [^{14}C]-HB-CoA, indicating that all observed signals result from covalently modified PhaC, presumably through the C149. The presence of four distinct groups of products seems to suggest that PhaCPhaE$_{Av}$ exhibits non-uniform loading of substrate *in vitro*, at least when compared to similar studies with D302A-PhaCPhaE$_{Av}$. In fact, most of the synthase remains at the monomeric position (~ 39 KDa) on the gel (labeled 'position of PhaC', Figure 3.1A) in the region labeled species I, as determined by Coomassie staining and Western blot with Abs to PhaCPhaE$_{Av}$ (data not shown).

Species I is believed to be similar to the 'intermediate species', (HB)$_n$-bound PhaC$_{Av}$ (n = 3 – 10), recently identified and isolated using the D302A-PhaCPhaE$_{Av}$ in a similar set of experiments (Chapter 2). Lane 1 in Figure 3.1A shows that at a S/E ratio of 5:1, species I is the dominant product. In an effort to maximize our chances of isolating and identifying species I, we lowered the S/E ratio to 1:1 and carried out trypsin digestion and HPLC analysis described previously (Chapter 2). The data revealed that peptides containing radioactivity eluted at acetonitrile concentrations >62% (data not shown). Difficulties were encountered when radiolabeled peptides were isolated for subsequent identification. All fractions contained more than one peptide, with the exception of one which gave clean N-terminal sequencing results. This fraction contained the same peptide that we had identified previously in studies with D302A-PhaCPhaE$_{Av}$ incubated with HB-CoA (Chapter 2). ESI-MS analysis of this fraction

gave a single peak with a [M+H$^+$] mass of 6039.0 Da; this corresponds to the molecular weight of the 52mer peptide containing the active site cysteine attached with $(HB)_3$, minus the MW of water (data not shown).

3.4.2 Chemical competence of species I. The definitive distribution of radioactivity observed in Figure 3.1A suggests that species I, II, III, and IV may each represent a different stage of the synthase during the polymerization process, and that the transition from one stage to the next may be mechanistically informative. While species IV might have resulted from protein/polymer aggregation due to *in vitro* conditions and may not be relevant to what is occurring inside the cell, we feel that species I, II, and III may reflect the initiation and elongation process *in vivo*. Since recombinant PhaCPhaE$_{Av}$ is a tetramer (320 KDa), species III could have $(HB)_n$ similar to that of species II but resides in different quaternary structures. Results from our studies with D302A-PhaCPhaE$_{Av}$ strongly suggested that species I might represent a self-primed synthase. To demonstrate the chemical competence of species I, a reaction was performed at a S/E ratio of 5000:1. The results are shown in Figure 3.1B. At this S/E ratio, species I and II are no longer observed, and most of species III has disappeared. Only species IV was observed in significant amount. One could argue that since the SA of substrate was lower than that in reaction shown in Figure 3.1A, the radioactive signal might not have been detected after just ~15 h of exposure to the phosphorimager screen. Therefore, another experiment was carried out to monitor the disappearance of PhaC$_{Av}$ (equivalent to species I) by Coomassie staining as a function of S/E ratio. As shown in Figure 3.2, PhaC$_{Av}$ gradually disappeared from the monomeric position. When a higher amount of synthase was used in the reactions and loaded onto the gel, PhaC$_{Av}$ reappeared near top of the gel and in the well area where species III and IV reside in lanes containing reactions at S/E ratio of 500 and higher (data

not shown). Interestingly, the migratory properties of $PhaE_{Av}$ did not change in any of these reactions. These studies demonstrate that species I and II can be chased into products and are thus chemically competent.

3.4.3 Time-dependence Phenomenon. During the investigation of the polymerization reaction catalyzed by $PhaCPhaE_{Av}$, an initially puzzling but interesting observation was made. Reactions described in Figure 3.1A contain a high concentrations of $PhaCPhaE_{Av}$ (3.3 μM), and a low concentrations of [^{14}C]-HB-CoA (16.5 to 148.5 μM). High concentration of synthase had to be used so that radiolabeled species I could be detected at low S/E ratios. With a specific activity of ~200 U/mg, the synthase consumes all of the substrate within milliseconds, well before the 5 min quenching time chosen for convenience. One would thus not expect the reaction products to differ if the quenching was after total substrate consumption. However, this was not the case. An increase in the amount of species I was observed as a function of quenching time. This phenomenon, hereafter referred to as the time-dependence phenomenon, was first observed when Abs to PHB were used to probed the reaction products by Western blotting (Figure 3.3). The Abs are found to be most specific for the PHB within species I, and they do not cross-react with $PhaCPhaE_{Av}$. The conclusion from this experiment is that, with time, $(HB)_n$ is transferred to apo-$PhaC_{Av}$ or $(HB)_n$-labeled PhaCs (n is low, = 1, 2, or 3) despite the fact that all of the substrate has been consumed. In order to confirm this unexpected result, reactions using radioactive substrate were carried out. The time-dependence phenomenon of species I was reproducible as shown in Figure 3.4B. While the intensity of species I increased from Lane 1 through 4, that of species II gradually decreased (confirmed by quantitative analysis using ImageQuant™ TL software). Even more intriguing is that the amount of protein where species I resides does not appreciably change as a function of time, as shown in Figure 3.4A. This result,

i.e. the amount of $PhaC_{Av}$ remained detectably unchanged, was later confirmed with a more sensitive Western analysis using $PhaCPhaE_{Av}$ Abs, (data not shown).

3.4.4 Removal of CoA can stop the time-dependence phenomenon. The *in vitro* polymerization reaction contains only synthase and substrate HB-CoA. The reaction at the end of polymerization presumably contains $(HB)_n$ covalently labeled synthase and CoA. The observation of increasing amount of radioactivity or $[^{14}C]$-HB_n associated with species I, while the amount of protein associated with species I remained detectably unchanged suggested that somehow HB-CoA could be regenerated and used again by the synthase. Removal of CoA once all substrate is consumed should then eliminate the time-dependence phenomenon if our hypothesis is correct. In order to test this hypothesis, CoA was reacted with DTNB immediately after the substrate was consumed. As shown in Lane 3 of Figure 3.5A, the intensity of species I no longer increased despite the fact that reaction sat for 5 min before quenching with Laemmli buffer (compare results in Lane 2 and 3). In fact, the intensities of both species I and II (Lane 3) are similar to that in Lane 1. It is interesting that the intensity of species II decreased from Lane 1 to 2, suggesting that $[^{14}C]$-HB_n was released from species II.

3.4.5 D302A-PhaCPhaE$_{Av}$ also prevents the time-dependence phenomenon. To identify additional sources that contribute to the time-dependence phenomenon, we again directed our attention to D302. Earlier studies from our group investigating the reaction of wt $PhaCPhaE_{Av}$ with the saturated-trimer CoA (sT-CoA, **4** in Figure 1.9) revealed a 'burst' of 0.5 equivalents of CoA per equivalent of $PhaCPhaE_{Av}$, followed by slow release of CoA. The product of the reaction was identified as sT-acid. The slow release of CoA was no longer observed when D302A synthase was used. We proposed that, in the absence of HB-CoA, D302 could activate a

water molecule to hydrolyze the covalent thioester linkage at C149 (*13*). With this information, we predict that mutating D302 to alanine should maximize the amount of label observed with the synthase and perhaps never allow the time-dependence phenomenon to occur. Longer reaction incubation times were used since the activity of the D302A mutant is approximately 1000 to 1500 fold less than that of wt (*13, 14*). In fact, it takes 1 min for all of the substrate to be consumed in the reaction described in Figure 3.5B. As predicted, incubation of D302A-PhaCPhaE$_{Av}$ with substrate for various periods of time did not lead to increasing amounts of species I (Figure 3.5B). In fact, the amount of label associated with D302A-synthase at the first time point (Lane 1, Figure 3.5B) appeared to be much more than that associated with the wt synthase at any time point (Figure 3.5A). The number of [^{14}C]-HB associated with PhaC$_{Av}$ in each case was quantitated by an alternative method of gel analysis described previously in Chapter 2. Products from similar reactions (both reactions were at S/E=5) were resolved on SDS-PAGE gel which was then cut into pieces and extracted for scintillation counting. In the case of the mutant, there were 2-3 HB units associated with D302A-PhaC$_{Av}$ after the reaction had been incubated for 20 min. In the case of the wt synthase, there were ~ 0.5 HB associated wt-PhaC$_{Av}$ after 5 min of incubation time.

3.4.6 Chasing of radiolabeled species I with cold HB-CoA: species I is chemically competent.

We have recently proposed that species I, synthase with short HB oligomers (HB$_{3\sim10}$), represents an important stage of the synthase during polymerization (*14*). Species I could be the primed synthase or intermediate species on the pathway of PHB polymer elongation. Therefore, species I is required to be chemically competent to fulfill its proposed role(s). As shown in Figure 3.6, when radiolabeled species I, formed at S/E ratio of 45 (Lane 1), was chased with cold HB-CoA at S/E ratio of 1000, most of the radioactivity ended up being associated with species III and IV

(Lane 2). This result demonstrates not only that species I are intermediates on the pathway of PHB polymer formation, but also the transition from species I to species II, III or IV is non-processive since cold HB-CoA is directly added onto the pre-formed [^{14}C]-HB oligomers to form longer oligomers. In fact, all species observed in Lane 1 (Figure 3.6) are intermediates on the pathway of PHB polymer formation, since their intensity decreased significantly (Figure 3.6, Lane 2).

3.4.7 Reactivity of species I, II, and III. Information on the reactivity of species I ~ III can be gained if one monitors the distribution of radiolabel as a small amount of [^{14}C]-HB-CoA is introduced into the reaction mixtures that contain species I, II, and III which are pre-formed with unlabeled HB-CoA. Species IV was not considered since it does not enter the gel and quantitative analysis of this species is therefore not feasible. Results from this study are complicated but informative, and are shown in Figure 3.7. In all reactions, the same amount of [^{14}C]-HB-CoA was added in after the synthase's reaction with cold HB-CoA. We chose a low [^{14}C]-HB-CoA/synthase ratio of 5:1, which is just enough to detect the signals using the phosphorimager. In addition, we chose to react the synthase with cold HB-CoA at two S/E ratios. Reactions at a S/E ratio of 5 allows the detailed study of species I and II, since these two are the dominant intermediate species observed at this ratio, while reaction at a S/E ratio of 180 allows the study of species III. Lane 1 of Figure 3.7 reveals that almost all of the radiolabel is associated with species II after the synthase is reacted with cold HB-CoA at a S/E ratio of 5 for 10 s first, followed by addition of [^{14}C]-HB-CoA and incubated for an additional 10 s. This was not surprising since species II is the dominant species when the synthase was incubated with substrate at a S/E ratio of 5 for only 10 s, as previously shown in Figure 3.5A (Lane 1). When the period of incubation with the labeled substrate is extended to 5 min, the time-dependence

phenomenon of species I is once again observed (Lane 2, Figure 3.7). However, it is now clear that the source of HB or $(HB)_n$ required for the formation of species I after all of the initial substrate is consumed comes from species II. In fact, it comes from the HB units that were most recently added onto the synthase. Quantitative analysis of the phosphorimage revealed that the observed signal intensity of species II in Lane 2 is 50% of that in Lane 1, and the signal intensity of species I in Lane 2 is four fold higher that that in Lane 1. Overall, the total amount of the observed signal intensity in Lane 2 is 20% less than that in Lane 1, despite the fact that the same amount of radioactivity was used in both reactions. Lane 2 of Figure 3.7 provides a preview to what was contained in the reaction shown in Lane 3 before [^{14}C]-HB-CoA was added in (since the synthase in Lane 3 was incubated with cold substrate for 5 min initially). Species I observed in Lane 2 was mostly gone in Lane 3, suggesting that species I is more reactive or as reactive as species II. When incubation with labeled substrate is extended to 5 min, species I again returns as shown in Lane 4, although the amount seems to be less. The same type of analysis was applied to the reactions shown in Lane 5 and 6, which contained cold HB-CoA/synthase ratio of 180. Results from Lane 5 suggest that species III is far more reactive than II, since most of the radioactivity is associated with III. It is rather difficult to compare the activity of I and III, since the amount of I present is limited, and one cannot distinguish whether I disappeared first before, during, or after additional [^{14}C]-HB-CoA was added onto III. It is clear however that the amount of species I shown in Lane 6 is much less than that shown in Lanes 2 and 4. One explanation is that the extent of the time-dependence phenomenon decreases as S/E ratio increases. This is reasonable since, at higher S/E ratios, longer HB oligomers are expected to form which may be less prone to hydrolysis. Overall, the sum of the radiolabel intensity shown in Lane 5 and 6 is much greater than that shown in Lanes 1 through 4 despite the fact that the same amount of

radiolabel was applied in all reactions. This observation confirms that species formed at low S/E ratios, such as 5, are prone to hydrolysis which leads to a low recovery of radioactivity; those formed at higher S/E ratios are more stable.

3.4.8 Kinetics of the polymerization reaction catalyzed by wt PhaCPhaE$_{Av}$ monitored by anti-PhaCPhaE$_{Av}$ Western blot. All reactions described above contained high concentrations of synthase (μM range) and low S/E ratios. As a result, only the end-products of the reactions were analyzed. In an effort to better understand the *in vitro* polymerization catalyzed by PhaCPhaE$_{Av}$, we decided to follow the kinetics of the reaction by Western blotting using Abs to PhaCPhaE$_{Av}$. This method is appropriate since only small amounts (ng) of synthase are used in the reaction, and this amount can be detected by Western. Autoradiography monitoring the formation of [^{14}C] labeled species I and II would not be informative since the specific activity of the substrate would need to be on the order of 10^{10} cpm/μmol in order for them to be detectable by phosphorimage given the low amounts of protein. To slow down the reaction, it was carried out at room temperature rather than the normal temperature of 30°C. Release of CoA was also monitored in a duplicate reaction by the standard DTNB assay (*12*). At 10 nM of PhaCPhaE$_{Av}$ and 0.7 mM of HB-CoA (S/E=70,000) (typical Class III synthase assay conditions), a typical profile of CoA release was obtained as shown in Figure 3.8B. The surprise observation is apparent from the Western blot shown in Figure 3.8A. Within the first 10 s of the reaction, all of the PhaC$_{Av}$ has disappeared. This was anticipated since results from Figure 3.2 have already demonstrated that all PhaC$_{Av}$ of the synthase associates with the product at S/E >1000. The time-dependence phenomenon is irrelevant at such high S/E ratios. Therefore, at a S/E ratio of 70,000, one does not expect to see PhaC$_{Av}$ at its monomeric position during any time period. However, as the reaction proceeds, PhaC$_{Av}$ gradually reappears, most clearly in Lanes 6, 7 and 8

(Figure 3.8A), which contain reactions that were quenched after 120, 240, and 480 s, respectively. This was unexpected! Where does this PhaC come from? The CoA release assay (Figure 3.8B) shows that at 120 s, approximately 16% of the substrate has been consumed. This corresponded to a S/E ratio of 11200, indicating that at 120 s, the molecular weight of the polymer formed should be about 1 MDa if the synthase exhibits uniform loading. The molecular weight of a PHB polymer formed by PhaCPhaE$_{Av}$ *in vitro* has previously been determined by Jossek *et al.* to be (1- 2) x 10^6 g/mol (*17*). Thus, it is interesting that PhaC precisely re-appears once the synthesis of a PHB polymer is complete. The interpretation of this result will be discussed below.

3.4.9 Labeling of recombinant Class I synthase PhaC$_{We}$. The observation of intermediate species in the reactions catalyzed by recombinant Class III synthase PhaCPhaE$_{Av}$ led us to apply similar study to the recombinant Class I synthase PhaC$_{We}$. Autoradiography results in Figure 3.9 unambiguously show that recombinant PhaC$_{We}$ does not exhibit uniform loading of the substrate, supporting previous studies (*6*). All radioactivity ends up in the well area of the gel at low S/E ratios (e.g., 30) while most of the synthases remain unmodified as revealed when the gel used for autoradiography is Coomassie-stained or probed with Abs to PhaC$_{We}$ (data not shown). In fact, even at S/E ratios of 5, the same results are observed (data not shown). However, at high enough S/E ratios (>200:1), small amounts of radioactivity are observed at the monomeric position of PhaC (Figure 3.9, Lanes 4 and 5). These species are proposed to be similar to the species I observed with the Class III PhaCPhaE$_{Av}$ system.

3.5 DISCUSSION

In the present chapter, we report our continuing efforts to understand the *in vitro* polymerization catalyzed by recombinant Class III synthase PhaCPhaE$_{Av}$, with the hope to better understand this non-template driven process. Previously, we presented the first direct evidence of HB oligomers ranging in length from trimers to decamers covalently attached to the active site cysteine (C149) through thioester linkage by using D302A-PhaCPhaE$_{Av}$, a mutant that is severely impaired in the elongation process (Chapter 2). Those intermediate species are believed to be the same as those categorized as species I described in this chapter, given the similarities of their migratory properties on SDS-PAGE gel. In addition, we have also isolated and identified the same 52mer peptide with (HB)$_3$ attached from a reaction containing wt PhaCPhaE$_{Av}$ at a S/E ratio of 1. When compared to D302A-PhaCPhaE$_{Av}$ at low S/E ratios (<100) (*14*), it is clear that uniform loading is not occurring in the reaction containing wt synthase and HB-CoA at low S/E ratios. In other words, the polydispersity of the polymers or oligomers formed is greater for the wt enzyme than for D302A mutant. Uniform loading may occur if all the synthase can be loaded. The polymerization process *in W. eutropha* is a carefully orchestrated process and most likely involves additional proteins such as PhaP. In addition, the rate of delivery of substrate is also controlled, unlike the *in vitro* conditions. Therefore, although it initially appeared that wt PhaCPhaE$_{Av}$ does not uniformly load (Figure 3.1), the reaction catalyzed by the synthase is more uniform than expected considering that only the synthase and substrate were in the reaction. The reaction catalyzed by recombinant Class I synthase PhaC$_{We}$, on the other hand, is non-uniform (Figure 3.9).

We have gone on to demonstrate that species I is chemically competent, and represents intermediates in the synthesis of large PHB polymers. Species I can only be observed at low S/E

ratios when there is not enough substrate to form large polymers. Our model is that species I results from self-priming by the synthase. Self-priming is a mechanism of initiation that is observed with some polymerases, such as bacterial glycogen synthase from *Agrobacterium tumefaciens* (*11*), that drives the non-template polymerization process. *In vitro*, the *A. tumefaciens* glycogen synthase is able to synthesize its own primers by transferring glucose residues from ADP-glucose onto itself; the primed synthase then serves as a substrate for elongation (*11*). This is what we have also observed with the Class III synthase PhaCPhaE$_{Av}$ *in vitro*. In addition, it seems that there are additional stages that the synthase goes through during polymerization. Species II, III, and IV are indicative of those stages. In fact, we have demonstrated that species II and III are also intermediates in the synthesis of PHB polymer. Their identification is currently unknown. Possibilities include a different oligomeric state of the synthase with the same size of HB oligomer or a much longer HB oligomer attached. It is possible that only when the HB oligomer reaches a certain length, then does the transition from species I, to II, to III occurs.

The time-dependence phenomenon observed with species I at low S/E ratios (< 200), and the re-appearance of PhaC at its monomeric position subsequent to the completion of the synthesis of a PHB polymer with a molecular weight of 1 MDa at high S/E ratios (Figure 8A) led us to propose that PhaCPhaE$_{Av}$ is a versatile enzyme (Scheme 3.3). In addition to being a polymerase, it has other undiscovered chemical roles, and these roles are highly dependent on the availability of the substrate HB-CoA.

Analysis of reactions with CoA removed by DTNB (Figure 3.5A) and those with D302A-PhaCPhaE$_{Av}$ (Figure 3.5B) suggests that the time-dependence phenomenon can be a result of several reactions. First, D302 of PhaC is directly responsible for this process. When this residue

is changed to A, the reaction described in Scheme 3.1 does not occur. This reaction has been previously observed with wt PhaCPhaE$_{Av}$ and sT-CoA (**4**, Figure 1.9), as described in the introduction. The detection of saturated-trimer acid (n = 2, Scheme 3.1) indicates that a HB oligomer that is 3 units long can still be hydrolyzed. Intuitively, this process will most likely occur more frequently with only 1 or 2 HB units attached to the active-site cysteine (n=0 or 1, Scheme 3.3). This explains the lower recovery of radioactivity for wt-PhaC$_{Av}$ when compared to that for D302A-PhaC$_{Av}$. This is also the reason why we were able to successfully isolate D302A-PhaC$_{Av}$ with (HB)$_n$ covalently bound, as the intermediate species is more stable (Chapter 2). Second, removal of the side product CoA from the reaction mixture seems to prevent the return of species I (Figure 3.5A), suggesting that the reaction shown in Scheme 3.2 occurs. The polymerization of HB-CoA by the synthase has always been considered irreversible. However, at low S/E ratios, Scheme 3.2 must be considered. Formation of HB-CoA through transesterification provides regenerated substrate that can be used. The increased levels of species I as a function of time strongly suggests the increased stability of species I, which can result when the newly formed HB-CoA is added onto primed synthase or synthase with longer HB oligomers which could be more reactive and less prone to hydrolysis. The caveat of this experiment is that the observed effect of DTNB may not be through removal of CoA. DTNB could interfere with other amino acid residues of the synthase, resulting in a synthase that is unable to carry out the reaction which is responsible for the time-dependence phenomenon. Third, the observation made in Lanes 1 and 2 of Figure 3.7 suggests that the reaction shown in Scheme 3.3 is possible. Currently, this is our favored model. When wt PhaCPhaE$_{Av}$ was briefly incubated with unlabeled substrate first at a S/E ratio of 5, followed by incubation with radiolabeled substrate for 10 sec or 5 min (envision that the HB oligomer already attached to the

cysteine is unlabeled and the incoming substrate is radioactive in Scheme 3.3), the increased amount of radioactivity associated with species I as a function of time (compare Lanes 1 and 2 in Figure 3.7) indicates that the most recent HB units that are being added onto species II now becomes associated with species I. Scheme 3.3 shows how this could happen. In the absence of additional substrates, species II could be unstable. Its HB oligomer chain is prone to attack by a nucleophile (this could be an amino acid or deprotonated water molecule; it is expressed as Nu in Scheme 3.3) that is positioned to catalyze the chain transfer step. Therefore, Scheme 3.3 predicts the loss of total recoverable radioactivity (resulting from the loss of the HB oligomers attached to Nu shown in Scheme 3.3) as species II transitions into species I. Quantitative analysis of the phosphorimage confirms this prediction. Approximately 20% of the total radioactivity (all from species II) was lost during this transition. Assuming ~ 5% of the $PhaC_{Av}$ is associated with species II in Lane 1, the average length of HB oligomers attached to $PhaC_{Av}$ is calculated to be 40 – 50 units long. Comparison of the signals of species II in Lane 1 and 2 revealed that half of the species II in Lane 1 had undergone the transition to form species I. During this process, half of the radioactivity was lost, while the other half remained attached to the $PhaC_{Av}$. It is calculated that a HB oligomer approximately 20 units long remain attached to $PhaC_{Av}$ originated from species II shown in Lane 1. The addition of 2.5% of $PhaC_{Av}$ with a HB oligomer of 20 units long to species I in Lane 1 can account for the increase of intensity of species I from Lane1 to Lane 2. Since the amount of $PhaC_{Av}$ remaining at the monomeric position (40 KDa) in Lane 1 and 2 only increased from 95% to ~ 97.5%, this difference cannot be detected by Coomassie staining and Western due to the detection limit of both methods. Therefore, the increasing amounts of species I as a function time observed in Figure 3.3, 3.4, 3.5A, and 3.7 most likely result from species II whose HB oligomers was cleaved off at approximately 20 HB units away

from the active site C149. Because the synthase with a 20 mer HB oligomer is less prone to hydrolysis by D302, this product (a member of species I) was observed to increase over time.

The re-appearance of $PhaC_{Av}$ (Figure 3.8A) at S/E ratios as high as 70,000 was also perplexing at first. From Figure 3.2, it is clear that as the S/E ratio increases from 100 to 5000, the amount of unmodified synthase decreases drastically. All $PhaC_{Av}$ was expected to be associated with PHB polymer; therefore, the return of unassociated $PhaC_{Av}$ was unexpected. Our recent *in vivo* quantitative study of *W. eutropha* under transient PHB formation and non-transient PHB accumulation conditions demonstrated that $PhaC_{We}$ is required to re-initiate in order to account for the amount of PHB granules generated inside the cell and the size of the polymer (*18, 19*). Jossek *et al* has also demonstrated that each $PhaCPhaE_{Av}$ generates ~25 polyester chains, each with a mass of ~ 1.6×10^6 g/mol, while studying the granules formed by $PhaCPhaE_{Av}$ *in vitro* at a high concentration of substrate (13.4 mM) and a low concentration of synthase (nM) (*17*). Therefore, the need for synthase to re-initiate is a common theme observed with both classes of synthase *in vivo* or *in vitro*. How is this accomplished if it is assumed that the synthase is attached to the polymer product? The Western results shown in Figure 3.8A suggests that this assumption is incorrect. It is interesting that the reappearance of free $PhaC_{Av}$ corresponds to when the synthesis of polymers with molar mass of 10^6 g/mol has been completed. Therefore, we believe that the $PhaC_{Av}$ observed in Lane 6 through 8 (Figure 3.8A) corresponds to the primed synthase ready for re-initiation. The re-appearance of $PhaC_{Av}$ at its monomeric position of the blot strongly suggests that, for synthase to re-initiate, $PhaC_{Av}$ is able to disengage from the polymer chain so that it can proceed with re-initiation. Therefore, the synthase is proposed to also have a hydrolase activity; this mechanism is proposed in Scheme 3.3. Note that Scheme 3.3 proposes that there are two channels within each monomeric

synthase. As no X-ray structure of the PHB synthase is available at present, this model is based on a similar model for the surfactin synthase, also an α/β hydrolase (*20*). In Scheme 3.3, a nucleophile is proposed to catalyze the chain-transfer reaction. Its candidate includes D84, D177, D251, S90, Y81, or H303 (numbering based on $PhaC_{Av}$), which are all conserved amino acid residues among the Class I and III synthases with no functions thus far unidentified. Hydrolysis can occur once the polymer chain is transferred onto to the putative amino acid residues. Alternatively, a water molecule can be activated by one of the conserved amino acids and can attack the polymer chain directly. The synthase is proposed to have the ability to sense the size of the polymer chain, perhaps by the curvature of the polymer. When the synthesis of one chain is complete, the synthase catalyzes chain termination. The breakpoint will mostly likely greater than $(HB)_3$ (the length of the oligomers associated with species I) to leave primed synthase for re-initiation. When the S/E ratio is low, the reaction shown in Scheme 3.3 may also occur to abort the polymerization. The amino acid(s) directly or indirectly responsible for the hydrolase activity do not have to be on the same monomer where the active cysteine resides. Although the active form of the synthase has been determined to be the dimeric form based on our radiolabeling result (0.5 equivalent of **4** (Figure 1.9) per monomer PhaC in the case of recombinant $PhaC_{We}$, and 0.5 equivalent of CoA release from **4** per monomer $PhaCPhaE_{Av}$), one monomer could play a role in synthesis while the other participates only in chain termination.

At nM concentrations of synthase and mM concentrations of HB-CoA, a typical CoA release profile (Figure 3.8B) by the Class III synthase has a burst phase followed by slow release of CoA. The sudden change in the rate of CoA release could be attributed to the time required for synthase re-initiation to take place. It is unclear whether $PhaC_{Av}$ returns as primed synthase (species I) or as the oligomer-free synthase (depends on the breakpoint of the polymer) since it is

difficult to distinguish between the two based on their position on the gel. In addition, we didn't have access to ^{14}C-labeled substrate that has a specific activity of 10^{10} cpm/μmol required to quantitate species I formed with nM amount of synthase.

We believe that primed synthase was also observed with recombinant Class I $PhaC_{We}$ (Figure 3.9). However, the study of this synthase is complicated by the fact that it does not uniformly load substrate. Comparing autoradiographs from Figure 3.1 and Figure 3.9, it is clear that wt $PhaCPhaE_{Av}$ loads substrate much more uniformly than $PhaC_{We}$. Otherwise, it wouldn't have been possible to capture $PhaC_{Av}$ with trimer HB units attached at a S/E ratio of 1. It is evident that the polymerization reaction catalyzed by recombinant $PhaC_{We}$ *in vitro* system is missing a factor or factors, perhaps a $PhaE_{Av}$ equivalent. We attempted to isolate the native $PhaC_{We}$ from its host by using a mutant *W. eutropha* strain with this synthase gene replaced with the same gene with $(His)_6$-tag attached at its N-terminus. The his-tag did not facilitate synthase isolation, and synthase was isolated with low purity (~20%, data not shown). The kinetics of CoA release of this 'protein mixture' however differs from that of recombinant $PhaC_{We}$, in that the lag phase was no longer observed. The discrepancy observed is a clear indication that either native and recombinant Class I synthase are different, or that the 'protein mixture' contains factor(s) that are important in initiation.

To summarize, we have demonstrated that Class III $PhaCPhaE_{Av}$ synthase initiates polymerization through self-priming. The primed synthase, species I, can serve as substrates for further PHB elongation. Since HB units can be added onto existing polymers when fresh HB-CoA is introduced into a reaction mixture containing pre-formed intermediate species, the reaction catalyzed by $PhaCPhaE_{Av}$ is non-processive. The caveat is that we have only observed species I, II, and III at low S/E ratios. Therefore, when enough HB-CoA is available to form a

polymer, the polymerization may be processive, similar to what has been observed with the polyphosphate kinase (*21*). The synthase is also proposed to have hydrolase activity that allows the synthase itself to control the polymer size and reinitiate. Further investigations are necessary and are underway in our lab.

3.6 ACKNOWLEDGEMENTS

I would like to thank Metabolix, Inc. for providing us with anti-PHB antibodies.

3.7 REFERENCE

1. Byrom, D. (1987) Polymer Synthesis by Microorganisms: Technology and Economics, *Trends Biotechnol. 5*, 246-250.
2. Anderson, A.J. and Dawes, E.A. (1990) Occurrence, Metabolism, Metabolic Role, and Industrial Uses of Bacterial Polyhydroxyalkanoates, *Microbiol. Rev. 54*, 450-472.
3. Madison, L.L. and Huisman, G.W. (1999) Metabolic engineering of poly(3-hydroxyalkanoates): From DNA to plastic, *Microbiol. Mol. Biol. Rev. 63*, 21-53.
4. Rehm, B.H. and Steinbüchel, A. (1999) Biochemical and genetic analysis of PHA synthases and other proteins required for PHA synthesis, *Int. J. Biol. Macromol. 25*, 3-19.
5. Rehm, B.H. (2003) Polyester synthases: natural catalysts for plastics, *Biochem J 376*, 15-33.
6. Stubbe, J. and Tian, J. (2003) Polyhydroxyalkanoate (PHA) homeostasis: the role of PHA synthase, *Nat Prod Rep 20*, 445-457.

7. Gerngross, T.U., Snell, K.D., Peoples, O.P., Sinskey, A.J., Cushai, E., Masamune, S., and Stubbe, J. (1994) Overexpression and purification of the soluble polyhydroxyalkanoate synthase from *Alcaligenes eutrophus*: Evidence for a required posttranslational modification for catalytic activity, *Biochemistry 33*, 9311-9320.

8. Liebergesell, M., Sonomoto, K., Madkour, M., Mayer, F., and Steinbuchel, A. (1994) Purification and characterization of the poly(hydroxyalkanoic acid) synthase from *Chromatium vinosum* and localization of the enzyme at the surface of poly(hydroxyalkanoic acid) granules, *Eur J Biochem 226*, 71-80.

9. Alonso, M.D., Lomako, J., Lomako, W.A., and Whelan, W.J. (1995) A new look at the biogenesis of glycogen, *FASEB J. 9*, 1126-1137.

10. Zeeman, S.C., Smith, S.M., and Smith, A.M. (2002) The priming of amylose synthesis in *Arabidopsis* leaves, *Plant Physiol 128*, 1069-1076.

11. Ugalde, J.E., Parodi, A.J., and Ugalde, R.A. (2003) De novo synthesis of bacterial glycogen: *Agrobacterium tumefaciens* glycogen synthase is involved in glucan initiation and elongation, *Proc Natl Acad Sci U S A 100*, 10659-10663.

12. Müh, U., Sinskey, A.J., Kirby, D.P., Lane, W.S., and Stubbe, J. (1999) PHA synthase from *Chromatium vinosum*: Cysteine 149 is involved in covalent catalysis, *Biochemistry 38*, 826-837.

13. Jia, Y., Kappock, T.J., Frick, T., Sinskey, A.J., and Stubbe, J. (2000) Lipases provide a new mechanistic model for polyhydroxybutyrate (PHB) synthases: Characterization of the functional residues in *Chromatium vinosum* PHB synthase, *Biochemistry 39*, 3927-3936.

14. Tian, J., Sinskey, A.J., and Stubbe, J. (2004) Detection of Intermediates from the Polymerization Reaction Catalyzed by a D302A Mutant of Class III Polyhydroxyalkanoate (PHA) Synthase, *Biochemistry.*

15. Yuan, W., Jia, Y., Tian, J., Snell, K.D., Muh, U., Sinskey, A.J., Lambalot, R.H., Walsh, C.T., and Stubbe, J. (2001) Class I and III polyhydroxyalkanoate synthases from *Ralstonia eutropha* and *Allochromatium vinosum*: characterization and substrate specificity studies, *Arch Biochem Biophys 394*, 87-98.

16. Laemmli, U.K. (1970) Cleavage of structural proteins during the assembly of the head of bacteriophage T4., *Nature 227*, 680-685.

17. Jossek, R., Reichelt, R., and Steinbüchel, A. (*1998*) *In vitro* biosynthesis of poly(hydroxybutyric acid) by using purified poly(hydroxyalkanoic acid) synthase of *Chromatium vinosum*, *Appl. Microbiol. Biotechnol. 49*, 258-266.

18. Tian, J., He, A., Lawrence, A., Liu, P., Watson, N., Sinskey, A.J., and Stubbe, J. (2004) Analysis of Transient Polyhydroxybutyrate Production in *Wautersia eutropha* H16 by Quantitative Westerns and Transmission Electron Microscopy, *manuscript submitted for publication.*

19. He, A., Tian, J., Lawrence, A., Liu, P., Sinskey, A.J., and Stubbe, J. (2004) Expression Analysis of Proteins Involved in Polyhydroxybutyrate Homeostasis in *Wautersia eutropha* H16, *submitted for publication.*

20. Bruner, S.D., Weber, T., Kohli, R.M., Schwarzer, D., Marahiel, M.A., Walsh, C.T., and Stubbs, M.T. (2002) Structural basis for the cyclization of the lipopeptide antibiotic surfactin by the thioesterase domain SrfTE, *Structure (Camb) 10*, 301-310.

21. Ahn, K. and Kornberg, A. (1990) Polyphosphate kinase from *Escherichia coli.* Purification and demonstration of a phosphoenzyme intermediate., *J. Biol. Chem. 265*, 11734-11739.

3.8 SCHEMES AND FIGURES

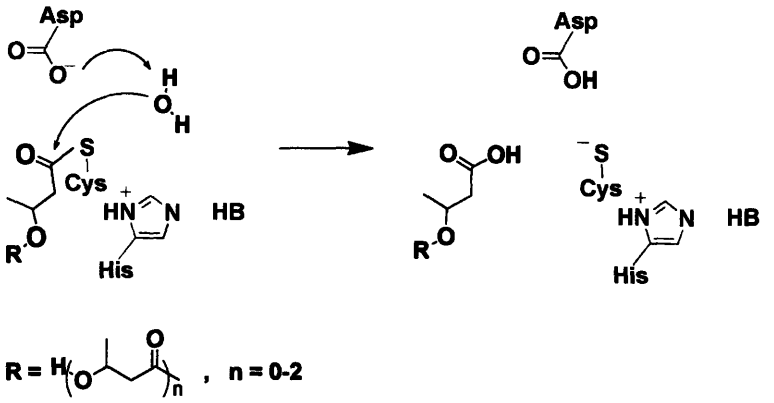

Scheme 3.1 Hydrolysis of covalently attached HB oligomer by D302 of $PhaC_{Av}$ at low S/E ratios.

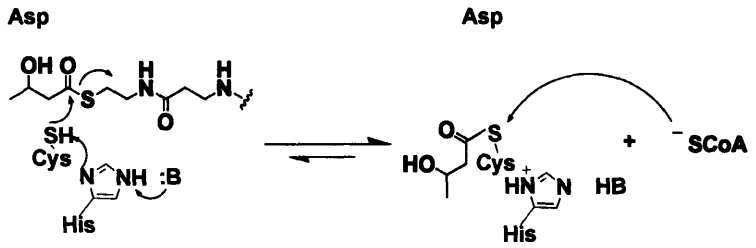

Scheme 3.2 Regeneration of HB-CoA through transesterification by the synthase at low S/E ratios.

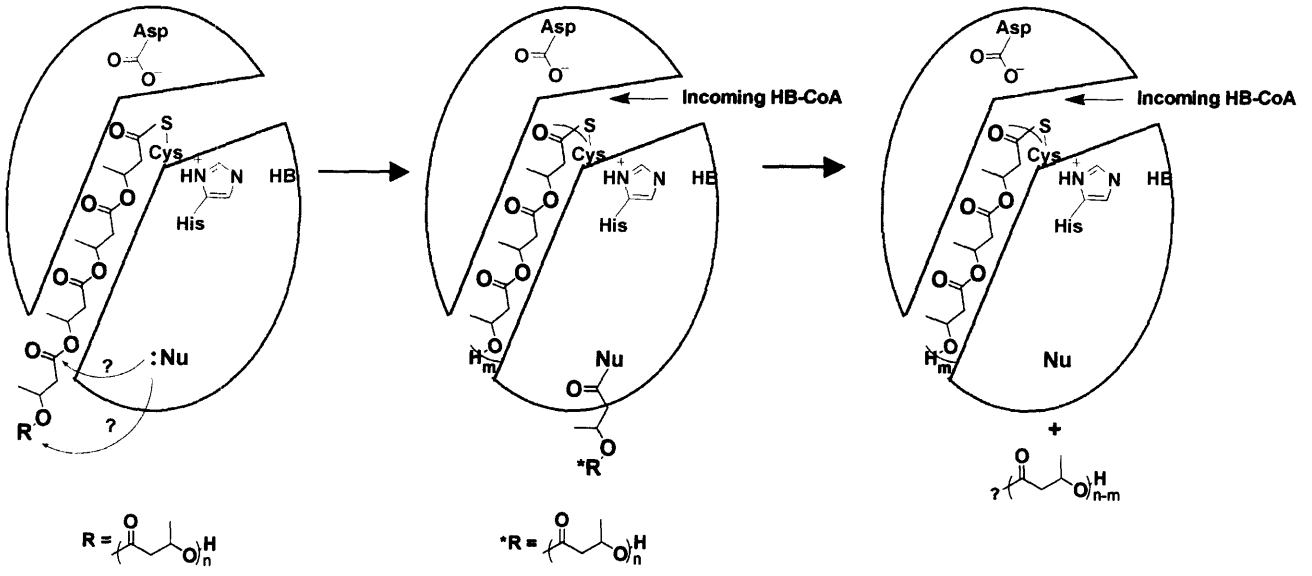

Scheme 3.3 A nucleophile (Nu) of the synthase is proposed to catalyze the polymer chain transfer, resulting in primed synthase.

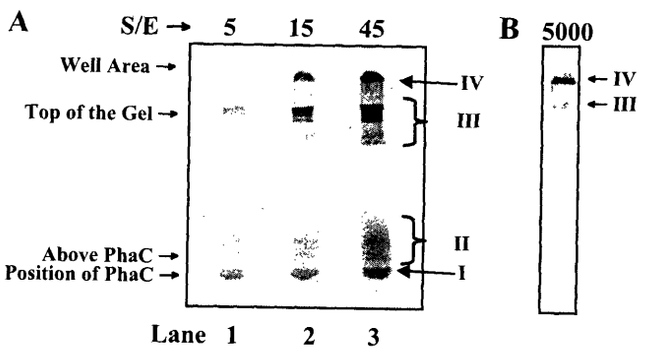

Figure 3.1 10% SDS-PAGE gel analyzed by phosphorimaging. The reaction contained 3.3 μM of PhaCPhaE$_{Av}$ and [^{14}C]-HB-CoA (SA of 2.6 x 10^{7}cpm/μmol) at increasing S/E ratios. (**A**) Lanes 1 through 3 correspond to S/E ratio of 5, 15, and 45, respectively. The specific activity (SA) of the substrate used. Species III but not species IV is able to enter the stacking gel. (B) Phosphorimage demonstrating the chemical competence of species I and II at a S/E of 5000. SA of substrate was 2.4 x 10^{5} cpm/μmol.

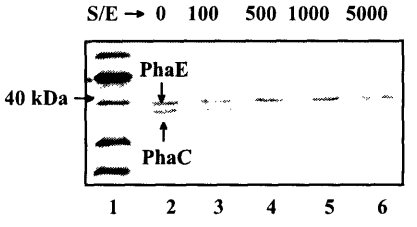

Figure 3.2 Coomassie-stained SDS-PAGE gel shows disappearance of $PhaC_{Av}$ as the S/E ratio increases. [$PhaCPhaE_{Av}$]=0.37 μM. Lane 1, MW stds; Lanes 2 through 6 have a S/E ratio of 0, 100, 500, 1000, and 5000, respectively. Unlabeled (*R*)-HB-CoA was used in this experiment.

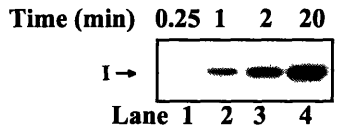

Figure 3.3 Western blot using PHB Abs showing the time-dependence associated with species I. PhaCPhaE$_{Av}$, 1.25 μM, was incubated with 18.75 μM of unlabeled (*R*)-HB-CoA (S/E=15) in a final volume of 70 μL at 30°C. At this concentration of synthase, all of the substrate is consumed in < 1 sec. At 0.25, 1, 2, and 20 min (Lanes 1 through 4, respectively), 15 μL was removed from the reaction mixture and quenched with an equal volume of Laemmli buffer without reducing reagent. All reaction products were resolved on SDS-PAGE gel, then transferred onto a PVDF membrane and probed with PHB Abs. Each lane contains equal amounts of protein (~1.5 μg).

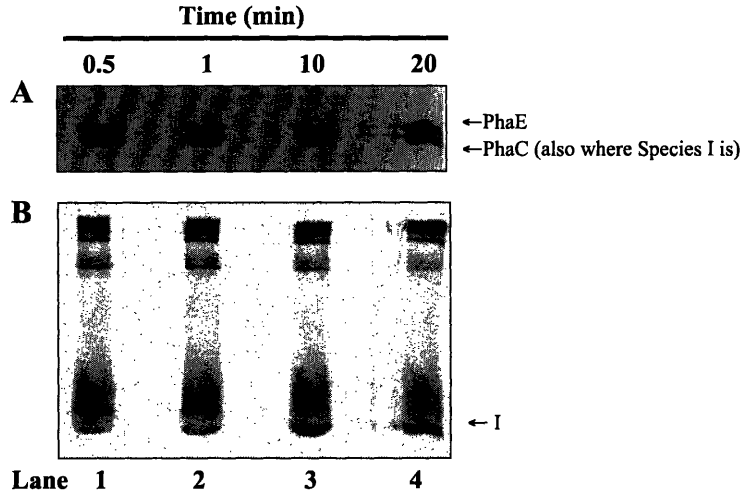

Figure 3.4 Time-dependence phenomenon observed with wt PhaCPhaE$_{Av}$ and [^{14}C]-HB-CoA. In a final volume of 45 μL, 3.5 μM of PhaCPhaE$_{Av}$ was reacted with 158 μM of [^{14}C]-HB-CoA (S/E=45) in assay buffer. At 0.5, 1, 10, and 20 min, 10 μL of the reaction mixture was removed and quenched with equal volumes of Laemmli buffer without reducing reagent. The reaction products were resolved on SDS-PAGE gel. (**A**) Part of the Coomassie-stained gel. (**B**) Autoradiography of the same gel shown in (**A**) after it was dried.

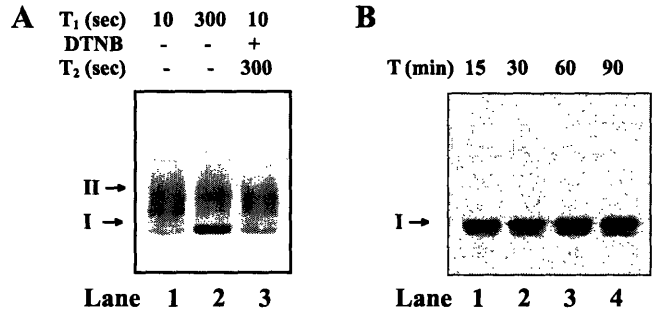

Figure 3.5 Autoradiography demonstrating the elimination of the time-dependence phenomenon by (**A**) removal of CoA, or (**B**) use of D302A-PhaCPhaE$_{Av}$. (**A**) Triplicates of reaction containing 3.3 μM wt PhaCPhaE$_{Av}$ and 16.5 μM of [^{14}C]-HB-CoA (S/E=5) were prepared and treated as follows: Lanes 1 and 2, reaction stopped after 10 sec and 5 min, respectively; Lane 3, DTNB was added after 10 sec at a DTNB:HB-CoA ratio of 91 and the reaction was incubated for another 5 min before Laemmli buffer was added. (**B**) A reaction containing 5 μM of D302A-PhaCPhaE$_{Av}$ and 50 μM of [^{14}C]-HB-CoA was prepared in quadruplicates. Lanes 1 through 4, the reaction was quenched at 15, 30, 60, and 90 min, respectively.

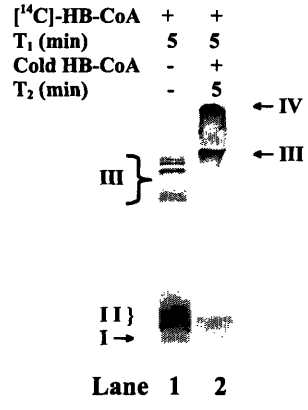

Figure 3.6 Chasing radiolabeled species with cold HB-CoA. A reaction containing 3.3 μM PhaCPhaE$_{Av}$ and 148 μM [^{14}C]-HB-CoA (S/E=45) was prepared in duplicates. After 5 min of incubation (T_1), one reaction was quenched with Laemmli buffer (Lane 1) while additional cold HB-CoA was added to the other at a S/E ratio of 1000 and the reaction was allowed to proceed for another 5 min (T_2) before being quenched (Lane 2). Autoradiography of the gel that resolved the reaction products is shown.

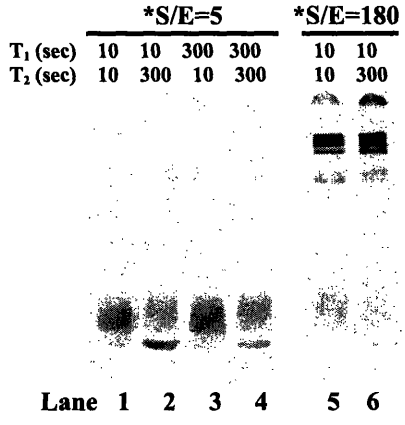

Figure 3.7 Autoradiography revealing the reactivity of species I, II, III, and IV. A reaction containing 3.3 μM PhaCPhaE$_{Av}$ and 16.5 μM of cold HB-CoA (*S/E=5) was prepared in quadruplicates and treated as follows: Lanes 1 and 2, additional [^{14}C]-HB-CoA was added after 10 sec and was allowed to react for either 10 sec or 5min, respectively, before quenching with Laemmli buffer; Lanes 3 and 4, additional [^{14}C]-HB-CoA was added after 5 min and was allowed to react for either 10 sec or 5 min before being quenched. Lanes 5 and 6 contain reactions that were treated similarly as those described in Lanes 1 and 2, with the exception that 600 μM of cold HB-CoA was used in the initial reaction (*S/E=180). The amount of [^{14}C]-HB-CoA added to each reaction was exactly the same, at [^{14}C]-HB-CoA:PhaCPhaE$_{Av}$ ratio of 5. T_1 and T_2 refers to the reaction time with cold and hot substrate, respectively.

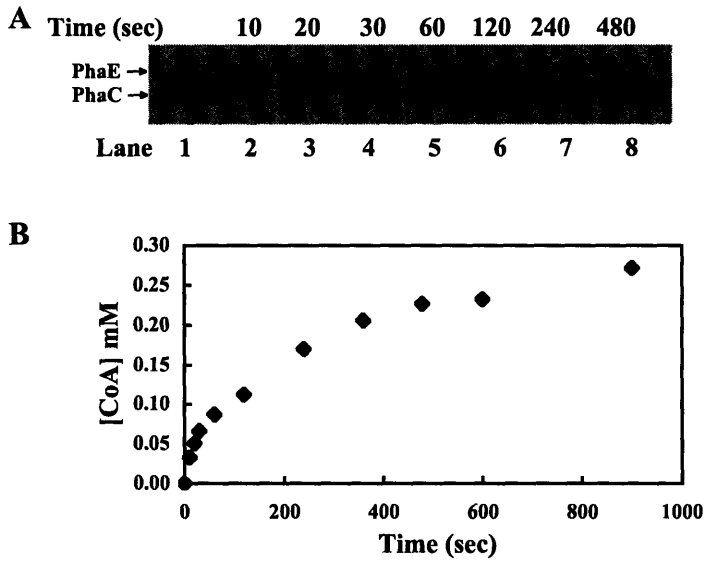

Figure 3.8 Kinetics of wt PhaCPhaE$_{Av}$ monitored by Western blot using Abs to PhaCPhaE$_{Av}$ (**A**). In a final volume of 80 μL, 10 nM PhaCPhaE$_{Av}$ was reacted with 0.7 mM cold HB-CoA (S/E=70,000) in assay buffer at RT. At 10, 20, 30, 60, 120, 240, and 480 s (Lane 2 through 8, respectively), 10 μL was removed from the reaction mixture and quenched with equal volumes of Laemmli buffer. From this quenched mixture, 18 μL (containing ~ 7.2 ng of PhaCPhaE$_{Av}$) was loaded onto the gel and resolved, followed by transfer to a PVDF membrane and probing with PhaCPhaE$_{Av}$ Abs. Lane 1 contains 7.2 ng of PhaCPhaE$_{Av}$ only. (**B**) Kinetics of the reaction described in (**A**), monitored by release of CoA.

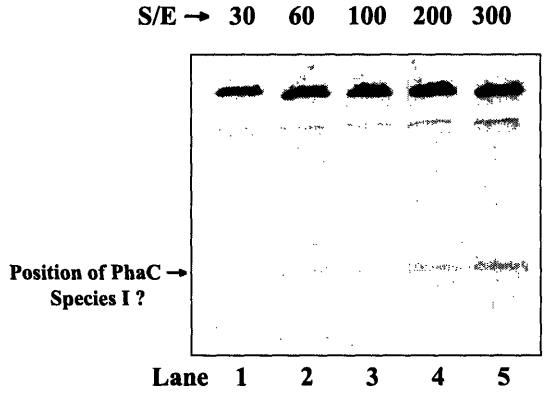

Figure 3.9 Autoradiography of products from reactions containing recombinant $PhaC_{We}$ and [^{14}C]-HB-CoA (7.9 x 10^6 cpm/μmol) at various S/E ratios. [$PhaC_{We}$]=3 μM. Lane 1 through 5, S/E=30, 60, 100, 200, and 300, respectively. The phosphorimage was obtained after 2 days of exposure to the Low-energy screen.

CHAPTER 4

Mechanistic Investigation of the Class I Synthase

4.1 ABSTRACT

Class I synthases catalyze the conversion of β-hydroxybutyryl coenzyme A (HB-CoA) to PHB. The native molecular weight of the protein is a monomer and at high concentrations, it becomes dimeric. The kinetics of polymer production exhibit a long and variable lag phase. Class I synthase from *Wautersia eutropha* has been purified by numerous labs. The reported specific activities vary from 1 to 160 U/mg. An N-terminal $(His)_6$-synthase was constructed, over-expressed in BL21(DE3)pLysS, and purified with specific activity of ~ 40 U/mg. In addition, wt synthase was also over-expressed in UT5600 strain and purified by a modification of the procedure reported by Song *et al* (*1*). In our hands, the synthase purified by this method also has a specific activity of ~ 40 U/mg. The presence of fructose in the reaction buffer did not remove the kinetic lag phase in product formation as reported by Song *et al.* Recombinant synthase was further studied mechanistically with the hope of identifying the active form of the synthase in the initiation process *in vitro* and *in vivo*. Monomeric and dimeric forms of the synthase were separated on and isolated from size-exclusion column, and assayed for activity. Results show that the lag phase is not due to the dimerization of monomer and that the fraction containing protein monomer is as active as that containing protein dimer. The K_D for the protein monomer-dimer equilibrium and the rate constant for dimer dissociation to monomer were determined. It has been well established that recombinant Class I synthase has a much greater rate of elongation than initiation. The mechanism observed *in vitro* would thus make it difficult to control granule formation *in vivo* and hence the *in vitro* results suggested that a factor was missing to make the initiation and elongation rates more equivalent. We therefore constructed a $(His)_6$-tagged Class I synthase gene and carried out a gene replacement with the wt synthase gene in the host organism, *W. eutropha*. The tag was used to facilitate protein purification from

crude cell extracts readily. Despite the successful use of this tag *in vitro*, the synthase from *W. eutropha* could only be purified to 20% homogeneity. The native synthase exhibits different kinetics from the recombinant Class I synthase, and has kinetics similar to the Class III synthase. Thus *W. eutropha* appears to require an additional factor or factors to facilitate uniform loading of its synthase *in vivo*. These factors remain to be identified.

4.2 INTRODUCTION

The prototypical Class I synthase from *Wautersia eutropha* uses short chain 3-hydroxybutyryl-CoA (HB-CoA) and 3-hydroxyvalerate-CoA (HV) thioesters as substrates. It has a subunit molecular weight of 64 KDa and is designated as PhaC. The enzyme over-expressed in *Escherichia coli* and isolated exists in both monomeric and dimeric forms (*2*). The active form of the synthase has always been the subject of interest. Based on results from studies with [^{3}H]-saturated-trimer (**4**, Figure 1.9), a putative primer of the polymerization process from our lab, it has been proposed that dimer is the active form of the synthase during the elongation process (discussed in detail in Chapter 1, section 1.3.4). The active form of the synthase during initiation has not been addressed. Elucidating the active form(s) of the synthase during different stages of polymerization is crucial to understanding the mechanism of the initiation process. Another unusual feature of the recombinant PhaC is its slow release of CoA in the initiation stages of ester formation. The synthase thus exhibits a long and variable lag phase, the basis for which is not understood.

In 1994, we reported the first isolation of *W. eutropha* synthase ($PhaC_{We}$) with a specific activity (SA) of 5-8 U/mg (*2*). Since that time, purification of the same enzyme from a baculovirus expression system has appeared (*3*), as have other purification schemes using our

expression vector (*1, 4-6*). The SAs reported for "homogeneous" protein, however, have varied from 1 to 160 U/mg using the same assay method. In an effort to obtain synthase with reproducible SA and to understand the basis of this variability, we undertook and now report an alternative purification procedure using an N-terminal hexa-histidine tagged synthase ($(His)_6$-synthase) construct. Recently, Song *et al* also developed an alternative purification procedure using a hydrophobic-interaction-column (HIC) (*1*). The homogeneous protein had a reported specific activity (SA) of ~ 10 U/mg. We have purified non-$(His)_6$-tagged synthase using their procedure. Both purification methods (affinity tag and HIC) have resulted > 95% homogeneity synthase with a reproducible SA of ~ 40 U/mg. Purified non-$(His)_6$-tagged synthase was further used in a set of experiments designed to determine the active oligomeric form of the synthase during initiation of polymer formation.

To date, characterization of the Class I synthase has been limited to the recombinant synthase expressed heterologously. The characteristics of the recombinant synthase to that isolated from *W. eutropha* have thus remained unexplored. In Chapter 3, evidence that the Class III synthase/HB oligomer complex is the primed synthase was presented. Although a similar complex was also observed in the recombinant Class I synthase (Chapter 3, section 3.4.9), this synthase does not follow the same kinetic mechanism of initiation. In this case, the elongation rate is much greater than the initiation rate and thus only a small amount of protein is primed. Large polymers or aggregates of polymers are formed immediately by a small fraction of the enzyme. Most of the protein remains unmodified. In the present chapter, results will be presented that show that the Class I synthase PhaC isolated from *W. eutropha* exhibits no lag phase in CoA release used to monitor polymer formation. The reason why recombinant $PhaC_{We}$

does not load HB-CoA uniformly could be that the protein is not appropriately modified or that a factor is missing when the enzyme is over-expressed in *E. coli*.

4.3 MATERIALS AND METHODS

4.3.1 Materials. Hecameg [6-O-(N-heptylcarbamoyl)-methyl-α-D-glucopyranoside] was obtained from Vegatec (Villejuif, France). Isopropyl thio-β-D-galactoside (IPTG) was purchased from Boehringer Mannheim. The expression of plasmids pKAS4 and pHAS carrying $PhaC_{We}$ and $(His)_6$-$PhaC_{We}$, respectively, have been reported (*2, 7*). Production of antibodies to $PhaC_{We}$ has been described previously (*8*). Edman sequencing of protein was carried out by the MIT Biopolymer Laboratory.

4.3.2. Over-expression and purification of $(His)_6$-tagged W. eutropha synthase. $(His)_6$-PhaC was purified from *Escherichia coli* strain BL21(DE3)pLysS harboring pHAS. The culture was grown at 30°C to an OD_{600nm} of 0.6, at which time expression of $(His)_6$-PhaC was induced by adding IPTG to a final concentration of 0.1 mM. After growth for an additional 3 h at 30°C, 2.3 g/L cells were harvested by centrifugation and stored at -80°C.

All purification steps were carried out at 4°C. Cells (~ 13.8 g wet weight) were resuspended in 40 ml of Buffer A (50 mM KPi, pH=7.5, 300 mM NaCl). Cells were lysed by two passes through a French pressure cell at 12,000 psi, and cell debris was removed by centrifugation at 18,000 rpm for 1 h. The crude extract was mixed with Ni-NTA (~20 ml, Qiagen) that had been pre-equilibrated with Buffer A for 30 min. The mixture was poured into a column. The column was washed with 250 ml Buffer B (Buffer A + 20 mM imidazole), and then with 120 ml of Buffer C (20 mM imidazole, pH=7.5, 5% glycerol, 0.05% hecameg). $(His)_6$-PhaC was eluted with Buffer D (250 mM imidazole, pH=7.5, 5% glycerol, 0.05% hecameg), and fractions of 5 ml

were collected. Fractions were analyzed by 12% SDS-PAGE, and those containing the desired protein were combined, concentrated, and buffer exchanged into Buffer E (20 mM KPi, pH=7.5, 5% glycerol, 0.05% hecameg) using an Amicon with YM-30 membrane. Aliquots of the protein were quick-frozen in liquid N_2 and stored at -80°C. To remove protein aggregate, $(His)_6$-PhaC was passed through an analytical size-exclusion column (Bio-Silect SEC250, Biorad) in 50 mM KPi, pH=7.8, 75 mM NaCl at a flow rate of 1 ml/min.

4.3.3 Over-expression and purification of non-$(His)_6$-tagged W. eutropha synthase. The procedure of over-expression of PhaC (no his-tag) in *Escherichia coli* strain UT5600 carrying plasmid pKAS4 is adapted from Gerngross et al (*2*). The culture was grown at 30°C to an OD_{600nm} of 0.6, at which time expression of PhaC was induced by adding IPTG to a final concentration of 0.4 mM. After growth for an additional 4 h at 30°C, 4.5 g/L cells were harvested by centrifugation and stored at -80°C.

The purification procedure reported by Song *et al* (*1*) was modified to isolate the synthase. All purification steps were carried out at 4°C. Cells (~ 7 g wet weight) were resuspended in ~21 ml of 50 mM KPi, pH=7, 5% glycerol buffer. The cell suspension, 7 mL at a time, was sonicated using a microtip on a XL2020-Sonicator (Misonix, NY) at power level 4 for 90 s (0.8 s on, 0.2 s off). Cell debris was removed by centrifugation at 15,000 g for 30 min. The crude extract was filtered through a 0.45 μm Sterile Acrodisc filter (Gelman Science) attached to a syringe. To the filtrate, ammonium sulfate ($(NH_4)_2SO_4$) was added slowly until its final concentration was 15%. The suspension was centrifuged at 15,000 g for 20 min to remove the precipitant. Additional $(NH_4)_2SO_4$ was then added slowly to the supernatant until its final concentration reached 50%. The suspension was centrifuged again at 20,000 g for 20 min. The pellet, which contained PhaC, was saved and redissolved in Buffer A (50 mM KPi, pH=7, 1M

$(NH_4)_2SO_4$, 5% glycerol, and 0.05% hecameg). The mixture was then loaded onto a methyl-hydrophobic interaction column (HIC, ~ 40 mL bed volume, Bio-rad) that had been pre-equilibrated with Buffer A. The column was eluted with a linear gradient of 250 mL Buffer A and 250 mL Buffer B (50 mM KPi, pH=7, 5% glycerol, and 0.05% hecameg). Forty-eight fractions of ~10 ml each were collected and analyzed by 10% SDS-PAGE. Those containing the desired protein (Fraction 35-48) were combined, concentrated, and the buffer was exchanged into Buffer B using an Amicon with YM-30 membrane. PhaC continued to elute at the end of the linear gradient. Additional Buffer B (~ 100 mL) was therefore used to remove the remaining synthase from the column. Seven additional fractions (Fraction 49-55, ~ 10 mL each) containing PhaC were combined and concentrated, separately from Fraction 35-48. Aliquots of the protein were quick-frozen in liquid N_2 and stored at -80°C. To remove protein aggregate, PhaC was passed through an analytical size-exclusion column (Bio-Silect SEC250, Biorad) in 50 mM KPi, pH=7.8, 75 mM NaCl at a flow rate of 1 ml/min. For details, see Section 4.3.5.

4.3.4 Enzyme assay. The synthase was assayed following the procedure described in Jia *et al* (*9*).

4.3.5 Isolation of aggregate, dimer, and monomer fractions of the synthase. Seventy μL of 10 mg/mL recombinant $PhaC_{We}$ without his-tag (700 μg) was injected onto a size-exclusion column (Bio-silect SEC 250-5 column, 300 x 7.8 mm, with a guard column, 50 x 7.8 mm, Bio-rad) running on a BioCAD®SPRINT™ System. This HPLC system was kept in the cold room at 4°C, the temperature at which all column-chromatography was carried out. The running buffer consists of 50 mM KPi, pH=7.5, and 75 mM NaCl. The flow rate was at 1 mL/min. During the 20 min HPLC analysis, fractions containing aggregate, dimer, or monomer were collected and

kept on ice. By measuring A_{280nm} and using an extinction coefficient of 162,000 $M^{-1}cm^{-1}$ (*7*), the concentration of protein in the aggregate, dimer, and monomer fractions were determined to be 0.06, 0.15, and 0.12 mg/mL, respectively. All fractions were then assayed immediately, and 2 μg of protein was used in each assay. The results from these procedures are highly reproducible. Thus, these procedures were routinely used to collect the aggregate, dimer, and monomer fraction of the synthase.

4.3.6 Kinetic studies of dimer-monomer interconversion at 0°C. The same procedure described above was used to collect the fraction containing mostly synthase dimer for this analysis. The dimer fraction was kept at 0°C during the entire analysis. The dimer fraction (100 μL, ~ 15 μg) was analyzed by SEC after 50 min, and its HPLC trace served as the reference for the initial dimer/monomer ratio. We were unable to analyze the dimer fraction immediately upon its collection from the column since each HPLC run took 20 min, and a blank run (also 20 min) with running buffer was run in between each protein injection to wash the column. The dimer/monomer ratio in the dimer fraction was also evaluated after 85, 150, 235, and 1173 min of incubation at 0°C by removing and injecting 100 μL of the same dimer fraction onto the same SEC column at these time points.

4.3.7 Kinetic studies of dimer-monomer interconversion at 22°C. In contrast to incubating the fraction containing mostly dimer synthase at 0°C described above, all incubations were carried out at 22°C. SEC analysis was still carried out at 4°C. The fraction containing mostly synthase dimer was again collected using the procedure described above and kept at 0°C. The first aliquot (100 μL) of the dimer fraction was analyzed by SEC after 50 min, and its HPLC defining the dimer/monomer ratio at this time point is taken as time (T) = 0 at 22°C. The same amount of

dimer fraction was then transferred from 0°C to 22°C. After 5.5 min of incubation at 22°C, this sample was analyzed by SEC. Its HPLC profile is defined as the dimer/monomer ratio at T=5.5 min. This procedure was repeated for samples that had been incubated at 22°C for 10, 15, 30, 45, 75, 137, 360, and 480 min. Buffer injection, that is a blank run, was included after analysis of each protein sample.

A small aliquot of the dimer fraction incubated at 22°C was also removed at T = 0, 1, 2, 3, 4, 5, and 6 h for SDS-PAGE gel analysis. It was important to verify that $PhaC_{We}$ in the dimer fraction remained intact and that no proteolysis occurred.

4.3.8 Growth of W. eutropha gene replacement strains. Growth condition 1. A glycerol stock of gene replacement *W. eutropha* strain Re1092 containing a $PhaC_{We}$ with $(His)_6$-tag engineered at its N-terminus was plated on a Tryptic soy broth-dextrose free (TSB) plate and incubated at 30°C for 2 days. A single colony was then used to inoculate a starting culture of 10 mL TSB medium. The culture was grown at 30°C overnight and used to inoculate 2 × 2L in TSB medium in 6 L-size flasks. The cultures were harvested when the OD reached ~1. A yield of 1.2 g of *W. eutropha* cells per L of culture was obtained. The cells were stored at –80°C until purification.

Growth Condition 2. All growth media used in this condition contained 10 μg/mL gentamicin. A glycerol stock of Re1092 was plated on a LB plate and grown at 30°C for 2 days. A single colony was used to inoculate 2 mL of TSB medium which was then used to inoculate 100 mL of TSB medium. After 12 h (OD = 4.8), 3×10 mL of the 100 mL culture was used to inoculate 3 × 2-L of TSB medium. The cells were grown for 72 h at 30°C. Approximately 50 g of cells were harvested from the 6 L of culture (8.3g/L). The cells were flash frozen and stored at –80°C until purification.

4.3.9 PHB Quantitation. The amount of PHB accumulated by *W. eutropha* cells was quantitated following the procedure described previously (*10*).

4.3.10 Purification of $(His)_6$-PhaC from its native host W. eutropha ($PhaC_{We\_N}$) using Ni-NTA column. Cells grown under Growth Condition 1, 2.5 g, were resuspended in Buffer A (50 mM Kpi, pH=7.5, 300 mM NaCl) at a ratio of 3 mL per g of cells. The mixture was stirred at 4°C until an uniform suspension was reached. The cells were then lysed by sonication using a microtip on XL2020-Sonicator at Power level 4 for 1min (0.8 s on, 0.2 s off). After centrifugation at 18,000 rpm for 25 min, the supernatant was loaded onto a 2.5 mL Ni-NTA column. The flow-through was collected. The column was sequentially washed with 25 mL of Buffer A, 25 mL of Buffer B (50 mM Kpi, pH=7.5, 300 mM NaCl, 20 mM imidazole), 25 mL of Buffer C (60 mM imidazole, pH=7.5, 5% glycerol), and 25 mL of Buffer D (250 mM imidazole, pH=7.5, 5% glycerol). Fractions (6 mL) were collected from each of the above buffer washes, with the exception of the Buffer D wash, from which 1 mL fractions were collected. All fractions were analyzed by 10% SDS-PAGE gels. The fractions from the Buffer D wash were too dilute to observe synthase by a SDS-PAGE gel. Therefore, fractions from this wash were combined and concentrated to 1 mL using Centriprep YM-30 (Millipore). All fractions were stored at –80°C until analysis. A Western blot using antibody (Ab) to $PhaC_{We}$ was carried out to quantitate the amount of synthase present in each fraction.

4.3.11 Purification of $(His)_6$-PhaC from W. eutropha using methyl-HIC column. Native synthase ($PhaC_{We\_N}$) was purified from 30 g of *W. eutropha* cells grown under Growth Condition 2 using a methyl-hydrophobic interaction column following a modification of the procedure by Song *et al* (*1*). The cells, resuspended in 90 mL of 50 mM KPi, pH-7, 5% glycerol, were lysed

by sonication, and DNAse (1200 units) and hecameg (0.05%) were added. After centrifugation, $(NH_4)_2SO_4$ was added to 25% saturation. The solution was spun down and supernatant was collected. To the supernatant, additional $(NH_4)_2SO_4$ was added until 50% saturation. The mixture was centrifuged, and the pellet was redissolved in ~ 9 mL of Buffer 1 (1M $(NH_4)_2SO_4$, 50 mM KPi, pH=7, 5% glycerol, and 0.05% hecameg), and then loaded onto the methyl-HIC column (~ 30 mL) which had been equilibrated in Buffer 1. The column was eluted with a linear gradient of 150 mL of Buffer 1 × 150 mL of Buffer 2 (50 mM KPi, pH=7, 5% glycerol, and 0.05% hecameg). Fractions (~ 6.7 mL) were collected (41 total, named F1-F41). The column was further washed by an additional 50 mL of Buffer 2, the same fraction size was collected (named F42-F48). All fractions were analyzed by 10% SDS-PAGE gel and activity assays. The fractions (F43, 44, 45) that contained the most synthase activity were concentrated individually using a Centricon YM30 (Millipore) and stored at –80°C until analysis. Concentration of the synthase was determined by Western blots.

4.4 RESULTS

4.4.1 Purification and characterization of recombinant W. eutropha PHB synthase with and without $(His)_6$. Since the initial report of recombinant $PhaC_{We}$ purification, the SAs of the protein ranging from 1 to 160 U/mg have been reported for protein that is 95 % homogeneous based on SDS-PAGE. A summary of the SAs from various research groups can be found in Yuan *et al* (*7*). In an effort to obtain an enzyme preparation that results in reproducible activity, we generated an N-terminal $(His)_6$-tagged version of $PhaC_{We}$ (*7*). When over-expressed in *E. coli* BL21(DE3)pLysS strain, a large amount of the synthase (80-90% judging from the induction gel) was found in the insoluble cell suspension (Figure 4.1A, compare lane 2 and 4). $(His)_6$-

$PhaC_{We}$ can be purified using a Ni-NTA agarose column (Figure 4.1B) with a SA of 20 to 30 U/mg. When examined by size-exclusion chromatography (SEC), a significant amount of larger molecular aggregate was revealed in addition to monomer and dimer (data not shown, but similar to that shown in Figure 4.3A). The aggregate is active with a SA of 10-20 U/mg, and the SA of $(His)_6$-$PhaC_{We}$ with the aggregate removed is ~ 40 U/mg (Figure 4.2). Once the aggregate is removed, it does not reappear.

Recently, Song *et al.* also reported a one step purification procedure of synthase using a methyl-HIC column (*1*). The SA of their $PhaC_{We}$ was ~ 10 U/mg. To reproduce their data, PhaC without the $(His)_6$-tag was over-expressed in *E. coli* UT5600 strain. From a comparison of the expression of this construct to that in BL21(DE)3pLysS (Figure 4.1A), it is clear that although the amount of PhaC over-expressed is less in the UT5600 strain (compare Lane 2 vs. 7), most of the PhaC is in the soluble fraction of the cell lysate in this strain (compare Lane 8 vs. 9). A modified version of the Song's purification procedure was used to yield >95% homogeneous synthase (Figure 4.1C) with a SA of ~ 40 U/mg. When examined by SEC, high molecular weight aggregates were also present (Figure 4.3A). Isolated protein aggregate did not reform dimer or monomer (Figure 4.4) and vice versa. The aggregate also had a SA of ~ 20 U/mg (Figure 4.5A). Removal of the aggregate from recombinant $PhaC_{We}$ purified using this method did not improve the SA much (47 vs. 40 U/mg). Therefore, synthase with and without $(His)_6$-tag purified using two different over-expression systems and purification methods yield protein with similar SAs, ~ 40 U/mg.

4.4.2 Effect of fructose. Goodwin and coworkers have recently reported that the presence of high concentrations of fructose (50-70%) in the synthase reaction mixture promotes synthase dimer formation and eliminates the lag phase for CoA release (*6*). They claimed that dimer is the

only active form of the recombinant Class I synthase from *W. eutropha*, and that the monomeric form of the synthase is inactive. We attempted to evaluate the effect of fructose by making our assay buffer 50% in fructose (150 mM KPi, pH=7.2, 0.2% glycerol, 0.05% hecameg, and 50% fructose). We failed to see any increase in CoA release catalyzed by the synthase under these conditions. In fact, not only did the lag phase for CoA release increase, but the synthase also lost most of its activity. Since their publication did not describe the assay in detail, Dr. Zhang, the primary author of the paper, was contacted. According to Dr. Zhang, the assay buffer (100 mM Tris-HCl, pH=8) should not contain any fructose. The synthase should be pre-incubated in 50% fructose solution before being diluted into assay buffer. In addition, their assay mixture does not contain hecameg, although their protein was purified in the presence of this detergent. Despite the fact that these protocols were followed and the recombinant $PhaC_{We}$ was purified by using their HIC procedure, we were unable to detect the removal of the lag phase (Figure 4.6). Instead, a much longer phase was present, and SA of the synthase was only ~ 6 U/mg. When we tried to assay the synthase in their assay buffer alone without introducing fructose at any time as a control, it was found that synthase had lower SA in the Tris-buffer, 17 U/mg vs. our standard 40 U/mg (Figure 4.6).

4.4.3 Determination of K_D for D↔M and k_d for dissociation of dimer (D) to monomer (M). An understanding of the kinetics and thermodynamics of $PhaC_{We}$ dimer/monomer (D/M) interconversion in the presence and absence of HB-CoA is essential in designing experiments to test the active form of the synthase in the initiation process. We have used SEC in an effort to determine the equilibrium constant, K_D, for D↔M and the rate constant, k_d, for dissociation of D to M. Our approach is based on that of Goody *et al*, in their studies on the dimerization of HIV reverse transcriptase (*11, 12*). Since the purified native synthase is inaccessible, recombinant

$PhaC_{We}$ without his-tag was used for these studies. Two criteria were essential for the successful determination of these constants. First, a SEC method was required to isolate the dimeric form of the synthase (referred to subsequently as the 'dimer fraction'), reproducing in large amounts. The analytical SEC column used can separate 1 mg of the stock protein at a time. Second, the equilibration of dimer to monomer must be slow at 0°C as the 'dimer fraction' is kept at this temperature in between time points. A 50 min sampling time (20 min for SEC analysis and 20 min of column wash) is required. As shown in Figure 4.7 and Figure 4.8, criteria one and two are met. First, consistent D/M ratios in the 'dimer fraction' could be obtained from different injections (Figure 4.7B). Second, the equilibration between D and M is extremely slow, with a $t_{1/2}$ of at least > 4 h at 0°C. Note that all SEC studies were carried out at 4°C. This is an important experimental condition since it is essential that the dimer/monomer ratio is minimally perturbed while being analyzed on the SEC column.

A sample of the dimeric $PhaC_{We}$, isolated by SEC at 4°C was then incubated for various time periods of time at 22°C prior to reanalysis at 4°C by SEC. Ideally, the protein fraction should also be analyzed at 22°C as a control to determine if transferring the protein from 22°C to 4°C would cause a shift in the D/M ratio. However, the HPLC profile of this control would not give an accurate D/M ratio at the end of the desired incubation time at 22°C since SEC analysis takes 20 min and the protein will equilibrate during this time. Therefore, it was assumed that switching the protein from 22°C to 4°C would not lead to changes in the D/M ratio. The results of a typical experiment are shown in Figure 4.9A. The total amount of protein (area under the curve) recovered by this method remained constant through 2 h. Unfortunately as the incubation time increased to 6 and 8 h, protein loss most likely due to precipitation was observed. The synthase remained intact however, no proteolysis was observed (Figure 4.9B). The dimer and

monomer peaks from each chromatogram shown in Figure 4.9A was cut and weighed in order to determine the ratio between D and M at each time point. The height of their peak was also measured as a way to verify the weight measuring method. Results from the two methods gave similar ratios. The concentration of dimer was plotted as a function of time in order to calculate K_D and k_d. Analysis of the data to obtain a k_d is complex as the data is best fit to double exponentials (a fast phase and a much slower phase). Fits to the fast phase gives a k_d (22°C) of 0.14 min^{-1}. An accurate K_D cannot be obtained as loss of protein starts to occur before equilibrium is reached. Using the concentration of D and M at 137 min, K_D was estimated to be ~ 4 μM.

4.4.4 Isolation and specific activity of synthase dimer and monomer. The basis for the lag phase observed with the recombinant $PhaC_{We}$ is not understood. One working hypothesis that has been put forth in the literature is that it is due to dimerization of the monomer, and that the dimer is the only active form of the synthase. Moderately slow D to M dissociation at 0°C has provided an opportunity to determine if the monomeric form of $PhaC_{We}$ is catalytically active and if the interconversion of M to D alone is responsible for the lag phase. Protein fractions containing mostly dimer or monomer using $PhaC_{We}$ without a his-tag were collected through SEC, as shown in Figure 4.3B and C, respectively. Both fractions were assayed immediately using equal amount of protein (2 μg). As shown in Figure 4.5A, the extent of the lag phase was similar in both cases. The SA of the fractions containing mostly dimer or monomer was 45 U/mg and 47 U/mg, respectively. In order to observe the lag phase more clearly, less protein from each fraction, 1 μg, was used in a similar experiment. Both fractions were isolated from an independent study. As shown in Figure 4.5B, the extent of the lag phase and the rate of CoA release by both fractions were similar. The lag phase of the CoA release by the 'dimer fraction'

was only slightly shorter than that for the 'monomer fraction'. Thus, the conversion of M to D alone is not responsible for the lag phase and the basis of the lag phase remains unknown.

4.4.5 Growth of W. eutropha under different conditions and quantitation of their PHB content. Since recombinant $PhaC_{We}$, with or without his-tag, purified from *E. coli* does not exhibit uniform loading ((*2*), Chapter 3) and behaves kinetically different from the recombinant Class III $PhaCPhaE_{Av}$ synthase, we became interested in isolating the synthase directly from its native host, *W. eutropha* with the hope to characterize the native synthase. In order to facilitate the purification of $PhaC_{We\_N}$, a gene replacement strain containing PhaC with a N-terminus $(His)_6$-tag was generated by Dr. G. York. Ideally, we would like to find growth conditions that minimize the amount of PHB produced and maximize the amount of soluble synthase present in the cell. However, we were unable to find growth conditions in which *W. eutropha* cells accumulate no PHB. In growth condition 1 (Methods), *W. eutropha* grown in TSB medium was harvested at an early time point (OD ~ 1) with the hope that minimal amounts of PHB had been produced. However, PHB quantitation showed that these cells contained 8-10% PHB of cell dry weight (cdw). In addition, a large volume of culture had to be grown in order to have enough cells for synthase purification. Growth condition 2, harvesting *W. eutropha* after 72 h of cultivation, was then pursued. This condition was chosen based on our previous observation that in TSB medium, the percent of PHB per cdw inside the cells peaks at about ~ 4 h, and then dramatically decreases. After 72 h, less than 1% of PHB per cdw remains. Therefore, harvesting cells at this time point would minimize the amount of granule-bound synthase. This condition also gave high yield of cells per liter of culture.

4.4.6 Isolation of $(His)_6$-$PhaC_{We}$ from W. eutropha using Ni-NTA column. Our previous studies expressing the same His-$PhaC_{We}$ in *E. coli* greatly facilitated its purification using a Ni affinity column. Thus, we thought that this construct would successfully allow synthase purification from the native host. Unexpectedly, although the synthase contained a $(His)_6$-tag, the presence of the tag did not enhance purification from *W. eutropha* as expected. The synthase eluted at all concentrations of imidazole, ranging from 20 mM to 250 mM, in the absence or the presence of hecameg. Since the amount of synthase expressed in *W. eutropha* is low, approximately 1% or less judging from SDS-PAGE gels, the amount of synthase present in the fractions collected during increasing concentration of imidazole buffer wash had to be quantitated by Western using Ab to PhaC. As shown in Figure 4.11A, the predominant amount of $PhaC_{We\_N}$ eluted at 20 mM and 60 mM imidazole (note that the lanes showing $PhaC_{We\_N}$ from 250 mM imidazle wash had been concentrated). Native $(His)_6$-$PhaC_{We}$ could only be purified to ~10% by the Ni-NTA column method, as shown in Figure 4.11B. Its identity was confirmed by N-terminal sequencing. When this partially purified synthase was assayed, no lag-phase was observed (will be discussed more in the next section).

4.4.7 Isolation of $(His)_6$-$PhaC_{We}$ from W. eutropha using Methyl-HIC Column. Purification methods other then Ni-NTA were therefore pursued. The most successful one used the methyl-HIC column developed by Song *et al* (*1*). This procedure gives $(His)_6$-$PhaC_{We\_N}$ judged to be 20 to 30% pure based on Coomassie-stained gel shown in Figure 4.11C. The purification was followed using activity assays. Although most of the fractions contained small amounts of PhaC, the fractions collected from 0 mM ammonium sulfate buffer wash (F43 and F44) contained PhaC with the highest activity. Although the intensity of the PhaC band seemed to be the same in most of the fractions judging from SDS-PAGE gels, the percent of PhaC in these fractions were much

higher due to the absence of other protein bands. The most interesting observation made during the purification was that when the activity of the synthase was measured at all stages of purification, CoA release did not display any lag phase (Figure 4.12). Western analysis was used to determine the final concentration of isolated $PhaC_{We\_N}$. Using this number, the SA of the native synthase was estimated to be ~200 U/mg. Upon freezing the dilute protein, the activity of the synthase dropped to ~40 U/mg, equivalent to the specific activity of recombinant $PhaC_{We}$. This, the synthase expressed in its host organism appears to be modified in some form.

4.5 DISCUSSION

The ability to purify recombinant $PhaC_{We}$ in soluble form was first reported in 1994 (*2*). Since that time several labs have reported SAs for this protein that vary from 1 to 160 U/mg, despite that apparent homogeneity of the enzyme (*1, 4-6*). Possible explanations for variable SAs are misfolded protein or substoichiometric post-translational modification of an essential residue of the protein. We have now purified his-tagged and non-tagged $PhaC_{We}$ using Ni-NTA agarose column and HIC column, respectively. Both methods yield pure protein with similar SAs. The observed propensity of the recombinant $PhaC_{We}$ to aggregate and the low activity of the aggregate provide the simplest explanation for the variability in activity. This explanation is also consistent with the requirement for hecameg, a non-ionic detergent below its critical micelle concentration levels, for optimal protein purification. A consensus of 40 U/mg has been reached with one exception. Zhang *et al.* (*6*) using our vector have reported an activity of 160 U/mg in the presence of 50 % fructose. We have purified recombinant $PhaC_{We}$ using a modified version of their procedure and have attempted to assay the enzyme in the presence of 50% fructose. Pre-

incubation of synthase with fructose resulted longer lag phase and an activity of only 6 U/mg. The basis for the discrepancy between our work and theirs is unknown.

The dimer mechanism model (Figure 1.7), based on our ^{3}H-saturated-trimer (**4**, Figure 1.9) data (*9*), postulates that the dimer of $PhaC_{We}$ is the active form of the synthase for the elongation process. The active form of the synthase during initiation is unclear. Activity assays at 22°C, using equal amounts of the monomeric and dimeric forms of $PhaC_{We}$ isolated from SEC (4°C), show that the lag phase and rates of CoA release from both are very similar. These studies support a model in which the monomeric PhaC is active, at least in the initiation process (Figure 1.8) and eliminate a slow conversion of the M to D (without substrate) as a possible mechanism for the lag phase. The k_d is established to be 0.14 s^{-1}, and the K_D is estimated to be ~ 4 μM. Given the *in vivo* concentrations of $PhaC_{Re\_N}$ is ~ 1 μM (assuming all synthase is soluble) from our studies (*13, 14*), all synthase is likely to be a monomer at least in its 'apo' form.

Successful isolation of the synthase PhaC from its native host *W. eutropha* has been unprecedented in the field of PHA. So far, all experiments designed to study and understand the polymerase have relied on $PhaC_{We}$ (Class I) and $PhaCPhaE_{Av}$ (Class III) over-expressed and purified from *E. coli* systems. Although the kinetic behavior of $PhaCPhaE_{Av}$ is also unusual and multiphasic, its relative rate of elongation to initiation are much closer than that in the Class I synthase case (Chapter 3). The lag phase of PhaC has made interpretation of kinetic data impossible. It is therefore crucial to determine whether the recombinant synthase $PhaC_{We}$ is similar to the synthase expressed in its native environment. Toward that end, we recently engineered *W. eutropha* to contain the gene encoding either the N-terminal $(His)_6$-tagged synthase or an N-terminus $(His)_6$-tagged C149A synthase in place of the wt synthase gene in an effort to isolate the protein from the host organism. To our surprise, the purification was not

successful despite the fact that the same purification conditions were used to successfully purify $(His)_6$-$PhaC_{we}$ from *E. coli*. Using the Ni-NTA column, the native synthase eluted during all washes regardless of the imidazole concentrations. Unlike the recombinant synthase which elutes mostly at 250 mM, more native synthase eluted at 20 and 60 mM imidazole. The presence of 0.05% hecameg did not make a difference in the elution profile. These results are reminiscent of our efforts to purify the recombinant protein from *E. coli* in the absence of hecameg. Initially, we thought perhaps the native synthase was PHB bound since there is always a small amount of PHB present under the growth conditions tested. The presence of PHB could either interfere with purification since it may be covalently bound to the enzyme, or change the conformation of synthase, making the N-terminus inaccessible. However, the same imidazole elution profile was observed when we attempted to purify the mutant C149A synthase from the *W. eutropha* strain Re1095 which is incapable of producing PHA (data not shown). Clearly, the conformation of the native synthase is different from the recombinant synthase. The Ni-NTA method allowed us to purify the synthase to only ~10% homogeneity. The presence of the synthase was identified by Western and confirmed by N-terminal sequencing. Interestingly, when the crude extract and the partially purified synthase were assayed, no lag phase was observed. Other purification methods were then pursued; methyl-HIC column gave the best results. The native synthase could be purified to 20 - 30% homogeneity. The synthase had an activity of ~ 200 U/mg, and was also free of a lag-phase when assayed. However, upon freezing, its activity dropped to ~ 40 U/mg. The higher SA of the native synthase supports our hypothesis that the constitutively expressed synthase is modified in *W. eutropha*, perhaps residing in the host organism in the primed form. The absence of lag phase observed with synthase isolated from its native hosts suggests the possibility that the recombinant $PhaC_{We}$ lacks a modification or other factor(s) that

are important in initiation. Elucidating the difference between these two sources of synthase is our next goal.

4.6 REFERENCE

1. Song, J.J., Zhang, S., Lenz, R.W., and Goodwin, S. (2000) *In vitro* polymerization and copolymerization of 3-hydroxypropionyl-CoA with the PHB synthase from *Ralstonia eutropha, Biomacromolecules 1*, 433-439.
2. Gerngross, T.U., Snell, K.D., Peoples, O.P., Sinskey, A.J., Cushai, E., Masamune, S., and Stubbe, J. (1994) Overexpression and purification of the soluble polyhydroxyalkanoate synthase from *Alcaligenes eutrophus*: Evidence for a required posttranslational modification for catalytic activity, *Biochemistry 33*, 9311-9320.
3. Williams, M.D., Fieno, A.M., Grant, R.A., and Sherman, D.H. (1996) Expression and Analysis of a Bacterial Poly(hydroxyalkanoate) Synthase in Insect Cells Using a Baculovirus System, *Protein Expres. Purif. 7*, 203-211.
4. Gerngross, T.U. and Martin, D.P. (1995) Enzyme-catalyzed synthesis of poly[(R)-(-)-3-hydroxybutyrate]: Formation of macroscopic granules in vitro, *Proc. Natl. Acad. Sci. USA 92*, 6279-6283.
5. Wodzinska, J., Snell, K.D., Rhomberg, A., Sinskey, A.J., Biemann, K., and Stubbe, J. (1996) Polyhydroxybutyrate synthase: Evidence for covalent catalysis, *J. Am. Chem. Soc. 118*, 6319-6320.
6. Zhang, S., Yasuo, T., Lenz, R.W., and Goodwin, S. (2000) Kinetic and mechanistic characterization of the polyhydroxybutyrate synthase from *Ralstonia eutropha, Biomacromolecules 1*, 244-251.

7. Yuan, W., Jia, Y., Tian, J., Snell, K.D., Muh, U., Sinskey, A.J., Lambalot, R.H., Walsh, C.T., and Stubbe, J. (2001) Class I and III polyhydroxyalkanoate synthases from *Ralstonia eutropha* and *Allochromatium vinosum*: characterization and substrate specificity studies, *Arch Biochem Biophys 394*, 87-98.

8. York, G.M., Junker, B.H., Stubbe, J.A., and Sinskey, A.J. (2001) Accumulation of the PhaP phasin of *Ralstonia eutropha* is dependent on production of polyhydroxybutyrate in cells, *J Bacteriol 183*, 4217-4226.

9. Jia, Y., Yuan, W., Wodzinska, J., Park, C., Sinskey, A.J., and Stubbe, J. (2001) Mechanistic studies of Class I polyhydroxybutyrate (PHB) synthase from *Ralstonia eutropha*: Class I and III synthases share a similar catalytic mechanism, *Biochemistry 40*, 1011-1019.

10. York, G.M., Lupberger, J., Tian, J., Lawrence, A.G., Stubbe, J., and Sinskey, A.J. (2003) *Ralstonia eutropha* H16 Encodes Two and Possibly Three Intracellular Poly[D-(-)-3-Hydroxybutyrate] Depolymerase Genes, *J Bacteriol 185*, 3788-3794.

11. Divita, G., Rittinger, K., Geourjon, C., Deléage, G.C., and Goody, R.S. (1995) Dimerization Kinetics of HIV-1 and HIV-2 Reverse Transcriptase: a Two Step Process, *J. Mol. Biol. 245*, 508-521.

12. Divita, G., Rittinger, K., Restle, T., Immendorfer, U., and Goody, R.S. (1995) Conformational stability of dimeric HIV-1 and HIV-2 reverse transcriptases, *Biochemistry 34*, 16337-16346.

13. Tian, J., He, A., Lawrence, A., Liu, P., Watson, N., Sinskey, A.J., and Stubbe, J. (2004) Analysis of Transient Polyhydroxybutyrate Production in *Wautersia eutropha* H16 by

Quantitative Westerns and Transmission Electron Microscopy, *manuscript submitted for publication.*

14. He, A., Tian, J., Lawrence, A., Liu, P., Sinskey, A.J., and Stubbe, J. (2004) Expression Analysis of Proteins Involved in Polyhydroxybutyrate Homeostasis in *Wautersia eutropha* H16, *submitted for publication.*

4.7 FIGURES

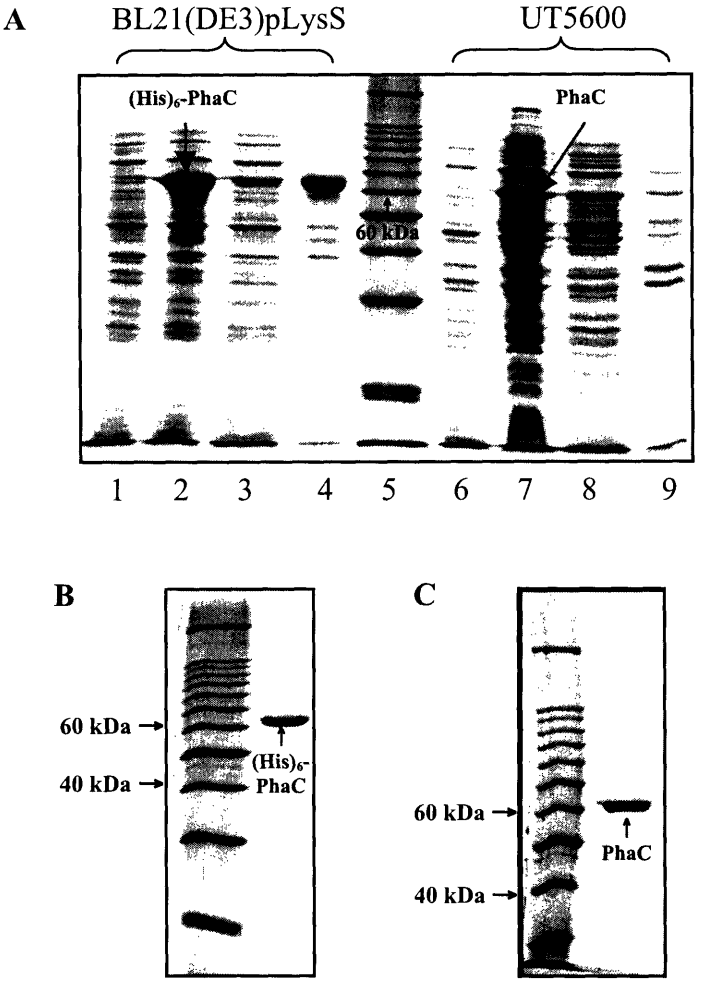

Figure 4.1 (**A**) SDS-PAGE gel examining the over-expression of $(His)_6$-PhaC (Lane 1 through 4) and PhaC (Lane 6 through 9) in BL21(DE3)pLysS and UT5600 *E. coli* strains, respectively. Lanes 1 and 6: uninduced cells; Lanes 2 and 7: induced cells; Lanes 3 and 8: soluble cell free extract; Lanes 4 and 9: insoluble cell suspension; Lane 5: Molecular weight standards. (**B**) $(His)_6$-PhaC after Ni-NTA agarose column. (**C**) PhaC after methyl-hydrophobic interaction column.

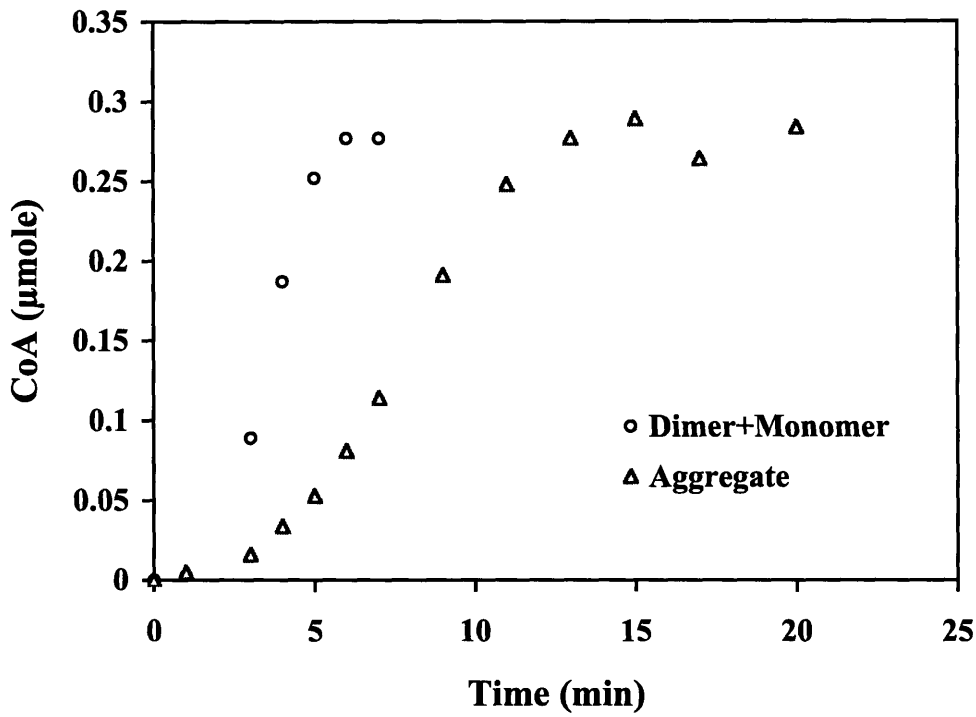

Figure 4.2 Time course of CoA release from HB-CoA catalyzed by protein aggregate (Δ) and synthase dimer + monomer (o). Both fractions were isolated from recombinant synthase $(His)_6$-PhaC purified by Ni-NTA resin. The reaction mixtures contained 2 µg of protein aggregate or dimer+monomer.

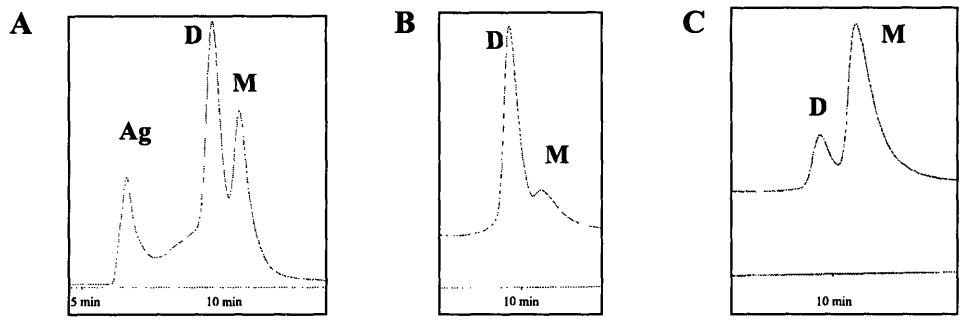

Figure 4.3 Bio-Silect SEC250 size-exclusion chromatography analysis of recombinant synthase and fractions collected. (**A**) Synthase $PhaC_{We}$ after HIC, revealing the presence of protein aggregate (Ag), synthase dimer (D), and synthase monomer (M). (**B**) Typical profile of the fraction collected containing mostly D. (**C**) Typical profile of the fraction collected containing mostly M.

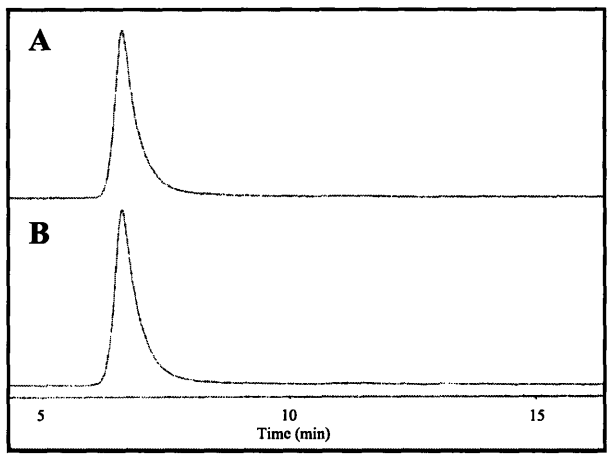

Figure 4.4 SEC chromatographs showing protein aggregate of recombinant $PhaC_{We}$, once separated from the synthase dimer and monomer, does not reform dimer or monomer. Isolated protein aggregate was incubated at 0°C for (**A**) 186 min, and (**B**) 404 min before being reanalyzed.

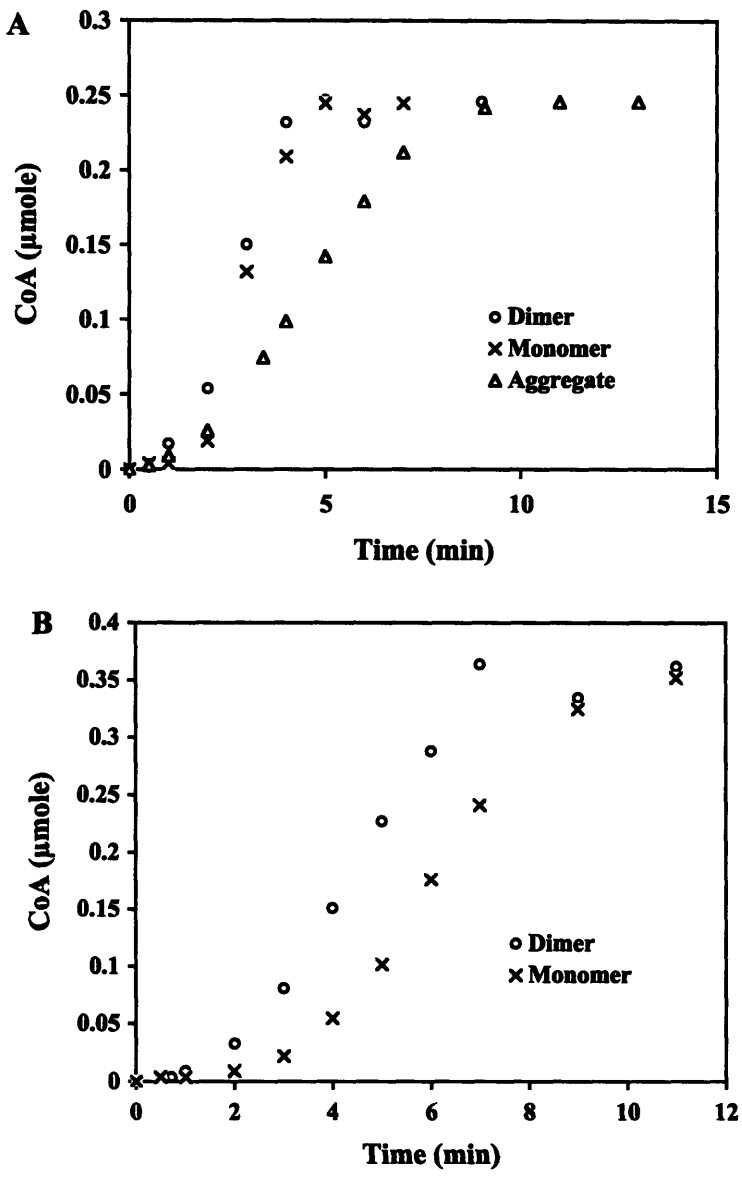

Figure 4.5 Time course of CoA release from HB-CoA catalyzed by protein aggregate (Δ), synthase dimer (O), and synthase monomer (×). All fractions were isolated from recombinant synthase PhaC purified by the method of HIC. (**A**) The reaction mixtures contained 2 μg of protein aggregate, dimer, or monomer. (**B**) The reaction mixtures contained 1 μg of synthase dimer or monomer isolated from an independent experiment.

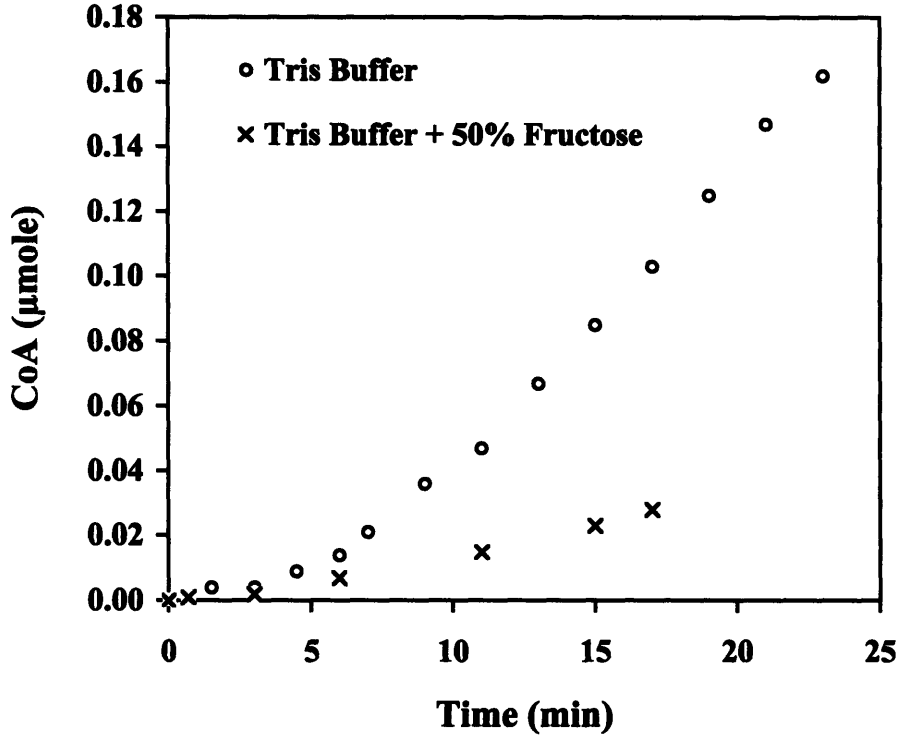

Figure 4.6 Effect of fructose on lag phase for synthase assay. Recombinant $PhaC_{We}$ was pre-incubated in a fructose solution (50% final concentration) on ice for 1 h, from which 0.5 µg of $PhaC_{We}$ was used to initiate a reaction containing 1 mM HB-CoA in 100 mM Tris-HCl, pH=8 (×). A control with synthase not pre-incubated with fructose was also carried out (o). Release of CoA was detected by the discontinuous DTNB assay.

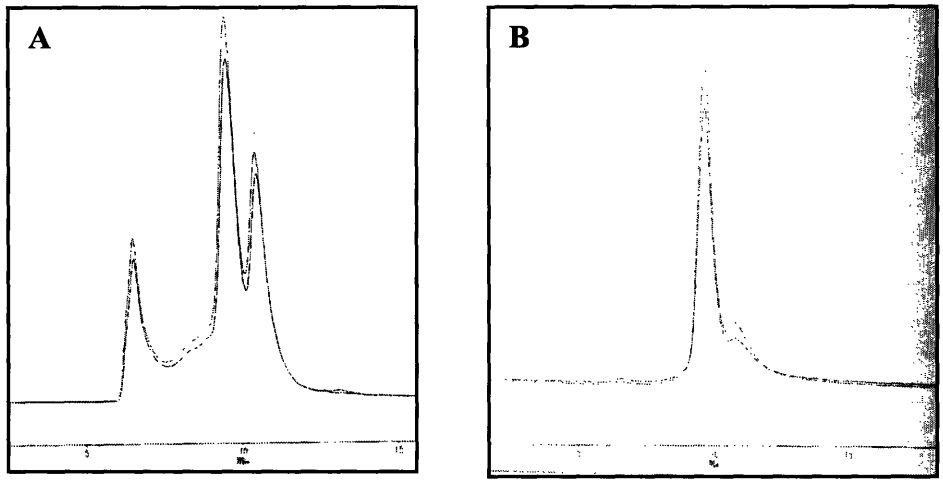

Figure 4.7 SEC chromatographs of two independent experiments demonstrating the reproducibility of the methods used: HPLC and manual collection of the dimer fraction: (**A**) Synthase PhaC after HIC; (**B**) Dimer fraction collected.

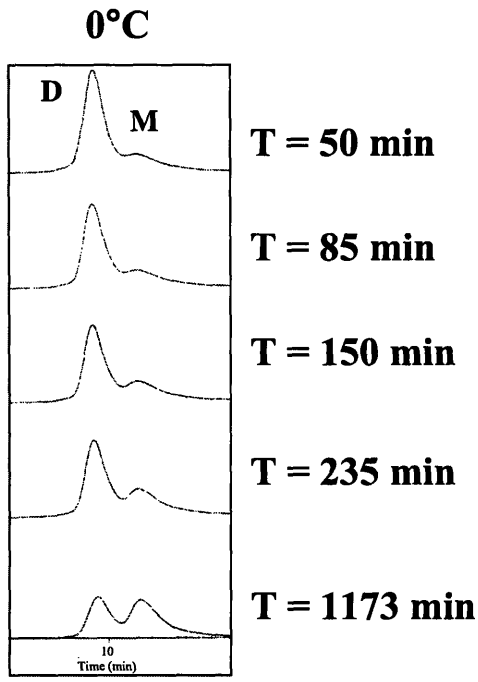

Figure 4.8 SEC chromatographs showing dimer↔monomer interconvation at 0°C. Recombinant $PhaC_{We}$ dimer isolated by SEC at 4°C was incubated for various periods of time (T) at 0°C and reanalyzed at 4°C.

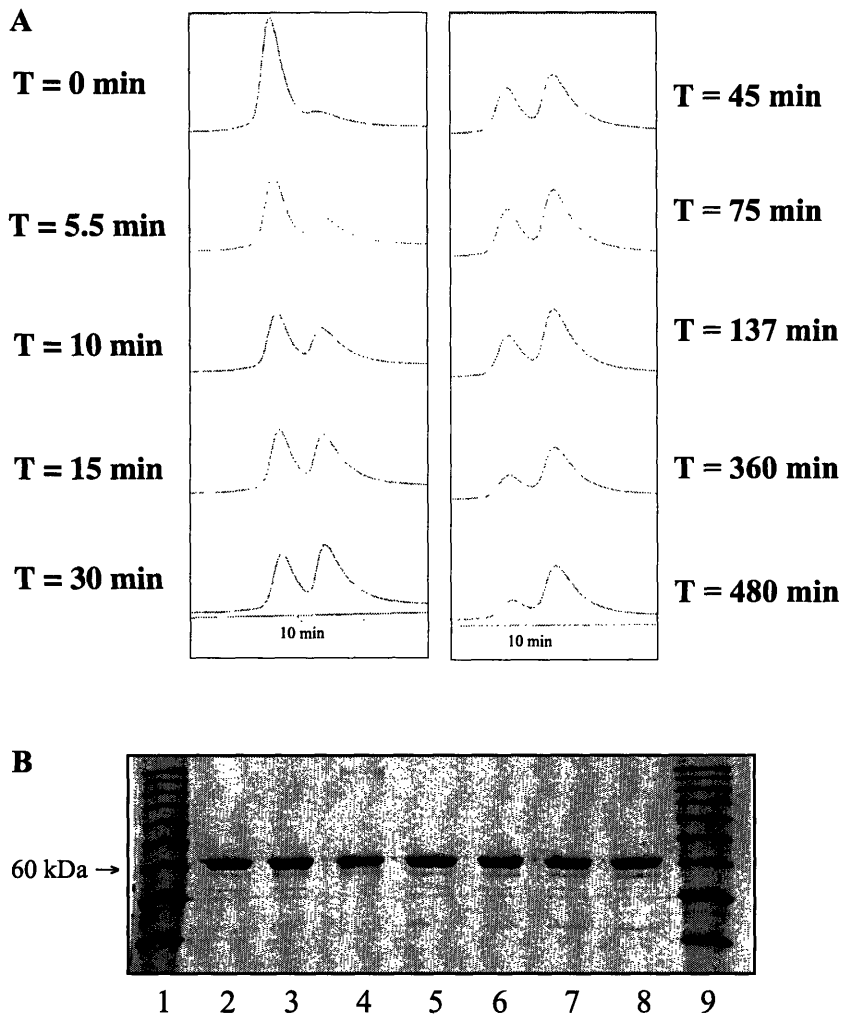

Figure 4.9 **(A)** SEC chromatographs showing dimer↔monomer interconvation at 22°C. Recombinant $PhaC_{We}$ dimer isolated by SEC at 4°C was incubated for various periods of time (T) at 22°C and reanalyzed at 4°C. **(B)** SDS-PAGE gel examinning the integrity of the synthase dimer upon incubation at 22°C for 0, 1, 2, 3, 4, 5, and 6 h (Lane 2 through 8, respectivley). Lanes 1 and 9 contain protein molecular weight standards.

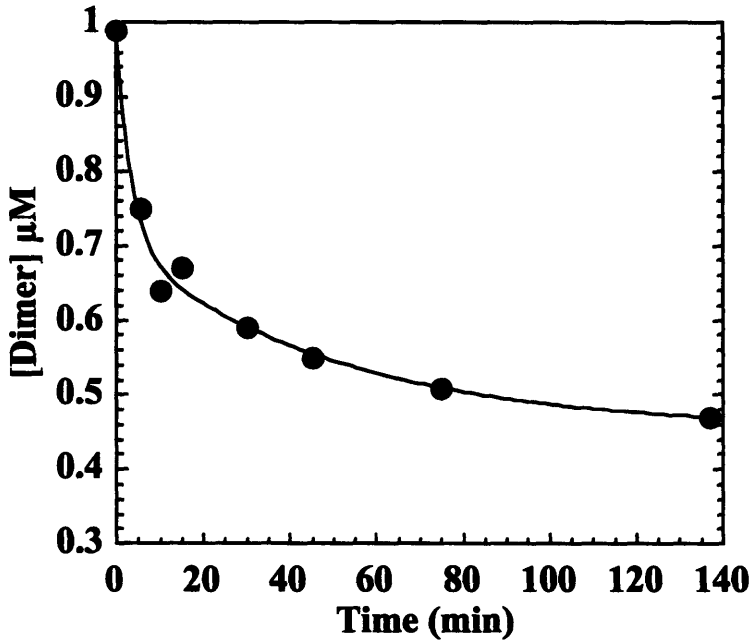

Figure 4.10 Dissociation of synthase dimer to monomer at 22°C based on the data shown in Figure 4.9A.

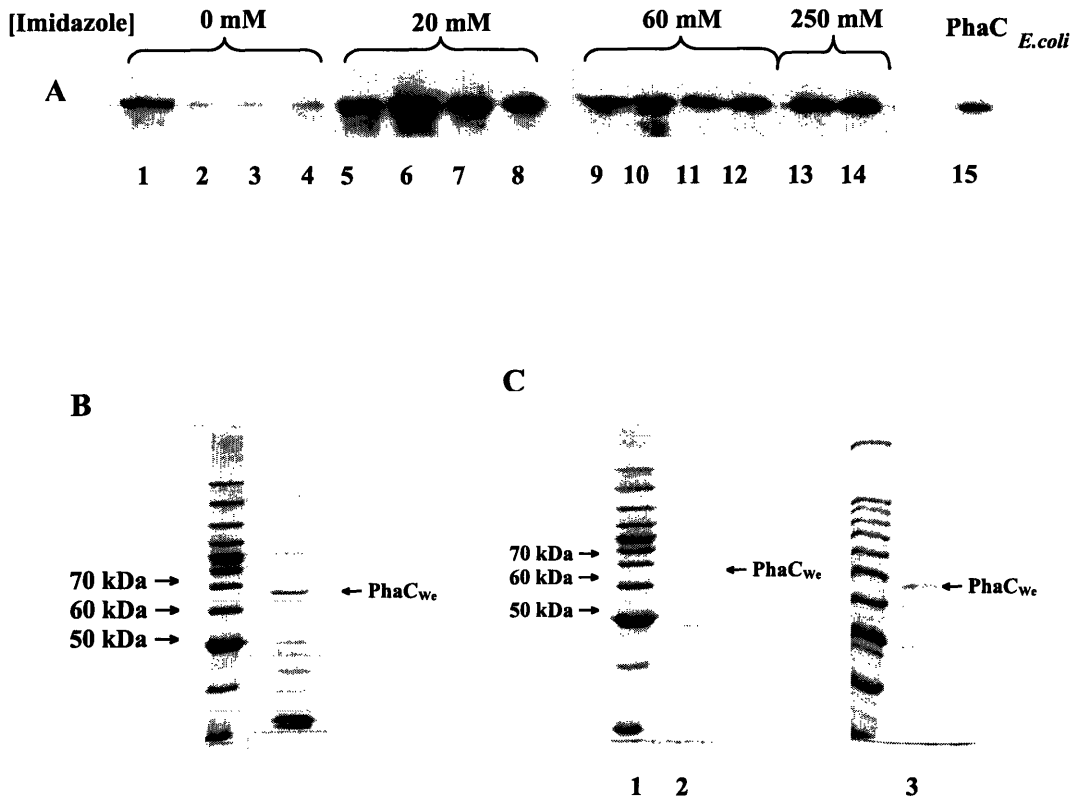

Figure 4.11 Purification of $(His)_6$-$PhaC_{We}$ from *W. eutropha* whose synthase gene was replaced with $(His)_6$-synthase. (**A**) Elution profile of $PhaC_{We\_N}$, monitored by Western using antibodies to PhaC, at increasing concentrations of imidazole (Imid) using Ni-NTA column. Lane 1 through 4, fraction 1~4 at [Imid]=0 mM; Lane 5 through 8, fractions 1~4 at [Imid]=20 mM; Lane 9 through 12, fractions 1~4 at [Imid]=60 mM; Lanes 13 and 14, concentrated fractions from [Imid]=250 mM; Lane 15, western of $(His)_6$-PhaC isolated from *E. coli*. (**B**) Coomassie-stained SDS-PAGE gel showing $PhaC_{We\_N}$ isolated using the Ni-NTA method. (**C**) Coomassie-stained SDS-PAGE gel showing $PhaC_{We\_N}$ isolated using methyl-HIC column. Lane 1, MW; Lane 2, F43; Lane 3, concentrated F43.

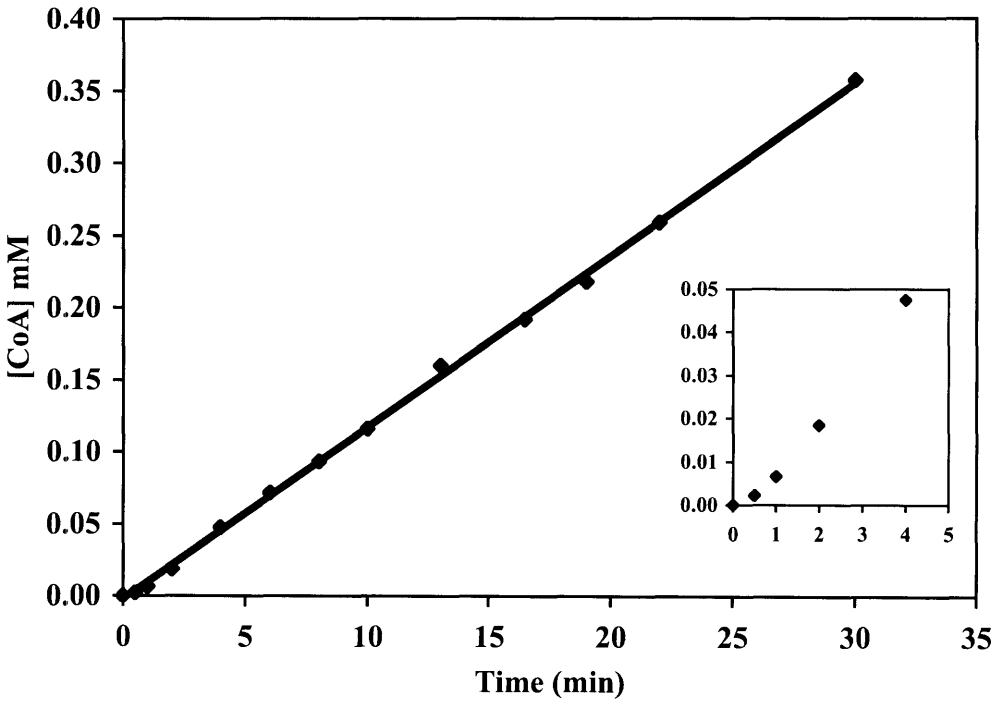

Figure 4.12 Activity assay measuring the rate of CoA release by $PhaC_{We\_N}$. No lag-phase was observed.

CHAPTER 5

Kinetic Studies of Polyhydroxybutyrate Granule Formation in *Wautersia eutropha* H16 by Transmission Electron Microscopy

5.1 ABSTRACT

Wautersia eutropha, a gram-negative bacterium, accumulates polyhydroxybutyrate (PHB) as insoluble granules inside the cell when nutrients other than carbon are limited. In this chapter, we report findings from kinetic studies of granule formation and degradation in *W. eutropha* H16 using Transmission Electron Microscopy (TEM). In nitrogen-limited growth medium, the phenotype of the cells at the early stages of granule formation is revealed for the first time. At the center of the cells, dark-stained features with small granules attached are observed. These 'features' are proposed to serve as nucleation sites for granule initiation. TEM images also reveal that when *W. eutropha* cells are introduced into nitrogen-limited medium from nutrient-rich medium, their cell size increases 2 to 3 fold, and the cells undergo additional volume changes during the growth conditions. Unbiased stereology was used to analyze the 2-D TEM images, from which the average volume of a *W. eutropha* H16 cell and the total surface area of granules per cell in nutrient-rich and PHB production media were obtained. These parameters have been essential in the calculation of the concentration of proteins involved in PHB formation and utilization and their changes with time, and the extent of protein coverage of the granule surface area presented in our recent papers (J. Tian, A. He, A. Lawrence, P. Liu, N. Watson, A.J. Sinskey, and J. Stubbe, submitted for publication; A. He, J. Tian, A. Lawrence, P. Liu, A.J. Sinskey, and J. Stubbe, submitted for publication).

5.2 INTRODUCTION

Polyhydroxyalkanoates (PHAs), polymers composed of polyoxoesters, are accumulated in granular form by various micro-organisms under nutrient-limited conditions when a carbon source is readily available (*1*). They serve as reserves of carbon and reducing equivalents to preserve cell survival during stressful conditions. Little do these bacteria know that their biodegradable PHAs have properties ranging from thermoplastics to elastomers, and could potentially replace the non-environmental friendly petroleum-based plastics that are heavily used in our society. Production of economically competitive PHAs and those with new properties have been the impetus for many research groups to study the biosynthesis, degradation, and homeostasis of PHA in microorganisms. Biosynthesis of PHAs involves transforming soluble substrates, such as hydroxyalkanoate coenzyme A esters, into insoluble inclusions during polymer elongation; these inclusions are stored in a fashion that can be rapidly degraded when needed (*2*).

In an effort to elucidate the mechanism of PHA biosynthesis and degradation, various research groups have identified important proteins that play a role in these processes. In *Wautersia eutropha*, the most extensively studied micro-organism, a synthase (PhaC), three intracellular depolymerases (PhaZs), an oligomer hydrolase, a phasin protein (PhaP), and a putative transcription factor (PhaR) have been characterized (*3-9*). In addition, through genomic analysis, two additional depolymerases and three additional phasin proteins have been identified recently in *W. eutropha* (*10*). This organism uses 3′-hydroxybutyryl-CoA (HB-CoA) to make polyhydroxybutyrates (PHBs). To maximize the production of PHB, *W. eutropha* are typically grown in nitrogen-limited medium with an available carbon source such as fructose (PHB production medium, PHB_P) (*5*). At late stages of PHB accumulation, the polymer can account

for 80-85% of the dry cell weight. Transmission electron microscopy (TEM) and immuno-gold labeling experiments examined by TEM at a late stage of PHB production have revealed that the entire inside of each cell is filled with 8 to 12 PHB granules that are 0.2 - 0.5 μm in diameter (*1*). The synthase and phasin proteins were shown to be located on the granule surface (*7, 11, 12*), although the extent of coverage appeared to be low. Early electron microscopy studies of PHB granules from *Bacillus cereus*, *Bacillus megaterium* (*13*), *Rhodospirillum rubrum* (*14*), and *Chlorogloea fristschii* (*15*) all revealed an atypical membrane-like material surrounding the surface of granules, varying in thickness from 3 nm to 20 nm, depending on the species. Recent atomic force microscopy (AFM) studies on granules freshly isolated from *W. eutropha* with minimum perturbation also demonstrated a 3-4 nm thick boundary layer surrounding the surface of the granules (*16*). In addition, globular structures, 35 nm in diameter with a central pore, were also reported to be on the surface of the granule and proposed to be centers for PHB synthesis and depolymerization. Based on these observations, two models have been proposed for granule formation. The first is the micelle model in which the extended PHB chains covalently attached to the synthase aggregate initially into a micelle structure (Figure 1.12) (*3, 17*). The physical properties of the polymer are thus proposed to be the driving force for inclusion formation. The second is the budding model we proposed recently, in which the hydrophobic synthase binds to the inner face of the plasma membrane and buds from this membrane leading to a granule surface covered with a lipid monolayer (Figure 1.13). In this model, the biology of the system and the physical properties of the polymer both are required for granule formation.

Our lab has been interested in the mechanism of granule formation and degradation. Studying granule formation from its inception, that is the early stage of PHB biosynthesis, has not

previously been reported and may allow a distinction between these two models (Figure 1.12 and Figure 1.13).

In the present chapter, TEM has been used to study the kinetics of granule formation and degradation in *W. eutropha* H16. The TEM images of cells at the early stages of PHB production revealed dark-stained features near the center of the cell, ringed by small granules ($\leq$ 0.1 μm in diameter). These images have led to an alternative model for granule formation in which granules are localized and that these new features function as granule initiation sites. In addition, these time course studies revealed changes in cell and granule sizes, which have been quantitatively analyzed by unbiased stereology. Stereology, a branch of applied mathematics, is the three-dimensional interpretation of flat images by criteria of geometric probability (*18*). Using this analysis method, we report for the first time, the average volume of *W. eutropha* H16 cells and the total surface area of granules per cell at different stages of granule formation. These parameters, along with results from quantitative Western analyses described in our recent manuscripts ((*19, 20*), Chapter 6), have identified the proteins involved during PHB biosynthesis and degradation, and their changes in concentration as a function of time. The kinetic information is essential for proposing functional roles of the proteins in PHB homeostasis.

5.3 MATERIALS AND METHODS

5.3.1 Cultivation conditions. Wild-type (wt) *W. eutropha* H16 was cultivated with aeration at 30°C. Gentamicin was included in all growth media, except when PHB utilization was being measured. A single colony from a Tryptic soy broth-dextrose free (TSB, Becton Dickinson Microbiology Systems, Cockeysville, MD) plate was cultivated in 5 mL of TSB medium to saturation (~40 h), at which time 2 mL was transferred into 100 mL of TSB medium in 500-mL

baffled flasks and grown for 24 h. The doubling time of *W. eutropha* H16 in TSB medium is between 3 to 4 h. These cells harvested by centrifugation were washed and transferred into 200 mL TSB medium or 200 mL of PHB production medium (PHB_P, minimal medium supplemented with 1% fructose and 0.01% ammonium chloride) in 1 L baffled flasks to yield cultures with an initial OD_{600nm} of 0.5. For cells grown under TSB conditions, 5 mL of cells were removed at 4 and 24 h for TEM analysis. For cells grown under PHB_P, 5 mL of cells were removed from the culture at 2.5, 5, 9, 24, and 73 h. In all cases, cells were immediately fixed for TEM studies. For PHB utilization, 100 mL of cells grown in PHB_P for 73 h were harvested, washed with 0.85% saline and transferred into 200 mL of PHB utilization medium (PHB_U, minimal medium supplemented with 0.5% ammonium chloride). Samples were harvested at 48 h for TEM analysis.

5.3.2 TEM reagents. All TEM reagents were purchased from Electron Microscopy Sciences (Hatfield, PA)

5.3.3 Fixation. Five mLs of the cell culture in TSB, PHB_P, or PHB_U at various time points were transferred to a 15 mL falcon tube containing 5 mL of fresh fixative solution (2% gluteraldehyde, 3% paraformaldehyde made fresh, 5% sucrose, and 0.1M sodium cacodylate buffer, pH 7.4). After 5 min of manual mixing, the cells were spun down at 5000 rpm for 10 min. The supernatant was removed, and an additional fresh 10 mL of the fixative solution was added to resuspend the cell pellet. After 1 h of incubation at room temperature with occasional mixing manually, the cells were pelletted again. Sodium cacodylate buffer, 0.1M at pH 7.4 (1.5 mL), was added to resuspend the pellet. The cell suspension was transferred to an Eppendorf tube (1.7 mL), where after 2 min of mixing, the cells were spun down at 9,000 rpm for 1 min in a mini-

centrifuge. The supernatant was removed, and the pellet was washed 3× with 1.5 mL of 0.1M sodium cacodylate buffer. The pellet was dislodged from the bottom of the Eppendorf tube to ensure good washing each time.

The cell pellet was then fixed with 1.5 mL of a 1% osmium solution prepared by mixing 1.25 mL of 4% osmium tetraoxide (OsO_4), 1 mL of 0.1N HCl, 1.75 mL dH_2O, and 1 mL of acetate-veronal stock (1.2% of sodium acetate (anhydrous) and 2.9% of sodium barbituate (veronal) in dH_2O). The pellet was dislodged from the bottom of the tube and incubated in the osmium solution for 1 h.

The fixed cells were then pelletted and 1.5 mL of a third fixative solution, the Kellenberger uranyl acetate solution (0.5% uranyl acetate in veronal-acetate buffer) was added. The pellet was initially washed with this solution briefly (< 1 min), and then incubated in 1.5 mL of fresh solution overnight in the dark.

5.3.4 Dehydration. Upon the completion of uranyl acetate staining, the pellet was rinsed with ~ 1.5 mL dH_2O quickly after being dislodged and was then pelletted by centrifugation. To dehydrate the cells, they were subjected to increasing amounts of ethanol. The pellet was first placed in 50% ethanol/water for 10 min, and subsequently in 70% ethanol for 10 min, 95% ethanol for 10 min, and then 3× in 100% ethanol for 15 min. The cells were spun down after each ethanol treatment to remove the supernatant, and the pellet was dislodged during each incubation to ensure homogeneous dehydration. The pellet was further dehydrated in 50% ethanol/50% propylene oxide for less than 5 min before being transferred to 100% propylene oxide (~1.5 mL). After 5 min, the pellet was then placed in 50% propylene oxide/50% low viscosity embedding resin (containing vinyl-4-cyclohexene dioxide, DER 736 Resin, nonenyl

succinic anhydride, and 2-dimethylaminoethanol; these components are mixed in proportions to obtain hard blocks following the instruction of the Spurr Kit) and rotated on a rotator for 12 h.

5.3.5 Embedding. All of the pellet was transferred into ~ 1.5 mL 100% low viscosity embedding resin and placed under vacuum in a dessicator for 4 h. This process was repeated at least 3× with fresh embedding resin. The pellet was then cut into small sections randomly, and embedded into beam capsules containing 100% low viscosity embedding resin. The beam capsules were then placed at 60°C overnight to allow embedding.

5.3.6 Sectioning and Scoping. Ultra-thin sections were cut on a Reichert Ultracut E microtome at a thickness of ~70 nm using a Diatome diamond knife. The sections were picked up with 200 mesh Nickel grids coated with Formvar (0.3% dissolved in ethylene dichloride) and a layer of carbon. Serial sections were also prepared for the wt *W. eutropha* cells grown in PHB_P for 5 h. The thickness of each section was ~ 70 nm. The sections were examined using a Philips EM410 or JOEL JEM-1200EXII electron microscope at 80 kV. For each condition, images were recorded on film at high and low magnifications.

5.3.7 TEM image data analysis: calculation of the average cell volume at 5 h of wt strain grown in PHB_P. *W. eutropha* cells appear to be rod-shaped under a light microscope and all calculations of volumes are based on this premise. The volume of the cell has thus been approximated by using the equation describing the volume of a cylinder: $V_C = \pi d^2 h/4$. V_C is defined as the volume of a cylinder or a single cell, d is the diameter of the cylinder or the width of the cell, and h is the height of the cylinder or the length of the cell. Serial sections (~70 nm, 5 h in PHB_P) are required to obtain the actual length and width of a cell by selecting the longest and widest cell profiles, respectively, in images. Here and in the rest of this chapter, cell profiles

refer to the cross-section of cells resulting from a single cut. Long cell profiles that do not change length and angle from one section to the next are measured with a ruler in length (*h*); similarly, wide cell profiles that do not change width and angle from one section to the next are measured in width (d). All measured values are corrected by the magnification factor. The average cell volume of this sample is referred to as V_{C5h}. This analysis assumes that the cells are uniform in size at this time point, which is not the case. At 5 h under these growth conditions, the cells are dividing. Since the analysis involves examination of successive sections for the longest cells which are on the verge of dividing, V_{C5h} is the average cell volume at this stage. The average cell volume of freshly divided cells at 5 h is assumed to be half of that of V_{C5h}. Thus as noted in Table 1, a range of volumes is reported for the time points in which cells are dividing. In the stationary phase (TSB medium at 24 h and PHB_P at 9 to 73 h), the cells are assumed to be uniform.

5.3.8 Calculation of the area of cell profiles on 2-D images using unbiased stereology at given times. The Cavalieri-Point counting method has been used for this analysis (*21, 22*). A multipurpose test system is used: the probe contains parallel lines (also called test lines) spaced 19.85 mm apart, and points spaced 39.7 mm apart evenly on each line (Figure 5.1). The probe is overlaid randomly on a TEM image containing cell profiles. The number of points (P) that hit cell profiles is then tabulated. This process is repeated with images of other random sections of the same sample until enough points are obtained so that the coefficient of error (CE) is less than 10%. CE, also known as sampling error, is defined as the (Standard deviation/Mean)/(sample number)$^{1/2}$, where the sample number is equal to the number of images used for the study. Typically, a minimum of 100 to 200 points is needed. The area of the cell profiles covered in all images is calculated using Equation 5.1 (*23, 24*).

$$A_{CP} = \sum P_{CP} \times a(p) \qquad \textbf{Equation 5.1}$$

Here, A_{CP} is the total area of the cell profiles on all images, $\sum P_{CP}$ is the number of points hitting the cell profiles, summed over all images, and a(p) is the area per point, the product of the distances between points in the x- and y-directions (19.85 mm x 39.7 mm). Since all images are magnified, a(p) is corrected by the magnification factor.

5.3.9 Calculation of the average volume of cells at each time point using A_{CP} of the corresponding sample and V_{CSh}. The Delesse principle states that the two-dimensional areas of profiles of tissue components are related to the three-dimensional volumes occupied in space by these components, assuming random distribution and random orientation of components (*25*). The relationship between area and volume is that shown in Equation 5.2.

$$A_A = V_V \qquad \textbf{Equation 5.2}$$

A_A is the area fraction and V_V is the volume fraction, both are further defined as shown in Equation 5.3.

$$A_A = \frac{A_{obj}}{A_{ref}} = \frac{V_{obj}}{V_{ref}} = V_V \qquad \textbf{Equation 5.3}$$

A_{obj} is the area of the object of interest on flat images, which in our case is equal to the area of total cell profiles (A_{CP}) described above. A_{ref} is the area of the reference space that contained A_{obj}, which can be obtained by counting the total number of points (ΣP_T) on the point-grid probe used to obtain A_{CP}, and multiplying ΣP_T by the area per point (Equation 5.1). Similarly, V_{obj} is the volume of object of interest, which in our case is the total volume of the cells observed on images from which A_{obj} was measured; V_{ref} is the reference volume that contained V_{obj}. Since A_{CP} is a function of $\sum P_{CP}$ (Equation 5.1), a value that is highly dependent on the number of observed cell profiles present on EM images which are all taken at random, a normalization

procedure is necessary in order to compare A_{CP} calculated for samples collected at each time point. Therefore, the total number of cell profiles (N_{CP}) in all the images measured is counted. In order to avoid over-counting, a counting rule is applied. Cell profiles that lie within the reference area, and only those that are on the top and the left edge of the reference area are counted. Note that N_{CP} here only refers to the total number of cell profiles that are observed and therefore contributed to the measurement of A_{CP}. Therefore, A_{CP}/N_{CP} obtained from different samples is indicative of the trends in volume change. When comparing parameters of separate samples, such as PHB_P 2.5 h and 5 h, the relationship among their A_{CP}, V_{CP} (volume of cell profiles), and N_{CP} when the thickness of each section is the same can be found in the Equation 5.4.

$$\left(\frac{V_{CP2.5h}}{N_{CP2.5h}}\right) = \left(\frac{V_{CP5h}}{N_{CP5h}}\right) \times \frac{A_{CP2.5h}}{A_{CP5h}} \times \frac{N_{CP5h}}{N_{CP2.5h}} \qquad \textbf{Equation 5. 4}$$

Notice that we did not chose to cancel out the $N_{CP2.5h}$ and N_{CP5h} terms in this equation. This is because the terms in the parentheses (V_{CP}/N_{CP}) now represent the actual average volume of a cell (V_C). This representation is only valid when the number of cell profiles is equivalent to the number of cells present in the reference space, which is true in our system since a cylindrical cell can only appear once when sliced from any angle. The only exception is when the cells are dividing. Since the middle of the cell pinches in, sectioning the cell longitudinally on the edge could result in two profiles. However, the probability of this is low (≤ 2-3 % out of ~ a hundred of cell profiles, data not shown). In addition, cell division does not occur in PHB_P at 9, 24, and 73 h. Since we have obtained the actual average volume of a cell in PHB_P at 5h using images of serial sections described above, knowing $A_{CP2.5h}$, A_{CP5h}, $N_{CP2.5h}$, and N_{CP5h} allows us to calculate

the approximate average volume of a cell in PHB_P medium at 2.5 h. Similarly, an estimation of the average volume of a cell from other samples can be obtained using this method. Equation 5.4 is valid when the thickness of a section is the same for different samples, which is the case for this study.

5.3.10 Calculation of the total surface area of granules per cell (S_G) using unbiased stereology. The multipurpose test system (Figure 5.1) is again overlaid on TEM images of the same sample randomly (all images are of the same magnification). The size of the image defines the reference space. Since all images are approximately the same size, the total reference space is equal to the number of images times the size of an image. This time, instead of counting points, intersections (I) are counted when the test lines cross the surface of granules. Again, a large enough number of intersections must be counted so that the sampling error is less than 10%. The surface density of the granules (S_V), defined as the total surface area of granules per total reference space volume, can be calculated using Equation 5.5 (*26*).

$$S_V = 2 \times \sum I_G / \sum L \qquad \textbf{Equation 5.5}$$

$\sum I_G$ is the number of intersections of granules with test lines, summed over all images and $\sum L$ is the total length of test lines summed over all images. Again, the length L has to be corrected for magnification. Note that the unit of S_V is length^{-1} (e.g., μm^{-1}). The derivation of this equation is described in Elias *et al* (*27*) and also provided in Figure 5.2. Recall that V_V (V_{obj}/V_{ref}) is the total volume of observed cell profiles in total reference space in our case obtained from the same images. Therefore, dividing S_V by V_V gives the total surface area of granules in a unit volume of cells. The total surface area of granules in one cell (S_G) can be obtained using the following equation.

$$S_G = (S_V/V_V) \times V_{CP} \qquad \textbf{Equation 5.6}$$

Again, this analysis is applied to images of all our samples.

5.3.11 Measurement of the size distribution of cell and granule profiles on 2-D images. For all wt samples, the major and minor axis of all cell and granule profiles were measured on images recorded at the same low magnification (primary magnification: 3000×) so that a large field of cells could be sampled. Measurements were made by using the Scion Image for Windows software from Scion Corporation. These measurements were confirmed by random manual measurements with rulers.

5.4 RESULTS

5.4.1 Transition of cells from nutrient-rich medium (TSB) to PHB_P. The current literature on PHB has been mostly focused on studying the phenotype of microorganisms under conditions in which a maximum number of PHB granules are produced. A typical TEM picture shows a cell that is full of large granules (e.g., 24 h in PHB_P in Figure 5.4D). However, the fate of *W. eutropha* cells during the initiation stage of the PHB production has not, to our knowledge, been depicted. We were interested in using TEM to observe cells at these early stages. *W. eutropha* are typically grown in TSB rich medium for 20-24 h to minimize the amount of PHB in cells used to inoculate PHB_P. Ideally, the starting culture would contain cells in the early stationary phase and contain no PHB so that the PHB production in PHB_P could be monitored from the very beginning. However, in our hands, such growth conditions have not yet been identified. At 20-24 h in TSB medium, *W. eutropha* contains a low amount of PHB (<10% of cell dry weight) (*5*). Cells grown under these conditions were thus chosen to serve as the inoculum. Images of cells at 24 h in TSB medium and an early time point (2.5 h) in PHB_P are shown in Figure 5.3 and gave surprising results. Upon switching into PHB_P, *W. eutropha* expands its cell size, 2 to 3 fold

(Table 5.1, compare A_{CP}/N_{CP} values at TSB 24 h and PHB_P 2.5 h). The increased size could be associated with cell division, since the cells were transferred from nutrient depleted TSB medium at 24 h, when most of the cells are no longer dividing, to fresh PHB_P which contains 0.01% of nitrogen source and initially allows cell growth. A typical freshly divided rod-shaped cell (e.g. *Escherichia coli*) elongates with little or no increase in girth until it reaches approximately twice its original size and then separates into two cells nearly equal in size (*28*). Alternatively, increase in cell volume could be related to the ability of cells to sense nutrient limitation of nitrogen. Thus, the increased cell size may be a regulatory mechanism required to maximize the cell's capacity for granule storage. Support for this alternative explanation is the observation that the average cell volume at 2.5 h in PHB_P is still substantially larger than that at 4 h in TSB medium in which the cells were also dividing (Table 5.1). The basis for cell volume increase requires further investigation.

5.4.2 Kinetics of wt W. eutropha H16: unusual features accommodating small granules at early time points. Models in the literature for granule formation suggest granules may arise through physical association of PHB oligomers forming micelle-like structures (Figure 1.12) or by budding off the plasma membrane resulting in a granule covered with a monolayer of lipid (Figure 1.13). TEM may allow a distinction between these models as in the former case, the granules may be uniformly dispersed in the cytoplasm and in the latter case, the nascent granules should be adjacent to the inner leaflet of the plasma membrane of the cell. WT *W. eutropha* H16 has now been studied in PHB_P as a function of time, and the images of this time course are shown in Figure 5.4. At the early time points (2.5 and 5 h), striking dark-stained structures or features (0.4-0.5 μm) are observed near the center of the cross-section of many cells (Figure 5.4A, B and Figure 5.5) or along a longitudinal strip in the center of the cells (Figure 5.6). The

location of these dark-stained structures at the center of the cells is confirmed by images from serial sections (data not shown). These features are believed to be unique to *W. eutropha* H16 studied under PHB_P conditions since *E. coli* cells (which closely resemble *W. eutropha*) to our knowledge do not show this feature under normal growth conditions when fixed and stained under similar conditions and analyzed by TEM (*29, 30*). Of great interest is that very small PHB granules (Figure 5.5 and Figure 5.6A) localize around these dark-stained features. Examination of many images containing thousands of cells gave no evidence for PHB granules budding from the cell membrane or dispersed randomly within the cytoplasm. As the cells continue to grow in the PHB_P from 5 to 73 h, the dark features gradually disappear or become obscured by the increased size of the granules (Figure 5.6). Notice that the granules increase in size from 9 to 24 h in PHB_P, until the entire cell is filled with granules.

The dark features have also been observed in a *W. eutropha* H16 strain with its Class I synthase gene replaced with D302A-PhaCPhaE (Class III synthase) from *Allochromatium vinosum* (Figure 5.7). Although this strain was grown in PHB_P for 24 h (compare with the wt strain, Figure 5.4D), only small granules are observed to accumulate since the mutant is defective in its ability to elongate polymer (*31*). The dark-stained structures are again seen near the center of the cross-sections of cells where the small granules are found.

The observation of these dark stained features with attached granules is intriguing. However, it should be kept in mind that the cells have been cross-linked with gluteraldehyde and paraformaldehyde, fixed and stained with osmium tetraoxide and uranyl acetate, and extensively dehydrated with ethanol. The effects of this treatment on 'structure' are not known. A variety of additional methods to scrutinize these interesting structures to ensure their relationship to granule formation will be the focus of future experiments.

As shown in Figure 5.4B, C, D, E, and Figure 5.6, a significant amount of PHB is produced from 5 to 9 h, and from 9 to 24 h in PHB_P. Cells containing at as many as 18~ 25 granules per cell are occasionally observed from our images at 24 h. At 73 h, a significant coalescence of granules is observed as shown in Figure 5.8. Also of interest is the appearance of small white inclusions near the edge of the cell membrane (Figure 5.8). The identity of these inclusions is uncertain, and their origin is also unknown.

Upon transferring the cells into PHB_U after 73 h in PHB_P, *W. eutropha* H16 cells show a decrease in cell size by 48 h (Figure 5.4F and histogram). Furthermore, at this time point, the size and number of granules is much more heterogeneous than in PHB_P (Figure 5.4F and Figure 5.9). The observation of granules at this time point agrees with our previous PHB quantitation using the crotonic acid assay which showed that ~ 40% of PHB/cell dry weight remains at 48 h and thereafter (*5*). The TEM photographs clearly establish for the first time that almost all of this PHB is inside the cell and is not extracellular. The reason why the cell is unable to completely degrade PHB during these utilization conditions is at present not understood.

5.4.3 Changes of the cell volume during PHB production and utilization. Knowledge of the concentration of proteins involved in PHB homeostasis and how they change during PHB production and utilization is an essential component to understanding and unraveling this process. Calculation of the *in vivo* concentration of proteins requires knowledge of cell size at the time of interest. The TEM photographs shown in Figure 5.3 and 5.4 are unable to reveal cell volume change under PHB production and utilization conditions by direct examination. Since the TEM pictures present essentially flat profiles of cells obtained from random cuts through an embedded sample, the size of a cell profile is not representative of the size of the cell from which it arose. The method that has allowed the quantitation of changes in cell volume from 2-D

images such as those shown in Figure 5.4 is the theoretically unbiased stereology (*18, 22*). By taking measurements on the 2-D images, parameters from these measurements can be extrapolated to 3-D space, regardless of the shape and size of the object of interest. This estimation method has been used widely in geology, material science, neurosciences, and in the study of many biological tissues. Although stereology has not been used much in the study of bacterial cells, TEM images of bacteria are ideal for analysis by this method, since the cells in sections are embedded randomly and they are isotropic (having no preference in orientation). Stereology is practiced by superimposing line- and point-patterns on flat images of thin sections, from which the component(s) of interest can be quantified. Counted points and measured line segments are tabulated and entered into basic, assumption-free formulas, as described in the Materials and Method section. Since all cell samples are fixed by the same method, the effect of fixation on cell and granule size is assumed to be the same for all samples. This is however a caveat, since the amount of PHB differs in each sample, which could differentially effect fixation.

Using the point-counting method (Methods), the total area of cell profiles (A_{CP}) on all images was calculated for samples harvested at defined times during cultivation. As implied in Equation 5.1, A_{CP} is directly proportional to the size and the number of cell profiles (N_{CP}) on all images: the larger and the greater the number of cell profiles, the greater the number of hit points (P) with the test probe. While the size of cell profiles and its change from sample to sample is a result of the experimental testing conditions, the number of cell profiles on images is not since cells were randomly embedded and images were recorded randomly. Therefore, in order to be able to use A_{CP} for comparison purposes from sample to sample, A_{CP} must be normalized by the number of cell profiles, hence A_{CP}/N_{CP}. The change in cell volume among these samples is directly

reflected in this assumption-free (no assumption on the shape of the cell) value of A_{CP}/N_{CP}, as shown in Table 5.1. According to the Delesse principle, the area of cell profiles in a reference space (A_A) is equivalent to the volume of those profiles in the same reference space (V_V). Therefore, knowing the actual average volume of cells at one time point allows the calculation of the average volume of cells at other time points, as described in the Methods section.

In order to obtain the actual average volume of cells at one time point, images from serial sections of cells are required. We chose to examine cells in PHB_P at 5 h. An example of typical serial sections is shown in Figure 5.10. The average cell volume analysis for this time point is complicated by cell growth and division. We chose the longest cell profiles from images of serial sections and thus, the volume determined represents the population of cells just before cell division. Assuming the cells divided equally, the volume of the daughter cells is approximately half the size of the original cell. The determination of the length (*l*) and width (*d*) of the cell profiles from these sections is described in Methods. The average volume of the cell can be calculated using the volume equation of a cylinder assuming that *W. eutropha* is rod-shaped. The average cell volume at 5 h in PHB_P using the longest cell profiles was estimated to be 1.8 μm^3 or 1.8 $x10^{-15}L$ (Table 5.1). This value, chosen since most of the cells shown by TEM images and measured are in the cell division process (Figure 5.3B and Figure 5.4A, B) allowed the estimation of the average cell volume of the samples taken at other time points. The results are summarized in Table 5.1 and verified by a second approach described below. The largest change in volume is apparent between TSB 24 h and PHB_P at 2.5 h. This change reflects cell doubling. However, it is sufficiently large that an additional contribution to size might result from sensing nitrogen limitation and preparation for PHB storage.

The trends observed in cell volume change as a function of time in PHB_P was verified independently by measuring the size distribution of cell profiles on images recorded at a low magnification (negatives are at 3000×) so that a large number of cells was examined at each time point. A population of large cells should give higher frequency of long and wide cell profiles than a population of small cells if all cells are randomly embedded and examined. The major and minor axis of hundreds to thousands of cell profiles, regardless of shape and size, were measured for PHB_P 2.5, 5, 9, 24, and 73 h. Graphic representation of profile frequency in cell length is shown in the histograms of Figure 5.4. Less variation was observed in width and, therefore, only the average width is reported (Table 5.2). The average length of the cells decreased as a function of time, while the width decreased slightly from 2.5 to 9 h, and then increased slightly. As a result, the volume of the cell decreased from 2.5 to 9 h, and then gradually increased from 9 to 73 h in PHB_P, a trend similar to that measured by stereology (Table 5.1). In addition, using the average length of the longest cell profiles (usually ~ 4% of the total number of cell profiles measured) and the average width (Table 5.2) from images of each of these time points, the average volume of cells calculated using the volume equation of a cylinder (Table 5.2) are very similar to the volume values obtained from stereology. Note that the longest cell profile in PHB_P 9, 24, and 73 h should represent the actual length of the cell population, since cells are no longer dividing as indicated by the constant dry cell weight (with the weight of PHB subtracted) at these times (data not shown). Thus, it is appropriate to assume that all cells are of uniform size at these time points.

The average cell volume in TSB conditions were also measured for the 4 and 24 h samples using stereology. Again, a range of volumes is reported for the 4 h time point in Table 5.1 due to cell division. From 12 to 24 h in TSB medium, the mass of the cell (weight of PHB subtracted)

only increased by ~30% (data not shown), indicating that most of the cells are entering the stationary phase. Therefore, the average cell volume determined for TSB 24 h is close to that of a single cell.

5.4.4 Changes of the surface area of granules in wt W. eutropha H16 during PHB$_P$. Another piece of information that can contribute significantly to our understanding of PHB biosynthesis and degradation in *W. eutropha* H16 is the amount of each protein covering the surface of granules. Immuno-gold labeling studies using antibodies to the synthase (PhaC) and the phasin (PhaP), and TEM analysis revealed that these two proteins are on the surface of granules (*7, 11*). The large amounts of PhaP produced (estimated to be 3-5% of total amount of protein present under maximum PHB production conditions) were the basis for the proposal that the granules are mostly covered with PhaP (*32*). Substantial coverage, however, is not apparent in the TEM image (*7*). Immuno-gold labeling and TEM imaging also suggests very low coverage of the granule surface by PhaC. No quantitation of the surface coverage has been reported. In order to calculate the amount of protein covering granule surfaces, the total surface area of granules per cell (S_G) needs to be determined at each time point, as does the amount of each protein of interest. Again, stereology has been used to solve this problem. As shown in Figure 5.3 and 5.4, the granules at TSB 4 h (not shown), 24 h, and PHB$_P$ 2.5, 5, and 9 h appear to be spherical. However, those at the later time points alter their shape due to crowding and granule fusion. The beauty of the stereological method is that S_G can be derived without knowing the shape and number of the granules per cell since S_G is a function of the number of intersections between granule surfaces and test lines, and the length of the test line probes. The value of S_G for each time point is also reported in Table 5.1. Note that a range of S_G values are reported for TSB 4 h sample, which corresponds to the range of cell volumes reported. S_G is not reported for the 2.5

and 5 h samples in PHB_P since the granules are too small and not defined sufficiently to be quantitated.

The granules in TSB medium at 4 and 24 h appear to be roughly spherical and coalescence is not observed. Therefore, an alternative method is available to estimate S_G, providing confirmation of the results obtained from analysis using stereology. The diameter of every single granule profile on images containing 500 to 600 granules was measured for each sample. These granule profile diameters were averaged to give an apparent average granule diameter ($\overline{d}$) of 0.28 ± 0.02 μm and 0.19 ± 0.004 μm at 95% confidence interval for TSB 4 and 24 h samples, respectively. The $\overline{d}$ values were necessarily lower than the actual granule diameter ($\overline{D}$) since cross-sectioning intersects granules at random. $\overline{D}$ and $\overline{d}$ are related by Equation 5.7 (*18*).

$$\overline{D} = (4/\pi) \times \overline{d} \qquad \textbf{Equation 5.7}$$

The calculated $\overline{D}$ for 4 and 24 h TSB samples is 0.36 and 0.24 μm, respectively, if all granules are of the same size. Note that this assumption is more suitable for the 24 h time point than the 4 h time point since the granules appeared to be more heterogeneous at the early time point as revealed in serial sections of both samples (data not shown). The surface area of the granule can be calculated by using the formula for a sphere, $S=\pi\overline{D}^2$. Since there are approximately 2.5 - 5 granules per cell at TSB 4 h (depending on the choice of average cell volume) and 5 granules per cell at TSB 24 h ((*19*), Chapter 6), the total surface area of granules per cell at TSB 4 and 24 h was calculated to be 1-2 μm^2 and 0.9 μm^2, respectively. These values are very close to those obtained through stereology (Table 5.1).

5.5 DISCUSSION

Two models of PHB granule formation have been put forth in the current PHB literature: the micelle model (Figure 1.12) and the budding model (Figure 1.13). Both models account for the established location of the synthase and phasin on the surface of the granule. Earlier TEM studies revealing membrane-like material surrounding granules in intact cells (*14, 15, 33, 34*) or isolated granules (*13, 35*) also provided the basis for the budding model. We therefore studied the early stages of granule formation in *W. eutropha* H16 under growth conditions of nitrogen limitation with the hope of obtaining insight into the mechanism of this process. The cells examined by TEM have been fixed, stained, and dehydrated. The analysis that follows assumes that the observations made are not an artifact of the fixation method. Instead of observing granules randomly distributed in the cytoplasm or being close to the inner cell membrane as expected from Figure 1.12 and 1.13, respectively, nascent granules are found to arise from the center of the cell only. In addition, pronounced dark-stained features are also found at the center of the cells, and it is to these dark features that granules appear to be localized. As cultivation in PHB_P continues, the granules grow uniformly in size, and the dark features are no longer observed.

The molecular identity of these features is currently unknown. Osmium tetraoxide and uranyl acetate both serve as fixative and stains for lipid, protein, nucleic acids, and other cellular structures (*36*). The mechanism of staining is not well understood for either reagent. As a result of the nonspecific staining by both reagents, the dark-stained features could be any of the candidates listed above or other deposits that reacted with the staining reagents. Staining with more specific reagents may help in elucidating the composition of the dark stained features. Localization of nascent granules close to the unknown features have led us to propose a new

model for PHB granule formation: the dark-stained structures could serve as scaffolds, providing sites for the synthase to initiate granule formation. Subsequent to granule initiation, a number of possibilities for the fate of the scaffold have been considered. The first is that the scaffold (0.4-0.5 μm) becomes covered with granules. The second is that at some stage in granule growth, the scaffold is degraded. A third possibility is that the material that composes the scaffolds could be distributed over the surface of granule as it is being made. In any of these scenarios, the dark-stained features would not be observed at the late stage of PHB biosynthesis. The concept of scaffolds has been exemplified by cellulosome, the multicomponent, multienzyme complex from anaerobic cellulolytic bacteria that is used to degrade plant cell wall polysaccharides (*37*). The main component of the cellulosome is a multi-enzyme integrating protein unit called scaffoldin. The scaffoldin contains several cohesion domains, which recruit enzymes that play roles in cellulose degradation and contain a 'dockerin' domain. The cohesion-dockerin interaction allows the scaffoldin to organize the various cellulolytic components into a complex, which then allow all these enzymes to work efficiently and synergistically. The existence of this 'machinery' for cellulose degradation suggests that a similar complex could exist for orchestrating the proteins involved in PHB biosynthesis and degradation. Recently, Dennis *et al* have observed large structures on the surface of PHB containing granules from *W. eutropha* cells using AFM. They proposed that these structures might serve as synthesis/degradation centers (*16*). Isolation and identification of the dark-stained features observed by TEM, therefore, is important in verifying our new model and unraveling the process of PHB formation *in vivo*.

In this chapter, we have also reported the estimated average cell volume and total surface area of granules per cell from *W. eutropha* H16 cells grown in nutrient-rich TSB and in PHB_P using stereological analysis of TEM images. Once again, the assumption has been made that the

fixation of the cells has not effected the sizes of the cells or the granules. The growth conditions used in this study have been widely used in the PHB field, and therefore, these new parameters of cells should be useful to others interested in understanding PHB homeostasis. Recently, our laboratory has carried out a series of studies to quantitate the amount of PhaC, PhaZs, PhaP1, and PhaR in *W. eutropha* under these growth conditions using quantitative Western analyses ((*19, 20*), Chapter 6). Results of the Westerns, together with the cell volume and granule surface area calculated in this chapter, have provided new information on the homeostasis of PHB.

5.6 ACKNOWLEDGEMENT

I would like to thank Dr. Peter Mouton (CEO of the Stereology Resource Center, Inc, and consulting director of the Stereology Laboratory at the Laboratory of Neurosciences Gerontology Research Center, NIA/NIH, in Baltimore) for providing us with the multipurpose system probe and helpful discussions on stereological analysis. I also would like to thank Yu-Yao Tian, my father, for helpful discussions on stereological analysis, and Nicki Watson (Whitehead Institute for Biomedical Research) for helpful discussions on TEM sample preparation.

5.7 REFERENCE

1. Anderson, A.J. and Dawes, E.A. (1990) Occurrence, Metabolism, Metabolic Role, and Industrial Uses of Bacterial Polyhydroxyalkanoates, *Microbiol. Rev. 54*, 450-472.
2. Rehm, B.H. and Steinbüchel, A. (1999) Biochemical and genetic analysis of PHA synthases and other proteins required for PHA synthesis, *Int. J. Biol. Macromol. 25*, 3-19.
3. Gerngross, T.U., Snell, K.D., Peoples, O.P., Sinskey, A.J., Cushai, E., Masamune, S., and Stubbe, J. (1994) Overexpression and purification of the soluble polyhydroxyalkanoate synthase from *Alcaligenes eutrophus*: Evidence for a required posttranslational modification for catalytic activity, *Biochemistry 33*, 9311-9320.
4. Saegusa, H., Shiraki, M., Kanai, C., and Saito, T. (2001) Cloning of an intracellular Poly[D(-)-3-Hydroxybutyrate] depolymerase gene from *Ralstonia eutropha* H16 and characterization of the gene product, *J Bacteriol 183*, 94-100.
5. York, G.M., Lupberger, J., Tian, J., Lawrence, A.G., Stubbe, J., and Sinskey, A.J. (2003) *Ralstonia eutropha* H16 encodes two and possibly three intracellular Poly[D-(-)-3-hydroxybutyrate] depolymerase genes, *Journal of bacteriology 185*, 3788-3794.
6. Kobayashi, T., Shiraki, M., Abe, T., Sugiyama, A., and Saito, T. (2003) Purification and Properties of an Intracellular 3-Hydroxybutyrate-Oligomer Hydrolase (PhaZ2) in *Ralstonia eutropha* H16 and Its Identification as a Novel Intracellular Poly(3-Hydroxybutyrate) Depolymerase, *J Bacteriol 185*, 3485-3490.
7. Potter, M., Madkour, M.H., Mayer, F., and Steinbuchel, A. (2002) Regulation of phasin expression and polyhydroxyalkanoate (PHA) granule formation in *Ralstonia eutropha* H16, *Microbiology 148*, 2413-2426.

8. Maehara, A., Taguchi, S., Nishiyama, T., Yamane, T., and Doi, Y. (2002) A repressor protein, PhaR, regulates polyhydroxyalkanoate (PHA) synthesis via its direct interaction with PHA, *J Bacteriol 184*, 3992-4002.

9. York, G.M., Stubbe, J., and Sinskey, A.J. (2002) The *Ralstonia eutropha* PhaR protein couples synthesis of the PhaP phasin to the presence of polyhydroxybutyrate in cells and promotes polyhydroxybutyrate production, *J Bacteriol 184*, 59-66.

10. Potter, M., Muller, H., Reinecke, F., Wieczorek, R., Fricke, F., Bowien, B., Friedrich, B., and Steinbuchel, A. (2004) The complex structure of polyhydroxybutyrate (PHB) granules: four orthologous and paralogous phasins occur in *Ralstonia eutropha*, *Microbiology 150*, 2301-2311.

11. Gerngross, T.U., Reilly, P., Stubbe, J., Sinskey, A.J., and Peoples, O.P. (1993) Immunocytochemical analysis of poly-b-hydroxybutyrate (PHB) synthase in *Alcaligenes eutrophus* H16: Localization of the synthase enzyme at the surface of PHB granules, *J. Bacteriol. 175*, 5289-5293.

12. Liebergesell, M., Sonomoto, K., Madkour, M., Mayer, F., and Steinbuchel, A. (1994) Purification and characterization of the poly(hydroxyalkanoic acid) synthase from *Chromatium vinosum* and localization of the enzyme at the surface of poly(hydroxyalkanoic acid) granules, *Eur J Biochem 226*, 71-80.

13. Lundgren, D.G., Pfister, R.M., and Merrick, J.M. (1964) Structure of Poly-Beta-Hydroxybutyric Acid Granules, *J Gen Microbiol 34*, 441-446.

14. Boatman, E.S. (1964) Observations on the Fine Structure of Spheroplasts of *Rhodospirillum Rubrum*, *J Cell Biol 20*, 297-311.

15. Jensen, T.E. and Sicko, L.M. (1971) Fine structure of poly-beta-hydroxybutyric acid granules in a blue-green alga, *Chlorogloea fritschii*, *J Bacteriol 106*, 683-686.

16. Dennis, D., Liebig, C., Holley, T., Thomas, K.S., Khosla, A., Wilson, D., and Augustine, B. (2003) Preliminary analysis of polyhydroxyalkanoate inclusions using atomic force microscopy, *FEMS Microbiol Lett 226*, 113-119.

17. Ellar, D., Lundgren, D.G., Okamura, K., and Marchessault, R.H. (1968) Morphology of poly-beta-hydroxybutyrate granules, *J. Mol. Biol. 35*, 489-502.

18. Elias, H. and Hyde, D.M. (1983) *A Guide to Practical Stereology*. Karger, Basel.

19. Tian, J., He, A., Lawrence, A., Liu, P., Watson, N., Sinskey, A.J., and Stubbe, J. (2004) Analysis of Transient Polyhydroxybutyrate Production in *Wautersia eutropha* H16 by Quantitative Westerns and Transmission Electron Microscopy, *manuscript submitted for publication.*

20. He, A., Tian, J., Lawrence, A., Liu, P., Sinskey, A.J., and Stubbe, J. (2004) Expression Analysis of Proteins Involved in Polyhydroxybutyrate Homeostasis in *Wautersia eutropha* H16, *submitted for publication.*

21. Cavalieri, B. (1635) *Geometria Indivisibilibus Continuorum*. Bononi: Typis Clementis Ferronij.

22. Mouton, P.R. (2002) *Principles and Practices of Unbiased Stereology: An Introduction for Bioscientists*. The Johns Hopkins University Press, Baltimore, MD.

23. Thomson, W.R. (1930) Quantitative microscopic analysis, *J. Geology 38*, 193.

24. Glagolev, A.A. (1933) On the geometrical methods of quantitative mineralogic analysis of rocks., *Transactions of the Institute of Economic Mineralogy and Metallurgy 59*, 1.

25. Delesse, A. (1848) Procede mecanique pour determiner la composition des roches., *Annls. Mines 13*, 379.

26. Smith, C.S. and Guttman, L. (1953) Measurement of internal boundaries in three-dimensional structures by random sectioning., *Trans. AIME 197*, 81-111.

27. Elias, H., Hennig, A., and Schwartz, D.E. (1971) Stereology: applications to biomedicalresearch, *Physiol Rev 51*, 158-200.

28. Ingraham, J.L., Maaloe, O., and Neidhardt, F.C. (1983) *Growth of the Bacterial Cell.* Sinauer Associates, Inc., Sunderland, MA.

29. Fuller, R. and Lovelock, D.W. (1976) *Microbial Ultrastructure: The Use of the Electron Microsope.* Academic Press, London, U.K.

30. Iterson, W.V. (1984) *Inner Structures of Bacteria.* Benchmark Papers in Microbiology Series. Van Nostrand Reinhold Company Inc., New York, NY.

31. Tian, J., Sinskey, A.J., and Stubbe, J. (2004) Detection of Intermediates from the Polymerization Reaction Catalyzed by a D302A Mutant of Class III Polyhydroxyalkanoate (PHA) Synthase, *Biochemistry, manuscript accepted.*

32. Steinbüchel, A., Aerts, K., Babel, W., Föllner, C., Liebergesell, M., Madkour, M.H., Mayer, F., Pieper-Fürst, U., Pries, A., Valentin, H., and Wieczorek, R. (1995) Considerations on the structure and biochemistry of bacterial polyhydroxyalkanoic acid inclusions, *Can. J. Microbiol. 41 (suppl. 1)*, 94-105.

33. Dunlop, W.F. and Robards, A.W. (1973) Ultrastructural study of poly-β - hydroxybutyrate granules from *Bacillus cereus*, *J Bacteriol 114*, 1271-1280.

34. Wang, W.S. and Lundgren, D.G. (1969) Poly-beta-hydroxybutyrate in the chemolithotrophic bacterium *Ferrobacillus ferrooxidans*, *J Bacteriol 97*, 947-950.

35. Mayer, F., Madkour, M., Pieper-Furst, U., Wieczorek, R., Liebergesell, M., and Steinbuchel, A. (1996) Electron Microscopic Observations on the Macromolecular Organization of the Boundary Layer of Bacterial PHA Inclusion Bodies, *J. Gen. Appl. Microbiol. 42*, 445-455.

36. Bozzola, J.J. and Russell, L.D. (1999) *Electron Microscopy*. Jones and Bartlett Publishers, Boston, MA.

37. Bayer, E.A., Belaich, J.P., Shoham, Y., and Lamed, R. (2004) The Cellulosomes: Multienzyme Machines for Degradation of Plant Cell Wall Polysaccharides, *Annu Rev Microbiol 58*, 521-554.

5.8 TABLES AND FIGURES

Table 5.1 Estimated average cell volume (V_C) and total surface area of granules per *W. eutropha* H16 cell (S_G) by the method of stereology are reported as a function of time and cultivation condition. The change in cell volume is also reflected in the A_{CP}/N_{CP} values. Note that the CE associated with A_{CP}/N_{CP} is also the minimum CE associated with V_C.

Sample	[a] A_{CP}/N_{CP} (μm^2)	[b] CE	[c] V_C (μm^3)	[d] S_G (μm^2)
TSB 4h[e]	0.84	8%	0.9 - 1.8	1.3 - 2.5
TSB 24h	0.42	6%	0.9	1.3
PHB_P 2.5h[e]	1.09	6%	1.2 - 2.3	nd[f]
PHB_P 5h[e]	0.82	5%	0.9 - 1.8	nd[f]
PHB_P 9h	0.50	10%	1.1	3.6
PHB_P 24h	0.55	8%	1.2	7.3
PHB_P 73h	0.64	9%	1.4	11.2[g]
PHB_U 48h	0.49	4%	nd[h]	nd[h]

[a] total area of cell profiles/number of cell profiles

[b] sampling error associated with A_{CP}/N_{CP}, also applies to V_C

[c] average volume of cell

[d] average total surface area of granule per cell

[e] cells are under cell division at these time points; a range of V_c and S_G is reported.

[f] nd: not determined since granules were too small and ill defined

[g] the tiny granules observed at this hour was also counted during measurement

[h] nd: not determined since different phenotypes of cells seem to exist

Table 5.2 Estimated average cell volume calculated using the average length of longest cell profiles (~ 4% of the total cell profiles measured, see histograms of Figure 5.4) at each time point. The average width of all cell profiles shown in images used to measure the length of the cell profiles is also reported. The volume formula of a cylinder is used for calculation.

Sample	No. of Cell Profile Measured	[a] Width (μm)	Average Cell Vol. (μm^3)
PHB_P 2.5h	482	0.75 ± 0.015	2.4[b]
PHB_P 5h	768	0.69 ± 0.014	1.7[b]
PHB_P 9h	1596	0.66 ± 0.007	1.2
PHB_P 24h	600	0.68 ± 0.011	1.3
PHB_P 73h	754	0.74 ± 0.011	1.5

[a] with 95% confidence level

[b] volume of cells on the verge of cell devision

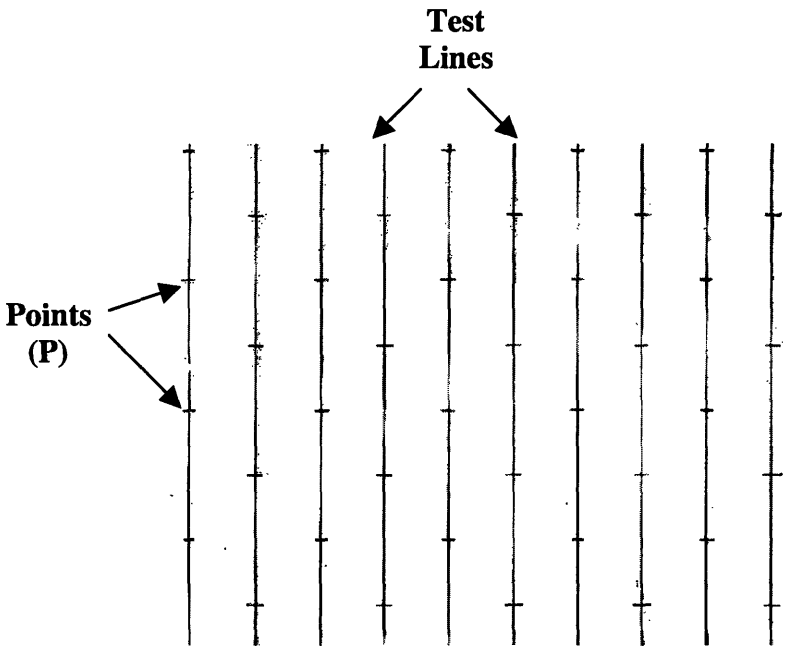

Figure 5.1 Multipurpose testing system, provided by Dr. Peter Mouton from Stereology Resource Center. Points are used to quantitate the area of cell profiles (Equation 5.1), and the test lines are used to quantitate the intersection between the granule surface and test lines (Equation 5.5)

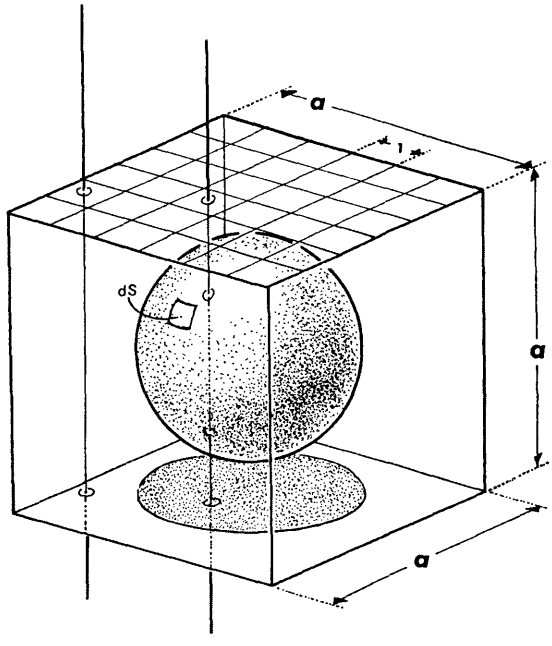

Figure 5.2 Derivation of the S_V equation. Reprinted with permission from H. Elias, A. Hennig, and D.E. Schwartz. Stereology: Application to biomedical research. Physiol. Rev. 51:158-200 (1971)]. "Let this sphere of radius *r* be enclosed in the reference volume, a cube whose edge equals α units. Divide the upper face of this cube into α^2 fields each one unit wide and one unit long. Now let straight lines pass through the center points of each little square. The length of each line within the cube measures α; their combined length is $L = \alpha \cdot \alpha^2 = \alpha^3$, which equals the volume of the cube. If all the vertical lines were parallel light rays, they would throw a shadow on the bottom of the cube. The area of such a shadow equals πr^2, while the surface of the sphere is $S = 4\pi r^2$. Each of the lines that intersects the surface of the sphere does so twice. Hence the number of points P of intersection of lines with the surface of the sphere equals $P = 2\pi r^2$. Of all the α^2 vertical lines that pass through the center points of the superficial little squares, πr^2 lines have achieved a total of $P = 2\pi r^2$ intersections with the surface of the sphere. Thus a surface of $S = 4\pi r^2$ suspended in a volume of α^3 has been intersected $2\pi r^2$ times by lines totaling $L = \alpha^3$. Since $S_V = 4\pi r^2/\alpha^3$ and $P_L = 2\pi r^2/\alpha^3$. $S/\alpha^3 = 2P/L$." Note that P defined in this excerpt is equivalent to I used in Equation 5.5 described in present chapter.

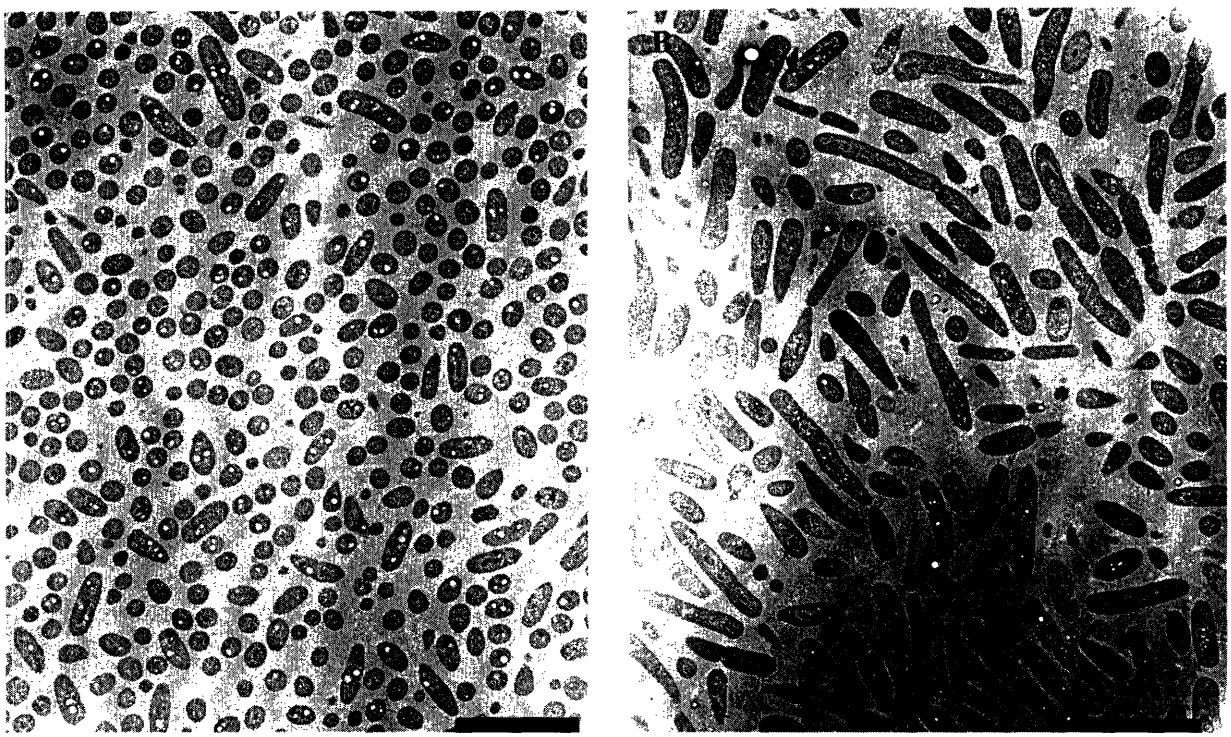

Figure 5.3 TEM images of (**A**) wt *W. eutropha* H16 grown in TSB medium for 24 h; (**B**) wt *W. eutropha* grown in PHB_P for 2.5 h after 24 h in TSB medium. Both images are recorded at the same magnification (bar size, 4.5 μm).

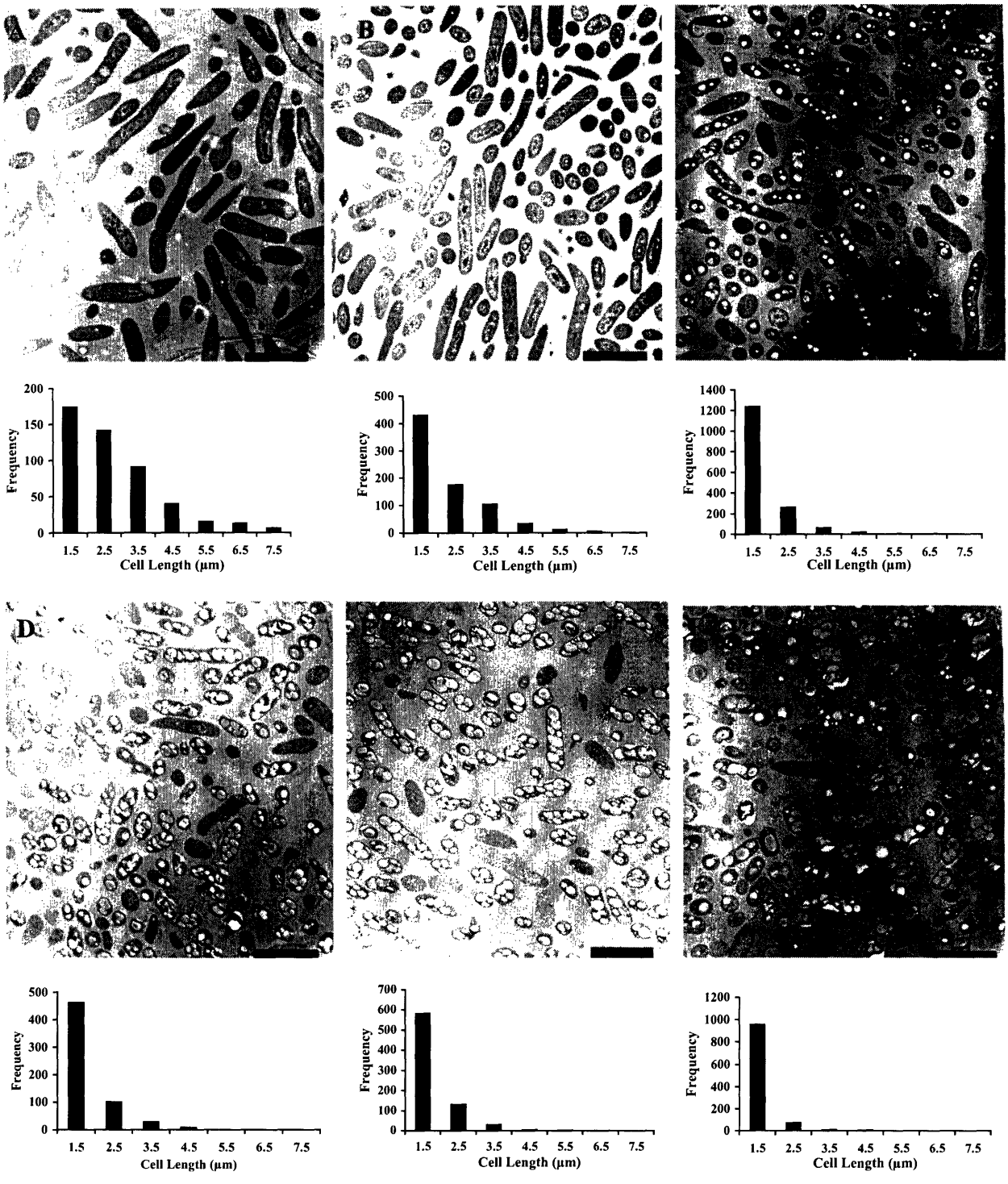

Figure 5.4 TEM images of wt *W. eutropha* H16 during its growth in PHB_P and PHB_U media. (**A**) PHB_P 2.5 h, (**B**) PHB_P 5 h, (**C**) PHB_P 9 h, (**D**) PHB_P 24 h , (**E**) PHB_P 73 h, and (**F**) PHB_U 48 h. Bar size, 3 μm. Change in cell size of these samples is reflected by the histograms. The histograms represent the size distribution of cell profiles (obtained by measuring the major-axis of all cell profiles) and are shown below each picture. Images in addition to the ones shown were also used for this analysis.

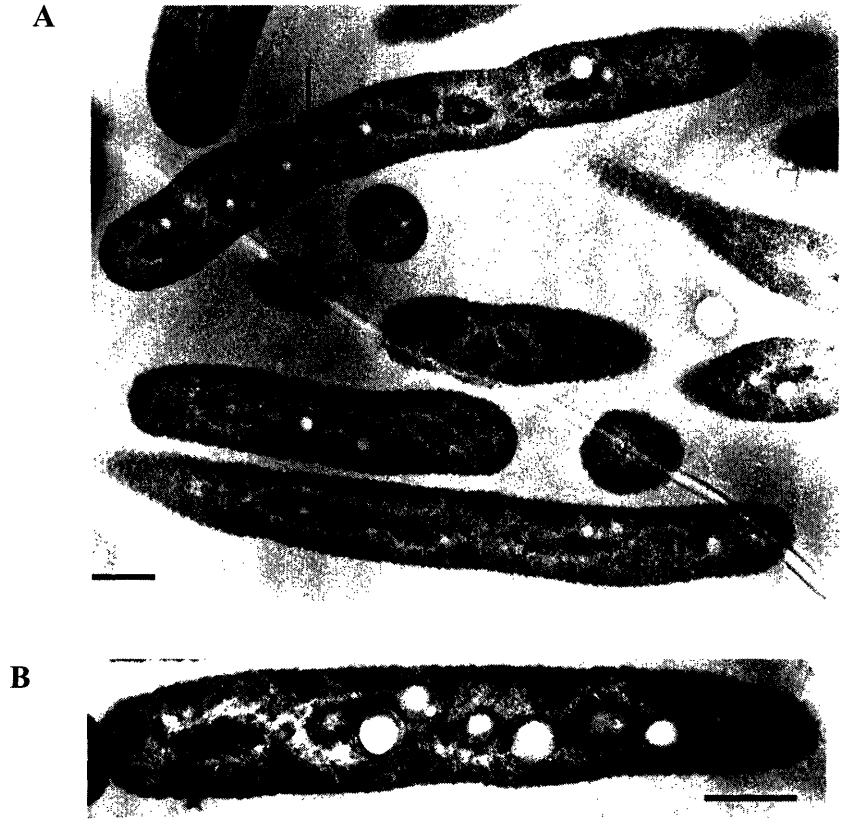

Figure 5.5 TEM images of wt *W. eutropha* H16 at 2.5 h in PHB_P. Nascent granules are revealed to be localized on dark-stained features observed near the center of the cell. Bar size, 0.5 μm. (**A**) Black arrow pointing at an example of dark-stained feature. (**B**) Image of a cell at higher magnification. Bar size, 0.5 μm.

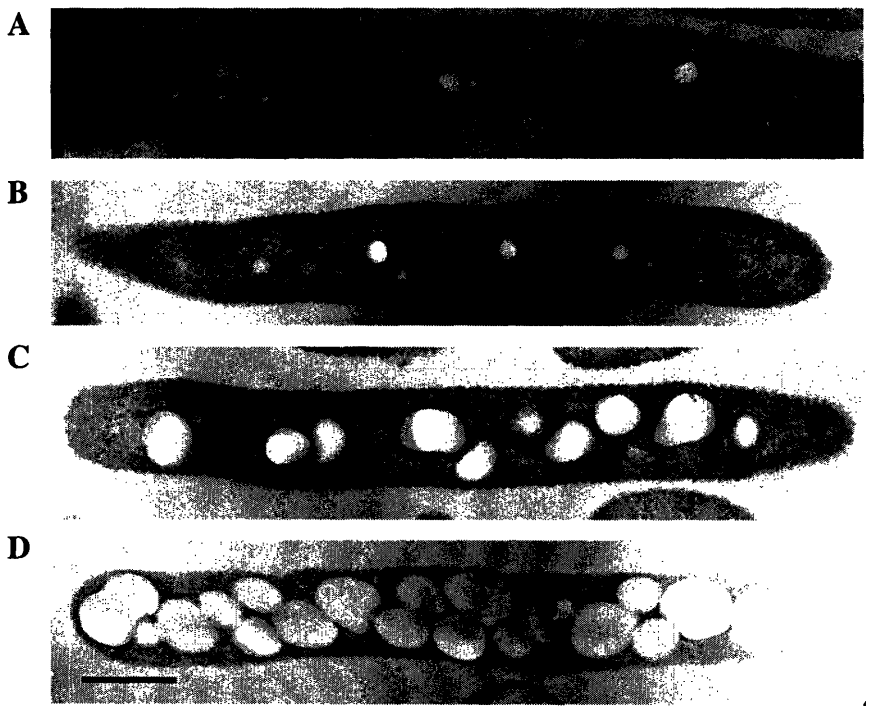

Figure 5.6 TEM images of wt *W. eutropha* H16 at PHB_P (**A**) 2.5 h, (**B**) 5 h, (**C**) 9 h, and (**D**) 24 h, showing the 'disappearance' of the dark-stained features. Bar size, 0.5 μm.

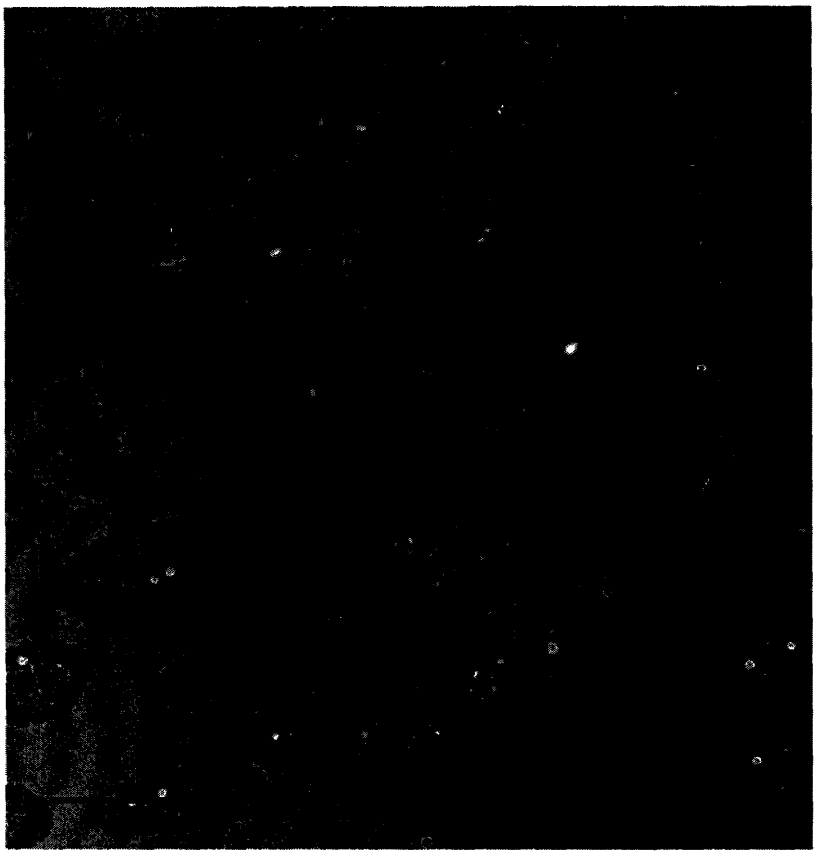

Figure 5.7 TEM of *W. eutropha* H16 with its synthase gene replaced with D302A-PhaCPhaE$_{Av}$ from *Allochromatium vinosum*, grown for 24 h in PHB$_P$. Examples of the dark-stained feature are indicated by black arrows. Bar size, 1 μm.

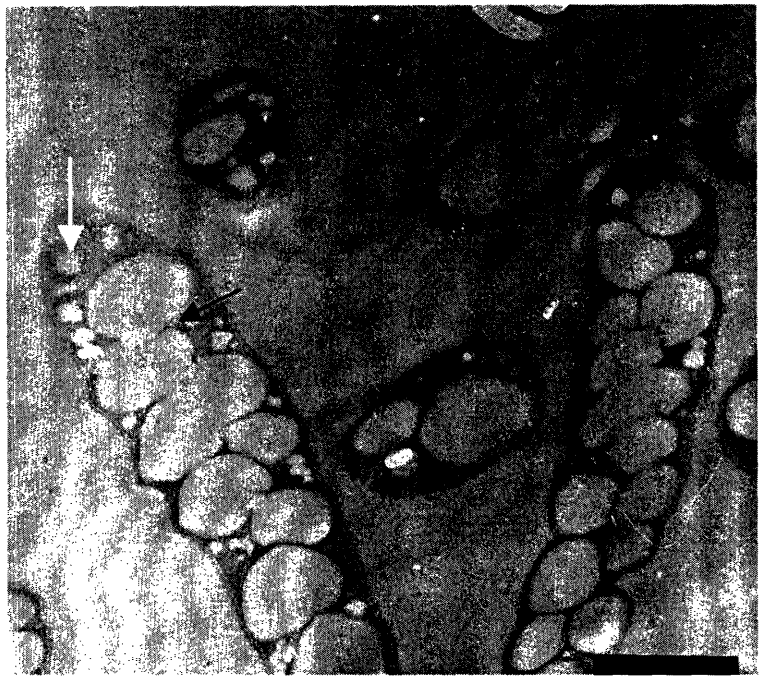

Figure 5.8 TEM image of *W. eutropha* H16 at 73 h in PHB_P. Significant granule coalescence (black arrow) was observed. In addition, small white features (white arrow) were observed. Bar size, 0.8 μm.

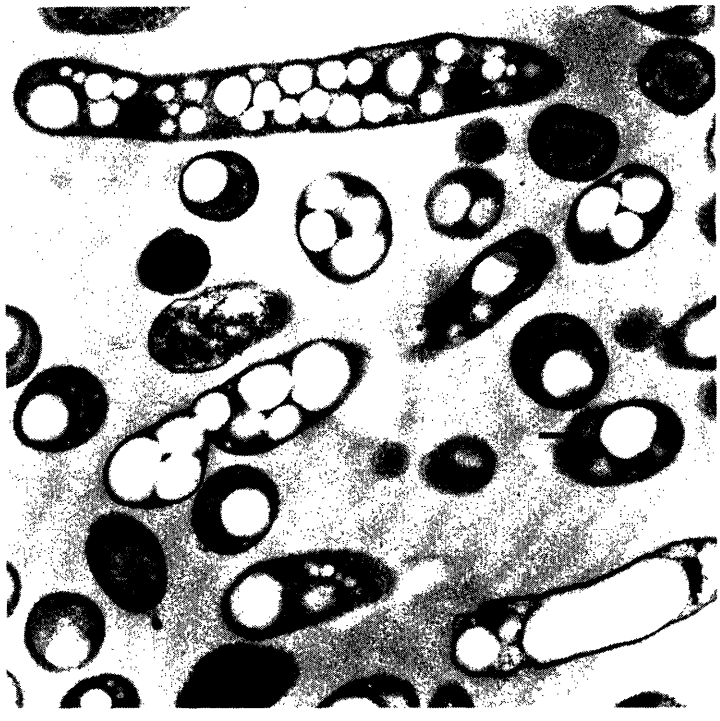

Figure 5.9 TEM image of *W. eutropha* H16 at 48 h in PHB_U. Different populations of cells seem to exist: some contained high number of smaller granules (compared to those at 24 h in PHB_P), while others contained a few of large granules. Bar size, 0.5 μm.

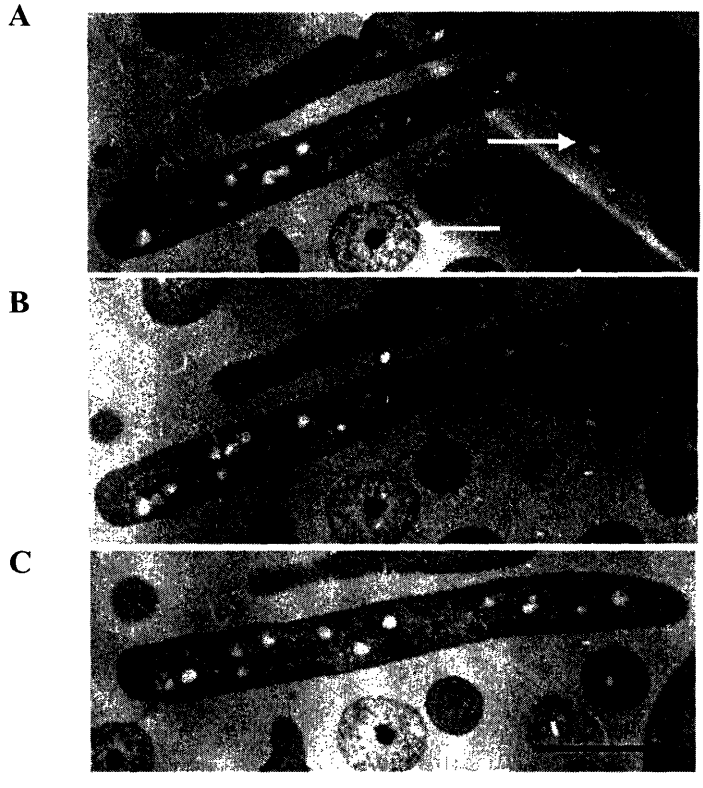

Figure 5.10 TEM images of consecutive serial sections (**A→B→C**) of the sample at 5 h in PHB_P. The longest cell profile appears to result from a cell that is lying parallel to the plane of sectioning knife, since its position does not change relative to the other two cell profiles (see white arrow) which seem to result from cells that were lying perpendicular to the place of section. Since the length of the long cell profile does not change from (**A**) to (**B**), this length represents the actual length of the cell. Notice that the cell length in (**C**) has decreased. These images also reveal that the size of the granules is fairly uniform. Bar size, 1 μm.

CHAPTER 6

Analysis of Polyhydroxybutyrate Biosynthesis and Degradation in *Wautersia eutropha* H16 by Quantitative Westerns and Transmission Electron Microscopy

6.1 ABSTRACT

Polyhydroxybutyrates (PHBs) are polyoxoesters generated from (*R*)3-hydroxybutyryl coenzyme A by PHB synthase. During the polymerization reaction, the polymers undergo a phase transition and generate granules. *W. eutropha* H16 can transiently accumulate PHB when grown in a nutrient-rich medium (up to 23% of cell dry weight (cdw) in tryptic soy broth-dextrose free, TSB). Under nitrogen-limited conditions (PHB production medium, PHB_P), up to 80% of cdw can be accumulated by these cells. Upon transferring to carbon-limited conditions (PHB utilization medium, PHB_U), 50% of the accumulated PHB can be degraded. Therefore, PHB homeostasis under nutrient-rich, nitrogen-limited, and carbon-limited conditions has been examined by quantitative Western analysis to monitor the levels of $PhaC_{We}$ (the synthase) and PhaP (a phasin), and their changes in levels over the growth period. These results show that $PhaC_{We}$ is constitutively present under both sets of conditions. The levels of phasin PhaP changed dramatically and corresponded kinetically to the levels of PHB. Transmission electron microscopy (TEM) provided the dimensions of the average cell and granule at 4 h and 24 h in TSB medium (Chapter 5). This information in turn allowed the calculation of the amounts of each protein detected (concentrations if soluble), the number of granules per cell and the granule surface coverage by PhaP and $PhaC_{We}$. The molecular weight of PHB (10^6 Da) was determined by dynamic light scattering at 4 h of growth in TSB medium, the time at which the maximum amount of PHB per cdw is accumulated. At this time, the surface area of the granules is maximally 27 – 54% covered with PhaP and there is 1-2 PhaP molecules/PHB chain. The ratio of PHB chains to $PhaC_{We}$ is ~ 60 which requires $PhaC_{We}$ to re-initiate polymer formation. Similar studies and analyses were also carried out for *W. eutropha* cells at 24 h in PHB_P. At this time, the amount of PhaP available can cover 20 – 30% of the granule surface, and there is 0.5 -

1 PhaP molecule/PHB chain. The ratio of PHB chains to $PhaC_{We}$ is 200 – 300, again demonstrating the requirement of $PhaC_{We}$ re-initation. Furthermore, the TEM studies of wt and Δ*phaR* strains in TSB medium provide further support for a new mechanism of granule formation proposed in Chapter 5.

6.2 INTRODUCTION

Polyhydroxyalkanoates (PHAs) are biodegradable polymers with properties of thermoplastics and elastomers depending on the structure of the R group (Figure 1.1). In times of nutrient limitation, many bacteria generate these polymers from 3-hydroxylalkanoate coenzyme A esters when an appropriate carbon source is available (*1*). The soluble substrate is transformed into insoluble granules in a non-template dependent polymerization process catalyzed by a synthase (PhaC) (*2*). When the bacteria find themselves in a more hospitable environment, they then degrade this polymer to generate building blocks and reducing equivalents for anabolism. However, bacteria in nutrient-rich medium can also make and degrade PHA. The biology of PHA production and utilization under these nutrient-rich growth conditions, however, remains to be elucidated.

The widespread detection of genes in many microorganisms that carry out PHA synthesis and degradation suggests that these pathways have evolved to be a general mechanism for bacterial cell survival in times of stress. Our labs have been interested in studying PHA homeostasis as a model of non-template driven polymerization processes that result in phase transitions during polymer accumulation. The mechanism by which the cells lay down the hydrophobic polymers so that they can be reused rapidly may be tractable in this 'simple'

system. The organism of our choice is *Wautersia eutropha* H16, which contains a Class I synthase that generates polyhydroxybutyrate (PHB, R=CH_3, Figure 1.1) (*3*).

In this chapter, we first report the studies of PHB production and utilization by *W. eutropha* H16 in TSB (Tryptic soy broth-dextrose free), a nutrient-rich growth medium. During the growth period, the amount of PHB changed from 15% (0 h) to ~ 23% (4 h), and then to ~0% (48 h) cell dry weight (cdw). Using antibodies (Abs) to $PhaC_{We}$ (the PHB synthase) and PhaP (a phasin), we have used time-resolved Western blots to measure the rates of their appearance and disappearance at 0, 4, 8, 12, 24, and 48 h. At 4 and 24 h, the average total surface area of PHB granules per *W. eutropha* H16 cell and the average cell volume have been recently determined by unbiased stereology analysis of images taken using transmission electron microscopy (TEM) (Chapter 5). In this chapter, the average number of granules per cell at 4 and 24 h in TSB medium has also been determined using stereology. Results from these studies, together with the molecular weight (M_W) determination of PHB, have allowed us to estimate the amount of each protein per cell, the percentage of the granule surface that is covered by $PhaC_{We}$ and PhaP, and the number of $PhaC_{We}$s per PHB polymer. These studies demonstrate that the granule surface is not entirely covered with PhaP, as previously suggested by others, and that re-initiation of polymer formation by the synthase is essential. Similar results were observed when these studies were applied to cells grown under nitrogen-limited condition. A comparison of the results from both nutrient-rich and nitrogen-limited conditions demonstrates the exquisite control by which bacteria ensure their survival. They further reinforce the differences between the structure and kinetics of granule formation *in vitro* and *in vivo*.

6.3 MATERIALS AND METHODS

6.3.1 Cultivation conditions. Wild-type (wt) *W. eutropha* H16 and the Δ*phaR* deletion strain were cultivated with aeration at 30°C. Gentamicin was included in all growth media. A single colony from a TSB plate was cultivated in 5 mL of TSB medium to saturation (~ 40 h), at which time 2 mL was transferred into 100 mL of TSB medium in 500-mL baffled flasks and grown for 24 h. These cells were washed and transferred into 200 mL TSB medium or 200 mL PHB production medium (PHB_P, minimal medium (*4*) supplemented with 1% fructose and 0.01% ammonium chloride) in 1-L baffled flasks to yield cultures with an initial optical density (OD) at 600 nm of 0.5. Cells, equivalent to an OD_{600nm} of 5, were harvested at 0, 4, 8, 12, 24, and 48 h. A 72 h time point was included for cells growing in PHB_P. PHB utilization was examined by transferring 100 mL of cells at 72 h in PHB_P to a minimal medium supplemented with 0.5% ammonium chloride (PHB_U). Cells were harvested at 0, 4, 8, 12, 24, 48, and 72 h. All cell samples collected were spun down, washed with saline solution, and stored at –80°C for Western analysis.

6.3.2 Cell counting. For cells grown under nutrient-rich conditions (TSB medium), wt *W. eutropha* H16 cells, at 0 h, were counted three times (OD_{600nm} = 0.5, containing ~ 15% PHB/cdw) using a hemocytometer (Petroff-Hausser Bacteria Counter, Hausser Scientific, Horsham, PA), and the average cell number was used in the calculations. The cell pellet at 0 h time point contained ~ 7.1×10^9 cells. The volume of culture collected at later time points was adjusted to contain ~ 7.1×10^9 cells based on OD_{600nm}. The number of cells per mL of culture was assumed to be directly proportional to the OD_{600nm} of the culture. The variation in the PHB content in samples was assumed to have minimal effect on OD_{600nm} since the difference in the

amount of PHB/cdw between the 0 h and any other time point sample is low, varying from 0 to 15%.

The presence of large amounts of PHB (>20% cdw) greatly affects the OD_{600nm} of the cell culture. For this reason, cells grown under nitrogen-limited (PHB_P) and carbon-limited (PHB_U) conditions were counted at each time point. Most of the cell counting has been done by A. He, and the details can be found in He *et al* (*5*).

6.3.3 Preparation of cell samples cultivated in TSB mediium for Western analysis. A cell pellet was thawed and resuspended in 500 μL of 50 mM Tris, 1 mM EDTA, 2% SDS, pH 8 buffer. The cell suspension was sonicated using a microtip on a XL2020-Sonicator (Misonix, NY) at power level 4 for 30 s (0.8 s on, 0.2 s off) and the sample was then heated at 95°C for 20 min before being spun down at 13,000 rpm for 6 min. The supernatant was saved for subsequent analysis by Western blotting. An appropriate amount of supernatant was chosen by trial and error to ensure that signals observed by Western analysis were not saturated. Protein, 600 to 1200 ng, from crude lysate, was loaded onto the gel. For detection of $PhaC_{We}$ and PhaP in wt *W. eutropha*, the equivalent of 0.4 and 0.4 μL, respectively, of the crude extract supernatant were loaded. Recombinant $PhaC_{We}$ and PhaP over-expressed and purified from *E. coli* were used to prepare standards; BSA at 0.1 mg/mL and SDS at 0.2% were added to all standards. All Westerns were carried out following a standard procedure, with minor adjustments in the percentage of the gel used for electrophoresis and the transfer conditions during blotting. PVDF membranes (Bio-Rad, CA) were used for electro-blotting. For $PhaC_{We}$ Western, 10% Tris-Tricine gel (Bio-Rad) was used. The gel was blotted for 2.5 h at 50V using the Criterion blotter (Bio-Rad). For PhaP Western, 15% self-made gel was used. The gel was blotted for 80 min at 100V using a Mini Trans-Blot Cell (Bio-Rad). The PVDF membranes were then incubated with

either anti-$PhaC_{We}$ (at 1/2000, dilution factor) or anti-PhaP (1/4000) Abs for ~1 h. After appropriate washings, the membranes were incubated with secondary Abs (goat anti-rabbit, conjugated with alkaline phosphatase) for ~45 min at appropriate dilutions. For $PhaC_{We}$, signals were detected by using the Western-Light Chemiluminescent Detection System (Applied Biosystems, CA). For PhaP, signals were detected by using the Immuno-Star AP chemiluminescent Kit (Bio-Rad). All Western images were recorded on a ChemiDoc XRS system and quantitated using Quantity One 1-D Analysis Software (Bio-Rad). The PhaP Western was carried out by A. He.

Preparation of cell samples cultivated in PHB_P and PHB_U for Western analysis is similar, and is described in He *et al* (*5*).

6.3.4 Solubilizing proteins from PHB granules generated under TSB growth conditions by SDS or using an extracellular PHB depolymerase. In order to determine whether 2% SDS can completely solublize all proteins from the surface of PHB granules, additional wt culture samples (1.7 mL x 2) were collected at 4 h when the maximum amount of PHB per cdw was produced. The cultures were spun down at 13,000 rpm for 3 min. After the supernatant was removed, the pellets were washed with 0.85% saline followed by centrifugation. The pellets were stored at –80°C until analysis. To one pellet, 0.5 mL of the solubilizing buffer (2% SDS, 50 mM Tris, 1mM EDTA, pH 8) was added to resuspend the cells. To the second pellet, 0.5 mL of the solubilizing buffer without SDS was added. Both cell suspensions were sonicated using conditions identical to those described above, and then heated at 95°C for 20 min. The cell suspension from the first pellet was stored at 4°C until the next step. To the cell suspension from the second pellet, 20 μL (~ 0.1 U) of extracellular depolymerase isolated from *Pseudomonas lemoignei* (specific activity 25 U/mg) in 50 mM Tris, 1 mM $CaCl_2$, 7.5% glycerol, pH 8 buffer

was added. An additional 5 μL of 100 mM $CaCl_2$ was also added so that the final $CaCl_2$ concentration was 1 mM. The reaction was incubated at 37°C for ~12 h. The sample was then brought to 2% final SDS concentration and heated for 20 min at 95°C. The cell suspension from both pellets was spun down. Additional solubilizing buffer had to be added to the first pellet suspension so that its final volume was the same as that of the second. These supernatants were analyzed by Western blotting. Similar controls were also carried out for granules generated under nitrogen-limited conditions, and are described elsewhere (*5*).

6.3.5 Extraction of PHB and M_W determination. The weight-averaged molecular weight (M_W) of PHB extracted from the 4 h sample in TSB medium, and the 24 h sample in PHB_P were determined by A. Lawrence. The details of this procedure can be found in Tian *et al.* (*6*).

6.3.6 Transmission electron microscopy. Five mL of *W. eutropha* wt and *W. eutropha* Δ*phaR* deletion strain cell samples were also collected from the cultures grown in TSB medium described above at the 4 h time point for EM analysis. An additional wt cell sample was also collected at 24 h in TSB medium. Samples were immediately fixed with gluteraldehyde and paraformaldehyde, followed by osmium tetraoxide and then by uranyl acetate. Upon fixation, the samples were dehydrated through a graded ethanol series (50%, 70%, 95%, and 100%), and finally embedded into 100% low viscosity embedding resin. All reagents were purchased from Electron Microscopy Sciences (Hatfield, PA). The detailed procedure for TEM sample preparation is described in Chapter 5. The block containing the sample was sectioned at a thickness of ~70 nm using a Diatome diamond knife on a Reichert Ultracut E microtome. The sections were examined using a Philips EM410 at 80 kV. Serial sections, each ~100 nm thick, were also obtained for the wt sample at 4 and 24 h.

6.3.7 TEM data analysis. Since TEM pictures present essentially flat profiles of organelles obtained from random cuts through the embedded sample, the size of a profile is not representative of the size of the structures from which it arose. In order to be able to interpret these cell cross-sections (will be referred to as cell profiles) in terms of three-dimensional structures, the TEM picture of wt samples were analyzed using unbiased stereology (*7*). Point and intersection-counting tests were designed to derive the average cell volume and average total surface area of granules per *W. eutropha* H16 cell. The detailed analysis is described in Chapter 5.

6.3.8 Determination of the average number of granules per cell at 4 and 24 h in TSB medium using stereology. In order to determine the average number of granules per cell from 2-D TEM images by stereology, serial section images from the 4 and 24 h time points were examined. The thickness of each section, for this analysis, should be smaller than the diameter of granules. From our previous analysis (described in Chapter 5), the mean diameter ($\overline{D}$) of granules at 4 and 24 h in TSB medium was measured to be 0.36 μm and 0.24 μm, respectively, assuming all granules are of uniform size at each time point. Therefore, the sample was sectioned so that each slice was ~ 100 nm. The methodology designed for estimation of the number of particles (e.g., number of granules) in a given tissue or specimen (e.g., cell) was developed by D. C. Sterio, and is known as the Disector Principle (*8*). The first of a pair of disector probes (the test system, shown in Figure 6.1) is placed randomly over the first of two images of adjacent sections. The second probe is then placed on the corresponding area of the second image. The first probe serves as the reference section, while the second serves as the look-up section. Each granule present in the cell is only counted once by counting the granule profile at the initial intersection between the sectioning plane and the granule. In other words, granule profiles were only

counted if they are present in the image of the reference section, and not in that of the look-up section. In order to avoid over-counting, only granules present within the frame or on the inclusion lines were counted. This procedure was continued with images of other adjacent sections until the sampling error was less than 10% (here, the number of samples is equal to the number of counting frames used). The total number of granules per unit volume of reference space (N_V) can be calculated using the following equation (*8*).

$$N_V = \Sigma Q^- / (\Sigma A \times h) \qquad \textbf{Equation 6.1}$$

Here, ΣQ^- is the number of disappearing granules summed over all counting frames, ΣA is the sum of the area of all counting frames, and h is the thickness of the section. Both ΣA and h need to be corrected by the magnification factor. This procedure was carried out for both TSB samples collected at 4 and 24 h. This exercise provides the distribution of granule particles in the volumes defined by sets of serial sections.

However, the value determined in Equation 6.1 gives the total number of granules in the reference space, which is not entirely filled with cells. Since we are interested in determining the number of granules per cell, we must now relate the volume occupied by cells in space to the reference volume, which is essentially V_V (Chapter 5). The average number of granules per cell (N_G) can be estimated using Equation 6.2.

$$N_G = (N_V/V_V) \times V_C = (N_V/A_A) \times V_C \qquad \textbf{Equation 6.2}$$

Here, V_V and A_A both refer to the cell, and not granule cross-sections. The term N_V/V_V gives the average number of granules in the volume of cells in the same reference space. Therefore, knowing the average volume of one cell (V_C), the average number of granules per cell can be obtained. The volume fraction is equal to the area fraction based on the Delesse principle, $V_V = A_A$, and determination of A_A and V_C has been described previously (Chapter 5).

In Chapter 5, the methods used to determine S_V (surface area of granules in reference space) and S_G (surface area of all granules per cell) were also described. Information on S_V and S_G allows N_G to be determined by an alternative method using Equation 6.3.

$$N_G = S_G/(S_V/N_V) \qquad \textbf{Equation 6.3}$$

Here, S_V/N_V gives the mean surface area of one granule. Knowing the total surface area of granules per cell (S_G), one can then calculate the number of granules.

6.4 RESULTS

6.4.1 Choice of TSB medium to study granule formation. As part of our effort to understand the mechanisms by which *W. eutropha* H16 synthesize and utilize PHB, we have studied the changes in protein levels involved in PHB homeostasis in different growth media as a function of time. The changes have been measured by quantitative Western blots using Abs to $PhaC_{We}$ and PhaP (Figure 6.2). One set of the growth conditions in the present studies utilizes a nutrient-rich medium (TSB). These nutrient-rich conditions have received minimal attention as most efforts have been focused on maximizing PHB production, a process that requires growth under nutrient-limited conditions (*9*). In TSB medium, we have previously shown that in wt *W. eutropha* H16 cells, the levels of PHB increase from 15 % to 23% of cdw over the first 4 h of growth and that by 48 h, the PHB is completely degraded (Figure 6.2A) (described in Chapter 7, (*10*)). The physiological reason for transient PHB production in TSB medium is presently not understood.

TSB medium was chosen to study transient PHB production and utilization based on our observations shown in Figure 6.3 using TEM. The pictures reveal that there are several small granules per cell, whose numbers can potentially be quantitated at 4 and 24 h. The granules at 24

h are also substantially smaller than those at 4 h, consistent with PHB degradation during this period. These images differ substantially from previous pictures of cells grown under nutrient-limited conditions, where the concentration of granules is so large that they are the only visible structures within the cells (*2*). It is interesting that the cells grown in TSB medium do not make granules as large as those grown in nitrogen-limited conditions.

The 4 h TEM images have been examined further by serial sections shown in Figure 6.4A through D. Examination of the features in the rectangular boxes (A-D) and the square boxes (A-D) and examination of the sections of hundreds of cells suggests that the granules within a cell are moderately uniform in size. The cells are dividing at this time point (4 h), which provides an explanation for the heterogeneity in granule size occasionally observed among cells. At 24 h, most of the cells have entered the stationary phase as indicated by the significantly reduced rate of increase in OD_{600nm} and of cdw with the weight of PHB subtracted (data not shown). At this time point, the granules are very uniform.

6.4.2 Determination of the average number of granules per cell at 4 and 24 h in TSB medium.

To determine the number of granules within the cell, one needs to know either the average cell volume (V_C) or the average total surface area of granules per cell (S_G). Unbiased stereology has recently been used to estimate each of these values in *W. eutropha* H16 grown in TSB medium at 4 and 24 h (Chapter 5). In the 4 h case, a range of V_C and S_G was reported based on the observation that the cells are dividing during this time frame (Table 5.1). The range for cell volumes varied from 0.9 μm^3 to 1.8 μm^3 with the former value being associated with cells that had newly undergone cell division, and the latter being associated with cells immediately before cell division. Thus, 0.9 μm^3 and 1.8 μm^3 are the minimum and maximum cell volumes at this time point and the average cell volume of the entire population of cells lies within this range.

For similar reasons, a range of S_G (1.3-2.5 μm^2) was therefore also reported. The V_C and S_G at the 24 h time point obtained from stereological analysis provided a close estimation of the cell volume and granule surface area of the actual population of cells as the cells are close to the stationary phase.

With this information, the average number of granules per cell can be extracted from the images of serial sections such as those shown in Figure 6.4 using the disector probe based on the Disector Principle (*8*). By counting the total number of disappearing granule profiles (ΣQ^-) from the reference section to the look-up section in a known reference volume, the average number of granules per cell can be calculated by two methods (see Equation 6.2 and Equation 6.3 in Methods). The first method relates the number of granules per reference space (N_V) to the volume of cells per reference space (V_V) and uses the information on the average cell volume (V_C) to obtain the average number of granules per cell (N_G). The second method uses the average surface area of 1 granule (S_V/N_V) and S_G to obtain N_G. The results from both methods agree. There are approximately 5 granules per *W. eutropha* H16 cell at 24 h in TSB medium. At 4 h, there are 2-3 granules per cell if the average cell volume of the freshly divided cells is used, and ~ 5 granules per cell if the average cell volume of the elongated cells before cell division is used. The number of granules is substantially reduced from the number reported in cells grown in nutrient-limited media ((*1*), Chapter5).

6.4.3 Quantitative Western analysis. As a first step in our Western analysis to determine the concentration of various proteins during PHB production and utilization, we required Abs to $PhaC_{We}$ and PhaP. In the case of PhaP, the Abs was generated from purified proteins (*11*) and further purified using the corresponding deletion strains, a process described in detail in He *et al* (*5*). $PhaC_{We}$ Abs required no additional purification. As noted in the introduction, $PhaC_{Av}$ and

PhaP at some point are attached to the PHB granules and we worried about our ability to remove these proteins quantitatively. Thus, a set of controls was carried out to convince ourselves that the standard procedure of boiling the crude cell extracts in 2% SDS for 20 min at 95°C was sufficient to recover all of the protein in the cell regardless of its location. The cells accumulating transient PHB (grown in TSB medium) were processed by two methods subsequent to sonication. The first method involved boiling the cell suspension directly in 2% SDS buffer (Figure 6.5, all lane 1s). The second method involved first treating the cell suspension with the extracellular PHB depolymerase from *P. lemoignei* to remove the PHB, followed by boiling in 2% SDS buffer (Figure 6.5, all lane 2s). In all cases, the amount of recovered $PhaC_{We}$ and PhaP was similar, indicating that the PHB is not interfering with our efforts to quantitate these proteins. Similar controls (*5*) were carried out for PHB granules produced under nitrogen-limitation, and the results are similar to those shown in Figure 6.5.

6.4.4 Analysis of proteins in wt W. eutropha H16. The changes in protein amounts as a function of growth conditions have been examined by quantitative Western blotting methods. The results of a typical set of experiments under the TSB growth conditions are shown in Figure 6.2. Note that in Figure 6.2B, the scale for PhaP on the right is different from the scale for $PhaC_{We}$ on the left. In addition, we chose to express the amount of each protein in fmol/μL of cell free extract (CFE). During the sample collection process designed to compensate for increased cell number, less volume of culture was used for pelletting (see Methods for details). This decision was based on the assumption that the number of cells per mL of culture is directly proportional to the OD_{600nm} in TSB medium. Each pellet should therefore contain the same number of cells. This method assumes that change in OD is a good reflection of change in cell number. We believe this is a good assumption as the cells do not make a large amount of PHB under these growth

conditions. The presence of 0.1 mg PHB/mL cell culture increases the OD_{600nm} by ~ 0.2 OD (data not shown). The error associated with the volume used to collect cells based on OD is < 10%, which is less than the error associated with cell counting (20 - 30%). By resuspending each pellet with the same volume of buffer, the amount of each protein at a given time point can be compared in terms of fmol/μL CFE. Figure 6.2B shows the relative amount of each protein as a function of time in the wt strain grown in TSB medium.

The OD_{600nm} assumption does not hold for cell cultures grown in nitrogen-limited condtions in which up to 80% PHB/cdw is produced. PHB is also present in significant amount (from 80% to 40% PHB/cdw) throughout the PHB utilization stage. For this reason, the number of cells/mL of culture at the chosen times in PHB_P and PHB_U were counted. Figure 6.6 shows the relative amount of each protein as a function of time in the wt strain grown in PHB_P and PHB_U. Note that the amount of protein is expressed in terms of number of protein molecule per cell.

6.4.5 Relationship between PhaP and PHB. Previous studies have demonstrated that increasing amounts of PhaP occur with increased PHB production (*11*). The results in Figure 6.2A and B and Figure 6.6A and B, however, demonstrate the first kinetic correlation between these two species under nutrient-rich and nutrient-limited conditions. The rate at which PHB is produced and utilized is correlated with the rate at which PhaP is produced and degraded.

6.4.6 Time course of $PhaC_{We}$. Under nutrient-rich conditions, the amount of $PhaC_{We}$ does not appear to change appreciably between 0 and 12 h as shown in Figure 6.2B and are constitutively expressed. The slight downward trend in the amount of $PhaC_{We}$ from 0 to 4 h may reflect the <10% (~ 6 % for the 4 h time point) error associated with the assumption that OD_{600nm} is proportional to cell number. The amount of PHB/mL cell culture increased from 0.03 mg to 0.14

mg between 0 to 4 h, respectively, and this additional amount of PHB increased the OD_{600nm} by ~ 0.2. Between 12 and 48 h, the amount of $PhaC_{We}$ increased. From 24 to 48 h, all of the PHB is completely degraded, indicating the amount of carbon in the medium is low. Other metabolites could also be limiting such that cells are stressed and consequently are preparing themselves to produce more PHB. As a result, $PhaC_{We}$ expression could be upregulated, ready to make PHB when the appropriate nutrient conditions are encountered.

Under nutrient-limited conditions (PHB_P and PHB_U), $PhaC_{We}$ is also constitutively expressed with little fluctuation in its amount over time (Figure 6.6A and B).

6.4.7 In vivo concentrations and molecules per cell of $PhaC_{We}$ and PhaP at 4 and 24 h in TSB medium. Quantitative Western analysis has provided information about the amount of each protein in the cells. Previously, the average cell volume of a *W. eutropha* H16 cell at 4 and 24 h in TSB medium was reported to be 0.9 -1.8 μm^3, and 0.9 μm^3, respectively (Chapter 5, Table 5.1). Knowing the number of cells and the amount of each protein they contain allows the calculation of a concentration of each protein and the number of molecules of each protein per cell. The results are summarized in Table 6.1. Note that in this table, the amount of PhaR (a putative transcription regulator) and $PhaZ1_a$ (an intracellular depolymerase) is also included since both proteins have been demonstrated to be involved in PHB homeostasis in TSB medium. Western quantitation of these two proteins was carried out by P. Liu and A. He, and has been described in our recent manuscript (*6*). The choice to report concentrations (μM) of each protein assumes that they are soluble and not localized to granules or membrane. Since different populations of cells are present at 4 h in TSB medium, a range of protein concentrations or the number of protein molecules per cell are reported for this time point. The ratio of $PhaZ1_a$ to $PhaC_{Av}$ is approximately 5:1 at 4 h and 1:1 at 24 h. Also of interest is the ratio of PhaR to

$PhaC_{We}$ (2:1). The concentration of PhaR is particularly striking as PhaR is a regulatory protein. The μM levels of PhaR and the close stoichiometry relative to PhaC suggest that it plays a role other than that of a transcription factor. Finally, PhaP is present at a much higher concentration (~ 40 μM) than the rest of the proteins studied, consistent with reports from others (*12*).

6.4.8 Protein coverage of granule surface area per cell at 4 and 24 h in TSB medium.

Previous immuno-gold labeling experiments have shown that $PhaC_{We}$ and PhaP are located on the granule surface under nitrogen-limited conditions (*13, 14*). The amount of PhaP produced under these conditions has been estimated to be 3-5% of total amount of protein present (*12*). Results from our present studies indicate that PhaP is ~ 9% of the total amount of protein present at 4 h in TSB medium. No information at present is available on the location of $PhaC_{We}$ and PhaP under nutrient-rich conditions. For calculation purposes, we have assumed that both proteins are granule bound. With this assumption, the extent of granule surface coverage by $PhaC_{We}$ and PhaP under nutrient-rich conditions can be calculated. The calculation requires a knowledge of the average total surface area of granules per cell (S_G) determined by stereology at 4 and 24 h in TSB medium to be 1.3-2.5 μm^2, and 1.3 μm^2, respectively (Chapter 5, Table 5.1). Assuming PhaP (20 KDa) and $PhaC_{We}$ (64 KDa) are both globular in structure, the Stokes radius (R) of the two proteins can be approximated to be 2.1 nm and 3.5 nm, respectively, using chymotrypsinogen A (25 KDa) and BSA (66 KDa), globular proteins of comparable size, as models. From the size, one can estimate the theoretical number of each of these proteins required to cover the entire surface of granules per cell. In this calculation, we assumed the area of the protein that is in contact with the granule is equivalent to the area of a square with its length equal to the diameter of each globular protein (Area $= (2 \times R)^2$). Dividing the total surface area of granules per cell by this contact area gives the maximum number of each protein

molecule that can occupy the surface of the granules (Table 6.2). Given that we know the amount of protein extracted from a known number of cells, the actual number of $PhaC_{We}$s and PhaPs per cell can be obtained (Table 6.1). A comparison between experimentally determined number and the maximum give ranges of protein coverage at 4 h in TSB medium due to the complications associated with cell division. At 4 h, there are approximately 330 molecules of $PhaC_{We}$ and 39,000 molecules of PhaP per cell. The total surface area of granules per cell is 1.3 μm^2 to 2.5 μm^2, and the coverage by $PhaC_{We}$ and PhaP is 1.6% to 0.8% and 54% to 27%, respectively. The results are summarized in Table 6.2. Similar values of PhaP surface coverage (35%) were obtained for cells at 24 h. However, $PhaC_{We}$ coverage increased significantly between 4 to 24 h from 0.8 - 1.6% to 5.5%, due to the increasing amount of $PhaC_{We}$ and the decrease in the total granule surface area per cell. It is important to reemphasize that the partitioning of $PhaC_{We}$ and PhaP between soluble and granule bound states is unknown, but by analogy with limiting nitrogen growth medium, they are likely to be granule bound. Thus, the low surface coverage even for PhaP suggests that the granules formed under TSB conditions are likely covered by lipid or other unknown components.

6.4.9 Protein coverage of granule surface area per cell at 24 h in PHB_P. Since the density of the PHB granule generated under nitrogen-limited conditions has been previously reported in literature (*15*), two independent methods are available to quantitate the coverage of granule surface by $PhaC_{We}$ and PhaP at 24 h in PHB_P medium. In the first method, the estimated average total granule surface area per cell (S_G) is determined from stereology analysis of TEM images (Chapter 5, Table 5.1). Analysis using this method does not require the knowledge of the shape, size or number of the granules. Knowing the amount of each protein per cell then allows the calculation of its granule surface coverage. In the second method, the total granule surface area

per volume of cell culture (e.g., 1 mL) is calculated using information on the amount of PHB present in that volume of cell culture and the density of amorphous PHB. In addition, the dimension of an individual granule is needed. Note that the calculations involved in the first method are cell based, whereas those in the second method are culture volume based. Thus, cell counting is a source of error in the first method, and granule dimension along with the density of amorphous PHB granule are the major source of error in the second method. Each method of calculation is described below in details.

Method 1: Calculation of protein coverage of granule surface using S_G derived from stereological method. Previously, S_G at PHB_P 24 h was determined to be ~ 7.3 μm^2 (Chapter 5, Table 5.1). Knowledge of the approximate Stoke radius of $PhaC_{We}$ and PhaP (described in Section 6.4.8) allows the estimation of the theoretical number of each of these proteins required to cover the entire surface of granules per cell by the same calculation method described in Section 6.4.8). The theoretical numbers are summarized in Table 6.3. Western analysis and cell counting (each carried out 3 times) provided the information regarding the average amount of each protein per cell at PHB_P 24 h. There are ~ 750 and ~ 86400 molecules of $PhaC_{We}$ and PhaP present in a cell at this time point. For calculation purposes, we have assumed that all proteins are granule bound. With this assumption, the extent of granule surface coverage by each protein can be calculated. The amount of $PhaC_{We}$ and PhaP available is only enough to cover 0.5% and 21%, of the granule surface, respectively. The results are summarized in Table 6.3. Again, the values of PhaR, $PhaZ1_a$, and $PhaZ1_b$ (a putative intracellular depolymerase) are also included since their presence has been demonstrated and quantitated in nutrient-limited conditions (*5*).

Method 2: Calculation of protein coverage of granule surface using density of PHB granules. The density (ρ) of PHB granules can provide the information on the total volume (V) of granules per volume of culture if the mass (M) of PHB present in that volume of culture is known (ρ = M/V). The amount of PHB can be determined by the crotonic acid analysis. At 24 h in PHB_P medium, there is 1.13 mg PHB per mL of culture, which corresponds to a total PHB volume of 1.5 × 109 μm^3 per mL of culture assuming the density of amorphous PHB is 0.75 g/mL (Note that the density of crystalline PHB has been previously determined to be 1.25 g/mL (*15*); amorphous PHB presumably contains 40% water, and therefore it's density is approximated to be 0.75 g/mL). Information of the total PHB volume can then be used to obtain the number of granules per mL of culture if the dimension of granules is known. To accomplish this, the length of the major and minor axis of approximately 550 granule profiles on TEM images were measured; their average was determined to be 0.42 μm and 0.3 μm, respectively. These values were necessarily lower than the actual length of the granule major and minor-axis since cross-sectioning intersects granules at random. These values were therefore multiplied by a factor of (4/π) to obtain the actual length of the major and minor axis of the granules assuming all granules are uniform in size (Chapter 5). Although these values suggest that granules are not spherical at 24 h in PHB_P medium, at least by the method of TEM, we decided to assume the shape of granule to be spherical since we are interested in obtaining an approximate size of the granule. The average of the above two values (0.46 μm, after correction) was used as the average diameter of spherical granule at this h. Using the volume formula of a sphere, the average volume of a granule is calculated to be 5.1×10^{-2} μm^3. Therefore, there are ~ 3×10^{10} PHB granules per mL of culture. Knowing this number and the average surface area of 1 granule (using surface area formula of a sphere), the total surface area of granules per mL of culture was

calculated to be 2×10^{16} nm^2. Similarly, the theoretical number of each protein required to cover this amount of granule surface area completely can be determined as described in the above section (6.4.8). These values are summarized in Table 6.4. The data from the same Western analysis can also be used to provide the information on the amount of each protein per mL of culture at PHB_P 24 h (since the amount of crude extract quantitated by Western and the volume used to pellet the cell are known). These values are also summarized in Table 6.4. By this method, the amount of $PhaC_{We}$ and PhaP available can cover 0.8% and 33% of the granule surface, respectively.

6.4.10 M_W of PHB at 4 h in TSB medium and 24 h in PHB_P allows determination of the $PhaC_{We}$/PHB and PhaP/PHB ratios: Evidence for re-initiation of PHB biosynthesis in vivo.

The M_W of PHB prepared from two independent samples collected at the 4 h time point in TSB medium, and at 24 h in PHB_P medium was determined by dynamic light scattering by A. Lawrence. In the case of PHB generated in TSB medium, the average M_W was 1 MDa with a polydispersity of 1.2. Surprisingly, PHB polymer produced under nutrient-limited conditions has the same M_W (1 MDa) and polydispersity (1.2). The M_W number, the amount of PHB in a given volume of cell culture determined by the crotonic acid assay ((*16*), and Chapter 7), and the amount of $PhaC_{We}$ obtained from the same volume of cell culture (by Westerns), allowed the calculation of the ratio of molecules of PHB to $PhaC_{We}$. At 4 h in TSB medium, this ratio is ~ 60. At 24 h in PHB_P, this ratio is 200 – 300. These results require that $PhaC_{We}$ can reinitiate polymer formation. The low polydispersity of the PHB molecular weight in both cases suggest that the re-initiation process is exquisitely controlled by either $PhaC_{We}$ itself or by $PhaC_{We}$ in conjunction with other factors such as PhaP or perhaps PhaR. Since the amount of PHB (Chapter 7, Figure 7.10A) and the amount of $PhaC_{We}$ present at each time point during the PHB

production phase in PHB_P is known, the specific activity of $PhaC_{We}$ *in vivo* is calculated to be 40 – 80 U/mg. The specific activity of $PhaC_{We}$ under nutrient-rich growth conditions was not evaluated since not enough time points were taken during the PHB production phase. The ratio of PhaP/PHB at 4 h in TSB medium can also be calculated from the data in Figure 6.2A and B. The ratio is 1-2. This ratio is determined to be 0.5 – 1 at 24 h in PHB_P using the data from Figure 6.6C. The PhaP/PHB ratio will most likely have important implications in establishing a function for PhaP in granule biogenesis.

6.4.11 Localization of granules observed in ΔphaR W. eutropha H16 strain. Our recent kinetic studies of wt *W. eutropha* grown in nitrogen-limited medium using TEM revealed nascent granules localized on dark-stained structures near center of the cell at the early stage of granule biosynthesis (Chapter 5). The analysis involved fixing and staining cells with paraformaldehyde, gluteraldehyde, osmium tetraoxide, and uranyl acetate followed by dehydration with increasing amounts of ethanol. The structures at 4 h in TSB medium (Figure 6.3A and Figure 6.7A) analyzed by a similar procedure are present, but are not as readily apparent as in our earlier studies. The results may differ because the features have disappeared, they are obscured by the granules, or the mechanism of granule formation differs from nutrient-limited conditions. The dark-stained features, however, are readily apparent at 24 h time point (Figure 6.3B and Figure 6.7B). Electron micrographs have also been obtained from a number of isogenic deletion strains grown in TSB medium. Interesting results have been obtained from Δ*phaR* cells previously shown to contain large numbers of small PHB granules in nitrogen-limited medium (*14*). Interestingly, when this Δ*phaR* strain was examined at 4 h in TSB medium, localization of small granules near the center of the cell is clearly observed (Figure 6.8).

6.5 DISCUSSION

Studies of PHB production and utilization under nutrient-rich and nutrient-limited conditions have confirmed some expectations about this process and have given us new insight about granule formation and PHB degradation. First, the kinetics of PhaP formation and disappearance in wt *W. eutorpha H16* are closely coupled to PHB levels, and there are 1-2 PhaPs/PHB polymer at the 4 h time point in TSB medium, and 0.5 – 1 PhaPs/PHB polymer at the 24 h time point in PHB_P. While previous studies have demonstrated unequivocally the importance of PhaP in PHB formation, a kinetic correlation, which has important implications in the mechanism of granule formation, has not been previously established.

Second, both $PhaC_{We}$ and $PhaZ1_a$ are detected throughout the nutrient-rich and nutrient-limited conditions (*5, 6*). Both are constitutively expressed and present in similar amounts. Comparison of our results with those recently reported from the Saito group reveal some discrepancies which may be associated with differences in sampling times and analysis methods. While they detected the presence of $PhaZ1_a$ in nitrogen-starved, carbon-rich medium (*17, 18*), they did not detect the presence of $PhaZ1_a$ in nutrient-rich medium similar to TSB medium. However, only a single time point after 2 days of cultivation was examined. In addition, Saito *et al* claimed that under nutrient-limited conditions, the ratio of $PhaZ1_a$: $PhaC_{We}$ was 1:500 (*18*). Instead of carrying out Western analysis on both $PhaC_{We}$ and $PhaZ1_a$ in the same cell extracts as we have done in this study, they only carried out $PhaZ1_a$ Westerns. They then used the number of $PhaC_{We}$ molecules per cell (18,000 molecules per cell) previously reported by Kawaguchi *et al* (*19*). This number appears to be a large overestimate for these growth conditions. Quantitative Western analysis in our studies reveals that the levels of $PhaZ1_a$ and $PhaC_{We}$ are close to 5:1 at 4

h and 1:1 at 24 h in TSB medium (Table 6.1). Similar ratios have also been found in cells grown in nitrogen-limited conditions (*5*).

At present, it is clear from our studies that $PhaC_{We}$ and $PhaZ1_a$ are present during the entire growth period in TSB medium, PHB_P, and PHB_U (the Western data on $PhaZ1_a$ can be found in Tian *et al* (*6*) and He *et al.* (*5*)). It is not possible to tell, however, if the synthase and the depolymerase are active at the same time. In part, the problem is associated with the lack of a good assay for the intracellular depolymerases in *vitro*. The turnover numbers of the enzymes measuring hydroxybutyrate are very low compared to turnovers measured *in vivo* (*5*). Studies from several groups examining PHB production and utilization under nutrient-limited and rich conditions have suggested that the synthase and the depolymerase are active simultaneously (*17-20*). Doi and coworkers previously reported that when *W. eutropha* cells containing PHB were transferred to a nitrogen-free medium containing pentanoic acid as the sole carbon source, the content of PHB decreased while that of the copolyester of HB and hydroxyvalerate (HV) units increased; when cells containing copolyesters were transferred to nitrogen-free medium containing butyric acid, the content of copolymer reduced, while that of PHB increased (*20*). Kobayashi *et al* have also reported that the $\Delta phaZ1_a phaZ2$ (PhaZ2, an intracellular oligomer hydrolase) double deletion strain was able to accumulate more PHB at the log phase when cultivated under nutrient-rich conditions, thus suggesting that the depolymerases and synthase are active simultaneously. However, since more than one depolymerase has been demonstrated by genetic and *in vivo* studies ((*10, 18*) and Section 7.7 in Chapter 7), it is unclear which depolymerase(s) is active simultaneously with the synthase.

We also attempted to determine the average number of granules per cell at 4 and 24 h in TSB medium. Change in cell size due to cell division complicates the analysis at the 4 h time point.

The fate of the granules during cell division, that is whether they are equally distributed between daughter cells is not known. Given this problem and assuming consequently a range of cell volumes and total granule surface per cell, we calculated using unbiased stereology that there are 2 to 5 granules per cell. At 24 h when the cells are more uniform and non-dividing, there are 5 granules per cell. The average size of the granule also decreases (Chapter 5). While further study is required, the degradation of the granules appears to be uniform. Serial sectioning of samples in TSB medium at time points not complicated by cell division is essential.

TEM studies of *W. eutropha* H16 wt and deletion strains grown in TSB conditions have given us additional support for the new granule formation model proposed in Chapter 5. We and others have previously considered two models for granule formation: one model involves micelle formation by aggregated PHB tails extending from the synthase and that granule formation is driven by the physical properties of the polymer (Figure 1.12). The second model involves granules budding from the cytoplasmic side of the plasma membrane (Figure 1.13). Neither model is in complete agreement with the results from the TEM studies of the early stages of PHB production under nitrogen-limited conditions presented in Chapter 5. These studies revealed that the granules were localized on dark-stained features near the center of the cells. The complexity of the sample preparation for TEM analysis leaves much room for caution of interpretation. However, these studies have suggested that maybe biology plays a much more important role in nucleation of granule formation than the community previously has considered.

The dark-stained features are again observed at the 24 h electron micrograph in TSB medium (Figure 6.7B) and less readily apparent at the 4 h time point. Analysis of many cells suggests granules also appear to be localized to the features. Localization of granules is also clearly shown by the TEM image of Δ*phaR* strain grown in TSB medim for 4 h. The dark-stained

structure is not, however, readily apparent at this time point. It is possible that these structures differ under different growth conditions. In neither case (Figure 6.7B or Figure 6.8) are the granules randomly distributed as might be expected for the micelle model, nor are they associated with the membrane as predicted by the budding model. Thus while caution is always required in interpretation of data by TEM subsequent to cell fixation, the TEM data suggest that alternative models for granule formation need to be considered.

Insight in granule formation is further elucidated by the calculations of the extent of phasin PhaP coverage of total granule surface area per *W. eutropha* H16 cell. Under nutrient-rich growth conditions, the coverage of transient PHB at best is 27 – 54% of the granule surface. Under nitrogen-limited conitions, the amount of PhaP available can cover 20 – 30% of the granule surface, as determined by two independent methods. EM studies of PHB granules from *Bacillus cereus*, *Bacillus megaterium* (*21*), *Rhodospirillum rubrum* (*22*), and *Chlorogloea fristschii* (*23*) all revealed a 3 nm to 20 nm layer (depending on species) surrounding the surface of granules. These studies along with biochemical analysis of changes in amounts of lipid during PHB production (*24*) suggest that a monolayer of lipid might be involved in surface coverage of granules. Recent atomic force microscopy analyses also suggested a structure(s) on the granule surface that are 350 Å in diameter and that they possess a pore like structure of 150 Å in the center (*25*). Clearly more careful analysis using multiple techniques is required to understand the biology of granule formation.

Finally the mechanism of PHB chain termination is of great interest to new material development. The present studies have given us some unexpected insight into this process. At the 4 h in TSB medium, there are approximately 60 PHB chains per $PhaC_{We}$. At 24 h in PHB_P, there are 200 –300 PHB chains per $PhaC_{We}$. The molecular weight of the PHB generated from

both conditions is amazingly monodisperse. Re-initiation of the polymerization process is required by these observations. These result support the hypothesis that synthase has an additional chemical role in polymer chain termination and re-initiation, proposed in Chapter 3. Recall in that chapter, the ability of the recombinant Class III synthase from *Allochromatium vinosum* to disengage itself from PHB once the polymer chain reaches 10^6 Da in size has been demonstrated *in vitro* (Scheme 3.3 and Figure 3.8). Given that the polymerization process involves covalent catalysis, the polymer must be hydrolyzed or undergo a transesterification onto a second site in the protein so that it can be hydrolyzed and re-initiation can begin. The mechanism of regulation of this process is of great interest. The role of PhaP in this process with only 1 to 2 PhaPs per PHB chain, the role of PhaR present in similar amounts to $PhaC_{We}$ (Table 6.1 and 6.3), the importance of PhaC alone or the curvature of the granule all are of interest to investigate. Overall, the study of PHB production and utilization in TSB medium, PHB_P, and PHB_U has given us a glimpse into transient and non-transient PHB formation and degradation, although the biological basis for the transient formation process is not understood. Thus information learned from this study should help us in unraveling the granule formation and degradation processes.

6.6 ACKNOWLEDGEMENT

I would like to thank Dr. Peter Mouton (CEO of the Stereology Resource Center, Inc., and consulting director of the Stereology Laboratory at the Laboratory of Neurosciences Gerontology Research Center, NIA/NIH, in Baltimore) for providing us with the disector probe and helpful discussions on stereological analysis.

6.7 REFERENCE

1. Anderson, A.J. and Dawes, E.A. (1990) Occurrence, Metabolism, Metabolic Role, and Industrial Uses of Bacterial Polyhydroxyalkanoates, *Microbiol. Rev. 54*, 450-472.
2. Stubbe, J. and Tian, J. (2003) Polyhydroxyalkanoate (PHA) homeostasis: the role of PHA synthase, *Nat Prod Rep 20*, 445-457.
3. Rehm, B.H. and Steinbüchel, A. (1999) Biochemical and genetic analysis of PHA synthases and other proteins required for PHA synthesis, *Int. J. Biol. Macromol. 25*, 3-19.
4. Peoples, O.P. and Sinskey, A.J. (1989) Poly-b-hydroxybutyrate (PHB) biosynthesis in *Alcaligenes eutrophus* H16: Identification and characterization of the PHB polymerase gene (phbC), *J. Biol. Chem. 264*, 15298-15303.
5. He, A., Tian, J., Lawrence, A., Liu, P., Sinskey, A.J., and Stubbe, J. (2004) Expression Analysis of Proteins Involved in Polyhydroxybutyrate Homeostasis in *Wautersia eutropha* H16, *submitted for publication.*
6. Tian, J., He, A., Lawrence, A., Liu, P., Watson, N., Sinskey, A.J., and Stubbe, J. (2004) Analysis of Transient Polyhydroxybutyrate Production in *Wautersia eutropha* H16 by Quantitative Westerns and Transmission Electron Microscopy, *manuscript submitted for publication.*
7. Mouton, P.R. (2002) *Principles and Practices of Unbiased Stereology: An Introduction for Bioscientists*. The Johns Hopkins University Press, Baltimore, MD.
8. Sterio, D.C. (1984) The unbiased estimation of number and sizes of arbitrary particles using the disector, *J Microsc 134 (Pt 2)*, 127-136.
9. Madison, L.L. and Huisman, G.W. (1999) Metabolic engineering of poly(3-hydroxyalkanoates): From DNA to plastic, *Microbiol. Mol. Biol. Rev. 63*, 21-53.

10. York, G.M., Lupberger, J., Tian, J., Lawrence, A.G., Stubbe, J., and Sinskey, A.J. (2003) *Ralstonia eutropha* H16 Encodes Two and Possibly Three Intracellular Poly[D-(-)-3-Hydroxybutyrate] Depolymerase Genes, *J Bacteriol 185*, 3788-3794.

11. York, G.M., Junker, B.H., Stubbe, J.A., and Sinskey, A.J. (2001) Accumulation of the PhaP phasin of *Ralstonia eutropha* is dependent on production of polyhydroxybutyrate in cells, *J Bacteriol 183*, 4217-4226.

12. Wieczorek, R., Pries, A., Steinbüchel, A., and Mayer, F. (1995) Analysis of a 24-kilodalton protein associated with the polyhydroxyalkanoic acid granules in *Alcaligenes eutrophus*, *J. Bacteriol. 177*, 2425-2435.

13. Gerngross, T.U., Reilly, P., Stubbe, J., Sinskey, A.J., and Peoples, O.P. (1993) Immunocytochemical analysis of poly-b-hydroxybutyrate (PHB) synthase in *Alcaligenes eutrophus* H16: Localization of the synthase enzyme at the surface of PHB granules, *J. Bacteriol. 175*, 5289-5293.

14. Potter, M., Madkour, M.H., Mayer, F., and Steinbuchel, A. (2002) Regulation of phasin expression and polyhydroxyalkanoate (PHA) granule formation in *Ralstonia eutropha* H16, *Microbiology 148*, 2413-2426.

15. Mas, J., Pedros-Alio, C., and Guerrero, R. (1985) Mathematical model for determining the effects of intracytoplasmic inclusions on volume and density of microorganisms, *J Bacteriol 164*, 749-756.

16. Karr, D.B., Waters, J.K., and Emerich, D.W. (1983) Analysis of poly-beta-hydroxybutyrate in *Rhizobium japonicum* bacteroids by ion-exclusion high-pressure liquid-chromatography UV detection, *Appl Environ Microbiol 46*, 1339-1344.

17. Saegusa, H., Shiraki, M., Kanai, C., and Saito, T. (2001) Cloning of an intracellular Poly[D(-)-3-Hydroxybutyrate] depolymerase gene from *Ralstonia eutropha* H16 and characterization of the gene product, *J Bacteriol 183*, 94-100.

18. Kobayashi, T., Shiraki, M., Abe, T., Sugiyama, A., and Saito, T. (2003) Purification and Properties of an Intracellular 3-Hydroxybutyrate-Oligomer Hydrolase (PhaZ2) in *Ralstonia eutropha* H16 and Its Identification as a Novel Intracellular Poly(3-Hydroxybutyrate) Depolymerase, *J Bacteriol 185*, 3485-3490.

19. Kawaguchi, Y. and Doi, Y. (1992) Kinetics and Mechanism of Synthesis and Degradation of Poly(3-Hydroxybutyrate) in *Alcaligenes eutrophus*, *Macromolecules 25*, 2324-2329.

20. Doi, Y., Segawa, A., Kawaguchi, Y., and Kunioka, M. (1990) Cyclic nature of poly(3-hydroxyalkanoate) metabolism in *Alcaligenes eutrophus*, *FEMS Microbiol Lett 55*, 165-9.

21. Lundgren, D.G., Pfister, R.M., and Merrick, J.M. (1964) Structure of Poly-Beta-Hydroxybutyric Acid Granules, *J Gen Microbiol 34*, 441-446.

22. Boatman, E.S. (1964) Observations on the Fine Structure of Spheroplasts of *Rhodospirillum Rubrum*, *J Cell Biol 20*, 297-311.

23. Jensen, T.E. and Sicko, L.M. (1971) Fine structure of poly-beta-hydroxybutyric acid granules in a blue-green alga, *Chlorogloea fritschii*, *J Bacteriol 106*, 683-686.

24. Thiele, O.W., Dreysel, J., and Hermann, D. (1972) The "free" lipids of two different strains of hydrogen-oxidizing bacteria in relation to their growth phases, *Eur J Biochem 29*, 224-236.

25. Dennis, D., Liebig, C., Holley, T., Thomas, K.S., Khosla, A., Wilson, D., and Augustine, B. (2003) Preliminary analysis of polyhydroxyalkanoate inclusions using atomic force microscopy, *FEMS Microbiol Lett 226*, 113-119.

6.8 TABLES AND FIGURES

Table 6.1 *In vivo* concentration of $PhaC_{We}$, PhaP, PhaR, and $PhaZ1_a$ in wt *W. eutropha* H16 at 4 and 24 h in TSB medium, assuming that all proteins were soluble. Number of molecules of each protein is also reported.

	4 h in TSB medium		24 h in TSB medium	
	Concentration (μM)	**No. of Molecules Per Cell**	**Concentration (μM)**	**No. of Molecules Per Cell**
PhaC	0.3 - 0.6	3.3×10^2	2.6	1.4×10^3
PhaP	36 - 72	3.9×10^4	48	2.6×10^4
PhaR	1 - 2	1.1×10^3	4.5	2.4×10^3
$PhaZ1_a$	1.4 - 3	1.5×10^3	3.2	1.8×10^3

Table 6.2 Protein coverage of the granule surface at 4 h and 24 h time points in TSB medium.

Time (h)	(T)[a] No. of PhaC	(E)[b] No. of PhaC	% PhaC[c]	(T) No. of PhaP	(E) No. of PhaP	%PhaP
4	2.5 - 5.1 x 10^4	3.3 x10^2	**0.8 - 1.6**	0.7 - 1.4 x 10^5	3.9 x 10^4	**27-54**
24	2.7 x 10^4	1.4 x 10^3	**5.5**	7.4 x 10^4	2.6 x 10^4	**35**

[a] Theoretical number of protein covering the total surface area of granule per cell (Note that for 4 h, a range is given due to the complication associated with cell diviosn. The total surface area of granules in a freshly divided cell is half of that in an elongated cell before cell division)

[b] Experimental number of protein covering the total surface area of granule per cell

[c] Experimental / Theoretical (x 100)

Table 6.3 Protein coverage of granule surface area per cell at 24 h in PHB_P using S_G (Method 1)

Protein	(T)[a] No. of Protein	(E)[b] No. of Protein	% of S_G covered by Protein
PhaC	1.5×10^5	750	**0.5**
PhaP	4.2×10^6	86400	**21**
PhaR	4.2×10^6	1200	**0.3**
$PhaZ1_a$	2.3×10^5	1100	**0.5**
$PhaZ1_b$	2.3×10^5	1000	**0.4**

[a] Theoretical number of protein covering the total surface area of granule per cell

[b] Experimental number of protein covering the total surface area of granule per cell

Table 6.4 Protein coverage of granule surface area per mL of cell culture at 24 h in PHB_P using density of amorphous PHB (Method 2).

Protein	(T)[a] No. of Protein	(E)[b] No. of Protein	% of Granule Surface covered by Protein
PhaC	4.0×10^{14}	3.2E+12	**0.8**
PhaP	1.1×10^{15}	3.6E+14	**33**
PhaR	1.1×10^{15}	5.0E+12	**0.5**
$PhaZ1_a$	6.3×10^{14}	4.6E+12	**0.7**
$PhaZ1_b$	6.3×10^{14}	4.2E+12	**0.7**

[a] Theoretical number of protein covering the total surface area of granule per mL of culture

[b] Experimental number of protein covering the total surface area of granule per mL of culture

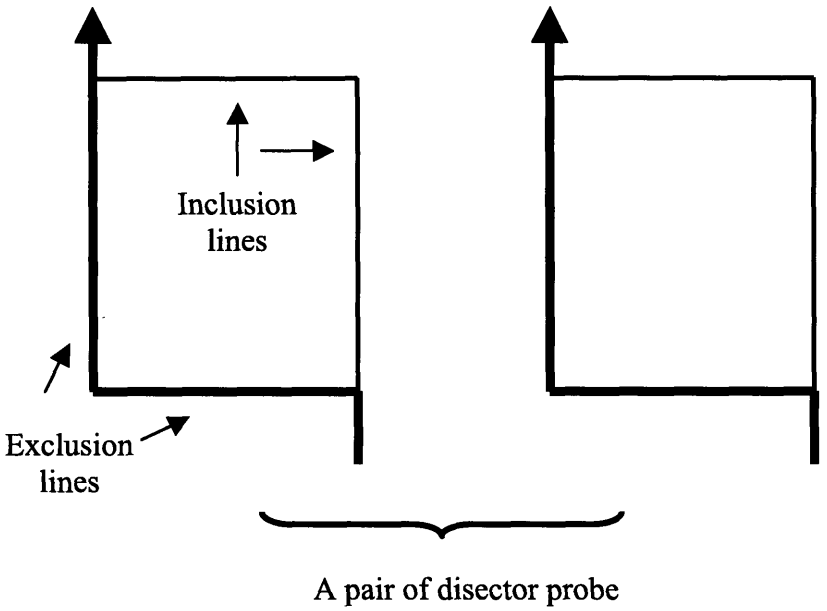

Figure 6.1 Disector probes used to quantitate the number of granules per cell using images of consecutive serial sections. A transparency with a pair of dissector probe is laid over serial images of cells randomly. The first image covered by one disector probe serves as the reference, while the second image covered by the other disector probe serves as the look-up section, where the disappearance of granules is counted.

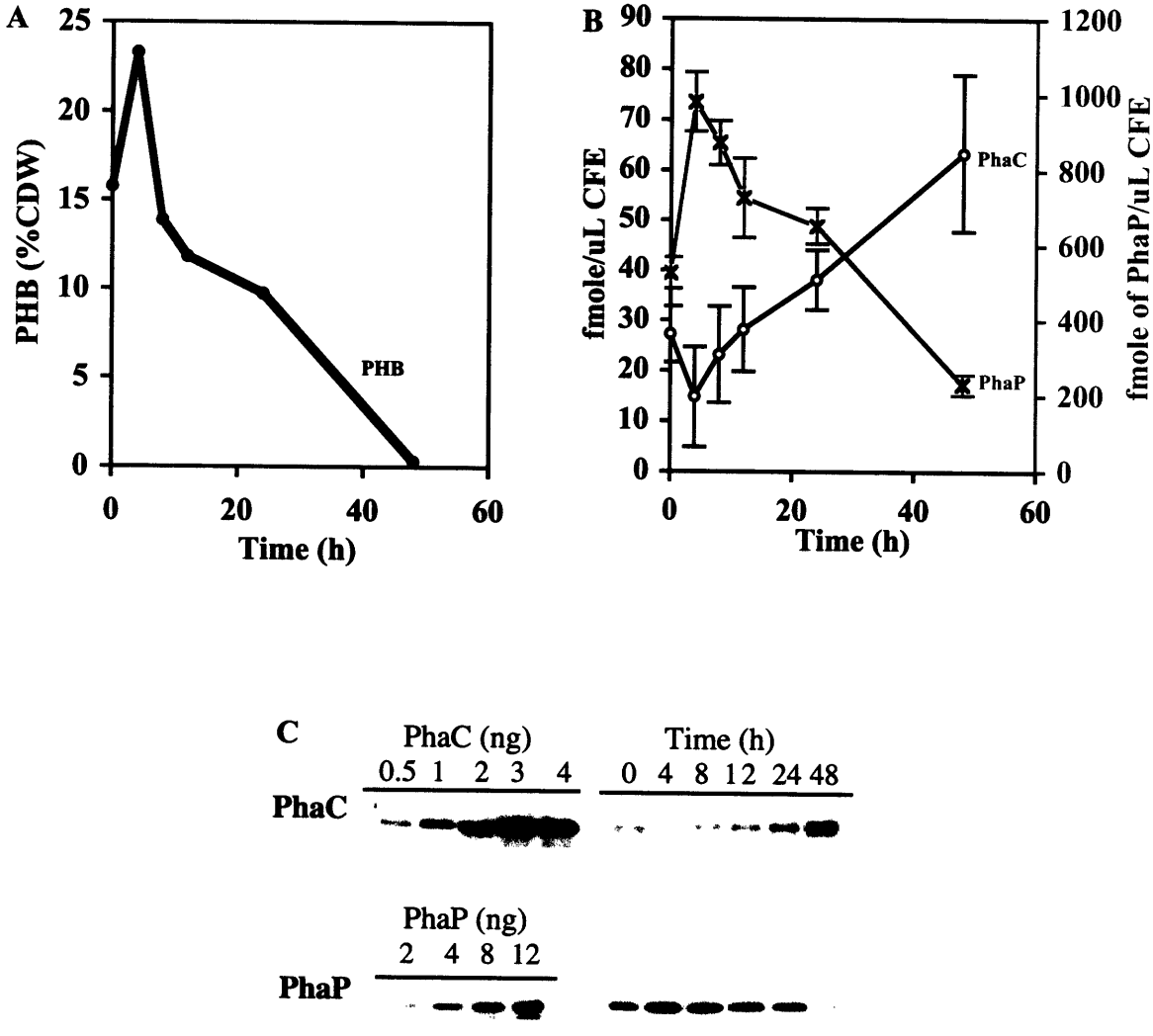

Figure 6.2 (**A**) Profile of PHB accumulation by wt *W. eutropha* H16 in TSB medium. (**B**) Expression of $PhaC_{We}$ and PhaP in wt *W. eutropha* from 0 to 48 h in TSB medium. (**C**) Western blots of $PhaC_{We}$ and PhaP in crude extract of wt *W. eutropha*. Westerns in comparison to standards were used to generate the data in (**B**).

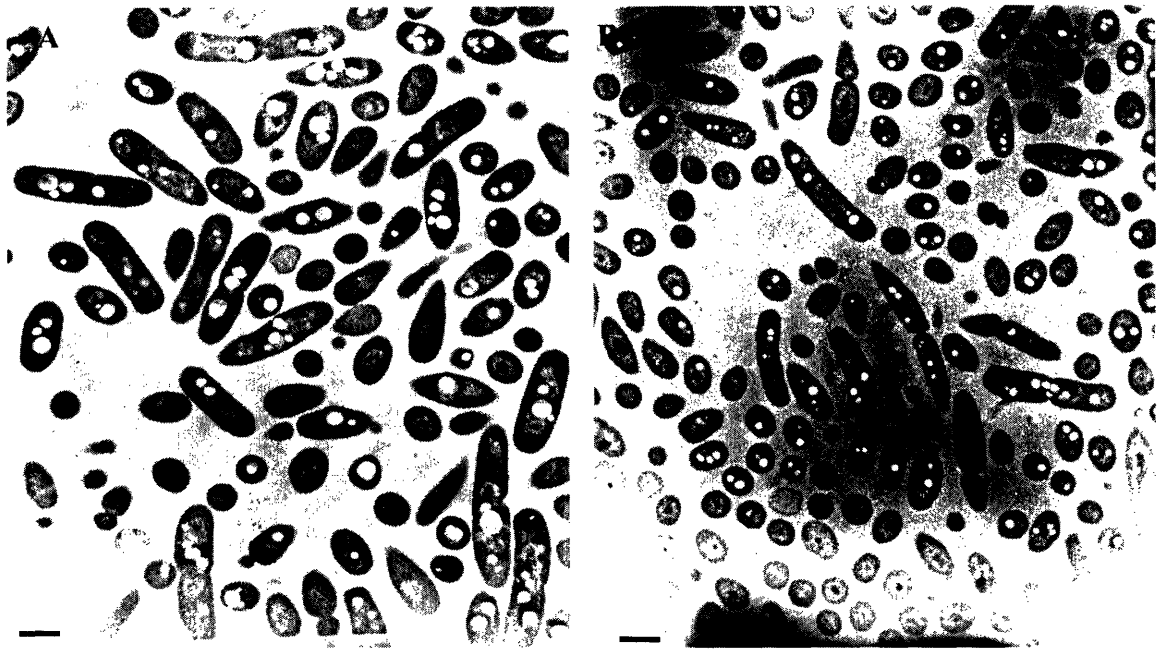

Figure 6.3 TEM images of wt *W. eutropha* H16 grown in TSB medium for (**A**) 4 h, and (**B**) 24 h. Both images are at the same magnification. Bar size, 1 μm.

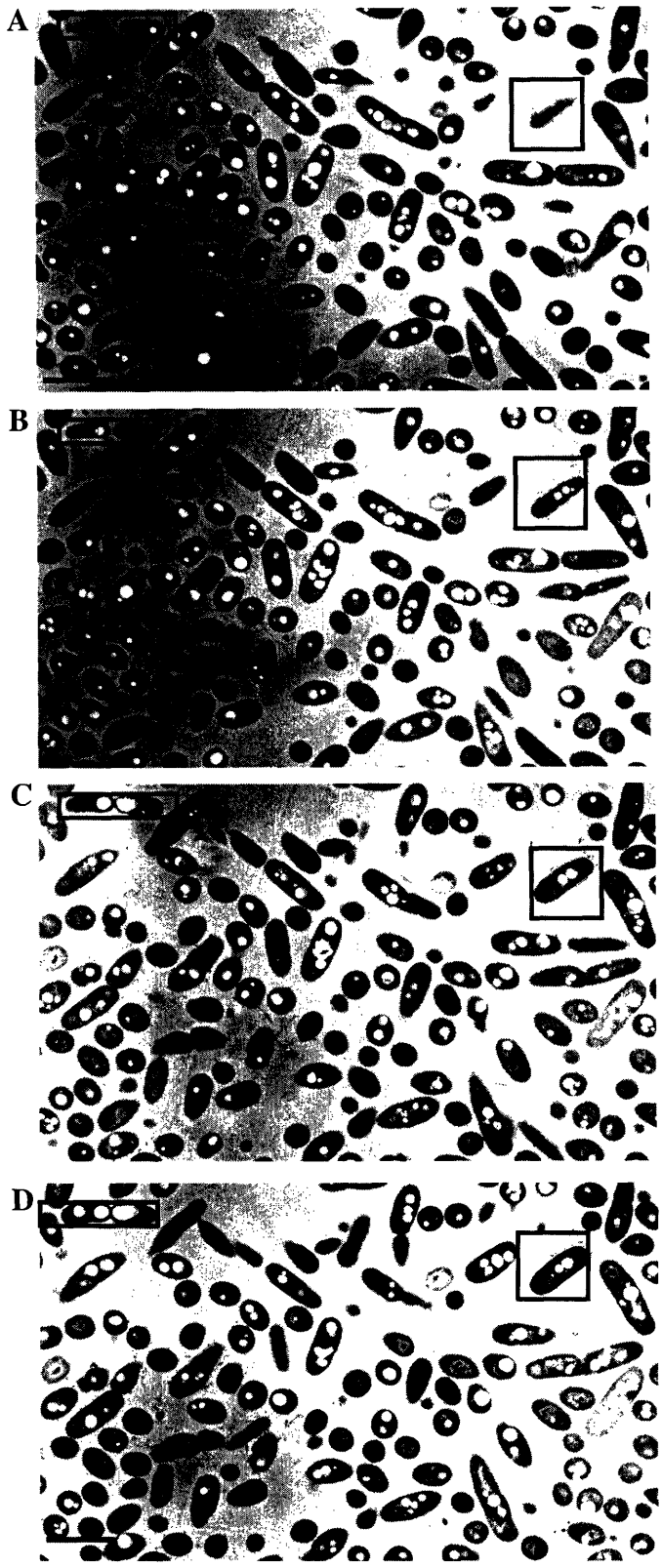

Figure 6.4 TEM images of consecutive serial sections of wt *W. eutropha* H16 grown in TSB medium for 4 h. Bar size, 2 μm.

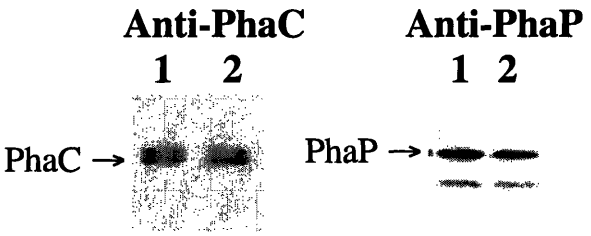

Figure 6.5 Control experiment for Western analyses showing that the amount of protein ($PhaC_{We}$ and PhaP) extracted from cells grown in TSB medium using 2% SDS followed by 20 min boiling at 95°C (all the lane 1s) is similar to that extracted from cells which had been treated with extracellular depolymerase prior to 2% SDS treatment (all the lane 2s).

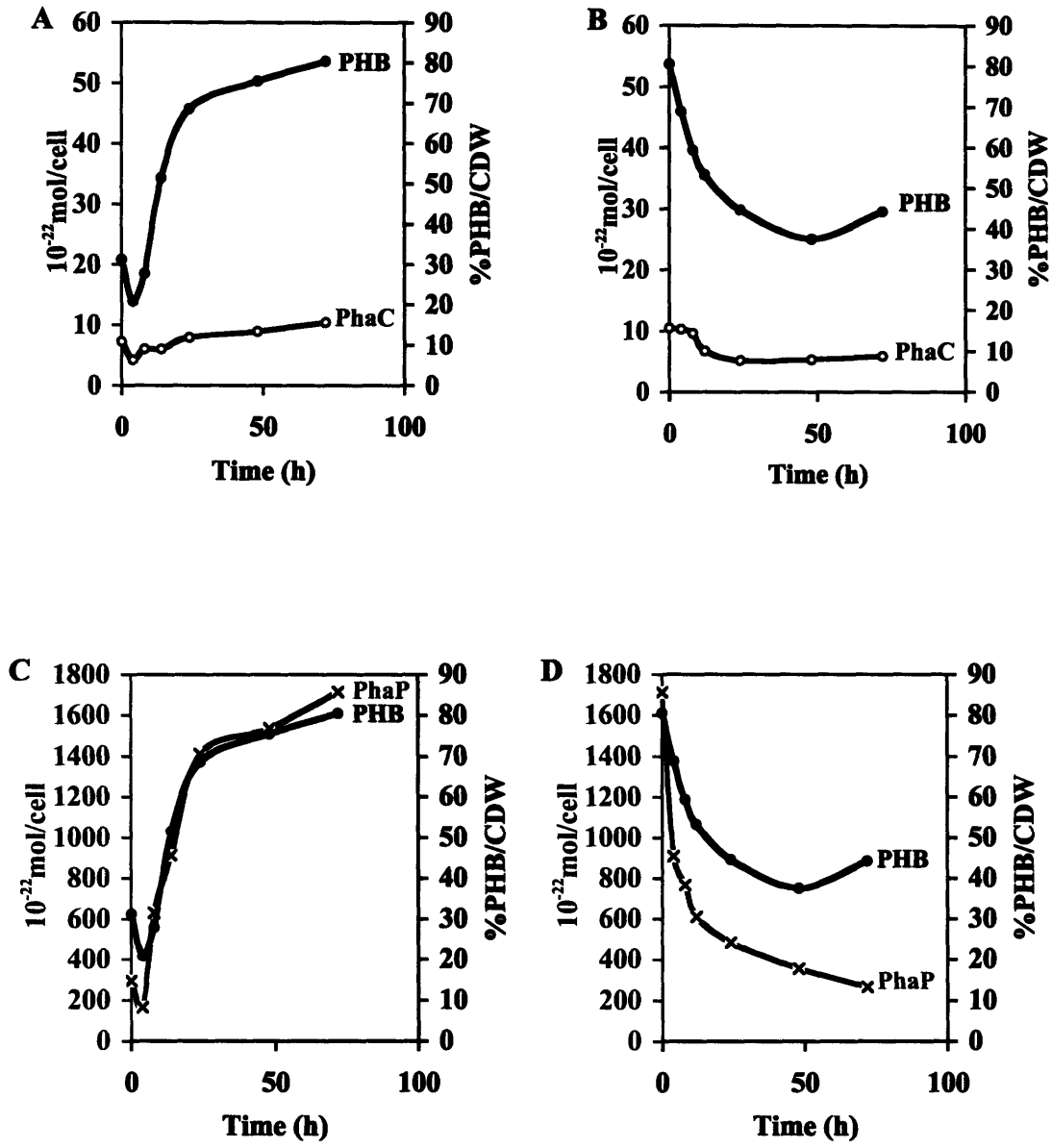

Figure 6.6 (**A**) Expression of $PhaC_{We}$ in wt *W. eutropha* in PHB_P and (**B**) in PHB_U. (**C**) Expression of PhaP in wt *W. eutropha* H16 in PHB_P and (**D**) in PHB_U.

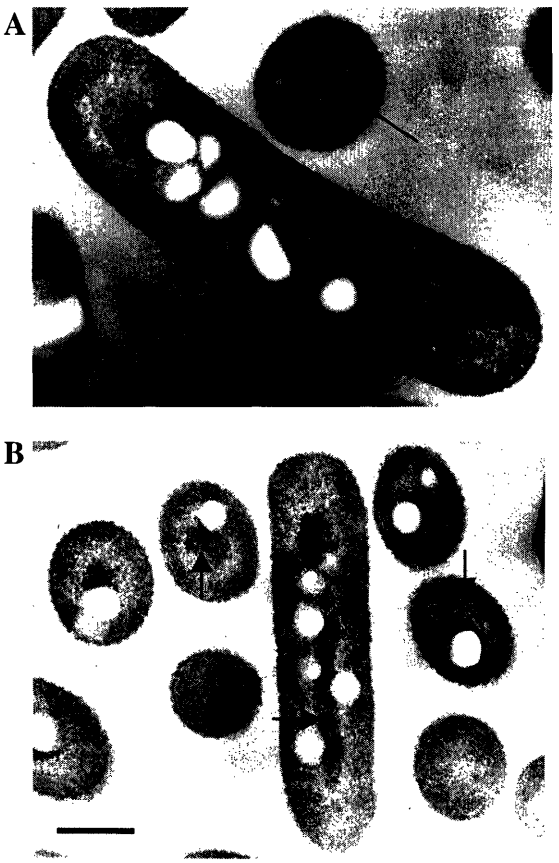

Figure 6.7 TEM images of wt *W. eutropha* H16 cells at (**A**) 4 h and (**B**) 24 h in TSB medium showing dark-stained structures (black arrows). Bar size, 500 nm.

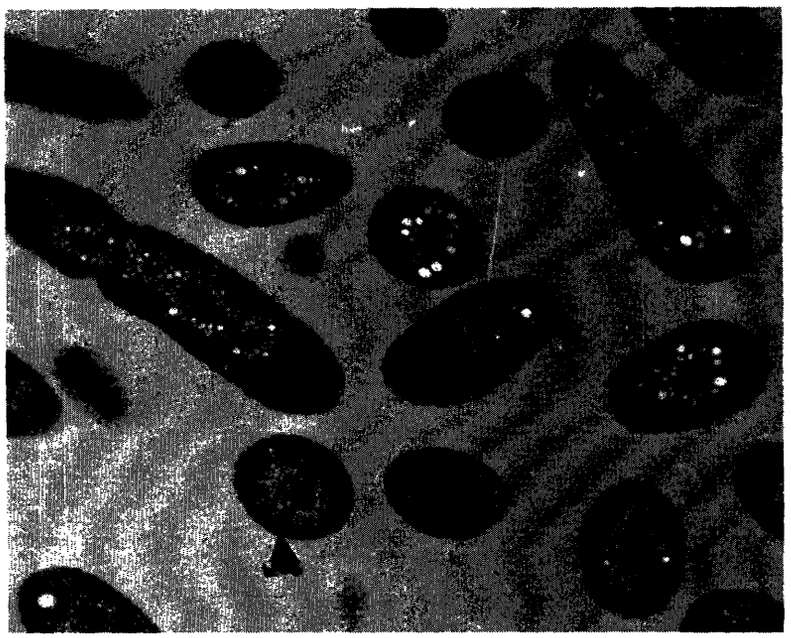

Figure 6.8 TEM image of Δ*phaR W. eutropha* H16 grown in TSB medium for 4 h showing localization of small granules. Bar size, 1.9 μm.

CHAPTER 7

Additional Observations and Proposal for Future Experiments

7.1 INTRODUCTION

Polyhydroxybutyrate biosynthesis, degradation, and regulation are complicated processes that are difficult to study, as are the other non-template driven polymerization systems. Studies in this field are challenged by the lack of methods for proper sample preparation, lack of appropriate substrates and consequently appropriate assays, and lack of biophysical techniques that can follow the polymerization and depolymerization processes. Despite these difficulties, researchers in this field have made significant advances over the past 15 – 20 years. These efforts include identifying and characterizing the major proteins involved in the synthesis, degradation, and regulation of PHB homeostasis, elucidating the physical state of the polymer *in vivo*, and producing homopolymers and copolymers in an economical fashion. Research in areas such as characterizing the granule surface, identifying new substrates for production of polymers with novel properties, sequencing the genome of *Wautersia eutropha* and other PHA producing bacteria, profiling mRNA and protein levels along with their changes, obtaining X-ray structures of the proteins involved are all underway.

Results from experiments presented and discussed in Chapter 2 and 3 have provided a glimpse into the mechanism of initiation and elongation by the Class III synthase from *Allochromatium vinosum*. The synthase was also proposed to play a role in controlling the size of the polymer chain, perhaps by polymer termination. Studies described in Chapter 4 suggested that an additional factor(s) was missing in the polymerization reaction catalyzed by recombinant Class I synthase from *W. eutropha*. The transmission electron microscopy studies presented in Chapter 5 and 6 have been mechanistically informative and exciting. Localization of the nascent granules near center of the cells and the dark-stained features have invoked a new mechanism of

granule initiation as a possibility. However, much more work is needed to verify these results and our hypothesis.

Over the years, many other interesting observations have been made while studying the recombinant synthases *in vitro* and the phenotypes of various mutant *W. eutropha* strains *in vivo*. They were not pursued at the time due to lack of a cogent hypothesis or lack of time. Further investigation of these observations could have a significant impact on our understanding of the polymerization process *in vitro* and *in vivo*. The results from these studies are presented here as food for thought. Some are presented in more detail than others since they are described for the first time. Each study is followed by a proposal of additional experiments that may shed new light on the PHB system. In addition, experiments designed to continue or to verify the results from studies presented in previous chapters are also presented. The format of this chapter differs from the others in that it is divided into sections by the area of research, and each section contains introduction, materials and methods, results, and a discussion which includes proposal for future experiments.

7.2 OLIGOMERIC STATE OF THE CLASS III SYNTHASE

7.2.1 Introduction

The oligomeric state of the recombinant Class III synthase (PhaCPhaE$_{Av}$) from *A. vinosum* has been an issue of debate. A molecular weight of 400,000 Da was determined by Liebergessell *et al* using gel filtration and native PAGE gel (*1*). They proposed that the native synthase might be composed of ten subunits. Results from size-exclusion column chromatography by Dr. Jia from our lab suggested that that the synthase exists as trimer and hexamer (unpublished). Therefore, the native molecular weight of the synthase was investigated again with the hope of

resolving the disagreement. Light scattering (LS) was chosen because in theory, it is an absolute method for measuring the molecular weight, shape, and polydispersity of polymers. The oligomeric state of PhaCPhaE$_{Av}$ over-expressed in *E. coli* was determined using LS coupled to size-exclusion chromatography (SEC) by HPLC. The purpose of the SEC is to separate the species. Synthase mutant W248A-PhaCPhaE$_{Av}$ was also analyzed by the same approach. W248 is located on PhaC, and is proposed to play an important role at the interface of dimerization in PhaCPhaE$_{Av}$. Disrupting this amino acid appeared to change the oligomeric state of the synthase to be mostly the smaller species (Y. Jia, unpublished). Thus, this mutant was used to determine the molecular weight of the smaller oligomeric species.

7.2.2 Material and Methods

Purification of recombinant PHA synthases. Recombinant wt and mutant Class III PHA synthases from *A. vinosum* were purified following the procedure described in Müh *et al* (*2*). W248A-PhaCPhaE$_{Av}$ was purified by Y. Jia, with a specific activity (SA) of 0.41 U/mg.

Calibration of the multiangle light scattering instrument. The Multiangle Light Scattering (MALS) instrument (Model DAWN EOS) and the refractive index (RI) detector from Wyatt Technology Corporation (Santa Barbara, CA) were calibrated and normalized with toluene. The auxiliary constant of the instrument was determined using different concentration of NaCl in dH_2O, and was determined to be 2.3371×10^{-4}. This value was close to the value determined by Wyatt Technology (2.2863×10^{-4}).

Determination of the dn/dc value of PhaCPhaE$_{Av}$. The amount of light scattered is directly proportional to the product of the polymer molar mass and its concentration (*3*). This

relationship is shown in Equation 7.1 where LSI = light scattering intensity, M_w = weight-average molar mass, C = concentration of the polymer, and dn/dc = change of refractive index/change of concentration.

$$\mathbf{LSI \propto M_w C (dn/dc)^2} \qquad \textbf{Equation 7.1}$$

Therefore, the dn/dc value for PhaCPhaE$_{Av}$ in the buffer of choice (150 mM NaCl, 50 mM KPi, pH = 7.8) and the temperature of choice (25°C, the temperature at which the light scattering experiment described below is carried out) must be obtained in order to determine the M_W of the protein. The concentration of the stock protein solution was determined to be 4.2 mg/mL by A_{280nm} and the extinction coefficient of the synthase. Solutions containing 0, 9.28, 25.4, 46.4, 74.2, 92.8, 139.3, and 185.6 μg/mL of PhaCPhaE$_{Av}$ were prepared by serial dilution using the same buffer described above. Each sample was injected onto the instrument and its refractive index value was measured. The Wyatt software DNDC plots the values (y-axis) obtained against the concentrations of the protein (x-axis), and reports a dn/dc value which is the slope of the line.

Analysis of wt and W248A-PhaCPhaE$_{Av}$ by multiangle light scattering. Analytical size-exclusion column (Bio-silect SEC400 column, 300 × 7.8 mm, with a guard column, 50 × 7.8 mm, Bio-rad) was connected to the MALS instrument. The column was equilibrated with the buffer described above overnight at 0.1 mL/min. Prior to analysis of the protein, the column was again equilibrated with the same buffer for several h at a flow rate of 0.8 mL/min. The same flow rate was used throughout the rest of the experiment. Wild-type PhaCPhaE$_{Av}$ (40 μL of 4.2 mg/mL) or W248A-PhaCPhaE$_{Av}$ (40 μL of 3.6 mg/mL) was each injected onto the column. Results were analyzed by the ASTRA software (Wyatt Technology) that was supplied with the light scattering instrument.

7.2.3 Results and Discussion

Determination of the dn/dc value for the synthase. The dn/dc value of the polymer of interest in a defined solvent, at a defined temperature must be known in order to calculate the M_w of the polymer. Since the dn/dc of PhaCPhaE$_{Av}$ has never been reported in literature, it was determined experimentally in 150 mM NaCl, 50 mM KPi, pH = 7.8, at 25°C to be 0.1948 ± 0.0053 mL/g. With this value, we were then able to determine the M_W of PhaCPhaE$_{Av}$.

Determination of the oligomeric state of wt and W248A-PhaCPhaE$_{Av}$. The extent of light scattering by the proteins was analyzed by the ASTRA software (Wyatt Technology). The relationship between the fraction of light scattered by the polymer (R(θ), also known as the Rayleigh ratio), the weight-average molecular weight (M_W) of the polymer and its concentration (c) is defined in Equation 7.2.

$$\mathbf{K^* c / R(\theta) = 1 / M_w P(\theta) + 2 A_2 c} \qquad \textbf{Equation 7.2}$$

K* and P(θ) are each defined in the following equations.

$$\mathbf{K^* = 4\pi^2 (dn/dc)^2 n_0^2 N_A^{-1} \lambda_0^{-4}} \qquad \textbf{Equation 7.3}$$

$$\mathbf{1/P(\theta) = 1 + (16\pi^2/3\lambda^2) \langle r_g^2 \rangle \sin^2(\theta/2) + ...} \qquad \textbf{Equation 7.4}$$

n_0 = refractive index of solvent
N_A = Avogadro's number
λ_0 = wavelength of the incident light in vacuum
c = concentration of the solute molecules (g/mL)
R(θ) = fraction of light scattered
A_2 = second virial coefficient
P(θ) = scattering function, indicating how the scattered light varies with angle
r_g^2 = mean square radius

Note that K* includes the dn/dc value and is a constant. The function P(θ) describes angular dependence of scattered light. Equation 7.4 is the first order expansion of 1/P(θ). The weight-averaged M_W in Equation 7.2 can be solved by several ways. The Debye fit method (provided by

the ASTRA software) plots $R(\theta)/K^*c$ (y-axis) against $\sin^2(\theta/2)$ (x-axis). Extrapolation of the Debye plot to zero scattering angle (note that when $\theta = 0$, the function $1/P(\theta)$ becomes 1), the M_W (the y-intercept) can be obtained. The Debye plot of wt PhaCPhaE$_{Av}$ is shown in Figure 7.1. Analysis of the data by the ASTRA software revealed the M_W of the major oligomeric species (**1**, inset of Figure 7.1) to be 324,100 Da. Since the molecular weight of PhaCPhaE$_{Av}$ is 80,000 Da per monomer of PhaC$_{Av}$ and PhaE$_{Av}$, this value suggests that the major peak (**1**, inset of Figure 7.1) represents a tetramer of PhaCPhaE$_{Av}$. The A_{280nm} profile indicated that PhaCPhaE$_{Av}$ exists not only as a tetramer, but also in a second smaller oligomeric state (**2**, inset of Figure 7.1). It is interesting that the two species do not equilibrate, and the tetramer remains to be the dominant state even under dilute conditions (Y. Jia, unpublished).

Since the peak representing the small oligomeric species was not well resolved from the major peak with wt synthase (inset of Figure 7.1), W248A-PhaCPhaE$_{Av}$ was analyzed by the same approach so that the molecular weight of the smaller oligomeric species could be determined. As shown in the inset of Figure 7.2, the ratio of the two oligomeric states changed. The amount of the larger species (**1**) decreased significantly and the smaller species (**2**) dominated. The Debye plot revealed that the M_W of the smaller species was 154,000 Da. Results from these light scattering experiments with wt and W248A-PhaCPhaE$_{Av}$, summarized in Table 7.1, strongly suggest that the recombinant synthase exists as dimer/tetramer *in vitro*. However, analysis assumes that PhaC$_{Av}$ and PhaE$_{Av}$ are always present at a 1:1 ratio.

One aspect of the Debye plots shown in Figure 7.1 and 7.2 is puzzling. The plot of $R(\theta)/K^*c$ vs. $\sin^2(\theta/2)$ usually fits to a straight line (first order fit) when the RMS (root mean square radius) of the polymer is < 50 nm (*3*). However, when the RMS $\geq$ 50 nm, the line shows curvature and requires a higher order fit to fit the data. In the two cases presented in Figure 7.1

and 7.2, second order fit was used. Assuming $PhaE_{Av}$ (40 KDa) and $PhaC_{Av}$ (39 KDa) are globular, each will have a Stoke radius of ~ 2.8 nm using ovalbumin (43 KDa) as a model. It is difficult to see how a tetramer of $PhaCPhaE_{Av}$ will have a radius larger than 50 nm. Therefore, how $PhaE_{Av}$ and $PhaC_{Av}$ are assembled in a tetramer, and what are the shape of these proteins is of interest since these aspects of the protein would most likely govern how PHB is synthesized.

7.3 THE ROLE OF $PhaE_{Av}$

7.3.1 Introduction

The presence of $PhaE_{Av}$ is critical for the high activity (~ 150 U/mg) of the recombinant synthase from *A. vinosum* (*2*). The key amino acid residues that catalyze the polymerization reaction, however, reside on $PhaC_{Av}$. How $PhaE_{Av}$ facilitates the initiation for $PhaC_{Av}$ is unclear. Is the presence of $PhaE_{Av}$ alone responsible for the difference observed between the recombinant Class I and III synthase? How does $PhaE_{Av}$ interact with $PhaC_{Av}$? Does $PhaE_{Av}$ play any other roles, such as that of PhaP in *W. eutropha*? Establishing the ratio of $PhaC_{Av}$ to $PhaE_{Av}$ in its native host will be important in understanding the mechanism of initiation.

To date, not many experiments have been designed specifically to study the function of $PhaE_{Av}$. Our lab, in collaboration with Prof. Catherine Drennan's lab at MIT, has been trying to obtain an X-ray structure of the Class I $PhaC_{We}$ and Class III $PhaCPhaE_{Av}$ PHA synthase. While no conditions tested have resulted crystals of $PhaC_{We}$, crystals of $PhaCPhaE_{Av}$ with saturated trimer aldehyde have been successfully obtained. However, the crystals only diffracted at ~ 7 Å. Geoff Stamper (Drennan lab) who was trying to improve the crystals of $PhaCPhaE_{Av}$, proposed to truncate parts of $PhaE_{Av}$ to remove the potential disordered peptide segment. He found that chymotrypsin has access to two cleavage sites near the C-terminus of $PhaE_{Av}$, suggesting the C-

terminus may correspond to a disordered peptide segment. Removing this segment could potentially give crystals that would diffract well. Thus, two truncated versions of PhaCPhaE$_{Av}$ (PhaCPhaE-A and PhaCPhaE-B) were cloned and purified by G. York and myself. Construct pJT3 encoding PhaCPhaE-A has 35 amino acids (aa) removed from the C-terminus of PhaE$_{Av}$, and construct pJT4 encoding PhaCPhaE-B has 22 aa removed. Biochemical analysis of these mutant proteins fortuitously provided interesting observations regarding the role of PhaE$_{Av}$.

7.3.2 Materials and Methods

Construction of expression plasmids for PhaCPhaE-A (pJT3) and PhaCPhaE-B (pJT4). The details of cloning can be found in G. York's 2001 year-end report (Chapter 6, p. 62). Table 3 (from G. York's report) lists the oligomers used for the construction of these plasmid.

Over-expression and Purification of PhaCPhaE-A and PhaCPhaE-B. Plasmid pJT3 encoding PhaCPhaE-A and pJT4 encoding PhaCPhaE-B were each transformed into BL21(DE3). Kanamycin, 30 μg/mL, was included in all growth media. Cells were plated on Lauria-Bertani (LB) plates and incubated at 37°C overnight. A single colony was then picked from each plate to inoculate 100 mL of LB medium. The cultures were grown at 37°C at 185 rpm for 12 h, which were then spun down and resuspended in fresh LB medium. Each was used to inoculate 10 L LB medium in 10-L fermenters. The cultures were grown at 37°C at 500 rpm. When the OD_{600nm} of BL21(DE3)/pJT3 and pJT4 reached 1.1 and 0.8, respectively, the cells were induced with IPTG (final conc. 0.4 mM) for 3.5 h. A yield of 5.5 g cells per L of culture was obtained for both strains. The cells were stored frozen at -80°C.

BL21(DE3)/pJT3 (32 g) and BL21(DE3)/pJT4 (31g) were used for protein purification following the standard procedure (*2*). Ten mg of PhaCPhaE-A and 20 mg of PhaCPhaE-B was obtained, each with a SA of 74 and 150 U/mg, respectively.

Size-exclusion column (SEC) chromatography analysis of PhaCPhaE-A and PhaCPhaE-B. Fifty μL of PhaCPhaE-A (3.3 mg/mL) and PhaCPhaE-B (4.7 mg/mL) was each injected onto analytical size-exclusion column (Bio-silect SEC400 column, 300 × 7.8 mm, with a guard column, 50 × 7.8 mm, Bio-rad) for analysis. The elution buffer contained 50 mM KPi, pH=7.8, and 150 mM NaCl, and the flow rate was 1 mL/min.

7.3.3 Results and Discussion

PhaE has 357 amino acid residues. Two chymotrypsin cleavage sites were found at the C-terminus of PhaE, and therefore two truncated versions of $PhaCPhaE_{Av}$ were made. Plasmids pJT3 and pJT4, encoding PhaCPhaE-A and PhaCPhaE-B, respectively, were cloned successfully. Although standard purification procedure was used (*2*), these proteins were only about ~90% pure judging from Coomassie stained SDS-PAGE gel (Figure 7.3). Approximately 20% of the 35 aa (PhaCPhaE-A) and 30% of the 22 aa (PhaCPhaE-B) removed are positively charged. It is thus possible that this change in isoelectric point altered purification. The specific activity (SA) of PhaCPhaE-B is similar to that of wt synthase, 148 U/mg vs. 150 U/mg, indicating that the last 22 aa of PhaE had no effect on the activity of synthase. The SA of PhaCPhaE-A (74 U/mg), however, is only half that of the wt. Somehow, the removal of an additional 13 aa altered the activity of the synthase.

Both proteins were further analyzed by SEC to determine the oligomeric state of the proteins. To our surprise, both mutant proteins exhibit a different oligomer distribution from that

of wt. While wt PhaCPhaE$_{Av}$ is mostly in the tetrameric state, both mutants are mostly in dimeric states (Figure 7.4). How the oligomeric state of the synthase changes in the presence of substrate is unknown. It is interesting to see that PhaCPhaE-B still has very high SA. Since PhaCPhaE-A has a significant SA change, its reaction with [^{14}C]-HB-CoA should be further characterized by SDS-PAGE analysis and autoradiography to observe the distribution of radioactivity or products. If more radioactivity is observed near top of the gel (indicating large polymer species) at low S/E ratios when compared to wt, then the presence of PhaE$_{Av}$ could explain the difference observed between the recombinant Class I and Class III synthase.

7.4 PRELIMINARY STUDIES OF MUTANT S90A CLASS III SYNTHASE

7.4.1 Introduction

Amino acid residue S90 of PhaC$_{Av}$ from the Class III PhaCPhaE$_{Av}$ is absolutely conserved among all classes of the synthases identified so far, and yet the function of this residue has not been elucidated. The polymerization reaction catalyzed by mutant S90A-PhaCPhaE$_{Av}$ was therefore briefly examined by SDS-PAGE analysis and autoradiography. Furthermore, a *W. eutropha* strain with its synthase gene replaced with S90A-PhaCPhaE$_{Av}$ was also examined by TEM with the hope of gaining insight into the function of this residue. Preliminary results suggest that S90 may function in controlling the size of the PHB polymer chain.

7.4.2 Materials and Methods

Source of recombinant S90A-PhaCPhaE$_{Av}$. S90A-PhaCPhaE$_{Av}$, with a SA of ~ 1 U/ mg, was previously purified by Y. Jia and had been stored at -80°C for 4-5 years. The enzyme was not assayed again prior to its use in the experiment described below.

Analysis of Reaction Products of S90A-PhaCPhaE$_{Av}$ with [^{14}C]-HB-CoA by SDS-PAGE: Coomassie Staining and Autoradiography. S90A-PhaCPhaE$_{Av}$, 5 μM, was incubated with 50 μM of [^{14}C]-HB-CoA in 20 mM Tris-HCl, pH 7.5, 50 mM NaCl (assay buffer) at 30°C. At 15, 30, 60, and 90 min, an aliquot of the reaction mixture (10 μL) was quenched with an equal volume of Laemmli buffer (*4*) with no reducing reagent. The reaction products were resolved on a SDS-PAGE gel, which was then dried and exposed to the Low-energy screen (Molecular Dynamics) for 14 h.

Transmission Electron Microscopy Analysis. A *W. eutropha* strain that contains the Class III S90A-PhaCPhaE$_{Av}$ replacing the native Class I synthase (constructed by G. York) was cultivated in PHB production medium (PHB$_P$) and PHB utilization medium (PHB$_U$) following the procedure described in Chapter 5. At 73 h in PHB$_P$ and 48 h in PHB$_U$, cell cultures were collected for TEM analysis. The detailed procedure for sample preparation is described in Chapter 5. The block containing the sample was sectioned at a thickness of ~70 nm using a Diatome diamond knife on a Reichert Ultracut E microtome. The sections were examined using a Philips EM410 electron microscope at 80 kV.

7.4.3 Results and Discussion

Analysis of in vitro reaction by Autoradiography. When the polymerization reaction catalyzed by recombinant S90A-PhaCPhaE$_{Av}$ with [^{14}C]-HB-CoA was examined by SDS-PAGE gel and autoradiography, interesting observations were made. First, a distribution of products that is different from the wt synthase at low S/E ratio was displayed (compare Figure 7.5A and B). Radioactivity smeared from the top to the bottom of each lane, with species III being the dominant product (Figure 7.5A). Furthermore, a wide distribution of species II (any radioactive

bands between species I and III) was observed. The transition from species II to III is no longer sharp. These observations suggest that perhaps S90 plays a role in controlling polymer size if species II represents synthase with different length of polymer attached. It is unlikely that species II represents different oligomeric state of the synthase since the smearing of species II is significant. However, it must be emphasized here that the effect of polymer length (> 60~100 mer, based on the studies with D302A-PhaCPhaE$_{Av}$, Chapter 2) on the migratory property of the synthase is unknown. In addition, the migratory properties of PHB polymer alone is also unknown. While it is known that most of the wt synthase remains at the monomeric position on SDS-PAGE gel at low S/E ratios (Chapter 3), the distribution of S90A synthase is unknown since the SDS-PAGE gel used for autoradiography was not Coomassie stained. Additional experiments determining the positions of proteins on the gel by Coomassie staining should be carried out in the future.

Second, the time-dependent phenomenon was observed from 15 to 30 min (compare the intensity of species I in Lanes 1 and 2, Fig. 7.5A), suggesting that S90 is not responsible for this phenomenon. As stated in the Methods section, the caveat of this experiment is that the S90A-PhaCPhaE$_{Av}$ used had been purified by Y. Jia 4-5 years ago, and its activity was not re-assayed prior to this experiment. The activity of this mutant is 0.75% of that of the wt synthase (determined by Y. Jia). At 5 μM, the mutant synthase should consume all substrate at S/E of 10 prior to 15 min if the protein did not deteriorate over the long storage time at –80°C. Given the interesting product size distribution, it would be worthwhile to purify this mutant and study it in detail by similar studies described in Chapter 2 and 3. Looking at the products formed at different S/E ratios and chasing the labeled or unlabeled products with unlabeled or labeled

substrates, respectively, can be informative. These experiments will provide mechanistic insight into the role of this serine residue.

TEM of W. eutropha with its Class I synthase gene replaced with S90A-PhaCPhaE$_{Av}$. The phenotype of this genetically engineered *W. eutropha* H16 strain differs significantly from that of the wt strain in PHB_P and PHB_U. Larger and fewer granules were observed per cell based on the images shown in Figure 7.6. The granules also appear to be shapeless; they seem to follow or adapt to the contour of the cell. While it is tempting to attribute the increase in granule size to the mutation of S90 to A, interpretation of the result awaits the control in which *W. eutropha* with its Class I synthase gene replaced with wt PhaCPhaE$_{Av}$ by TEM is examined. If the phenotype of this strain is similar to that of wt *W. eutropha*, then the function or one of the functions of S90 is associated with controlling granule size. It is important to characterize the S90A gene replacement strain using the tools used to study the wt *W. eutropha* strain. Quantitative Westerns of all proteins involved (especially PhaC, PhaE and PhaP), PHB quantitation by crotonic acid assay, M_W determination of the polymer, and stereology analysis of TEM photographs should all be carried out with the objectives to determine the granule surface area coverage, the number of times PhaC undergoes re-initiation, the ratio of PhaC to PhaP, and the number of PhaP or PhaE per polymer chain. A comparison of these results with those from the wt strain and the Δ*phaP* strain could be mechanistically informative. *W. eutropha* Δ*phaP* deletion strain also makes larger and fewer granules, as discussed below in Section 7.8.4. This analysis may reveal trends or rules that govern granule number and size. Kinetic studies of the S90A gene replacement strain at all stages by TEM will also be mechanistically informative. What appear to be larger granules (granules larger than the ones formed by wt *W. eutropha*) by TEM can result from coalescence of smaller granules, from the polymerases synthesizing longer

PHB chains, a combination of both, or other unknown mechanisms that may be phasin related. Determining the number of granules at the early stages of PHB accumulation will shed light on the mechanism for large granule formation. In addition, the number of 'dark-stained features' should also be estimated to see if there is a correlation between this number and the final number of granules. Of course, this should only be done once the presence of the 'dark-stained features' has been validated by cryo-EM or other control experiments (such as TEM examination of other deletion strains of *W. eutropha* at an early stage under nutrient-limited conditions, discussed in Section 7.8).

The TEM images of S90A gene replacement strain at 48 h in PHB_U (Figure 7.6C) cannot be easily interpreted without further analysis (by stereology and by PHB quantitation using crotonic acid assay). Some cell profiles are still completely filled with large granules, while some are empty. It appears that there are more empty cell profiles at this hour than at PHB_P 73 h (compare Figure 7.6B and C), suggesting PHB degradation occurred in this strain. More images are required for quantitative analysis in determining if the granule degradation occurs in a uniform fashion.

The function of this conserved serine residue in Class I synthase should also be assessed in *W. eutropha*. The studies described in this section are applicable to *W. eutropha* strain with S260 of its own synthase mutated to A. The interpretation of the results will be less complicated since the mutant synthase is in its native host.

7.5 PROBING THE FUNCTION(S) OF OTHER CONSERVED AMINO ACID RESIDUES OF CLASS III SYNTHASE BY SDS-PAGE GEL AND AUTORADIOGRAPHY

Analysis of radiolabeled reaction products catalyzed by recombinant wt, D302A, and S90A-PhaCPhaE$_{Av}$ by SDS-PAGE gel and autoradiography has been mechanistically informative and thought provoking. The methods described in Chapter 2 and 3 can be applied to other mutants so that the function(s) of other conserved amino acid residues residing on PhaC$_{Av}$ of the Class III synthase can be investigated. Those residues include P69, Y81, D84, G152, D177, W248, D251, H303, and G330 (Table 1.2). Detailed studies of synthase with these residues mutated will help to identify the residue(s) responsible for the re-initiation of the polymerization process.

7.6 FURTHER INVESTIGATION OF CLASS I SYNTHASE

7.6.1 Introduction

The study of recombinant Class I synthase from *W. eutropha* has always been complicated by the lag phase and the fact that the rate of elongation is much greater than the rate of initiation. One possibility is that protein purified from *E. coli* is not homogeneous. The heterogeneity could result from misfolded protein or post-translationally modified protein, perhaps by a small molecule initiator. Therefore, PhaC$_{We}$ with and without his-tag, purified from *E. coli*, were examined by ESI-MS. Surprisingly, two species were observed in both cases. In addition to the species with the expected molecular weight of the synthase, a second species with slightly larger molecular weight is also present. However, the identity of the second species is currently unknown.

7.6.2 Materials and Methods

Sample preparation for ESI-MS analysis. Concentrated recombinant $PhaC_{We}$ with (21.3 mg/mL) and without (10 mg/mL) $(His)_6$ tag were exchanged from 20 mM KPi, 5% glycerol, and 0.05% hecameg into distilled water using microcons (Microcon YM-50, MWCO: 50 KDa, Millipore). The exchange conditions for $(His)_6$-$PhaC_{We}$ are give in detail. To 50 μL of 21.3 mg/mL of synthase (~ 1 mg) in the buffer described above, 450 μL dH_2O was added. The diluted solution was transferred to the microcon and spun at 12,800 rpm for 4 min. The filtrate (~ 200 μL) was removed and its OD_{280nm} was measured to be 0.17. This corresponds to a loss of 13 mg of protein. To the protein remaining in the microcon, additional 200 μL of dH_2O was added. The sample was spun at the same speed for 8 min. The protein was concentrated to ~ 50 μL, which was then exchanged with another ~ 400 μL of dH_2O. This process was repeated three additional times. In the final round, the protein was concentrated to 60 μL, and its concentration was determined to be 6.3 mg/mL. The recovery of protein was ~ 40%. Recombinant $PhaC_{We}$ without his-tag was exchanged into dH_2O in a similar fashion. The protein was concentrated to 7 mg/mL, and its recovery was ~ 60%.

ESI-MS Analysis. Four protein samples were submitted to the MIT Biopolymers Lab for ESI-MS analysis. Sample 1 contained 126 μg (1.96 nmol) of $(His)_6$-$PhaC_{We}$ in dH_2O. Sample 2 contained 63 μg (984 pmol) of $(His)_6$-$PhaC_{We}$ in 50% acetonitrile and ~ 0.1% acetic acid in dH_2O. Sample 3 contained 140 μg (2.18 nmol) of $PhaC_{We}$ in dH_2O, and Sample 4 contained 70 μg (1.095 nmol) of $PhaC_{We}$ in 50% acetonitrile and ~ 0.1% acetic acid in dH_2O. The Biopolymers Lab usually prepares the submitted protein in 50% acetonitrile and ~ 0.2% acetic acid in dH_2O (for ESI analysis) for their customers. Therefore, as an internal control, Sample 2 and Sample 4 were prepared so that these samples could be directly analyzed without further

manipulation by others. However, it was determined by the researcher at the Biopolymer lab that 1% formic acid gave better spectrum (better signal to noise ratio). To 5 μL of Sample 1 and 3, 95 μL of 50% acetonitrile/1% formic acid was added. To10 μL of Sample 2 and 4, 90 μL of 50% acetonitrole/1% formic acid was added (this was all done by the Biopolymer Lab). The samples were analyzed by direct infusion at 5 μL/min on PE SCIEX API 365 (PerkinElmer). Note that all samples were submitted to the Biopolymer Lab immediately without freezing.

7.6.3 Results and Discussion

Obtaining a mass spectrum of recombinant $PhaC_{We}$ has been problematic and unsuccessful in the past. The problem was that MS analysis requires the protein to remain soluble in detergent-free and salt-free conditions. Recall that the detergent hecameg is required during the purification of recombinant $PhaC_{We}$. Although LC-MS can solve this problem, $PhaC_{We}$ fails to elute from the column. To solve this problem, concentrated synthase samples were exchanged into dH_2O using microcon. Despite the fact that a significant amount of protein (~ 60% in the case of $(His)_6$-$PhaC_{We}$, and ~ 40% in the case of $PhaC_{We}$) was lost during this process, most likely onto the membrane, soluble protein was still present in dH_2O.

ESI mass spectra of $(His)_6$-$PhaC_{We}$ and $PhaC_{We}$ were successfully obtained. The spectrum of each protein sample revealed two species, referred to as Peak 1 and 2 (Fig. 7.8, Table 7.3). Because MS is not quantitative, it is difficult to assess how much of each species was present in the sample despite the fact that Peak 1 appears to be the dominant species. The expected MW of $PhaC_{We}$ is 64,316 Da, and that of $(His)_6$-$PhaC_{We}$ is 66,480 Da due to the additional 20 amino acids at its N-terminus (MGSSHHHHHHSSGLVPRGSH, MW of 2163 Da). Peak 1 in both cases was assigned as the protein itself without the starting methionine (MW of Met: 131 Da). The protein in Peak 2 has not been identified since the MW difference between Peak 2 and Peak

1 could not be assigned. It appears that both $(His)_6$-$PhaC_{We}$ and $PhaC_{We}$, although over-expressed and purified from different *E. coli* strains using different methods (Chapter 4), are modified by the same compound with a MW of ~ 704 - 722 Da. The identity of this modified synthase might be interesting to establish.

While quantitating the native synthase in the crude extract of wt *W. eutropha* by Western, two bands were detected near the MW of $PhaC_{We}$ when a thin 10% SDS-gel (0.7 mm rather than 1 mm) was used (Figure 7.8). A thicker gel was unable to resolve the bands. It appears that the top band is the synthase since its position matched with that of the standard $PhaC_{We}$ purified from *E. coli*. More experiments should be done to confirm the position. The presence of the second band is intriguing, since the protein is recognized by the $PhaC_{We}$ Ab which is quite specific for $PhaC_{We}$. Does this band represent a form of the synthase that has undergone translational modification, a synthase primed with $(HB)_n$, or another synthase that is similar to $PhaC_{We}$ but catalyzes different substrate?

Ultimately, isolation of the synthase from its native host is necessary to understand and investigate the mechanism of the synthase. Preliminary studies described in Chapter 4 already suggest that the synthase isolated from *W. eutropha* behaves differently from that isolated from *E. coli*. Thus, acquiring a mass spectrum of the native synthase is critical. Genetically engineer an affinity tag that is much more accessible and specific than the his-tag (e.g., biotin) into the synthase gene may increase our chance of isolating the homogeneous synthase from its host. However, the location of the tag insertion needs to be considered.

7.7 CHARACTERIZATION OF INTRACELLULAR DEPOLYMERASE DELETION STRAINS IN VIVO

7.7.1 Introduction

Intracellular PHB depolymerases degrade PHB granules to oligomers and monomers of 3-hydroxybutyric acid. The first intracellular PHB depolymerase gene (*phaZ1*, renamed as $phaZ1_a$) from *W. eutropha* H16 was identified, cloned, and characterized by Saito's group (*5*). Results from their studies and those from Jendrossek's group (*6*) suggests that additional intracellular depolymerase(s) must be present to account for the degradation of PHB in $\Delta phaZ1_a$ *W. eutropha* H16 strains.

The availability of the $phaZ1_a$ sequence and the *Ralstonia metallidurans* sequenced genome allowed our lab (G. York and J. Lupberger) to successfully devise a strategy to find two additional candidate depolymerase genes in *W. eutropha*, designated *phaZ2* and *phaZ3* (*7*). PhaZ2 and PhaZ3 have been renamed as $PhaZ1_b$ and $PhaZ1_c$, respectively. $PhaZ1_a$, $PhaZ1_b$, and $PhaZ1_c$ share 40-45% sequence identity. In order to examine the function of $PhaZ1_b$ and $PhaZ1_c$, G. York and J. Lupberger generated *W. eutropha* H16 deletion strains ($\Delta phaZ1_a$, $\Delta phaZ1_b$, $\Delta phaZ1_c$, $\Delta phaZ1_{ab}$, $\Delta phaZ1_{ac}$, and $\Delta phaZ1_{abc}$) (*7*). We then analyzed these strains for PHB production and utilization under two sets of growth conditions. When cells were grown in nutrient-rich medium, $PhaZ1_a$ was sufficient to account for intracellular PHB degradation. When cells that had accumulated ~80% PHB/cell dry weight (cdw) were subjected to PHB utilization conditions, $PhaZ1_a$ and $PhaZ1_b$ were sufficient to account for PHB degradation. $PhaZ1_b$ is thus suggested to be an intracellular depolymerase. The role of $PhaZ1_c$ remains to be established.

7.7.2 Materials and Methods

Media and growth conditions. PHB production was examined in a nitrogen-limited medium (minimal medium (*8*) supplemented with 1% of fructose and 0.01% ammonium chloride, PHB_P). PHB utilization was examined in a carbon-limited medium (minimal medium supplemented with 0.5% ammonium chloride, PHB_U). Both processes were also studied in tryptic soy broth-dextrose free (TSB), a nutrient-rich medium.

Cultivation conditions. Wild-type (wt) *W. eutropha* H16 and depolymerase deletion strains ($\Delta phaZ1_a$, $\Delta phaZ1_b$, $\Delta phaZ1_c$, $\Delta phaZ1_{ab}$, $\Delta phaZ1_{ac}$, and $\Delta phaZ1_{abc}$) were cultivated with aeration at 30°C. Gentamicin was included in all growth media, except when PHB utilization was being measured. Each procedure was done in duplicate. A single colony from a TSB plate was cultivated in 5 mL TSB medium to saturation (~ 40 h) at which time 2 mL was transferred into 100 mL TSB medium in 500 mL baffled flasks and grown for 24 h. These cells were washed and transferred into 200 mL TSB medium or 200 mL PHB_P in 1 L baffled flasks to yield cultures with an initial OD_{600}=0.5. Cells (5 mL) were removed from the cultures at T = 0, 4, 8, 12, 24, 48, and 72 h. For PHB utilization, 100 mL of cells grown in PHB_P for 72 h were washed with 0.85% saline and transferred into the PHB_U. Cells (5 mL) were harvested at T = 4, 8, 12, 24, 48, and 72 h. In all cases, cells were analyzed for PHB content.

PHB quantification. Aliquots of cells (above) were washed twice with ice-cold water and dried overnight at 80°C under vacuum. PHB was quantitated as crotonic acid by the sulfuric acid/high-pressure liquid chromatography method of Karr *et al.* (*9*). The samples were analyzed using an Aminex HPX-87H column (Bio-rad, Hercules, CA); column temperature: 50°C;

gradient: isocratic; mobile phase: 5 mM sulfuric acid; flow rate: 0.6 mL/min. Crotonic acid was detected by a diode array detector at 210 nm.

7.7.3 Results and Discussion

To determine if the newly identified genes, *phaZ1$_b$ and phaZ1$_c$*, actually function as PHA depolymerases, Δ*phaZ1$_a$*, Δ*phaZ1$_b$*, Δ*phaZ1$_c$*, Δ*phaZ1$_{ab}$*, Δ*phaZ1$_{ac}$*, and Δ*phaZ1$_{abc}$ W. eutropha* H16 strains were examined for their ability to degrade PHB under two sets of growth conditions. WT strain was included in the study to serve as a control. The results from the experiments in TSB medium are shown in Figure 7.9A and B. The maximum amount of %PHB/cdw was found at the 4 h time point. In the wt, Δ*phaZ1$_b$*, and Δ*phaZ1$_c$* strains, all of the PHB was removed by 48 h. In all of the other strains, each of which has *phaZ1$_a$* deleted, the %PHB/cdw levels remain unchanged after 12 h. At present, it is not clear if the differences in %PHB/cdw observed for different strains during the first 12 hours are significant. Additional multiple independent studies are required to evaluate these differences. The results in TSB medium therefore provided no evidence that PhaZ1$_b$ or PhaZ1$_c$ can function as PHB depolymerases *in vivo*. Our recent Western analyses on cells grown in TSB medium have also failed to detect the presence of these two proteins (*10*).

The results from experiments in which PHB was accumulated to ~ 80% cdw in PHB$_P$ and then switched into PHB$_P$ are shown in Figure 7.10A and Figure 7.10B and C, respectively. During the 72 h cultivation period in PHB$_P$, the PHB accumulation pattern of each *phaZ* deletion strain was very similar to that of the wt strain, all approaching 80% cdw (Figure 7.10A). When each strain was switched into PHB$_U$, the wt strain had utilized 50% of its PHB content after 48 h, whereas the Δ*phaZ1$_{abc}$* strain lost a statistically insignificant amount of its PHB content after the same period. The Δ*phaZ1$_a$* strain utilized ~20% PHB content, the Δ*phaZ1$_{ac}$* strain utilized ~15%

to 20%, and the Δ*phaZ1*$_{ab}$ strain lost no statistically significant amount of its PHB content. Thus in contrast to the results in TSB medium, maximal PHB loss under these conditions appears to require the *phaZ1*$_a$ and *phaZ1*$_b$ genes. These results suggest that PhaZ1$_b$ is a PHB depolymerase. The PHB degradation in Δ*phaZ1*$_{ac}$ in several experiments appeared to be less than that in Δ*phaZ1*$_a$ strain. However at present, growth conditions have not yet been found to demonstrate unambiguously the function of PhaZ1$_c$ as a depolymerase. Recently, our lab studied the mRNA levels and protein expression levels of PhaZ1$_b$ and PhaZ1$_c$ in wt *W. eutropha* H16 cultivated under nutrient-limited conditions (*11, 12*). No amount of PhaZ1$_c$ has been detected during cell growth in PHB$_P$ or PHB$_U$. Interestingly, the expression of PhaZ1$_b$ increased after PHB production starts in PHB$_P$, and quickly decreased in PHB$_U$. In the light of these results, PhaZ1$_b$ could be functioning as a re-modelling enzyme. It may play a role in the proper packing of polymer chains. However, considering the same amount of PHB was degraded in Δ*phaZ1*$_b$ as that in wt, the role(s) exerted by PhaZ1$_b$ does not seem to effect the function of PhaZ1$_a$ and/or other depolymerase(s). Only in the absence of PhaZ1$_a$, then its effect was observed. Alternatively, PhaZ1$_b$ may be not a depolymerase. We can initially test this hypothesis by determining if it is active towards HB-CoA, the substrate of the synthase. Other short-chain or medium-chain length substrates (Figure 1.1) should also be tested.

7.8 STUDIES OF DARK-STAINED FEATURES

The intricacy and complexity of the cellular structures and their dynamics can often be better understood when viewed through sophisticated bioimaging techniques. Transmission electron microscopy studies of *W. eutropha* in the early stages of granule biosynthesis revealed nascent granules localized around the dark-stained features near the center of the cells. These images

prompted us to propose a new model that takes the dark-stained features and the location of granules into account (described in Chapter 5). This model is now considered as one of the possible working models for granule biogenesis. The details of these studies have been described and discussed in Chapter 5 and 6. As we have also emphasized in these chapters, sample preparation for TEM analysis involves extensive fixation and dehydration of the bacteria cells. The extent of structure alteration due to these harsh treatments is unknown and difficult to assess. Despite the problems associated with this method, TEM is still one of the few methods available to decipher and probe the interior of cells. With parallel studies carried out by methods such as cryoelectron microscopy validating the observations made with TEM, TEM can still contribute significantly to our understanding of the *in vivo* PHB biosynthesis and degradation processes.

Needless to say, the first priority is to confirm the location of granules and the presence of dark-stained features in *W. eutropha* cells. Several approaches can be considered. The first approach is to study an *E. coli* strain that is incapable of producing PHA in nitrogen-limited medium at an early stage by the conventional (fixing, staining, dehydration) TEM. The objective of this experiment is to determine if any cellular structure in *E. coli* could also give rise to the dark-stained structures observed in *W. eutropha*. *E. coli* and *W. eutropha* are similar in that both are gram-negative and cylindrical. The effect of fixing, staining, and dehydration on their cell membrane and shape, and through the membrane on other cellular structures may be similar. The absence of the dark-stained features in *E. coli* grown under PHB production conditions would suggest that these features are unique to *W. eutropha*, and are not an artifact. However, the presence of these features in *E. coli* does not eliminate our hypothesis since these features could still be formed as a result of nutrient-stress. The second approach is to examine wt *W.*

eutropha cells that are first grown in PHB_P for 2 to 5 h and then transferred to TSB medium for 4 to 8 h by conventional TEM. The observation that the dark-stained features are much more significant in cells harvested at 2.5 and 5 h in PHB_P (Chapter 5, Figure 5.5) than in cells collected at 4 h TSB medium (Chapter 6, Figure 6.4 and Figure 6.7A) suggests that the formation of these features may be stimulated by nitrogen-limitation. Thus, the objective of the second approach is to determine the fate of the dark-stained features in the early stages of PHB production phase as the cells are transferred into a nutrient-rich medium. Disappearance or reduced appearance of the dark-stained features in TSB medium would support the hypothesis that formation of these features is promoted under nitrogen-limited conditions. The third approach, discussed in detail in Section 7.10, is to examine the wt *W. eutropha* strain in the early granule accumulation stage by cryoelectron microscopy. Results by this method should be compared to our previous results by TEM to look for similarities and differences. The last approach (most important if the 'features' are real) is direct isolation of dark-stained features by ultracentrifugation and examination of each fraction by TEM or cryo-EM. The diameters of the dark-stained features are 0.4 ~ 0.5 μm when measured from 2D-images of *W. eutropha* cells at 2.5 and 5 h in PHB_P. At these stages, the presence and the size of these features are more prominent than any other structures within a *W. eutropha* cell. Therefore, the procedure used to isolate mitochondria which is ~ 0.5 μm from yeast cells may serve as a starting point (*13*).

7.9 PRELIMINARY TEM STUDIES OF DELETION STRAINS OF *W. EUTROPHA*

7.9.1 Introduction

Within the last year, various deletion strains of *W. eutropha* have been studied by TEM following the methods described in Chapter 5, with the hope to obtain new information regarding the importance of the synthase, phasin, a putative transcription regulator, and intracellular depolymerases. The deletion strains included in the studies were Δ*phaC*, Δ*phaP*, Δ*phaR*, Δ$phaZ1_a$, Δ$phaZ1_b$, Δ$phaZ1_c$, and Δ$phaZ1_{abc}$. Because these studies had been carried out prior to the kinetic studies of wt *W. eutropha* strain by TEM and the quantitative analysis of those images by stereology (described in Chapter 5 and 6), we were not aware of the granule coalescence at 72 h in PHB_P and the presence of the dark-stained features at the early time points in PHB_P. Therefore, each strain has only been studied in TSB medium at 4 h (with the exception of the last two strains listed above), in PHB_P at 72 h, and PHB_U at 48 h. These time points and growth conditions were chosen because the wt *W. eutropha* makes the most amount of PHB per cell dry weight at 4 h under nutrient-rich conditions and the change of phenotype of the granules before and after the cells enter PHB utilization conditions was of interest. The number of images obtained for each strain was also limited since quantitative analysis by stereology was not considered at the time. In this section, the preliminary TEM results of the deletion strains are presented. Although some images are suggestive of cell and granule size differences between the deletion strain and wt, stereology analysis will need to be done to confirm these observations, as described below.

7.9.2 ΔphaC W. eutropha H16 strain

At 4 h in TSB medium, *W. eutropha* cells with PhaC deleted did not produce any PHB (Figure 7.11B), as expected. The cells seemed to be healthy, and their cell size appeared to be similar to that of wt. Although some type of dark-stained features are observed, they are not as apparent which is similar to features observed with the wt strain at the same time point (Figure 7.11A). However, when examined in PHB_P at 72 h, significant differences were observed between the mutant and wt strains. Cells of the Δ*phaC* strain appeared irregular and abnormal (Figure 7.12 and 7.13). In addition, they were much smaller than wt cells examined at the same time point (compare to those in Figure 5.2E). A significant amount of cell death was also observed when Δ*phaC* cells were examined in PHB_U at 48 h (Figure 7.12B). The phenotypes of Δ*phaC* in TSB medium, PHB_P, and PHB_U suggest that PhaC is an essential gene when *W. eutropha* encounters nitrogen limitation, and that production of PHB is its major survival mechanism. Some type of dark-stained features that appear to be more condensed than those of wt at 2.5 and 5 h were also observed in PHB_P and PHB_U (Figure 7.12 and 7.13). While no granular features were observed in Δ*phaC* strain grown in TSB medium (Figure 7.11B), small granular features were observed in many cell profiles when this strain was grown in PHB_P and PHB_U (Figure 7.12 and 7.13). The composition of these granular features is unknown. Recently, Potter *et al* reported that there is no PhaC homologue in *W. eutropha* when searching through its sequenced genome (*14*). However, at the recent PHB International Symposium, the possibility of another synthase present in *W. eutropha* was proposed by Steinbuchel's group. Although our previous study has shown that PHB is not detectable in Δ*phaC* strain by the crotonic acid detection method, it is possible that *W. eutropha* does contain additional synthase(s), but their substrate may not be HB-CoA. It is interesting that the granular features observed in Δ*phaC* do

not appear to be associated with the dark-stained features (Figure 7.13). Instead, they are observed around the periphery of the cells.

Clearly, the absence of the synthase greatly affects the physiology of the cell under nitrogen-limited conditions. The synthase deletion strain can thus serve as a great tool in studying the effect of PhaC or its products, if there are any, on cell physiology of *W. eutropha*. In Chapter 5, we proposed that the increase in cell dimension observed when *W. eutropha* cells are transferred from TSB medium to PHB_P could be due to cell doubling and a regulatory mechanism that allows the cells to expand in preparation for granule storage. The Δ*phaC* strain can be used to test this hypothesis. Although it appears that the cells of Δ*phaC* strain are smaller than wt (suggesting that PhaC or its products may play a role in regulating cell size in nitrogen-limited conditions), we only have images at PHB_P 72 h and the data have not been quantitated. Stereology analysis should be applied to images of Δ*phaC* strain taken at 24 h in TSB medium and at early stages of PHB_P, such as 2.5, 5 or 9h, and at 24 h. The doubling time of Δ*phaC* in TSB medium is similar to that of wt, however, it takes Δ*phaC* strain 14 h to increase its OD_{600nm} from 0.5 to 1.2 and the OD remains the same thereafter. If the presence of PhaC or its product triggers a response in cell size regulation, then capturing images of Δ*phaC* while it's still dividing and comparing its cell size to that of wt can address our hypothesis. Comparing cell sizes at the stationary phase (24 h) can provide additional support for the role of synthase or its products in cell size regulation.

Additional TEM images of the Δ*phaC* strain in the early stage of PHB_P would also be valuable in confirming the presence of dark-stained features and granular features. If the results were confirmed, then Δ*phaC* strain would be ideal for isolating the dark-stained features since one does not have to worry about interference from PHB. To establish if the small granular

structures are composed of PHAs (with $R \geq C_4$, Figure 1.1), they can be extracted by trying the conditions used to isolate polymers composed of medium-chain length substrates. Nuclear magnetic resonance spectroscopy (NMR) and gas chromatography mass-spectroscopy (GC-MS) can then be used to determine their content. Preliminary Western data also revealed the presence of $PhaZ1_a$ and $PhaZ1_b$ in this strain, with $PhaZ1_a$ peaking at 4 h and $PhaZ1_b$ peaking at ~ 14 h (*12*). Therefore, Δ*phaC* strain is also useful for isolating these two proteins for analysis since there is no PhaC, PhaP, and PHB to interfere,

7.9.3 ΔphaR W. eutropha H16 strain

The phenotype of Δ*phaR* strain has previously been reported. Several research groups have shown in different organisms that as a result of deleting *phaR*, a large amount of PhaP is produced and a large number of small granules are formed (*15, 16*). This strain was also included in our study. In TSB medium, we have already observed non-random distribution of small granules within the cytoplasm at 4 h (Chapter 6, Figure 6.8). The number of granules appears to be greater than that in the wt strain. The expected granule phenotype was also observed at 72 h during PHB production. The cells were full of small granules (Figure 7.14). However, the cell size of the Δ*phaR* strain appeared to be much smaller than that of wt strain (compare Figure 7.15A and B). In fact, the cell size of Δ*phaR* at 72 h PHB_P is similar to that at 48 h in PHB_U (Figure 7.16A). The data suggest that deletion of *phaR* may have debilitated the cell's ability to increase in size. This result suggests that PhaR may play a role in controlling cell size and/or membrane synthesis (looking at early time points should be more informative) in addition to its regulation of PhaP.

Stereology analysis is required for cell size determination before any conclusion regarding the cell size of Δ*phaR* strain can be made. In fact, TEM images of cells at time points prior to 72

h in PHB_P may be more informative. TEM images of cells at 48 h in PHB_U also revealed a significant presence of dark-stained features (Figure 7.16A). Therefore, this strain may be of use to isolate the unknown features. The advantage of these conditions is that more cells per L of culture can be obtained for the isolation of the dark-stained features, since the cells in PHB_U can be cultivated starting with high ODs. There is not much PHB left at 48 h (compare Figure 7.16A and 7.16B which shows an image of the wt strain at this time point). Analysis of the PHB content in the Δ*phaR* strain by crotonic acid assay should also be established in different growth media. The current working model for PhaR in the literature proposes that the repression of PhaP production by PhaR is released as a result of PHB (or HB oligomers) production, thus leading to an increase in the amount of PhaP and large number of granules (*17, 18*). The preliminary Western analysis suggests that more PhaC is produced in the Δ*phaR* strain than the wt strain, indicating that there may be a relationship between PhaC and PhaR, and increasing amounts of PhaC could be the reason why the number of PHB granules increased. However, the Western analysis of Δ*phaR* strain has only been done once. This experiment should be repeated with cells from several independent growths, and cell counting is necessary. The number of granules produced in this strain, which can be quantitated by using serial sections and stereology, should be of great interest to us. Is the increase in number of PHB granules proportional to the production of PhaC or PhaP or both? What is the ratio of PhaP to PhaC? What is the granule surface area coverage by PhaP? What is the ratio of PhaP and PhaC to PHB polymer chain? Detailed studies of the Δ*phaR* strain similar to those we have carried out for the wt strain should shed more light on the mechanism of PHB production and the roles of PhaR.

7.9.4 ΔphaP W. eutropha H16 strain

One function of the phasin PhaP that has been proposed is to prevent granules from coalescing. One large granule has been presented as the typical phenotype of the Δ*phaP* deletion strain by Wieczorek *et al* using TEM (*19*). However, analysis of a large field of cells reveal that in addition to one large granule being present in the Δ*phaP* strain, tiny granular features are also found in cell profiles (Figure 7.17). If these tiny features are PHA granules, this observation then implies that in addition to PhaP, there may be other phasin proteins that could serve similar functions to PhaP. Recently, Potter *et al* reported the identification and isolation of three additional phasins. They demonstrated that under standard nitrogen-limitation growth conditions, PhaP (renamed PhaP1) is the most abundant phasin and is present at much higher concentration than the newly discovered ones (*14*). The function of the other PhaPs has not been identified. It is possible that they may play a role in coating the surface of PHB and/or other PHA granules. This could explain why small granules are observed in the Δ*phaP* strain, if the small white features (Figure 7.17) are indeed granules.

Since the Δ*phaP* strain generates granules much larger than those in wt strains, detailed studies similar to those on the wt strain should also be done for this strain. As mentioned earlier (Section 7.4.3), measurement of the number of times PhaC re-initiates polymer production and the M_W of polymer chain in the Δ*phaP* and the S90A-PhaCPhaE$_{Av}$ gene replacement strains may provide insight into the mechanism of large granules generation. In the former case, the lack of PhaP will most likely account for the large granules; and in the case of the S90A gene replacement strain, the synthase itself may account for the large size of granules. Thus, it is critical to monitor the amount of PhaP and the changes in its concentration in the S90A gene replacement strain as suggested in Section 7.4.3, over the course of granule formation. Another

unresolved issue is the identification of protein/lipids on the surface of the granules in the Δ*phaP* strain. This strain may be useful in isolating or identifying other components on the granule surface.

7.9.5 ΔphaZ1$_a$, ΔphaZ1$_b$, ΔphaZ1$_c$, and ΔphaZ1$_{abc}$ W. eutropha H16 strains

Currently, three proteins (PhaZ1$_a$, PhaZ1$_b$, and PhaZ1$_c$) and an oligomer hydrolase (PhaZ2) have been proposed to serve as intracellular depolymerases in *W. eutropha* (*7, 20*). Previous *in vivo* studies on Δ*phaZ1$_a$*, Δ*phaZ1$_b$*, or Δ*phaZ1$_c$* strains suggest that PhaZ1$_a$ is responsible for degrading the most amount of PHB ((*5, 7*), Section 7.7). Recently, our lab has also demonstrated that PhaZ1$_c$ does not seem to be present during PHB production or utilization through RT-PCR and Western methods (*11, 12*). Using the same methods, the presence of PhaZ1$_b$ was detected transiently during the PHB production phase. Its rapid disappearance in PHB$_U$ suggesting that this protein may play a role in polymer chain remodeling rather than functioning as a depolymerase similar to PhaZ1$_a$. The roles of PhaZ1$_a$, PhaZ1$_b$ and PhaZ1$_c$ are unclear. In fact, they may not be intracellular depolymerase. Therefore, the deletion strains were investigated by TEM. It turns out that the phenotypes of Δ*phaZ1$_a$* and Δ*phaZ1$_c$* appeared to be similar to that of wt *W. eutropha* strain at 72 h during the PHB production phase (Figure 7.18A and C) and 48 h during the PHB utilization phase (Figure 7.19A and C). Those of Δ*phaZ1$_b$* may be slightly different from wt, with slightly larger granules at the 72 h in PHB$_P$ (Figure 7.18B), and smaller amount of granules at the 48 h in PHB$_U$ (Figure 7.19B). However, stereology analysis is required before any conclusions on the amount of granule and granule size can be made. In addition, 72 h in PHB$_P$ is not a good time point for comparison in granule size since granule coalescence is typically observed at this stage. Overall, these results indicate that none of these proposed intracellular depolymerases functions alone.

Recently, degradation of PHB by the intracellular oligomer hydrolase (PhaZ2) has been demonstrated in *W. eutropha* by Kobayashi *et al.* (*21*). This result is rather puzzling in that if PhaZ2 were to play a major role in degradation, then how are the cells able to maintain a constant level of PHB throughout the utilization stage by the $\Delta phaZ1_{abc}$ strain as we have reported in York *et al*? The triple deletion strain was thus examined by TEM. While the phenotype of this strain at PHB_P 72 h (Figure 7.20A) is similar to that of wt, its phenotype at PHB_U 48 h (Figure 7.20B) differs from those of the single depolymerase deletion strains examined thus far. No degradation was observed. The cells are still intact and full of granules. This result clearly demonstrated that $PhaZ1_b$ and/or $PhaZ1_c$ is important for PHB degradation. How they exert their role(s) is unclear. It is likely that the presence of $PhaZ1_b$ (or $PhaZ1_c$) is required for the oligomer hydrolase and/or additional intracellular depolymerases to function properly in the degradation of PHB granules.

7.10 CRYOELECTRON MICROSCOPY

Advances in cryogenic preservation, automated data collection, and image reconstruction have allowed cryoelectron microscopy (cryo-EM) to become a powerful imaging tool in studying the structure and dynamics of macromolecular complexes and cellular components. Cryo-EM differs significantly from the conventional TEM in that the biological samples are maintained in or close to the native state of the samples. Instead of fixing samples with aldehydes at room temperature, the motion of molecules in a biological sample prepared for cryo-EM is stopped by quickly plunging the sample into liquid ethane. The vitreous, non-crystalline form of ice generated by this method of quenching presumably preserves the sample in its native state (*22*). The sample is cryo-transferred to the microscope and maintained at liquid nitrogen temperature

while being examined. No additional fixation or staining is involved. Thus, potential structural distortions and artifacts caused by fixatives, stains, and dehydration are avoided. There are, however, caveats associated with cryo-EM. The method assumes that vitrification does not perturb the native state of all parts of the sample significantly, which may not be the case. Because the samples are not stained, less contrast of the sample can be achieved. In addition, the electron beam damages the frozen samples. Using low electron dosage (1-20 electron/$Å^2$) is necessary, but leads to even less intrinsic contrast of the sample (*23*).

Single particle analysis and EM tomography are two methods used to reconstruct 3D images of the specimen from 2D images. The first method is usually used to study the structure and dynamics of isolated and purified macromolecules or complex(es) reconstituted *in vitro*. Many 'copies' of the same species are typically trapped in the vitreous ice layer in isotropic orientations, a requirement so that the 2D projections of the sample from every possible angle can be captured. To compensate for the low signal-to-noise ratio, an enormous 2D-image data set containing at least tens of thousands particles are required to regenerate the 3D images of the particle (e.g., ribosome, low-density lipoproteins) through sophisticated computational analysis (*23*). The resolution of the 3D image can be within 7 to 30Å. High-resolution X-ray structures or NMR of proteins involved in the complex are often mapped into the reconstructed 3D image of the complex to elucidate the interaction between the molecules in the complex. Lack of protein structural information (X-ray structure or NMR) as in the case of the PHB system, however, increases the difficulty of identifying the components in the complex significantly. "Computational purification" is a technique often used to identify sub-populations of molecules if they exist in different conformations. For example, three conformational states of an archaeal

chaperonin from *Sulfolobus shibatae* have been elucidated after 2D projections of 17,000 particles were computationally purified (*24*).

The second analysis method, EM tomography, is usually applied when the internal structure of cells or tissues are being studied. A series of images or projections of the same specimen is recorded as the sample is being tilted incrementally through a wide range of angles. These images are then used to reconstruct the 3D structures of the sample. However, radiation damage of the sample is more of a concern with this method since the sample experiences a longer exposure to the electron beam as it is being imaged from various angles. In addition, the thickness of the sample (>100 nm) prevents it from being vitrified homogenously and typically causes inelastic scattering of the electrons that leads to signal degradation. The resolution of the 3D image depends on the thickness of the sample and the number of projections recorded. A sample of 0.25 μm thickness would require 160 equally spaced projections to achieve a 3D resolution of 50Å (*25*), a daunting task. For these reasons, technical improvement and development of tomography are underway with the hope of overcoming the challenges of data collection, low resolution, and ambiguous interpretation of 3D reconstructs (*26*). Recently, successful cryo-EM of vitreous sections (CEMOVIS) of cells and tissues with unprecedented resolution and quality have been reported (*27, 28*). High-pressure freezing (HPF) and an improved sectioning apparatus are the reasons behind the success. HPF allows thick cell and tissue samples to be vitrified homogeneously. Needless to say, cryo-sectioning the sample is quite challenging and distortion of sample structures is possible as the knife cuts through the sample. However, these artifacts can be systematically evaluated. The end-result is that frozen-hydrated thin sections can be obtained and examined without further staining and yet achieve high resolution. There are several recent excellent reviews on cryo-EM, addressing sample

preparation, single particle analysis, 3D-reconstruction, EM tomography, CEMOVIS, and the caveats associated with these method (*23, 25, 29-31*). Overall, cryo-EM has demonstrated its importance in the native structural/functional studies of ribosome (*32*), photosystem II supercomplex (*33*), low-density lipoproteins (*34*), amyloid fibril (*35*) and many other macromolecular complexes. It will continue to be the method of choice to study the molecular machineries and internal structures of cells and tissues. Introducing cryo-EM to our lab and the PHB field is the next important step to take, as this method will bring a vast amount of information that would play a key role in unraveling PHA biosynthesis and degradation, *in vitro* and *in vivo*.

The Whitehead Institute/MIT Bioimaging Center has recently acquired the first of its kind cryoelectron microscopes, the JEOL JEM-2200FS. This high-resolution instrument is designed to image the smallest biological molecules at near-atomic resolution, surpassing what most other microscopes can offer. The scope is kept in a stable environment and can be controlled remotely to avoid perturbation of the electrons that pass through the sample. A built-in energy filter also alleviates inelastic scattering, thus increasing the image resolution. Having access to this state-of-the-art cryo-EM microscope on campus should allow us to attempt several interesting preliminary experiments using EM tomography and single particle analysis, despite the challenges associated with each method.

First, the kinetic studies of PHB production and utilization by *W. eutropha* in PHB_P and PHB_U by TEM should be repeated using CEMOVIS, with emphasis on the early stages of the PHB polymerization process. The location of nascent granules, whether they are close to the membrane or near the center of the cell, should be examined. The result of this experiment is crucial in verifying the current working models of granule initiation in *W. eutropha*. Cells

should also be examined for internal structures other than granules to see if features similar to the dark-stained features observed through TEM are present. However, since the samples are not stained, it is unknown how the 'dark-stained features' would appear and whether they can be distinguished clearly from the rest of the contents in the cytoplasm of the cells. EM tomography should be attempted to re-evaluate the cell dimensions determined previously from images of cells that were fixed, stained, dehydrated, and embedded in plastics (Chapter 5).

Second, time-resolved cryo-EM and single particle analysis should be attempted to study the *in vitro* polymerization reaction catalyzed by the recombinant synthases. The Class III D302A PhaCPhaE$_{Av}$ is a great candidate for this pilot study. Its slow rate of polymerization (1/1000 that of the wt synthase) can be used to our advantage again to study the initiation stage of the polymerization process. The reaction containing D302A mutant synthase and HB-CoA can be monitored by removing a drop from the reaction mixture at specific time points, placing it on a grid, and freezing the grid in liquid ethane. The sample can then be directly examined by cryo-EM. Thus, it may be possible for us to 'watch' the synthase catalyzing the reaction. Quenching the reaction rapidly at different time points provides the snapshots of the mutant synthase in action. Recently, visualization of the binding sites of *E. coli* DNA pol V on RecA-ssDNA has been demonstrated (*36*). If the technical difficulties can be overcome, then wt Class III and I synthases, their mutants, and the reaction they catalyze can be studied in this fashion. Substrate analogue N-acetyl-cysteamine can also be used when studying the wt synthase to slow down the reaction. The results from these experiments could potentially provide information on the following litany of questions: (1) what is the structure of the polymer as it is being synthesized (linear vs. curled up)? (2) What is the oligomeric state of the synthase during polymerization? (3) How many synthases are working on a single polymer or is there corporativity of the synthase?

(4) Is the polymer still associated with the synthase while a new PHB chain is being synthesized? (5) Is PhaE associated with the polymer (if we attempt to combine cryo-EM and immuno-labeling by treating the reaction mixture with immuno-gold labeled antibody (Ab) to PhaE before freezing the sample)? (6) Are the structures of PHB polymer produced by mutants different from that of wt? Most likely, cryo-EM will provide answers to many questions that are unforeseen, and play an important role in unraveling the process of PHB formation *in vivo* and *in vitro*.

7.11 REFERENCES

1. Liebergesell, M., Sonomoto, K., Madkour, M., Mayer, F., and Steinbuchel, A. (1994) Purification and characterization of the poly(hydroxyalkanoic acid) synthase from *Chromatium vinosum* and localization of the enzyme at the surface of poly(hydroxyalkanoic acid) granules, *Eur J Biochem 226*, 71-80.
2. Müh, U., Sinskey, A.J., Kirby, D.P., Lane, W.S., and Stubbe, J. (1999) PHA synthase from *Chromatium vinosum*: Cysteine 149 is involved in covalent catalysis, *Biochemistry 38*, 826-837.
3. Corporation, W.T. DAWN Course Manual.
4. Laemmli, U.K. (1970) Cleavage of structural proteins during the assembly of the head of bacteriophage T4., *Nature 227*, 680-685.
5. Saegusa, H., Shiraki, M., Kanai, C., and Saito, T. (2001) Cloning of an intracellular Poly[D(-)-3-Hydroxybutyrate] depolymerase gene from *Ralstonia eutropha* H16 and characterization of the gene product, *J Bacteriol 183*, 94-100.

6. Handrick, R., Reinhardt, S., and Jendrossek, D. (2000) Mobilization of poly(3-hydroxybutyrate) in *Ralstonia eutropha*, *J Bacteriol 182*, 5916-5918.

7. York, G.M., Lupberger, J., Tian, J., Lawrence, A.G., Stubbe, J., and Sinskey, A.J. (2003) *Ralstonia eutropha* H16 Encodes Two and Possibly Three Intracellular Poly[D-(-)-3-Hydroxybutyrate] Depolymerase Genes, *J Bacteriol 185*, 3788-3794.

8. Peoples, O.P. and Sinskey, A.J. (1989) Poly-β-hydroxybutyrate (PHB) biosynthesis in *Alcaligenes eutrophus* H16: Identification and characterization of the PHB polymerase gene (phbC), *J. Biol. Chem. 264*, 15298-15303.

9. Karr, D.B., Waters, J.K., and Emerich, D.W. (1983) Analysis of poly-beta-hydroxybutyrate in *Rhizobium japonicum* bacteroids by ion-exclusion high-pressure liquid-chromatography UV detection, *Appl Environ Microbiol 46*, 1339-1344.

10. Tian, J., He, A., Lawrence, A., Liu, P., Watson, N., Sinskey, A.J., and Stubbe, J. (2004) Analysis of Transient Polyhydroxybutyrate Production in *Wautersia eutropha* H16 by Quantitative Westerns and Transmission Electron Microscopy, *manuscript submitted for publication.*

11. Lawrence, A.G., Schoenheit, J., He, A., Tian, J., Liu, P., Stubbe, J., and Sinskey, A.J. (2004) Time-resolved expression profiling of *Wautersia eutropha* genes related to poly-(*R*)-hydroxybutyrate homeostasis during bach fermentation, *manuscript submitted for publication.*

12. He, A., Tian, J., Lawrence, A., Liu, P., Sinskey, A.J., and Stubbe, J. (2004) Expression Analysis of Proteins Involved in Polyhydroxybutyrate Homeostasis in *Wautersia eutropha* H16, *submitted for publication.*

13. Watson, K., Haslam, J.M., and Linnane, A.W. (1970) Biogenesis of mitochondria. 13. The isolation of mitochondrial structures from anaerobically grown Saccharomyces cerevisiae, *J Cell Biol 46*, 88-96.

14. Potter, M., Muller, H., Reinecke, F., Wieczorek, R., Fricke, F., Bowien, B., Friedrich, B., and Steinbuchel, A. (2004) The complex structure of polyhydroxybutyrate (PHB) granules: four orthologous and paralogous phasins occur in *Ralstonia eutropha*, *Microbiology 150*, 2301-2311.

15. Maehara, A., Ueda, S., Nakano, H., and Yamane, T. (1999) Analyses of a polyhydroxyalkanoic acid granule-associated 16-kilodalton protein and its putative regulator in the *pha* locus *Paracoccus denitrificans*, *J. Bacteriol. 181*, 2914-2921.

16. Potter, M., Madkour, M.H., Mayer, F., and Steinbuchel, A. (2002) Regulation of phasin expression and polyhydroxyalkanoate (PHA) granule formation in *Ralstonia eutropha* H16, *Microbiology 148*, 2413-2426.

17. Maehara, A., Taguchi, S., Nishiyama, T., Yamane, T., and Doi, Y. (2002) A repressor protein, PhaR, regulates polyhydroxyalkanoate (PHA) synthesis via its direct interaction with PHA, *J Bacteriol 184*, 3992-4002.

18. York, G.M., Stubbe, J., and Sinskey, A.J. (2002) The *Ralstonia eutropha* PhaR protein couples synthesis of the PhaP phasin to the presence of polyhydroxybutyrate in cells and promotes polyhydroxybutyrate production, *J Bacteriol 184*, 59-66.

19. Wieczorek, R., Pries, A., Steinbüchel, A., and Mayer, F. (1995) Analysis of a 24-kilodalton protein associated with the polyhydroxyalkanoic acid granules in *Alcaligenes eutrophus*, *J. Bacteriol. 177*, 2425-2435.

20. Saegusa, H., Shiraki, M., and Saito, T. (2002) Cloning of an Intracellular D(-)-3-Hydroxybutyrate-Oligomer Hydrolase Gene from *Ralstonia eutropha* H16 and Identification of the Active Site Serine Residue by Site-Directed Mutagenesis, *Journal of Bioscience and Bioengineering 94*, 106-112.

21. Kobayashi, T., Shiraki, M., Abe, T., Sugiyama, A., and Saito, T. (2003) Purification and Properties of an Intracellular 3-Hydroxybutyrate-Oligomer Hydrolase (PhaZ2) in *Ralstonia eutropha* H16 and Its Identification as a Novel Intracellular Poly(3-Hydroxybutyrate) Depolymerase, *J Bacteriol 185*, 3485-3490.

22. Dubochet, J., Adrian, M., Chang, J.-J., Homo, J.-C., Lepault, J., McDowall, A.W., and Schultz, P. (1988) Cryo-electron microscopy of vitrified specimens, *Quart. Rev. Phys. 21*, 129-228.

23. Frank, J. (2002) Single-particle imaging of macromolecules by cryo-electron microscopy, *Annu Rev Biophys Biomol Struct 31*, 303-19.

24. Schoehn, G., Quaite-Randall, E., Jimenez, J.L., Joachimiak, A., and Saibil, H.R. (2000) Three conformations of an archaeal chaperonin, TF55 from Sulfolobus shibatae, *J Mol Biol 296*, 813-819.

25. Steven, A.C. and Aebi, U. (2003) The next ice age: cryo-electron tomography of intact cells, *Trends Cell Biol 13*, 107-110.

26. McEwen, B.F. and Frank, J. (2001) Electron tomographic and other approaches for imaging molecular machines, *Curr Opin Neurobiol 11*, 594-600.

27. Matias, V.R., Al-Amoudi, A., Dubochet, J., and Beveridge, T.J. (2003) Cryo-transmission electron microscopy of frozen-hydrated sections of *Escherichia coli* and *Pseudomonas aeruginosa*, *J Bacteriol 185*, 6112-6118.

28. Al-Amoudi, A., Norlen, L.P., and Dubochet, J. (2004) Cryo-electron microscopy of vitreous sections of native biological cells and tissues, *J Struct Biol 148*, 131-135.

29. Ruprecht, J. and Nield, J. (2001) Determining the structure of biological macromolecules by transmission electron microscopy, single particle analysis and 3D reconstruction, *Prog Biophys Mol Biol 75*, 121-164.

30. Frank, J. (2001) Cryo-electron microscopy as an investigative tool: the ribosome as an example, *Bioessays 23*, 725-732.

31. Al-Amoudi, A., Chang, J.J., Leforestier, A., McDowall, A., Salamin, L.M., Norlen, L.P., Richter, K., Blanc, N.S., Studer, D., and Dubochet, J. (2004) Cryo-electron microscopy of vitreous sections, *Embo J 23*, 3583-3588.

32. Stark, H. (2002) Three-dimensional electron cryomicroscopy of ribosomes, *Curr Protein Pept Sci 3*, 79-91.

33. Nield, J., Orlova, E.V., Morris, E.P., Gowen, B., van Heel, M., and Barber, J. (2000) 3D map of the plant photosystem II supercomplex obtained by cryoelectron microscopy and single particle analysis, *Nat Struct Biol 7*, 44-47.

34. Orlova, E.V., Sherman, M.B., Chiu, W., Mowri, H., Smith, L.C., and Gotto, A.M., Jr. (1999) Three-dimensional structure of low density lipoproteins by electron cryomicroscopy, *Proc Natl Acad Sci U S A 96*, 8420-8425.

35. Jimenez, J.L., Guijarro, J.I., Orlova, E., Zurdo, J., Dobson, C.M., Sunde, M., and Saibil, H.R. (1999) Cryo-electron microscopy structure of an SH3 amyloid fibril and model of the molecular packing, *Embo J 18*, 815-821.

36. Frank, E.G., Cheng, N., Do, C.C., Cerritelli, M.E., Bruck, I., Goodman, M.F., Egelman, E.H., Woodgate, R., and Steven, A.C. (2000) Visualization of two binding sites for the

Escherichia coli UmuD'(2)C complex (DNA pol V) on RecA-ssDNA filaments, *J Mol Biol 297*, 585-597.

7.12 TABLES AND FIGURES

Table 7.1 Summary of Light Scattering Data Analyzed by ASTRA Software

	M_W of Peak 1		M_W of Peak 2	
WT PhaCPhaE$_{Av}$	324,100	(1.5%)[a]	202,700	(1.5%)
W248A-PhaCPhaE$_{Av}$	323,200	(8%)	154,000	(8%)

[a] error associated with the reported value

Table 7.2 Outer and inner oligonucleotides used in the construction of truncated versions of $PhaE_{Av}$ gene (this table is taken from G. York's 2001 Year-end report, p.62)

Outer oligonucleotides for use in construction of truncated versions of *phaE* gene.

```
              (region upstream of phaE)
PhaE-5-Xba:   TGCTCTAGACGCCCAACACCACGCGCC
                 XbaI

              *nt 462 phaCcv (reverse)
C149S rev:    GAAGGCGCCGCCCTGAGAGATACCGAGCAGATTG
```

Inner oligonucleotides for use in construction of truncated versions of *phaE* gene.

```
                          *nt 970 phaE (reverse)                *nt 949 phaE
(reverse)
PhaE-A-1:     5'-CTC CTC ACC GCGGCCGC TCA CAG GGC TGC GAC GCG ACG-3'
                           NotI     stop(rev)

                 *nt 955 phaE (forward)        *nt 970 phaE (forward)
PhaE-A-2:     5'-GTC GCA GCC CTG TGA GCGGCCGC GGT GAG GAG CCG GCC ACC-3'
                              stop NotI

                          *nt 1051 phaE (reverse)                 *nt 987 phaE
(reverse)
PhaE-B-1:     5'-GGT CTT GGT GCGGCCGC TCA GAG CGC AGT GGC AGG CTT G-3'
                           NotI     stop (rev)

                 *nt 994 phaE (forward)        *nt 1051 phaE (forward)
PhaE-B-2:     5'-GCC ACT GCG CTC TGA GCGGCCGC ACC AAG ACC AAT CCG GCC G-3'
                              stop NotI
```

Table 7.3 Summary of ESI-MS data of recombinant $(His)_6$-$PhaC_{We}$ and $PhaC_{We}$.

	Theoretical MW (Da)	MW of Peak 1 (Da)	MW of Peak 2 (Da)
$(His)_6$-$PhaC_{We}$			
Sample 1	**66480**	**66352**	**67074**
Sample 2	**66480**	**66352**	**67072**
$PhaC_{We}$			
Sample 3	**64316**	**64188**	**64892**
Sample 4	**64316**	**64192**	**64896**

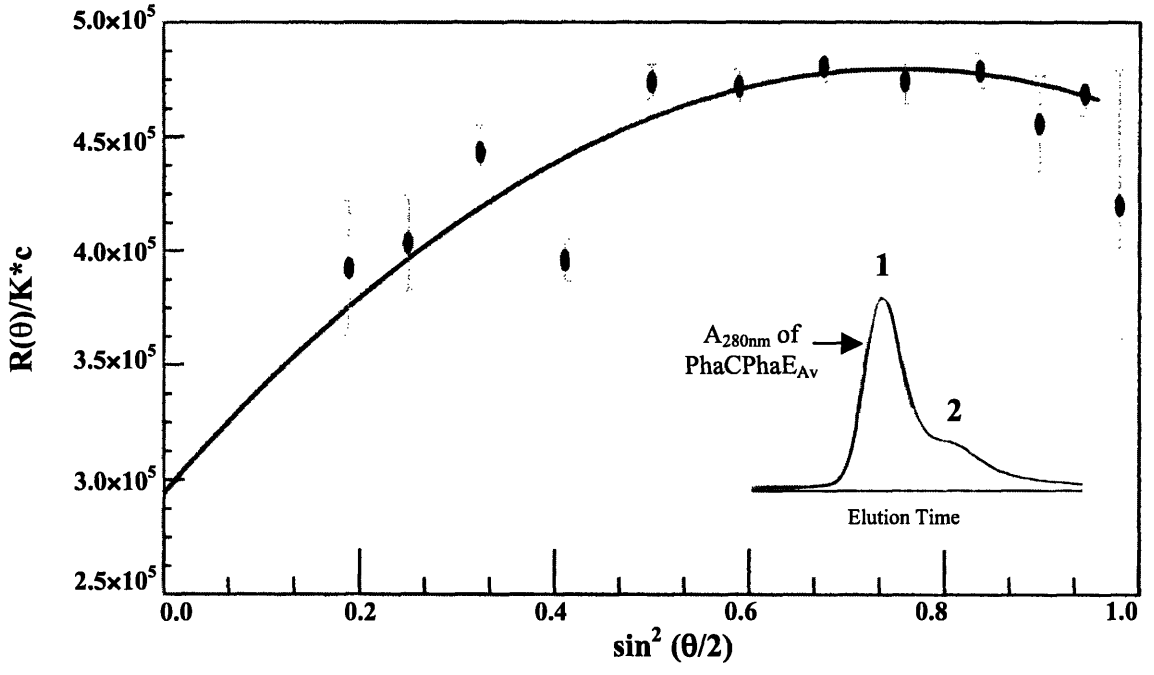

Figure 7.1 Analysis of wt PhaCPhaE$_{Av}$ by SEC coupled to multiangle light scattering instrument (MALS) and a refractive index detector (RI). The protein exists mostly in state **1**, which was determined to be a tetramer of PhaCPhaE$_{Av}$.

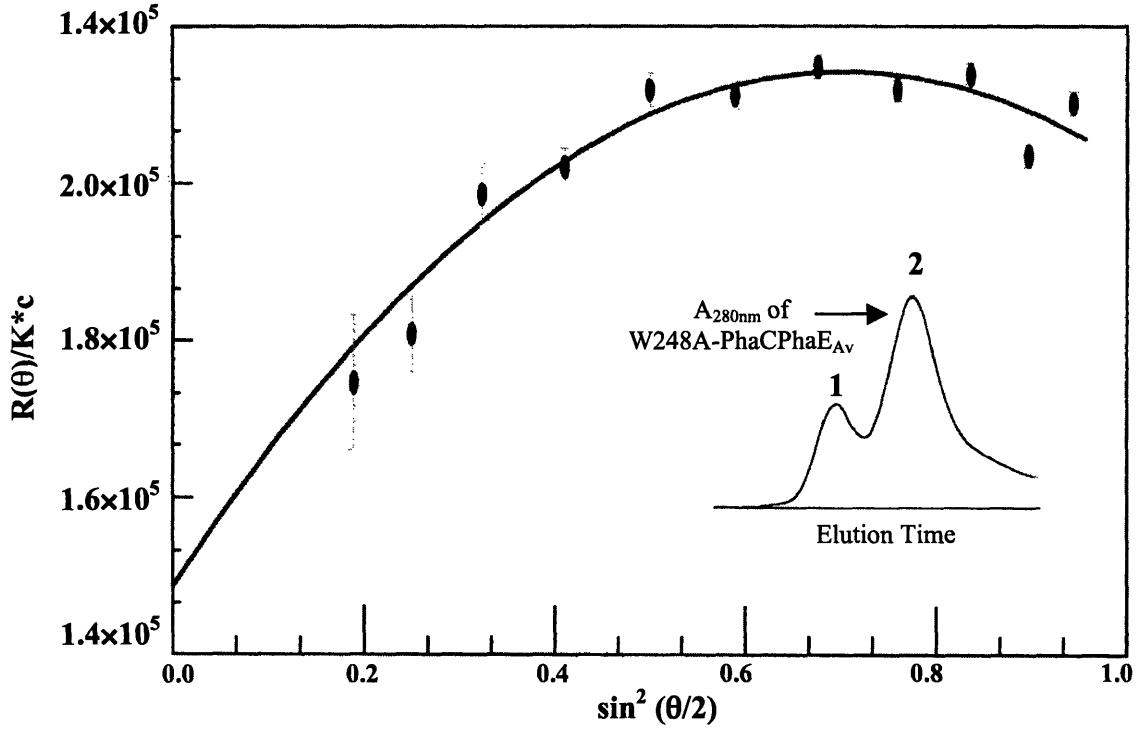

Figure 7.2 Analysis of W248A-PhaCPhaE$_{Av}$ by SEC coupled to MALS and RI. The ratio of protein in state **2** to that in state **1** increased with this mutant.

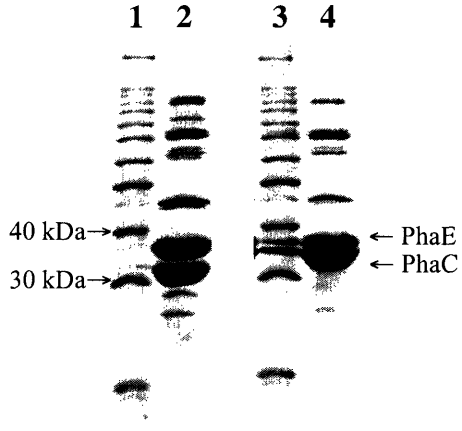

Figure 7.3 Coomassie-stained gel showing purified two truncated versions of PhaCPhaE$_{Av}$. Lanes 1 and 3, molecular weight standards; Lanes 2 and 3, PhaCPhaE-A and PhaCPhaE-B, respectively.

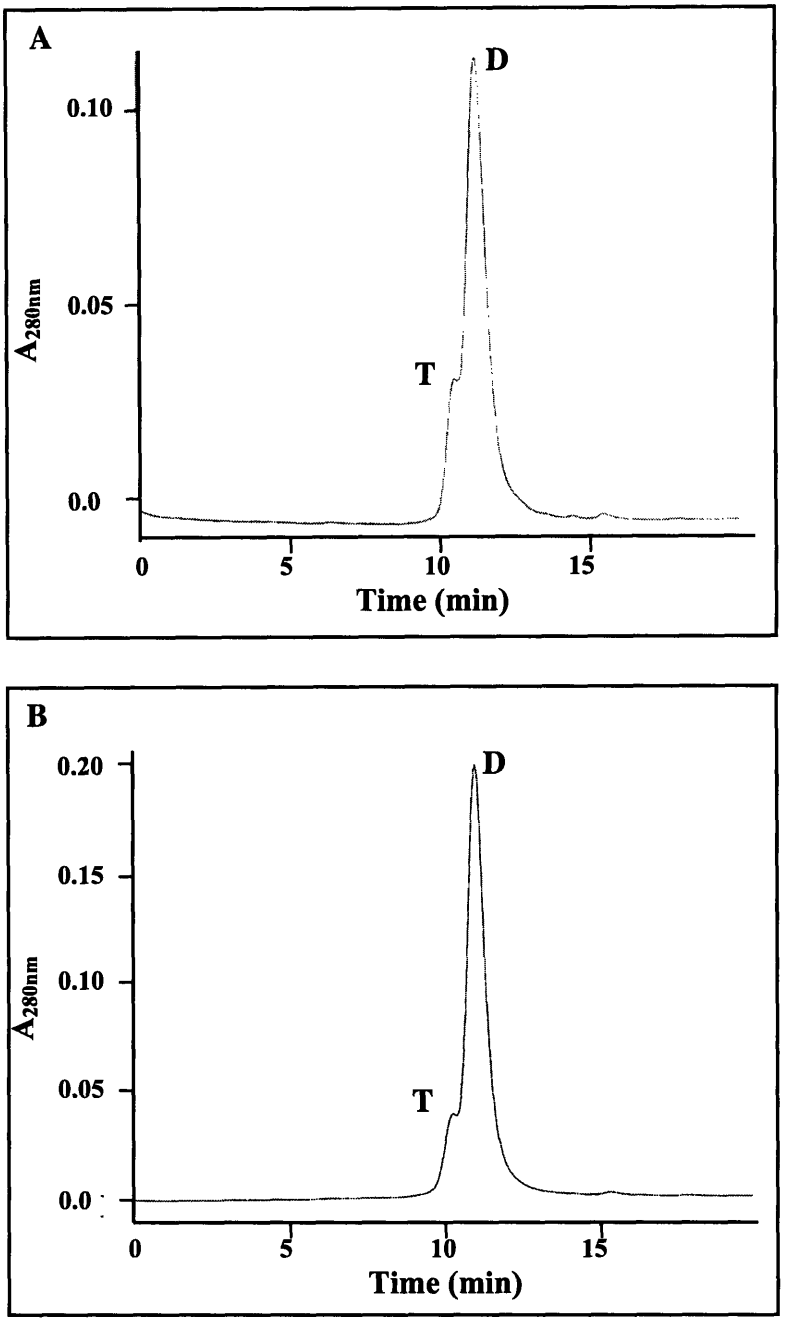

Figure 7.4 Size-exclusion chromatography analysis of (**A**) PhaCPhaE-A and (**B**) PhaCPhaE-B. D=dimer, T=tetramer.

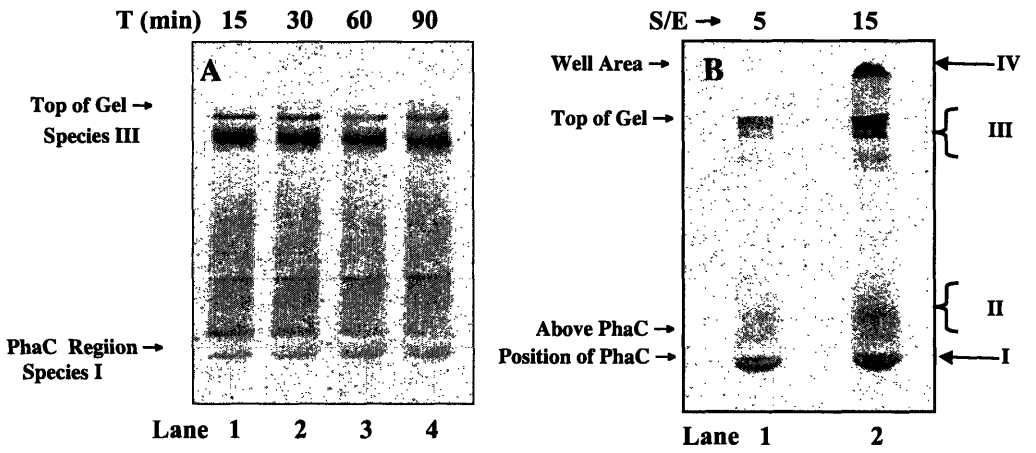

Figure 7.5 (**A**) Phosphorimage of reaction products from reactions containing 5 μM of S90A-PhaCPhaE$_{Av}$ and 50 μM of [^{14}C]-HB-CoA. Lane 1 through 4, reaction was quenched at 15, 30, 60, and 90 min, respectively. The time-dependence phenomenon was still observed with this mutant from 15 to 30 min (Lanes 1 and 2). For comparison purposes, part of Figure 3.1 revealing product distribution by wt PhaCPhaE$_{Av}$ (3.3 μM) is shown again in (**B**). The reactions shown in (**B**) were only incubated for 5 min. Lanes 1 and 2 contain reactions at S/E of 5 and 15 respectively.

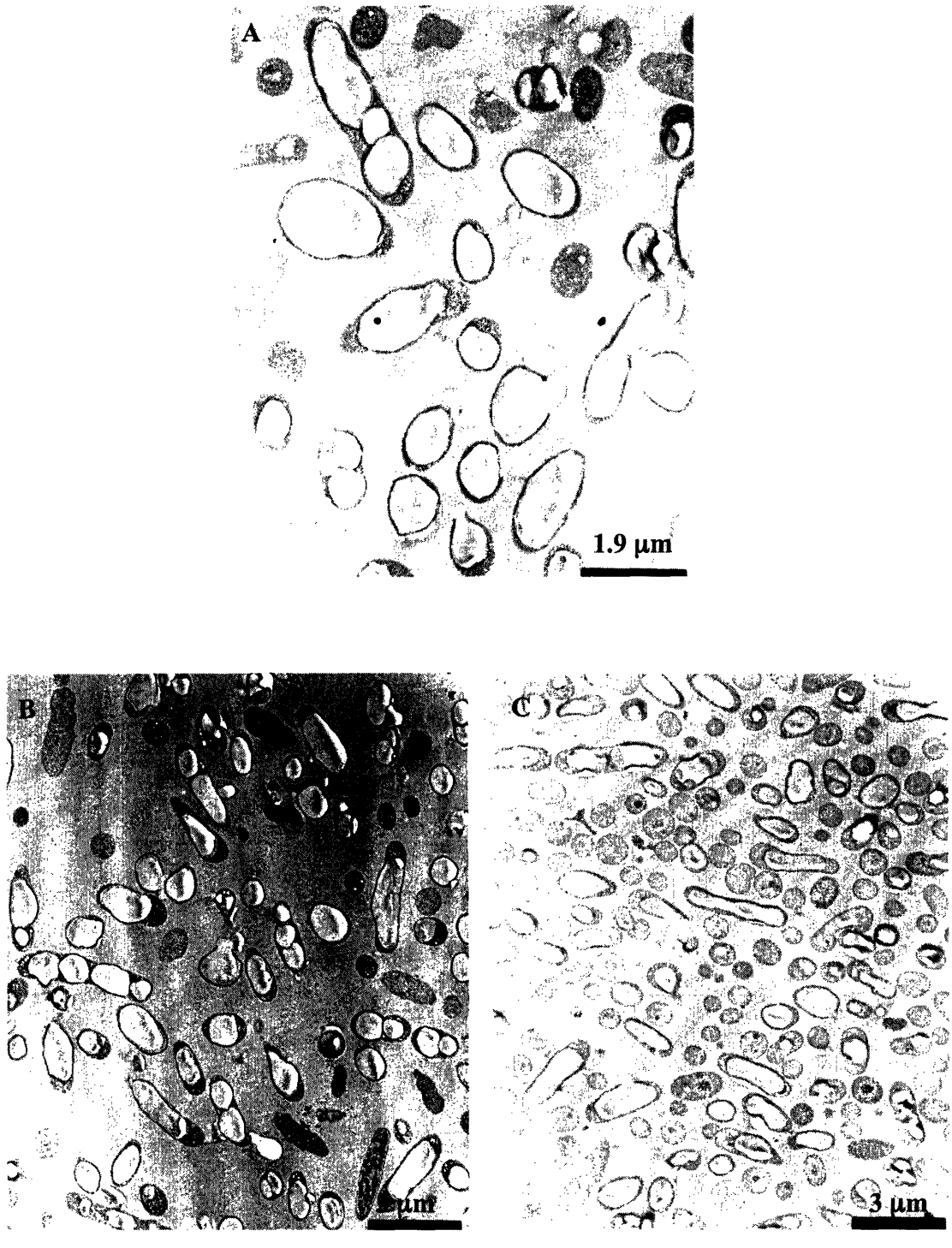

Figure 7.6 TEM of *W. eutropha* H16 with its synthase gene replaced with S90A-PhaCPhaE$_{Av}$. (**A**) and (**B**) at PHB$_P$ 73 h, and (**C**) at PHB$_U$ 48 h. Note that (**A**) is at a different magnification from the other two.

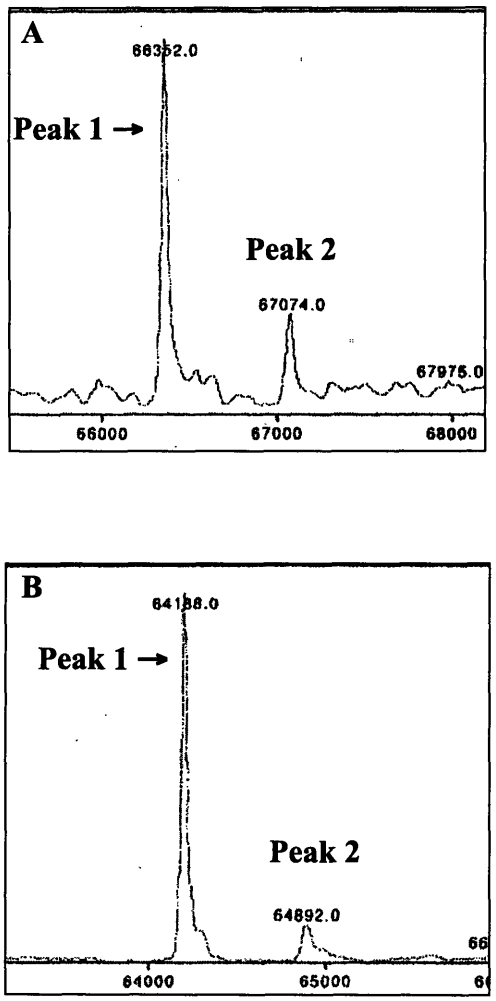

Figure 7.7 ESI mass spectra of (**A**) $(His)_6$-$PhaC_{We}$ (Sample 1, refer to text) and (**B**) $PhaC_{We}$ (Sample 3).

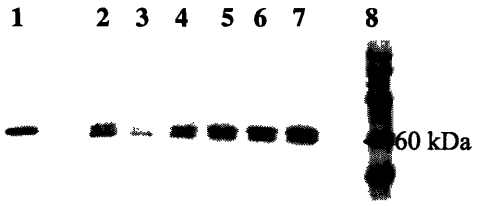

Figure 7.8 Two bands near the MW of $PhaC_{We}$ were detected by $PhaC_{We}$ Abs when the cell extract from *W. eutropha* cultivated in TSB medium were analyzed by Western using 0.7 mm 10% SDS-PAGE gel. Lane 1, recombinant $PhaC_{We}$ serving as a standard; Lane 2 through 7, cell extract of *W. eutropha* cells at 0, 4, 8, 12, 24, and 48 h, respectively; Lane 8, MW standards.

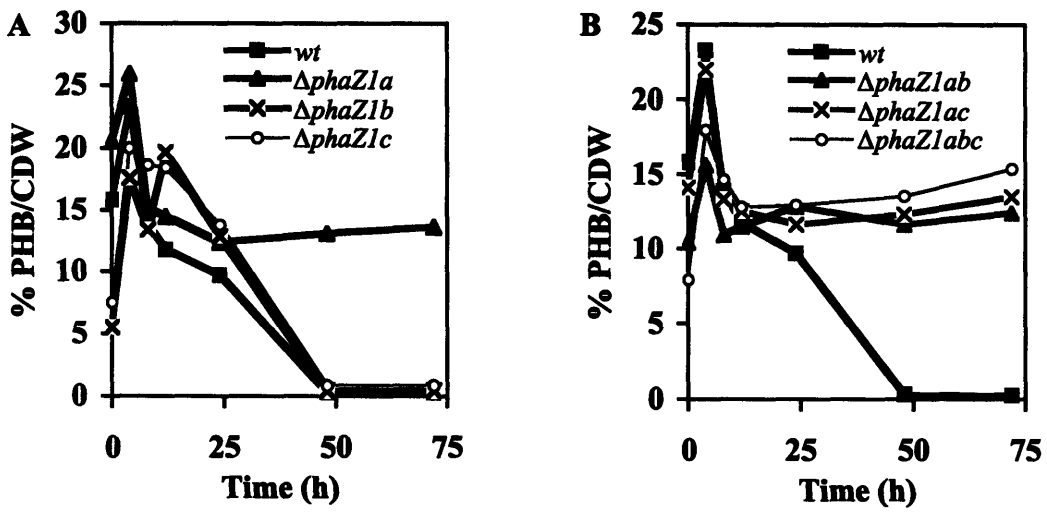

Figure 7.9 PHB production and utilization in TSB medium. **(A)** Results for wt, Δ*phaZ1*$_a$, Δ*phaZ1*$_b$, and Δ*phaZ1*$_c$. **(B)** Results for wt, Δ*phaZ1*$_{ab}$, Δ*phaZ1*$_{ac}$, and Δ*phaZ1*$_{abc}$.

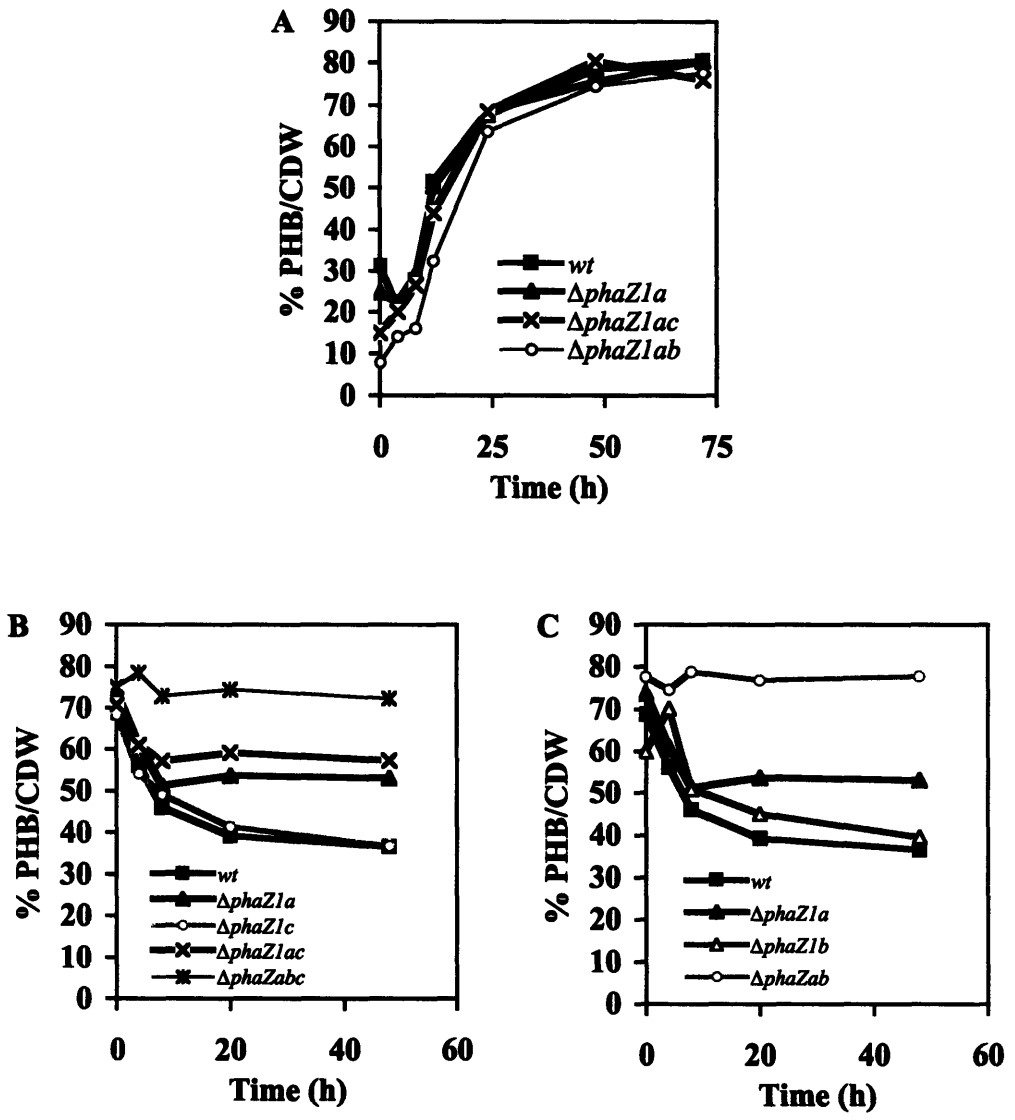

Figure 7.10 (A) PHB production in PHB_P by wt, $\Delta phaZ1_a$, $\Delta phaZ1_{ac}$, and $\Delta phaZ1_{ab}$ *W. eutropha* H16 strains. The production pattern is the same in all deletion strains (additional data not shown). PHB utilization in PHB_U by (B) wt, $\Delta phaZ1_a$, $\Delta phaZ1_c$, $\Delta phaZ1_{ac}$, $\Delta phaZ1_{abc}$; (C) wt, $\Delta phaZ1_a$, $\Delta phaZ1_b$, and $\Delta phaZ1_{ab}$ *W. eutropha* H16 strains.

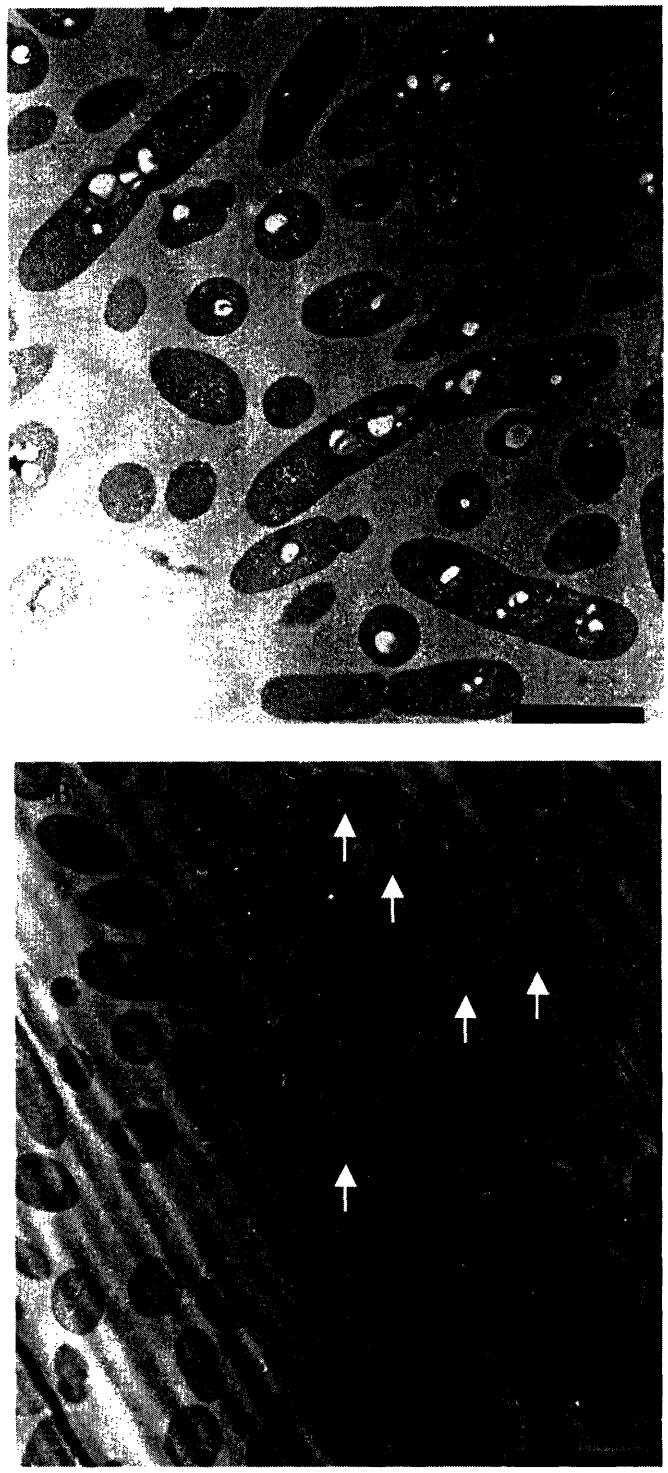

Figure 7.11 TEM photograph of (**A**) wt *W. eutropha* H16 in TSB medium at 4 h. (**B**) Δ*phaC W. eutropha* H16 in TSB medium at 4 h. Examples of the dark-stained feature are pointed by white errors. Bar size, 1.9 μm.

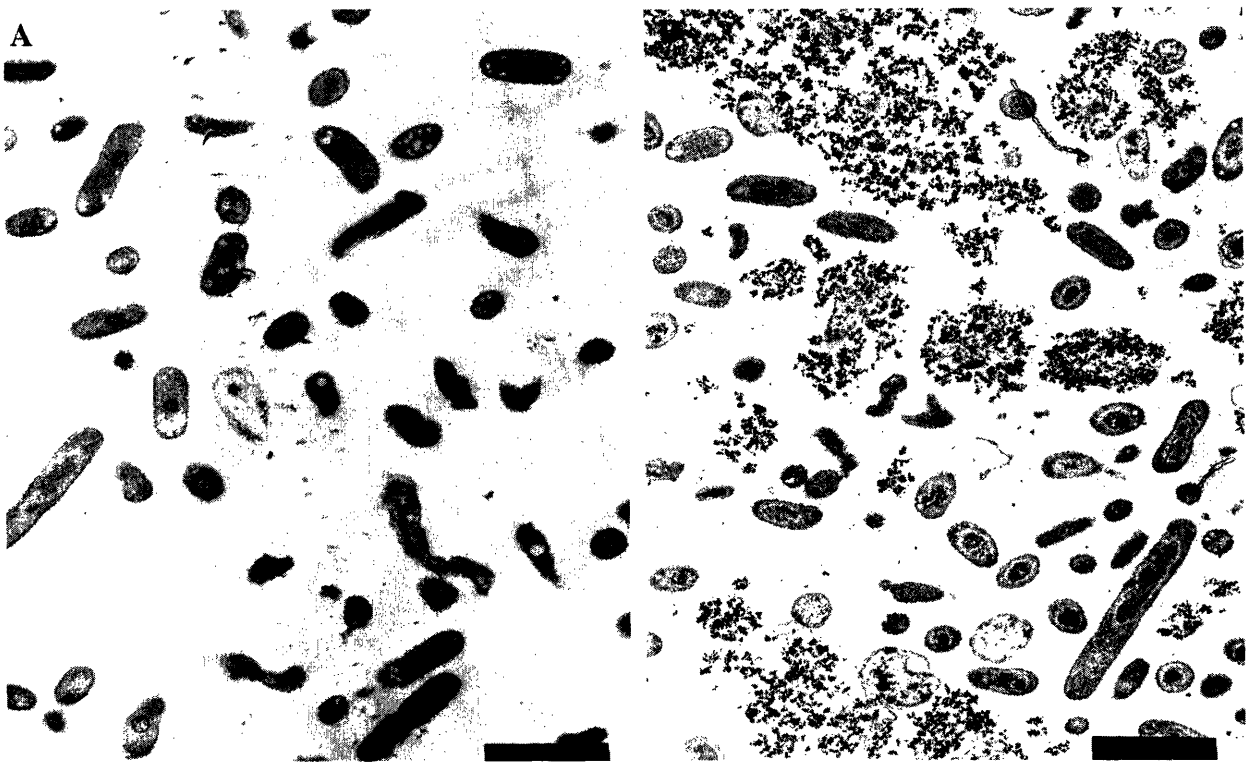

Figure 7.12 TEM images of (**A**) Δ*phaC W. eutropha* H16 strain grown in PHB_P for 72 h. (**B**) Δ*phaC* at 48 h in PHB_U. Bar size, 1.9 μm.

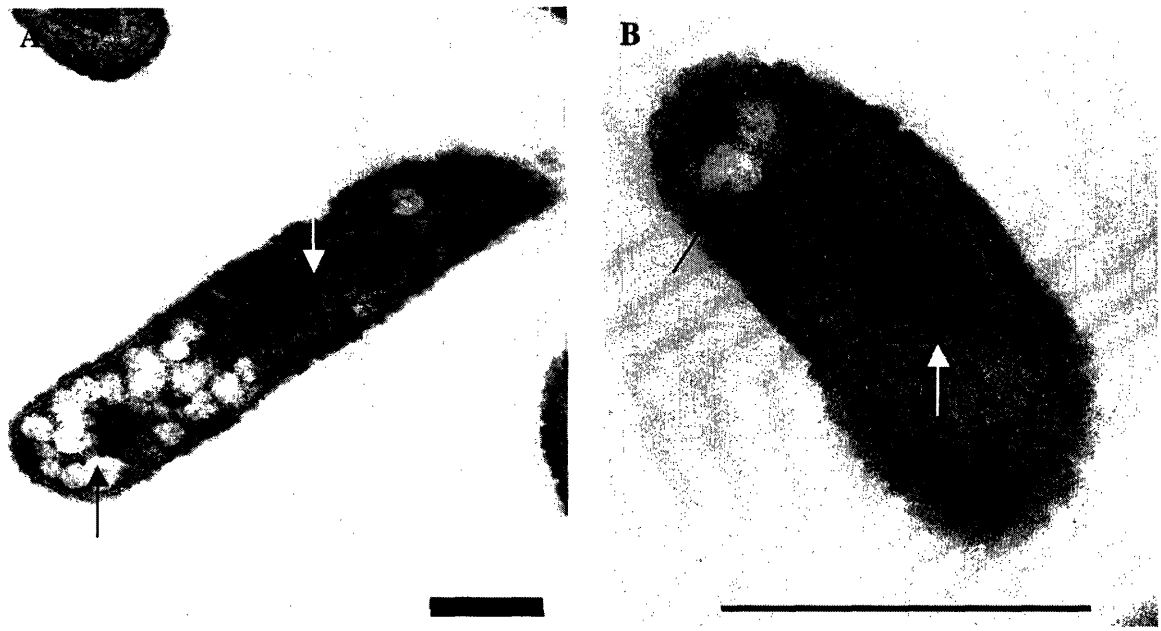

Figure 7.13 TEM images of Δ*phaC W. eutropha* H16 strain grown in PHB_P for 72 h, (**A**) bar size, 0.44 μm, (**B**) bar size, 0.8 μm. Small white granular features (black arrow), close to the cell membrane, are observed. They do not appear to be localized next to the dark-stained feature (white arrow).

Figure 7.14 TEM image of Δ*phaR W. eutropha* H16 at 72 h in PHB_P. Bar size, 0.64 μm.

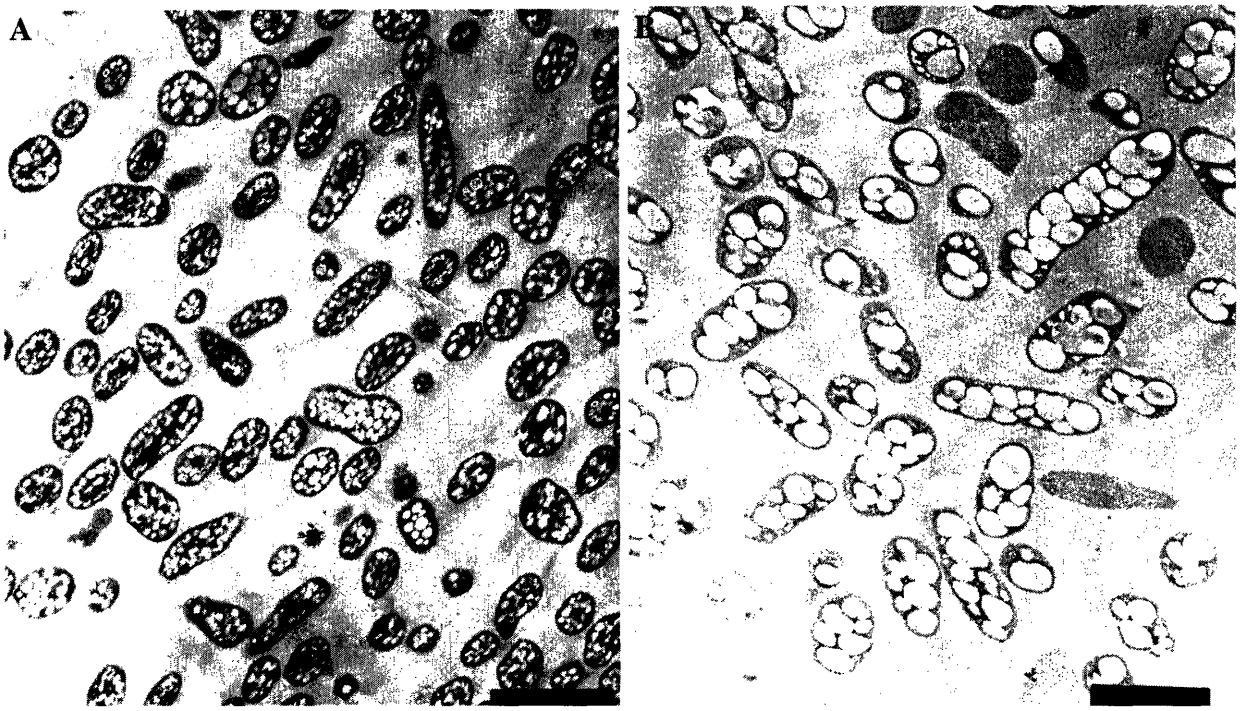

Figure 7.15 TEM images of (**A**) Δ*phaR W. eutropha* H16 strain at 72 h in PHB_P, and (**B**) wt strain at 72 h in PHB_P. Bar size, 1.9 μm. (**B**) is included for comparison purposes.

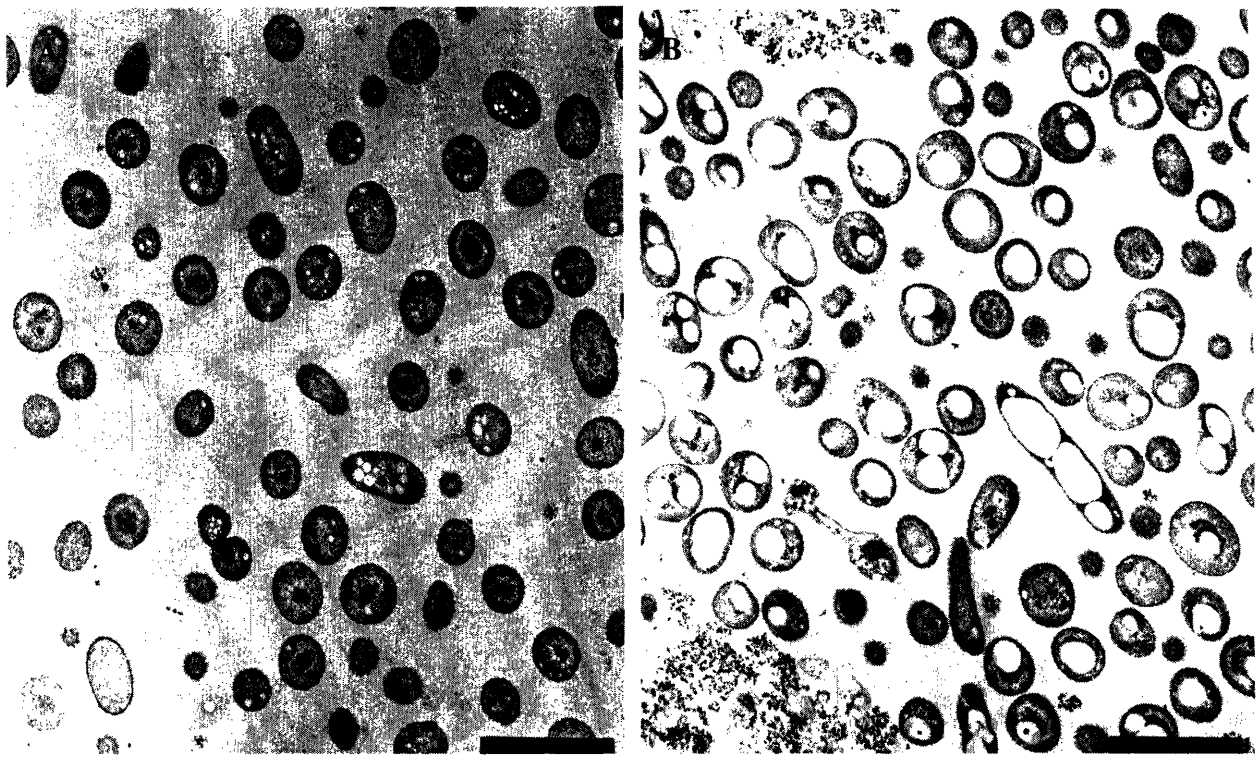

Figure 7.16 TEM images of (**A**) Δ*phaR W. eutropha* H16 strain at 48 h in PHB_U, and (**B**) wt strain at 48 h in PHB_U. Bar size, 1.9 μm. (**B**) is included for comparison purposes.

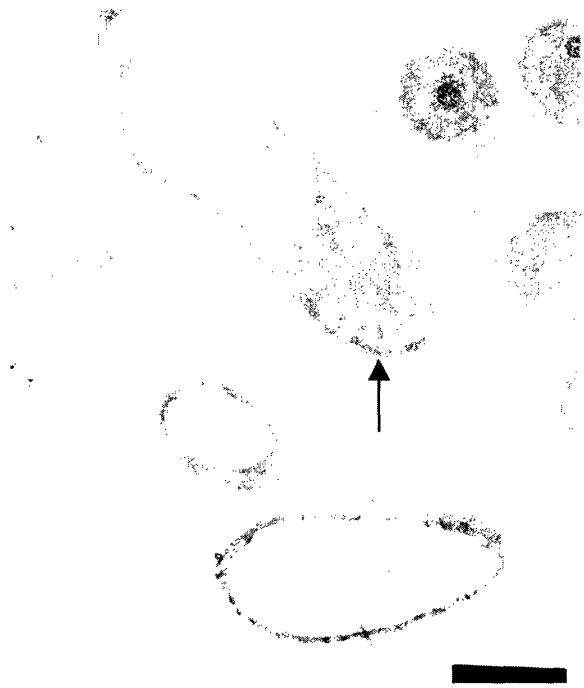

Figure 7.17 TEM image of Δ*phaP W. eutropha* H16 strain grown in PHB_P for 72 h. Bar size, 0.64 μm. Cells of Δ*phaP* strain are found to contain small granules (black arrow) close to the inner membrane of the cell in addition to one large granule.

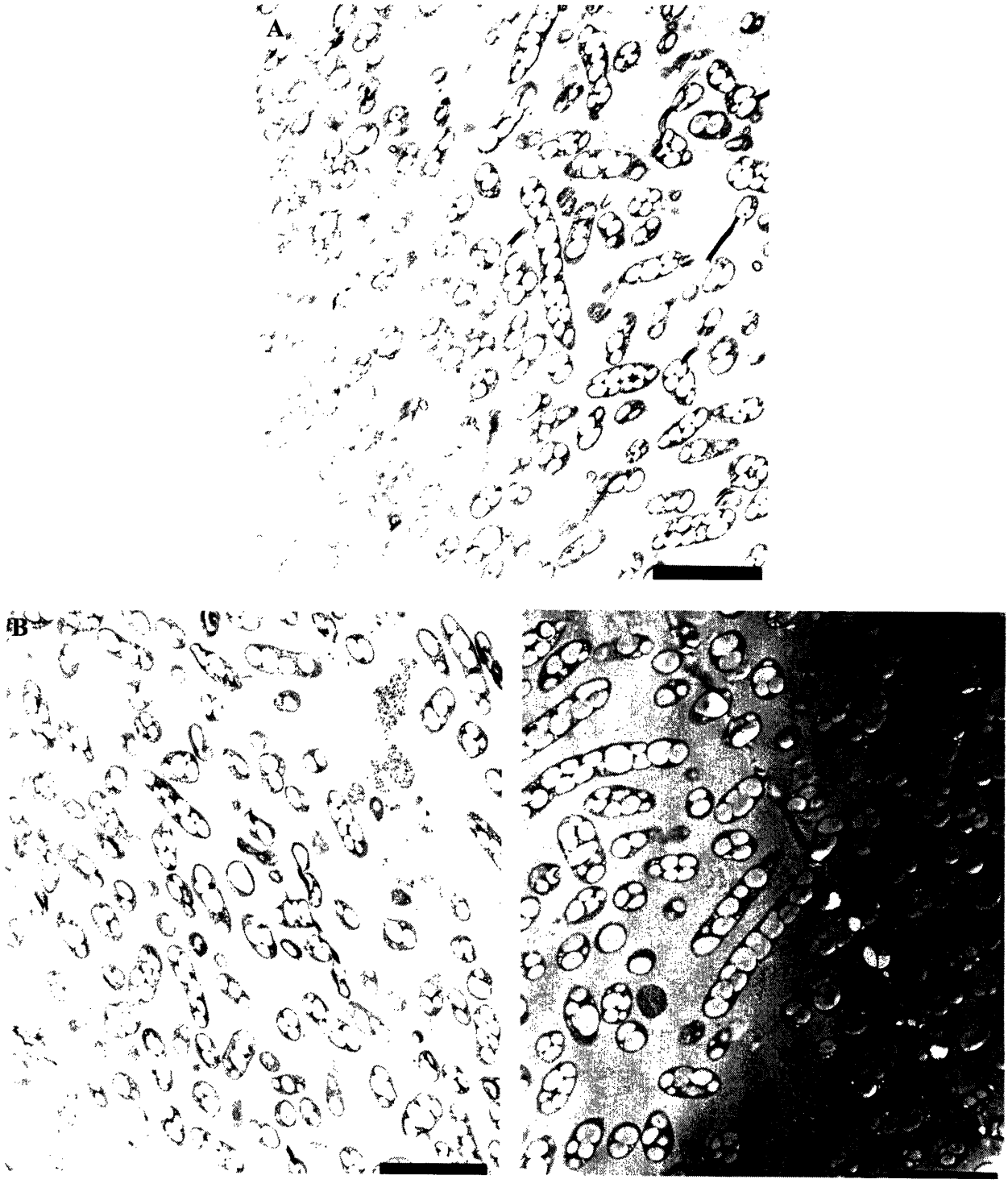

Figure 7.18 TEM images of (**A**) Δ*phaZ1*$_a$, (**B**) Δ*phaZ1*$_b$, (**C**) Δ*phaZ1*$_c$ *W. eutropha* H16 strains at 72 h in PHB_U. Bar size, 3 μm.

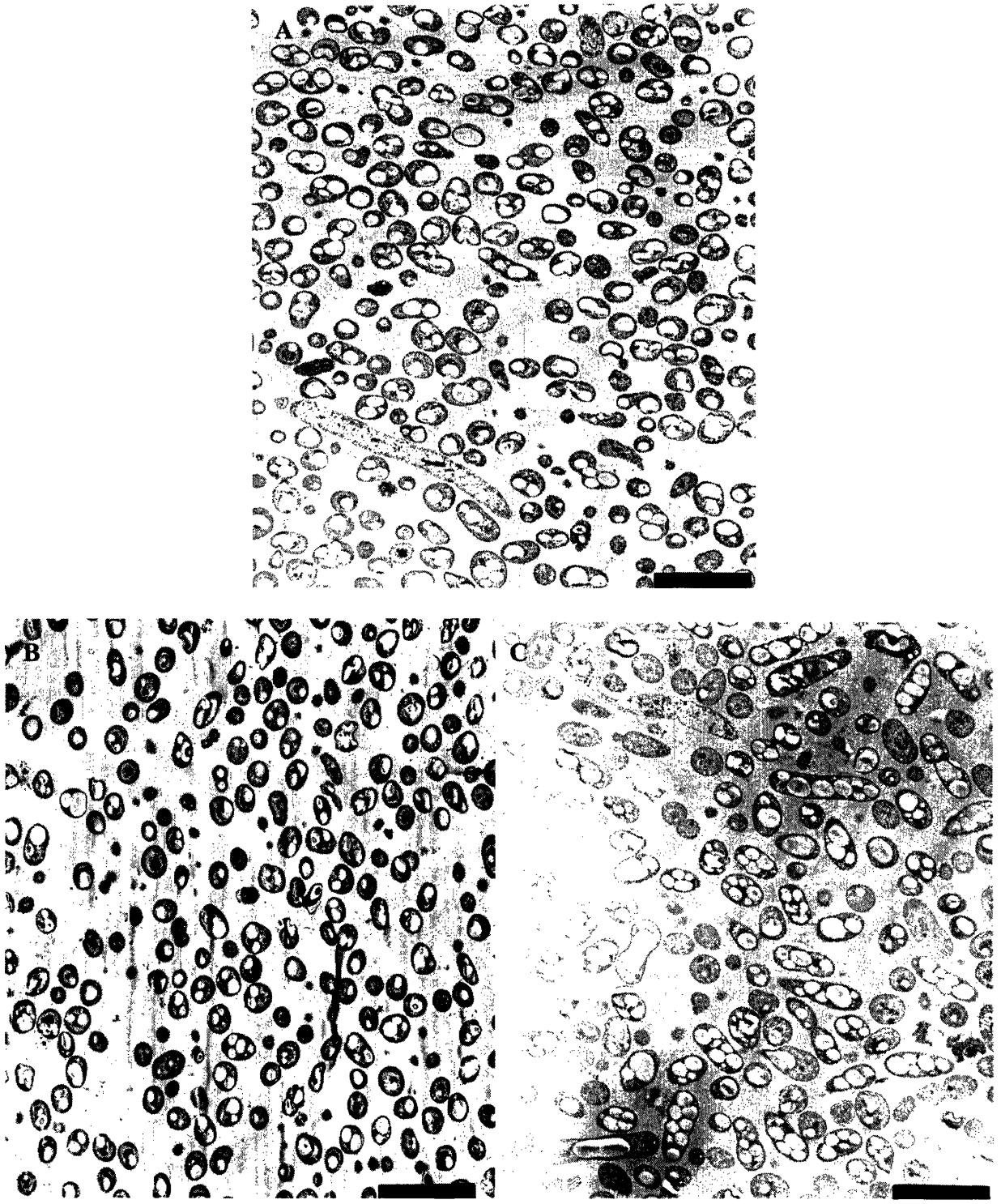

Figure 7.19 TEM images of (**A**) Δ*phaZ1*$_a$, (**B**) Δ*phaZ1*$_b$, (**C**) Δ*phaZ1*$_c$ *W. eutropha* H16 strains at 48 h in PHB_U. Bar size, 3 μm.

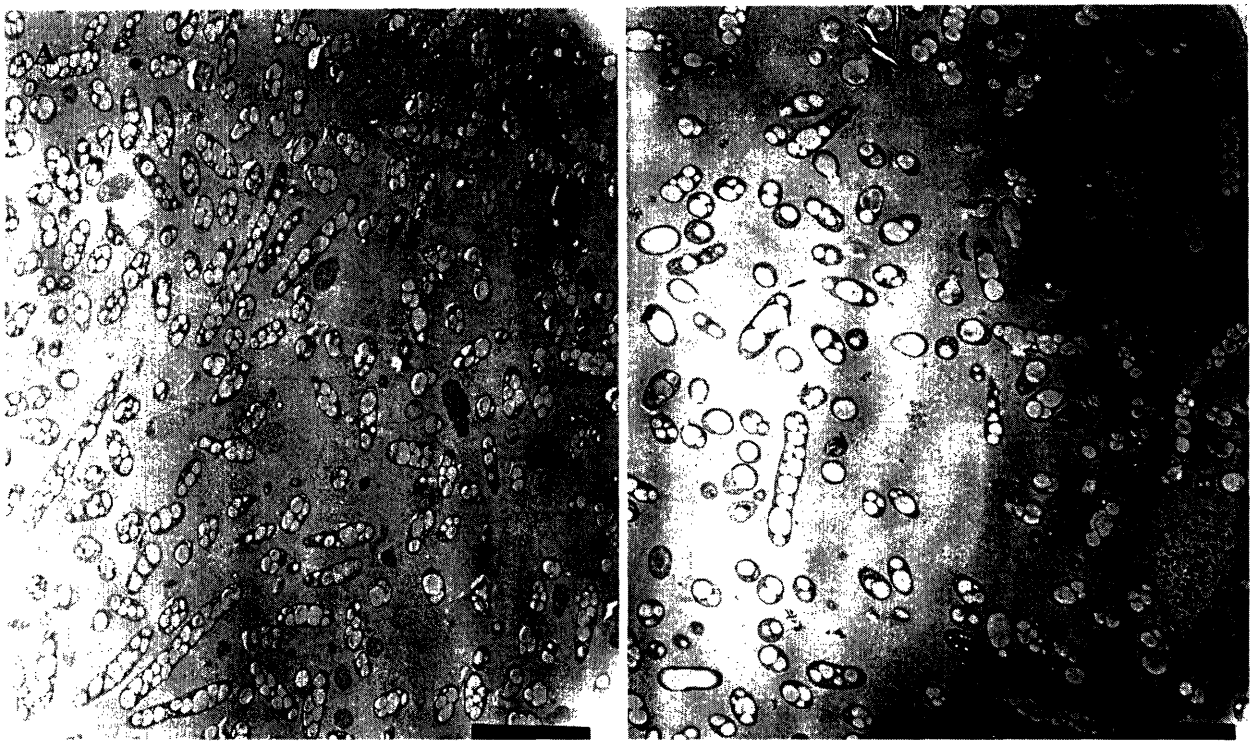

Figure 7.20 TEM images of $\Delta phaZ1_{abc}$ *W. eutropha* H16 strain at (**A**) 72 h in PHB_P and (**B**) 48 h in PHB_U. Bar size, 4.5 μm.